

RD-R139 419

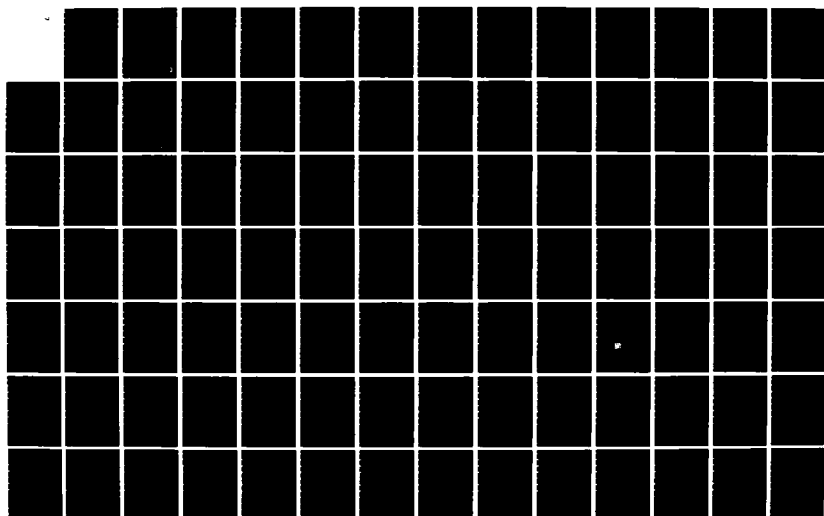
NCEL (NAVAL CIVIL ENGINEERING LAB) OCEAN PLATFORMS
SEMINAR(U) NAVAL CIVIL ENGINEERING LAB PORT HUENEME CA
D R SHIELDS NOV 83 NCEL-TN-1681

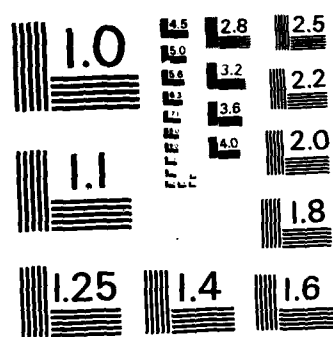
1/4

UNCLASSIFIED

F/G 13/13

NL





MICROCOPY RESOLUTION TEST CHART
NATIONAL BUREAU OF STANDARDS - 1963 - A

PN
TN NO: N-1681

(P)

TITLE: NCEL OCEAN PLATFORMS SEMINAR

AUTHOR: D. R. Shields

DATE: November 1983

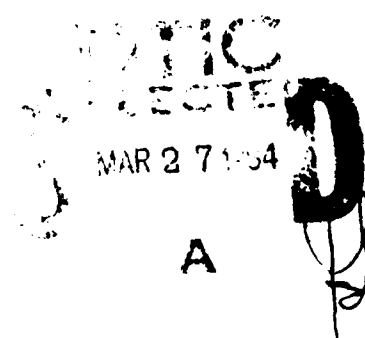
SPONSOR: Naval Facilities Engineering Command

PROGRAM NO: YF60.534.091.01.A351

NOTE

NAVAL CIVIL ENGINEERING LABORATORY
PORT HUENEME, CALIFORNIA 93043

Approved for public release; distribution unlimited.



DTIC FILE COPY

METRIC CONVERSION FACTORS

Approximate Conversions to Metric Measures

Symbol	When You Know	Multiply by	To Find	Symbol	When You Know	Multiply by	To Find	Symbol
			<u>LENGTH</u>				<u>LENGTH</u>	
in	inches	*2.5	centimeters	mm	millimeters	0.04	inches	in
ft	feet	30	centimeters	cm	centimeters	0.4	inches	in
yd	yards	0.9	meters	m	meters	3.3	feet	ft
mi	miles	1.6	kilometers	km	kilometers	1.1	yards	yd
			<u>AREA</u>				<u>AREA</u>	
in ²	square inches	6.5	square centimeters	cm ²	square centimeters	0.16	square inches	in ²
ft ²	square feet	0.09	square meters	m ²	square meters	1.2	square yards	yd ²
yd ²	square yards	0.8	square meters	km ²	square kilometers	0.4	square miles	mi ²
mi ²	square miles	2.6	square kilometers	ha	hectares (10,000 m ²)	2.5	acres	
			<u>MASS (weight)</u>				<u>MASS (weight)</u>	
oz	ounces	28	grams	g	grams	0.036	ounces	oz
lb	pounds	0.45	kilograms	kg	kilograms	2.2	pounds	lb
	short tons (12,000 lb)	0.9	tonnes	t	tonnes (1,000 kg)	1.1	short tons	
			<u>VOLUME</u>				<u>VOLUME</u>	
tsp	teaspoons	5	milliliters	ml	milliliters	0.03	fluid ounces	fl. oz
Tbsp	tablespoons	15	milliliters	ml	liters	2.1	pints	pt
fl oz	fluid ounces	30	milliliters	ml	liters	1.06	quarts	qt
c	cups	0.24	liters	l	cubic meters	0.26	gallons	gal
px	pints	0.47	liters	l	cubic meters	35	cubic feet	ft ³
qr	quarts	0.95	liters	l	cubic meters	1.3	cubic yards	yd ³
gal	gallons	3.8	cubic meters	m ³				
ft ³	cubic feet	0.03	cubic meters	m ³				
yd ³	cubic yards	0.76	cubic meters	m ³				
			<u>TEMPERATURE (exact)</u>				<u>TEMPERATURE (exact)</u>	
°F	Fahrenheit temperature	5/9 (after subtracting 32)	Celsius temperature	°C	Celsius temperature	9/5 (then add 32)	Fahrenheit temperature	°F

*1 in = 2.54 (exactly). For other exact conversions and more detailed tables, see NES Misc. Publ. 286, Units of Weight and Measures, Price \$2.25, SC Catalog No. C13-10-286.



Approximate Conversions from Metric Measures

Symbol	When You Know	Multiply by	To Find	Symbol	When You Know	Multiply by	To Find	Symbol
			<u>LENGTH</u>				<u>LENGTH</u>	
in	centimeters	0.39	inches	in	centimeters	0.04	inches	in
cm	centimeters	0.39	inches	in	centimeters	0.4	inches	in
m	meters	0.9	feet	ft	meters	3.3	feet	ft
km	kilometers	1.6	yards	yd	kilometers	1.1	yards	yd
			<u>AREA</u>				<u>AREA</u>	
cm ²	square centimeters	0.09	square centimeters	cm ²	square centimeters	0.16	square inches	in ²
m ²	square meters	0.8	square meters	m ²	square meters	1.2	square yards	yd ²
km ²	square kilometers	2.6	square kilometers	km ²	square kilometers	0.4	square miles	mi ²
ha	hectares	0.4	hectares	ha	hectares (10,000 m ²)	2.5	acres	
			<u>MASS (weight)</u>				<u>MASS (weight)</u>	
g	grams	0.035	ounces	oz	kilograms	2.2	pounds	lb
kg	kilograms	0.035	ounces	oz	tonnes (1,000 kg)	1.1	short tons	
t	tonnes	0.035	short tons	lb				
			<u>VOLUME</u>				<u>VOLUME</u>	
ml	milliliters	0.03	fluid ounces	fl. oz	liters	2.1	pints	pt
l	liters	0.03	fluid ounces	fl. oz	liters	1.06	quarts	qt
m ³	cubic meters	0.26	gallons	gal	cubic meters	35	cubic feet	ft ³
m ³	cubic meters	1.3	cubic feet	ft ³	cubic meters	1.3	cubic yards	yd ³
			<u>TEMPERATURE (exact)</u>				<u>TEMPERATURE (exact)</u>	
°C	Celsius temperature	9/5 (then add 32)	Fahrenheit temperature	°F	Celsius temperature	9/5 (then add 32)	Fahrenheit temperature	°F

Unclassified

SECURITY CLASSIFICATION OF THIS PAGE (When Data Entered)

REPORT DOCUMENTATION PAGE		READ INSTRUCTIONS BEFORE COMPLETING FORM
1. REPORT NUMBER TN-1681	2. GOV'T ACCESSION NO. DN387307	3. RECIPIENT'S CATALOG NUMBER ADA 139 419
4. TITLE (and Subtitle) NCEL OCEAN PLATFORMS SEMINAR		5. TYPE OF REPORT & PERIOD COVERED Final; Oct 1982 – Sep 1983
7. AUTHOR(s) D. R. Shields		6. PERFORMING ORG. REPORT NUMBER
9. PERFORMING ORGANIZATION NAME AND ADDRESS NAVAL CIVIL ENGINEERING LABORATORY Port Hueneme, California 93043		10. PROGRAM ELEMENT, PROJECT, TASK AREA & WORK UNIT NUMBERS 62760N; YF60.534.091.01.A351
11. CONTROLLING OFFICE NAME AND ADDRESS Naval Facilities Engineering Command Alexandria, Virginia 22332		12. REPORT DATE November 1983
14. MONITORING AGENCY NAME & ADDRESS (if different from Controlling Office)		13. NUMBER OF PAGES 297
16. DISTRIBUTION STATEMENT (of this Report)		15. SECURITY CLASS. (of this report) Unclassified
17. DISTRIBUTION STATEMENT (of the abstract entered in Block 20, if different from Report)		15a. DECLASSIFICATION/DOWNGRADING SCHEDULE
18. SUPPLEMENTARY NOTES		
19. KEY WORDS (Continue on reverse side if necessary and identify by block number) Ocean platforms, environmental specification, environmental forces, wave forces, offshore platforms, fixed platforms, guyed towers, tension leg platforms, semisubmersibles, discus buoys, spar buoys, buoy moorings, dynamic response of ocean structures, extreme statistics, reliability, probability, risk		
20. ABSTRACT (Continue on reverse side if necessary and identify by block number) The NCEL Ocean Platforms Seminar was held on 11-12 January 1983. Eleven experts, selected to represent the major disciplines relevant to ocean platforms, were invited to present papers and discuss R&D needs. The state-of-technology in ocean platforms was identified and R&D topics defined. This report provides the papers presented at the seminar and the conclusions from each participant concerning R&D needs.		

DD FORM 1 JAN 73 1473 EDITION OF 1 NOV 65 IS OBSOLETE

Unclassified

SECURITY CLASSIFICATION OF THIS PAGE (When Data Entered)

Unclassified

SECURITY CLASSIFICATION OF THIS PAGE(When Data Entered)

Library Card

Naval Civil Engineering Laboratory
NCEL OCEAN PLATFORMS SEMINAR (Final), by D. R. Shields
TN-1681 297 pp illus November 1983 Unclassified

1. Ocean platforms 2. Environmental forces I. YF60.534.091.01.A351

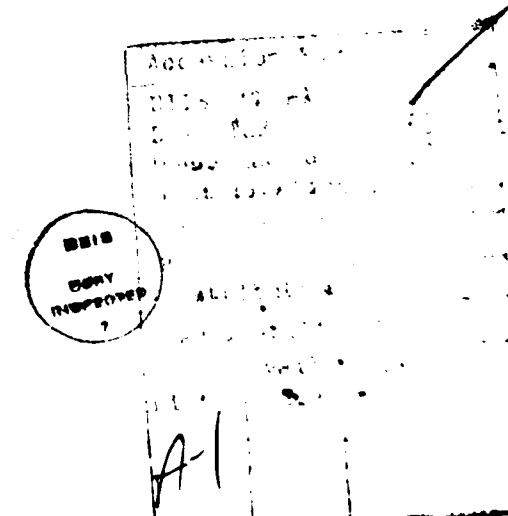
The NCEL Ocean Platforms Seminar was held on 11-12 January 1983. Eleven experts, selected to represent the major disciplines relevant to ocean platforms, were invited to present papers and discuss R&D needs. The state-of-technology in ocean platforms was identified and R&D topics defined. This report provides the papers presented at the seminar and the conclusions from each participant concerning R&D needs.

Unclassified

SECURITY CLASSIFICATION OF THIS PAGE(When Data Entered)

CONTENTS

	Page
INTRODUCTION	1
SEMINAR	1
Background	1
Participants	2
Format	3
Presentations	4
CONCLUSIONS	5
ACKNOWLEDGMENT	5
APPENDIX - Ocean Platforms Seminar Attendees	7
SEMINAR PRESENTATIONS:	9
Environmental Prediction for Offshore Platform Design	11
Environmental Forces on Ocean Platforms	27
Fixed and Guyed Tower Platforms State-of-the-Art	85
Semisubmersible and Tension Leg Platforms	101
Notes on Disc and Spar Buoys	137
Marine Cable Strumming and Its Prevention	169
Mooring Design, Deployment, and Operation	199
Full Scale Measurement, Model Tests and the Prediction of Dynamic Response	221
Extreme Statistics, Risk and Reliability	245
SEMINAR SUMMARIES BY PARTICIPANTS	265



INTRODUCTION

The Naval Civil Engineering Laboratory (NCEL) began research and development on ocean platforms in 1980 under the aegis of the Naval Facilities Engineering Command (NAVFAC). Two projects have evolved directed toward research and development on ocean platforms: (1) a work unit on long-term sensor platforms started in 1980 and (2) a project focusing on technology required to support design and construction of Offshore Air Combat Training Facilities.

Two previous technical seminars were conducted by NCEL to assist in the formulation of pertinent research topics for two other programs. During April 1979 the first seminar entitled "Environmental Loads on Fixed Offshore Structures" provided input to the development plan for the wave forces project.* The second seminar entitled "The 1980 CEL Mooring Dynamics Seminar" held in January 1980 was used as an aid in defining research and development topics for the mooring system prediction project.**

NCEL was tasked by NAVFAC to prepare a development plan for the technology option on Offshore Air Combat Training Facilities Technology. A seminar was conducted in January 1983 in order to assess the state-of-technology in ocean platforms for Offshore Air Combat Training Facilities. The seminar also included a workshop session to discuss research topics of importance to the Navy in an attempt to identify deficiencies in the technology required to design the ocean platforms required for Offshore Air Combat Training Facilities.

SEMINAR

Background

The Navy, Marine Corps and Air Force utilize Air Combat Training Facilities for personnel combat-readiness training. Because of environmental/social/political pressures and a shortage of real estate, these training facilities are being located over water. One Navy over-water training facility is the Tactical Air Crew Combat Training Systems (TACTS), located in the Atlantic Ocean off the outer banks of North Carolina. The fixed offshore platforms to support this TACTS range were installed in 1976. The Navy has identified three more TACTS ranges to be located offshore; these ranges and the tentative platform requirements are provided in Tables 1 and 2.

*T.M. Ward. Development plan for wave forces on ocean structures, Civil Engineering Laboratory, Technical Memorandum M-44-81-1. Port Hueneme, Calif., Oct 1980.

**P.A. Palo. The 1980 CEL mooring dynamics seminar, Civil Engineering Laboratory, Technical Note N-1604. Port Hueneme, Calif., Mar 1981.

The Air Force presently has two over-water training facilities, called the Air Combat Maneuvering Instrumentation (ACMI) System ranges. One range utilizes a caisson/mat structure in the shallow coastal waters off Florida; the second uses 33-foot-diam discus buoys in the relatively deep water of the Mediterranean Sea. The Air Force is presently developing a third over-water ACMI range to be located in the Philippine Sea, using 250-ton displacement semisubmersible buoys. The Air Force also has another shallow-water range scheduled for development in 1987 (see Table 1).

As presented in Table 1, two clear classes of offshore structures are required for the TACTS ranges: the shallow-water platform and the deep-water platform. Because the offshore petroleum industry has developed a great deal of technology on fixed offshore drilling and production platforms, the Navy may utilize this well-established technology for the design and construction of the shallow-water platforms.

Sites which have been identified for potential deep-water TACTS platforms are in water depths between 3,000 and 7,000 feet. These TACTS facilities may require platforms with a 20-year life cycle. Present technology does not provide reliable designs for these deep-water, long-term TACTS range platforms.

This seminar was organized in order to determine the state-of-technology in ocean platforms and to identify deficiencies in technology areas required for deep-water TACTS platform design.

Participants

NCEL invited to the seminar 11 prominent experts from the fields of coastal and oceanographic engineering, ocean engineering, offshore engineering, Naval architecture, statistics, and structural engineering to participate. These experts, each of whom presented a paper, were selected from the academic, industrial, and governmental sectors to provide a balanced mix of expertise. A list of the participants and their affiliations follows.

Mr. Henri O. Berteaux
Research Specialist and Instructor, M.I.T./W.H.O.I.
Woods Hole Oceanographic Institution

Dr. Leon E. Borgman
Professor of Geology and Statistics
University of Wyoming

Dr. Lyle D. Finn
Senior Research Associate
Exxon Production Research Co.

Dr. Owen M. Griffin
Mechanical Engineer
Marine Technology Division
Naval Research Laboratory

Dr. Robert T. Hudspeth
Professor, Ocean Engineering Program
Department of Civil Engineering
Oregon State University

Mr. Paul A. Palo
Mechanical Engineer
Ocean Structures Division
Naval Civil Engineering Laboratory

Dr. J. Randolph Paulling, Jr.
Professor of Naval Architecture
University of California

Mr. William O. Rainnie, Jr.
Chief, Engineering Division
NOAA Data Buoy Center
National Oceanic and Atmospheric Administration

Dr. Richard A. Skop
Head, Fluid Dynamics
Marine Technology Division
Naval Research Laboratory

Dr. J. Kim Vandiver
Associate Professor of Ocean Engineering
Massachusetts Institute of Technology

Dr. Charles L. Vincent
Chief, Coastal Oceanography Branch
Coastal Engineering Research Center
U.S. Army Corps of Engineers

Format

Requirements for the subject matter to be covered in the seminar sessions were outlined in advance by NCEL to assure that each participant clearly understood the purpose of the seminar. Also, the state-of-technology and technological deficiencies within each presenter's specialty were identified. The 2-day seminar was organized into two major parts. The first part was comprised of 11 individual sessions, eight long and three shorter sessions, covering the general state-of-technology for ocean platforms. Each of the eight longer presentations was made by a recognized expert, and each was approximately 1 hour long followed by a 15-minute discussion period. In the shorter sessions, the state-of-technology in mooring analysis and cable dynamics was presented by three Navy experts.

The second major part occurred during the afternoon of the second day when a workshop was conducted to identify technology deficiencies in ocean platforms for Navy TACTS range applications. Discussion among participants and attendees was encouraged in the workshop to establish pertinent research topics relating to these technology deficiencies.

Others attending the seminar were from within the NAVFAC ocean engineering community. This group of individuals was characterized primarily by research program managers, facilities program managers, research engineers, and design engineers (see the Appendix). The largest groups were the engineers who will provide the required design technology through the research program and the engineers who are responsible for design of Navy ocean platforms.

Presentations

First, the audience and the invited experts were introduced to the Navy's needs and requirements for TACTS platforms and to NCEL's development program requirements to support these platforms. The session schedule for the seminar presentations was as follows:

SEMINAR SCHEDULE

<u>TOPIC</u>	<u>SPEAKER</u>
Welcome	Mr. Robert Cordy
Navy Needs	Mr. Robert Peloquin
Tactical Air Combat Training	
Range Offshore Platforms	Dr. Shun Ling
Platform Requirements	Mr. David Shields
Technical Papers	
Environmental Specification	Dr. C. Linwood Vincent
Environmental Forces	Dr. Robert Hudspeth
Fixed Platforms and Guyed Towers	Dr. Lyle Finn
Semisubmersible and Tension Leg	
Platforms	Dr. J. Randolph Paulling
Discus and Spar Buoys	Mr. Henri Berteaux
NCEL Mooring Analysis	Mr. Paul Palo*
Recent Developments in Cable Dynamics . . .	Dr. Richard Skop and Dr. Owen Griffin*
Mooring Design, Deployment	
and Operation	Mr. William Rainnie
Full Scale Measurements, Model Test and	
the Prediction of Dynamic Response . .	Dr. J. Kim Vandiver
Extreme Statistics, Risk and	
Reliability	Dr. Leon Borgman
Workshop for Research and	
Development Needs for	
Ocean Platforms	Mr. David Shields

Because of the short time frame of the seminar, selection of the various topics and their material content for presentation during the seminar was carefully considered. Sessions which dealt with specific disciplines (e.g., environmental specifications, environmental forces,

*Short sessions.

extreme statistics, risk, and reliability) were presented at a fairly detailed level. Other sessions that covered topics which were composed of many specialized disciplines (e.g., fixed and guyed towers, semisubmersibles and tension leg platforms, and discus and spar buoys) had to be limited to a more general level of presentation because of the time limitations. The inequities in the detail level of the seminar sessions were recognized during the planning stage, but the time frame available made the inequities unavoidable.

The technical sessions opened with the environmental specifications and environmental forces as they are responsible for the description of the loads on surface ocean platforms. Each of the three sessions that followed, covering the generic ocean platforms, was organized to cover two similar platform classes (e.g., fixed and guyed towers, semisubmersibles and tension leg platforms, discus and spar buoys). The remaining sessions covered supporting technology required in design of ocean platforms (e.g., mooring design, deployment, and operation; full-scale measurements, model tests, and prediction of dynamic response; and extreme statistics, risk, and reliability). The shorter sessions dealt with NCEL mooring analysis capability and NRL's recent developments in cable dynamics. Eight of the papers presented are provided following the Appendix of this report.

CONCLUSIONS

The seminar satisfied its objective to define the present state-of-technology in ocean platforms and to identify research topics for ocean platforms. The workshop discussion was essentially a "brainstorming" session among the experts and attendees, with much stimulating dialogue, which provided Navy input for the post-seminar research recommendations given by the invited experts. The following four principal research areas were identified:

- Environmental specification
- Environmental forces
- Platform hydrodynamics
- Platform reliability analysis

The seminar summaries by the participants follow the seminar papers and may be consulted for details of the specific topics in each of these research areas. These recommendations provided the required input for the NCEL development plan for design and development of the TACTS ranges.

ACKNOWLEDGMENT

NCEL gratefully acknowledges the cooperation and enthusiasm displayed by the invited experts and their interests in Navy problems. The papers, presentations, and summaries they delivered are of a unique nature and have been of great benefit to this NAVFAC-sponsored program.

Table 1. Proposed Ranges and Platforms

Class of Problem	Range/Service	Proposed Platform	Water Depth (ft)	MILCON Fiscal Year
Shallow Water	Charleston/Navy	Caisson/Mat Steel Jacket Semisubmersible	60,66,108,132,150 120 250	86
	Key West/Navy	Caisson/Mat Buoy Semisubmersible	54 54,75,78 108	87
	Key West/Air Force	Caisson/Mat Buoy Semisubmersible	36,72 45,60,66 2 at 96	87
Deep Water	Southern California/Navy	Unknown	3 at 3600	88
	Kitty Hawk Expansion/Navy	Unknown	150;4800;5700; 5800; 2 at 6000	89

Table 2. Types of Platforms Required for TACTS Ranges

Type of Ocean Platform	No. Required
Steel Jacket	1
Caisson/Mat	8
Buoy	6
Semisubmersible	4
Unknown	9
Total	28

Appendix

OCEAN PLATFORMS SEMINAR PARTICIPANTS

Mr. Henri O. Berteaux
Research Specialist and
Instructor M.I.T./W.H.O.I.
Woods Hole Oceanographic Institution
Woods Hole, MA 02543

LCDR Arnold E. Bertsche, CEC
Assistant Program Manager
Naval Civil Engineering Laboratory
Program Manager's Office
Offshore Facilities
Port Hueneme, CA 93043

Dr. Leon E. Borgman
Professor of Geology and Statistics
University of Wyoming
Statistics Department
P.O. Box 3332
University Station
Laramie, WY 82071

Mr. Robert N. Cordy
Department Head
Naval Civil Engineering Laboratory
Ocean Engineering Department
Port Hueneme, CA 93043

Mr. James V. Cox
Research Structural Engineer
Naval Civil Engineering Laboratory
Civil Engineering Department
Structures Division
Port Hueneme, CA 93043

Mr. Robert V. Day
Program Manager
Naval Air Systems Command
Range Instrumentation Division
Jefferson Plaza II, Room 730
Washington, DC 20361

Mr. Jerome M. Dummer, Jr.
Civil Engineer
Naval Civil Engineering Laboratory
Ocean Engineering Department
Ocean Structures Division
Port Hueneme, CA 93043

Dr. Lyle D. Finn
Senior Research Associate
Exxon Production Research
P.O Box 2189
Houston, TX 77001

Dr. Owen M. Griffin
Mechanical Engineer
Naval Research Laboratory
Marine Technology Division
Code 5841
Washington, DC 20375

Mr. Herb G. Herrmann
Assistant Director of Engineering
Naval Facilities Engineering Command
Ocean Facilities Program Office
200 Stovall Street
Alexandria, VA 22332

Dr. Robert T. Hudspeth
Professor, Ocean Engineering Program
Oregon State University
Department of Civil Engineering
Corvallis, OR 97330

Dr. Shun Ling
Director, Engineering Analysis
Division
Naval Facilities Engineering Command
Chesapeake Division
Ocean Engineering and Construction
Project Office
Washington Navy Yard
Washington, DC 20374

Dr. William J. Nordell
Director, Ocean Structures Division
Naval Civil Engineering Laboratory
Ocean Engineering Department
Port Hueneme, CA 93043

Mr. Thomas J. O'Boyle
Civil Engineer
Naval Facilities Engineering Command
Chesapeake Division
Ocean Engineering and Construction
Project Office
Washington Navy Yard
Washington, DC 20374

Mr. Paul A. Palo
Mechanical Engineer
Naval Civil Engineering Laboratory
Ocean Engineering Department
Ocean Structures Division
Port Hueneme, CA 93043

Dr. J. Randolph Paulling, Jr.
Professor of Naval Architecture
University of California at Berkeley
Department of Naval Architecture and
Offshore Engineering
Berkeley, CA 94720

Mr. Robert A. Peloquin
Program Director
Naval Facilities Engineering Command
Ocean Facilities RDT&E
200 Stovall Street
Alexandria, VA 22332

Mr. William O. Rainnie, Jr.
Chief, Engineering Division
National Oceanic and Atmospheric
Administration
National Weather Service
NOAA Data Buoy Center
NSTL Station, MS 39529

Mr. David R. Shields
Civil Engineer
Naval Civil Engineering Laboratory
Ocean Engineering Department
Ocean Structures Division
Port Hueneme, CA 93043

Dr. Emil Simiu
Structural Research Engineer
National Bureau of Standards
Center of Building Technology
Washington, DC 20234

Dr. Richard A. Skop
Head, Fluid Dynamics
Naval Research Laboratory
Marine Technology Division
Code 5840
Washington, DC 20375

Mr. Edmund Spencer
Assistant Department Head
Naval Facilities Engineering Command
Chesapeake Division
Ocean Engineering and Construction
Project Office
Washington Navy Yard
Washington, DC 20374

Dr. John Kim Vandiver
Associate Professor of Ocean
Engineering
Massachusetts Institute of
Technology
Department of Ocean Engineering
Room 5-222
Cambridge, MA 02139

Dr. Charles Linwood Vincent
Chief, Coastal Oceanography Branch
Coastal Engineering Research Center
U.S. Army Corps of Engineers
Kingman Building
Fort Belvoir, VA 22060

Mr. Randal L. Wendt
Civil Engineer
Naval Civil Engineering Laboratory
Ocean Engineering Department
Ocean Structures Division
Port Hueneme, CA 93043

SEMINAR PRESENTATIONS

NCEL OCEAN PLATFORMS SEMINAR

ENVIRONMENTAL PREDICTION FOR OFFSHORE PLATFORM DESIGN

Charles L. Vincent
Coastal Engineering Research Center
Kingman Building
Fort Belvoir, VA 22060

INTRODUCTION

Design of platforms emplaced in shallow to deep seas requires specification of the forces expected to act on the platform during the lifetime of its proposed deployment. In practice this requires specification of the principal sources of hydrodynamic forces on the structure (short period wind waves, tides, currents and so forth) on a phenomena by phenomena basis with consideration of the interaction of the phenomena as necessary or practical. This paper provides a discussion of the capability to predict various of these phenomena with currently available techniques.

This paper will treat the prediction of winds, wind waves, water levels and currents in depths generally typical of continental shelves but outside of the surf zone at the beach. Since the topics addressed encompass a wide range of problems and techniques it is clear that so short a paper cannot address any of the areas in the fullness desired. The objective will be to present an overview of techniques available and relative errors obtained. The listing of techniques is by no means exhaustive; mention of any technique does not imply its endorsement nor does failure to mention a model imply any criticism.

The paper is organized as follows. A discussion of modelling and design scenarios will be given to illustrate typical situations encountered. Methods for estimating winds will then be addressed followed by a description of wind wave modelling. The modelling of water levels (unrelated to wind waves) and currents will be presented. The final section describes typical difficulties in applying model results to design problems.

DESIGN SCENARIOS

Models of the phenomena discussed in this paper are normally used in one of the following modes.

Forecast - the phenomena is predicted into the future in a real-time simulation of the forcing variables and phenomena.

Hindcast - the phenomena is simulated between two points in time based on a historical sequence of information about the forcing variables.

Design Synthesis - the phenomena is simulated for a specified event which has itself been hypothesized or synthesized from the statistics of the forcing variables.

The forecast mode is difficult because the forcing processes are themselves unknown. In the hindcast mode, the results of the model computation can be excellent if the details about the forcing process are well known and less than adequate if the forcing process is poorly known, irrespective of the quality of the model. In the design synthesis, the results are dependent on the quality of the model and the applicability of the design event selected.

Users of model results must recognize the effect of time scales in modelling. Simplistically, time scales of the processes can be divided into four scales. There are climatological scales in which interest is in the variation in the statistics of the phenomena over years to decades. There is a seasonal time scale in which the phenomena change on a month to month basis. On a synoptical time scale the phenomena may change on a day to day basis. At the meso-scale the changes may be hourly. Time scales exist below the meso-scale as well.

To each time scale there is accordingly a typical space scale. For wind waves, the statistics of the wave field may be significantly effected by the passage of a squall line within the context of a larger storm system moving across the region, i.e., on a meso-scale. The passage of the larger scale storm produces a variation in wave characteristics over several days, i.e., a synoptic event. There may be seasonal and yearly variation in the wave statistics as well. Tides however are fairly predictable based on subcycles of a basic nineteen year progression. The water level, if the water is shallow however, can be substantially altered by a severe storm tide which occurs on top of the normal tide. Any design problem should specify which time and space scales are included in the modelling and an assessment of the probable errors due to neglect of longer and shorter time scales is always in order. Most of the models described here can be driven at a meso- or synoptic time scale. However, there is rarely sufficient information to drive the models over the open ocean for meso-scale events. The models can be run for longer periods to synthesize the seasonal and climatological time scales if sufficient forcing data is available.

One final consideration is the degree to which the phenomena analyzed is a local effect. On continental shelves open to wide expanse of ocean, events occurring some distance away can effect the local area. Wind waves are particularly dispersive, traveling thousands of miles from their source. An assessment should always be made to assure that a design scenario which is primarily local does not ignore the possibility of an extreme event happening further away that could significantly effect a design value.

WINDFIELD PREDICTION

Winds in addition to exerting forces directly on a surface piercing platform are responsible for generation of wind waves, currents and adjustments to water levels. For many of the design parameters of interest to the

seminar the wind is a crucial forcing parameter which must be accurately predicted if the modelling of the other parameters is to have any reasonable hope of yielding realistic answers. It is crucial that poor estimates of winds not be combined with inadequate models of wind forced phenomena because it is unlikely that random errors and biases will be cancelled; instead it is possible that they may be significantly increased because of the entry of windspeed into the other models in a nonlinear fashion. It is essential therefore that the winds used have both minimum bias and random error.

The modelling of wind fields can be most difficult. In the open ocean case the problem is simplified by the absence of topographic features but complicated by the large area to be modelled often with low resolution (time and space) input information. Close to coasts topographic influences can be significant and meso-scale phenomena important. A further complication is that the primary information desired out of the windfield is ultimately some measure of the wind stress. Over the ocean the wind field, especially wind-stress, becomes dependent not only of the large scale pressure gradients but the local thermal and roughness characteristics of the sea surface.

The most sophisticated models for estimating windfields are the three dimensional global and hemispheric meteorological models run by the U.S. and other weather services and the U.S. Navy. These models are primitive equation models that are normally run in a forecast mode. In general they are too expensive to run for selected design cases. Scientists (1) are now beginning to apply these for smaller, meso-scale problems near coasts. Although they offer great promise, their complexity, expense and input data requirements make them, at this time, too difficult to use.

The most often used methods for estimating winds is to adopt a geostrophic wind model using surface pressure fields coupled with empirical relations between geostrophic and surface winds and modified by whatever wind observations are available. Used by a skilled meteorologist or engineer this methodology can produce very reasonable results. Recently the Corps of Engineers (2) extended and computerized this methodology to produce an oceanic wind model for wave hindcasts. This wind model is based on modifications to the geostrophic balance induced by the curvature of the pressure field, time rate of change of the pressure field, and use of a boundary layer model dependent upon thermal characteristics of the atmosphere and ocean to convert the "geostrophic" wind into a "surface" (in this case 19m level) wind. This model was used to create winds for every six hours for twenty years over the northern Atlantic Ocean. Windfields for the northern Pacific are currently being constructed. After the winds are constructed the winds are checked against ships observations and obvious discrepancies flagged for further study. Finally the observed ships' winds have been corrected for bias and blended into the data set. (In the Atlantic hindcasts over 7 million were used.) The resulting wind field is then largely based on a best estimate from the pressure and temperature fields as modified by observations available. The observations influence on the final wind speed estimate is dependent upon the number of observations in an area. The resulting windfields are expected to be typical of synoptic time scale events.

The quality of the hindcast winds have been examined in great detail (2). In comparison to the ships observations (corrected for bias) prior to their inclusion in the final windfields the bias in wind speed is between -0.5 and -1.3 m/sec while the root mean square error is between 2 and 3 m/sec over a range up to 30 m/sec. The bias in direction ranges between $\pm 5^\circ$. The root mean square error in direction decreased from 40° at a wind speed of 5 m/sec to about 20° at 25 m/sec. At low wind speeds the windfield is strongly influenced by small scale events that do not appear on weather charts; hence errors in direction and speed tend to be proportionately higher. Comparison of the wind speed data to wind speed measurements at buoys or other stations typically yield biases of order ± 1.5 m/sec and root mean square (RMS) errors of from 2 to 4 m/sec. When the nature of the measurements (typically 1 to 5 minute winds), the nature of the wind estimates (deduced from a quasi-equilibrium pressure assumption), and the fact that the wind model grid and observations locations essentially never coincide are considered, the bias and degree of random error appears minimal. It is concluded therefore that with a moderate level of effort reasonably accurate wind fields (± 3 m/sec RMS) can be obtained for synoptic events if adequate temperature and pressure data are available. It is of course possible to mis-hindcast a storm with much greater error if the storm is poorly specified. The question of whether the increased effort is worth the trouble is shown in Figure 1 where Corps wind estimates and a less sophisticated model are compared to observations at Sable Island for high wind cases over the same period.

Models such as those described above are adequate for midlatitude, synoptic events. They are not adequate in the tropics where the Coriolis force is weak or in tropical storms, and hurricanes. In the latter two cases parameterized models of the windfield are used with varying degrees of success. These models greatly simplify the windfield. The degree of success obtained is dependent upon how well the storms characteristics are known.

In summary, although the atmospheric processes that cause winds are difficult to predict, relatively good approximations for most purposes can be obtained by relatively simple methods. It is important however not to ignore principal variables such as temperature which effects on the boundary layer or curvature effects in pressure fields. Likewise it is important to recognize whether a proposed technique is appropriate to the region where it is to be applied.

PREDICTION OF WIND WAVES

The prediction of short period (1 to 30 second) wind waves for oceanic regions is normally performed using numerical models that simulate the evolution of the directional spectrum of these waves. This largely supersedes the use of nomograms developed just after World War II unless a small area is treated. These models simulate wave propagation using finite difference or ray methods and compute the evolution of the spectrum based on a variety of source and sink mechanisms. Among these are energy input through various mechanisms directly from the wind, transfers of energy within the wave field by nonlinear wave processes, dissipation due to turbulence and breaking, and, for shallow water models, dissipation through interaction with a bottom boundary layer. On a fast, large core computer the solution of the equations required

to simulate the wave growth on an oceanic scale for one day can take as little as a few seconds, even though the process is quite complex. Typically it takes far longer and requires more funds to generate the input wind data for the model than to do the actual wave computations.

In the deep water case, the ability to predict waves appears to have evolved further than agreement on the processes responsible. The reason for this apparent contradiction lies in the complexity of the processes and the large time and space scales over which these processes occur. Presently there are two major schools of thought. The first in historical context holds that the wave growth is predominantly due to the direct input of wave energy from the air to each wave component. Because early expression for this process did not appear to satisfactorily explain the patterns and growth rates of the wind waves an alternate theory was proposed. This theory holds that the wind excites short to medium length waves which through non-linearities in the wave motion generate longer waves with the effect that the spectrum grows to longer periods and higher energy. The theoretical predictions of this theory appears in reasonable agreement with observations, but it is not universally accepted. A review of the types of wave models and a fuller discussion of the problems is given in (3).

Wave models can be divided into the two classes outlined above which will be termed direct input and nonlinear models respectively. Within each class of models there is a diversity of numerical schemes and specific forms of particular source terms used. The net effect is to produce a wide variety of nearly equivalent to radically different models, all of which purport to predict the same phenomena reasonably accurately. In (3) it is shown that one major example of the direct input models does not predict growth with fetch, as presently understood, very well but does appear to simulate growth with time reasonably well. The recent nonlinear models could be shown to produce both reasonably well. Consequently there has been more of a trend in recent years toward practical models that are of the nonlinear type. However, wave research still continues.

One essential problem that remains is the selection of fetch and duration growth curves by which to judge wave model performance. There is reasonable agreement on the fetch curve, though not universal. There is less agreement on the duration curve because of a basic lack of information. Most modellers adopt a standard shape for the wind sea in simple generation cases that is given by the JONSWAP (4) shape. However an alternate formulation has been provided by Toba (5) which in practical sense does not differ greatly from the JONSWAP shape although its theoretical basis and equation is quite different. The basic growth curves are shown in Figure 2.

In finite depth water there is much less known than in the deep water case. In addition to the addition of bottom boundary layer effects there is considerable evidence that spectral shape is substantially different. Recent research at CERC, the University of Hamburg and The Royal Dutch Meteorological Office just completed has proposed a form for the depth dependent wind sea spectrum (Figure 3). This is in the process of being incorporated into new numerical models at these institutions. As reported in (6), the situation

in shallow water modelling is as confused as the deep water case because all of the deep water controversies extend to shallow water plus many new ones are added. Again there are several models that have widely differing source terms that perform with the same degree of error.

At this point it is desirable to consider the degree of accuracy that a wave prediction scheme for deep water might have. The model reported in (7) will be used as an illustration. Testing of a wave model is difficult because wave measurements have only been sporadically made. For an oceanic model there is often little data available for any given time period. Often there is only ship observations, which tend to be somewhat subjective. In (8) comparisons to ships observations and a selection of measurements (some back as far as 1961) indicate the performance of the meteorological and wave model combination.

In the case of ships observations data from one Marsden square were compared to the computed value at a grid point within the square for a twenty year period. For significant height the computed statistics agree well with the observed statistics based on 44,000 records, Figure 4. The means are within 0.04m and the extremes agreed within 1m. Thus, the combination appears able to predict the general statistics of waves in a region, based on the data available.

The study also compared the model results to instrumented observations of a series of storms and a few selected months. The mean significant wave height in these events ranged from 1.1 to 6.4m. The differences between the computed and measured means ranged from -.9 to 1.9 m and the mean absolute differences (absolute difference between time paired computed and observed values, averaged over an event) ranged from .5 to 2.7 m corresponding in general to an error of 15 to 25% for higher wave conditions. Part of the error is contributed by differences in location between the observation site and the hindcast grid point (typically 50 to 100 miles). Further, the plots of the hindcasts and measured data typically indicate that the two data sets are slightly out of phase which amplifies the random error and bias. Overall the statistics of the storm look quite similar for both data sets. The phasing problem is a result of the discretization of the model, the differences between hindcast grid location and measurement site, and the interpolation of the windfield in the model. The results therefore indicate that the model results may be reasonably accurate for the storm, but that for any given event, exact representation is less precise. If precise modelling of an event, so that all time phasing is kept is desired, the modelling will require a higher grid resolution and time resolution. However, given the level of error in the windfield it is not clear that such an increase in resolution will result in better representation unless the windfield representation is improved.

Comparison of the model to field data described above emphasized comparisons of wave height. Additional parameters of interest are the peak frequency of the wind wave spectrum, spectral shape and wave direction. Almost no deep water directional data are available for comparison. Tests of an earlier version of the model discussed above indicated a RMS error

of about 1 second in the wave period corresponding to the peak frequency for wave conditions with a range of 4 to 10 sec. Comparisons of spectra are only reasonable if the wave height and peak frequency are in agreement between model and measurement. In these cases the results vary from quite excellent to mediocre, but with the modelled spectrum within the confidence bands of the observed spectrum.

In summary, the ability to predict on the open ocean appears to be with a random error of 15 to 25%. This is reasonable considering that the windspeed enters the wave growth relationships as a square and the random error in the winds are of the same order. The degree of success in application of a model to a region appears to relate to how well the meteorological event can be specified and how fine a resolution is used in the modelling exercise. There are still several significant controversies existing in both deep and shallow water wave modelling that need a much better understanding of wave mechanics for resolution. It should be noted that almost all major wave models ignore the effects of currents. In many areas this is acceptable but in other areas can be a major mistake. Use of wave models should be predicated upon demonstration that the model generates acceptable growth curves for fetch and duration as well as acceptable theoretical spectral shapes. Application of the model to prior studies with comparisons to observations is also desirable.

PREDICTION OF WATER LEVELS AND CURRENTS

Prediction of either water level or currents requires prediction of both; hence the two must be considered jointly. Variations in water levels and the development of currents can be generated by tidal forces, temperature and density gradients and wind forces. The importance of these effects in a particular design situation significantly influence the type of model selected. The hydrodynamics of the situations are fairly well understood with the exception of many phenomena related to turbulence. Problems typically arise as a result of the mixture of scales involved in a particular problem and normally arise as a result of neglect or simplification. Often the problem of most concern arises out of poor initial or boundary conditions particularly if the site is open to the entire ocean. If the problem is meteorologically driven the problem of adequate meteorological specification is once again significant.

Modelling of water level and currents is practiced in a large number of research institutions, forecast offices, and consulting firms. As a result of historical development, advancement of computer technology, site specific nature of some practical problems, diversity of processes modelled and ingenuity, a truly extraordinary number of computer codes have been developed to handle the prediction problem. For example the U.S. Army Corps of Engineers has no less than 7 numerical models used for storm surge computations. Each has its relative merits and it is unlikely that any will be discarded in the near future.

Since there are so many different models, it is not possible to treat even a small portion of the models in any detail. Models can be broken into categories based on a number of technical considerations. Most models are two dimensional (horizontal plane using vertically averaged velocities), but three dimensional solutions, which in most instances are more appropriate, are now becoming more widespread. For economic reasons quasi-three dimensional solutions consisting of a basic two dimensional (horizontal) solution coupled

with a local, parametric solution for the vertical are also being used. Models can be either time dependent or steady state. Solutions may be made in square, rectilinear, stretched or polygonal coordinates by finite difference and finite element solutions. The time integration scheme may be either implicit or explicit. The model will either be one or multilayered. Finally models may include or exclude various terms in the equations depending on what type of problem is being solved. Within any set of combinations of the above, individual models may differ on some of the fine points of numerical simulation techniques. Usually the use of any particular model is based on the physics of the problem proposed, the availability of adequate boundary and forcing data, and cost.

With the large number of computer codes and the variation in situations in which they may be applied, it is difficult to site specific meaningful level of accuracies. In the situations in which the author have seen such codes applied the results in water levels were generally within 15% and the current velocities within 30%. However, most of these applications have been near the coast and have involved models which were run with reasonably good forcing data. The models had normally undergone a calibration procedure as well. The degree to which any simulation in an arbitrary location will meet or surpass these values probably depends upon having data to calibrate the model before hand.

DISCUSSION

The prediction methods discussed appear to have the capability of predicting phenomena with random errors of the range of 10 to 30%. It should be clear that this random error is not equivalent to an accuracy of the same amount. Some simulations will be quite excellent others marginal. It is the author's opinion that if a model incorporating an appropriate set of physics is selected and applied with proper resolution and forcing information the results will tend to be more accurate than the 30% level above. However it is unlikely that when a model is applied to a realistic case that the accuracy will ever be much lower than 10% in the near future because the forcing information is inadequate. The difficulty in getting adequate forcing data should not be considered a license however for applying an inadequate model as a short cut. A good model will minimize any amplification of error in the forcing processes, a bad model will most likely increase the random error and amplify any bias. The errors rarely cancel out.

Selection of any model of the phenomena discussed should be predicated on an analysis of what information is needed and the tolerance with which the information can be applied. Some of the key questions that should be resolved are discussed below.

When a parameter is required for design, it is necessary to specify the time frame over which the parameter is to be applied. It is important to ascertain whether a climatological value is needed, or whether extreme values are required. It is particularly critical to make sure that sampling of parameter does span all likely situations. As an example, Hurricane Iwa

was the first significant hurricane to hit Hawaii in 23 years. If the meteorology had only been examined for the last 15-20 years hurricanes might have been ignored. Of course hurricanes in Hawaii are rare and for many purposes could be ignored. However if a platform had been installed for this year and its survival were essential, then hurricanes should be considered.

Very often generation of a wave or current climate is time consuming and expensive. It may be possible to back into an answer by specifying the level of a particular parameter for which the platform may be expected to perform. Then events that can conceivably produce that level are considered and the result expressed in terms of some parameter such as storm intensity. By canvassing weather records to see how often such an event may occur, the chance of it occurring can be approximated. This can be adequate for many purposes.

When a model must be selected, cost, timeframe, model characteristics and error must all be balanced. It is important to obtain an adequate treatment of the technical problem involved. This may not require using a model that contains every possible physical process involved. By assessment of the errors of a code against the errors inherent in the proposed simulation it may be possible to compensate for the uncertainty induced. The degree to which this is acceptable is the degree to which the results are conservative, the cost of the conservatism in design, and the importance of the parameter to the design. The choices made should be deliberate and based on an adequate analysis of the impacts.

In the situation where there are many possible choices of models and where the physics is somewhat unclear, selection of a model can be difficult. It is important that any model selected be able to reproduce recognized theoretical or empirical relations. It is highly desirable to have a model that has been both calibrated and verified especially at the site of interest. Ultimately when a model is used in any area where there is little data or under extreme events outside the region of calibration, its chance of success depends on how closely the model simulates the physical processes involved and therefore important that the model meet the theoretical/empirical qualifications than a calibration/verification test.

In almost all the phenomena discussed, the process of obtaining a prediction for application in design can be quite lengthy. This is especially true if the codes used are new to the user or used in an area where little information is available. Very often the largest costs involved in a study arise from the personnel time required to establish grids and develop input information. Often the actual numerical simulations and their interpretation are a small part of the cost of the study. It is recommended that agencies that foresee frequent need of such parameters in their design work develop information systems or obtain access to such systems that have existing data sets cataloged and available for use. Further it would be prudent to support or participate in joint efforts to develop the types of information that they need so that the information can be gathered before hand. The specific modelling then may become a simple exercise of refining the computations. It is important to stress however that use of data from various outside sources in a design situation must be tempered by detailed knowledge as to how the information was generated or collected.

The design engineer must temper the results from model studies based on an appreciation of the difficulty of the problem, the uncertainties in the input forcing information, and the error characteristics of the model. Since the information used in development of a design scenario ultimately comes from statistics of the phenomena used (whether quantitatively or qualitatively derived) it is necessary to realize that the statistics are from a sample of possible events. Hence recurrence intervals, means etc., have an associated error that represents the natural variability of the process and our inability to explicitly define every parameter. No matter how well a specific event can be modelled, that event is unlikely to occur again in precisely the same way. Thus model results must be interpreted in this wider context.

In summary, the prediction of environmental phenomena such as wind, waves, tides and currents can be achieved with reasonable accuracy, especially when the spatial, temporal and natural variability of the processes is considered. The evolution of prediction techniques continues as our understanding of the basic processes increases. The design engineer has a choice of techniques in many cases some of which are more accurate than others. The problem often reverts to one of selecting the model technique that is appropriate to the problem, is cost effective, and realistically accounts for the uncertainties in our knowledge of the forcing functions and the natural variability of geophysical systems.

References

1. Pielke, R.A., 1982, Mesoscale Atmospheric Circulations Related to the Coast - A Summary, in First International Conference on Meteorology and Air/Sea Interaction of the Coastal Zone, (preprints), American Meteorological Society, Boston, pp.154-161.
2. Resio, D.T., C.L. Vincent, and W.D. Corson, Objective Specification of Atlantic Ocean Wind Fields From Historical Data, WIS Report 4, U.S. Army Engineer Waterways Experiment Station, Vicksburg, MS, 50pp., 1982.
3. Resio, D.T. and C.L. Vincent, A Comparison of Various Numerical Wave Prediction Techniques, Offshore Technology Conference Houston, TX, Paper OTC 3642, pp.2471-2481, 1979.
4. Hasselmann, K. et al., Measurement of the Wind Wave Growth and Swell Decay During the Joint North Sea Wave Project (JONSWAP), Deutsches Hydrographisches Institute, Hamburg, West Germany, 1973.
5. Toba, Y., Local Balance in the Air-Sea Boundary Processes II, Partition of Windstress to Waves and Currents, Journal of the Oceanographic Society of Japan, V. 20, pp. 20-25, 1973.
6. Vincent, C.L., Shallow Water Wave Modelling, in First International Conference on Meteorology and Air/Sea Interaction of the Coastal Zone, (preprints), American Meteorological Society, Boston, pp. 87-95, 1982.
7. Resio, D.T., The Estimation of Wind Wave Generation in a Discrete Model, Journal of Physical Oceanography, v.11, pp.510-525, 1981.
8. Corson, W.D. and D.T. Resio, Comparisons of Hindcast and Measured Deep-Water Significant Wave Heights, WIS Report 3, U.S. Army Engineer Waterways Experiment Station, Vicksburg, MS., 41pp., 1981.

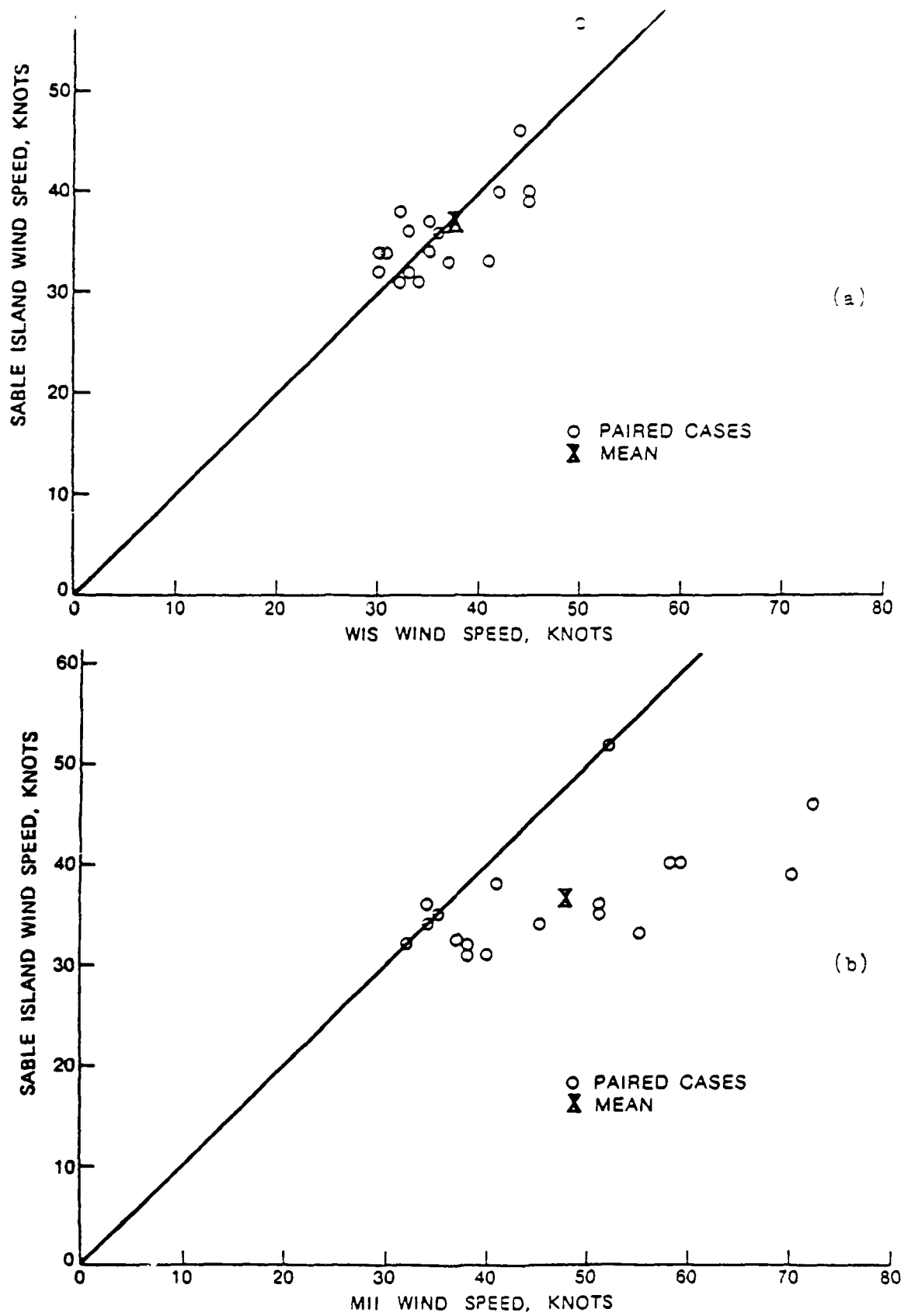


Figure 1. Comparison: wind model in (Ref.2) to observed winds at Sable Island in (a) versus comparison of predictions from a geostrophic model without planetary boundary layer module to same winds in (b) for high wind conditions.

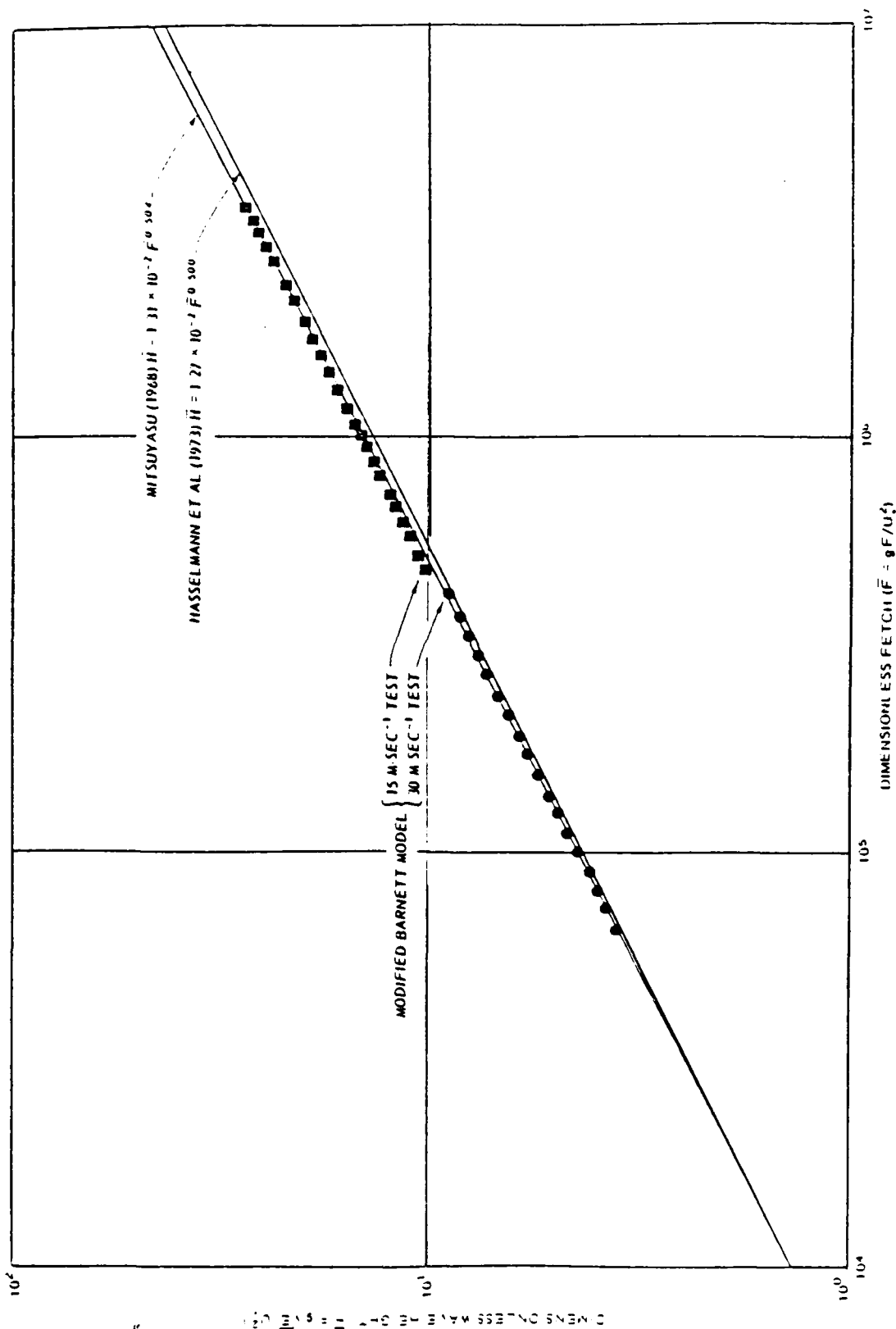


Figure 2A. Wave Growth with Fetch

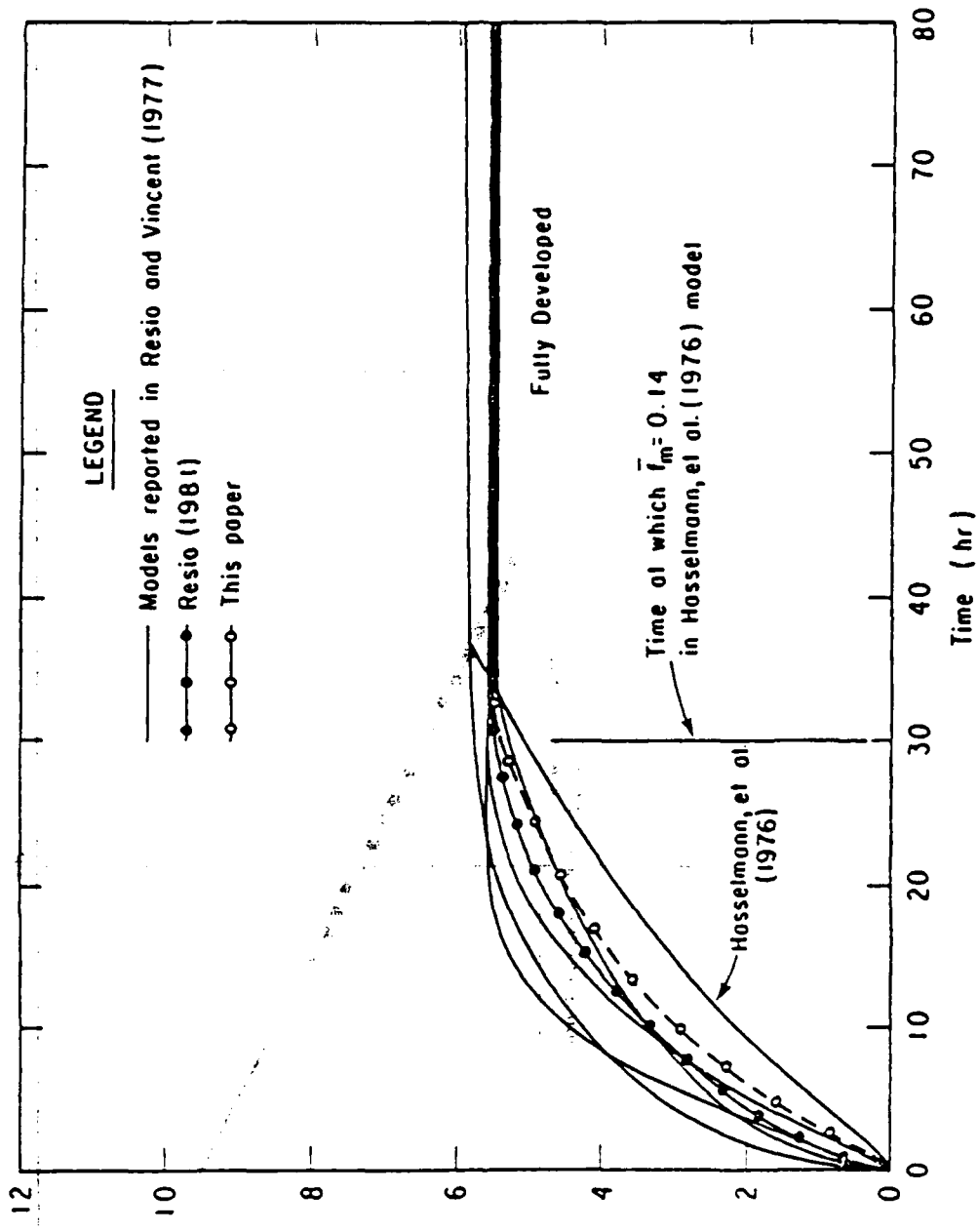
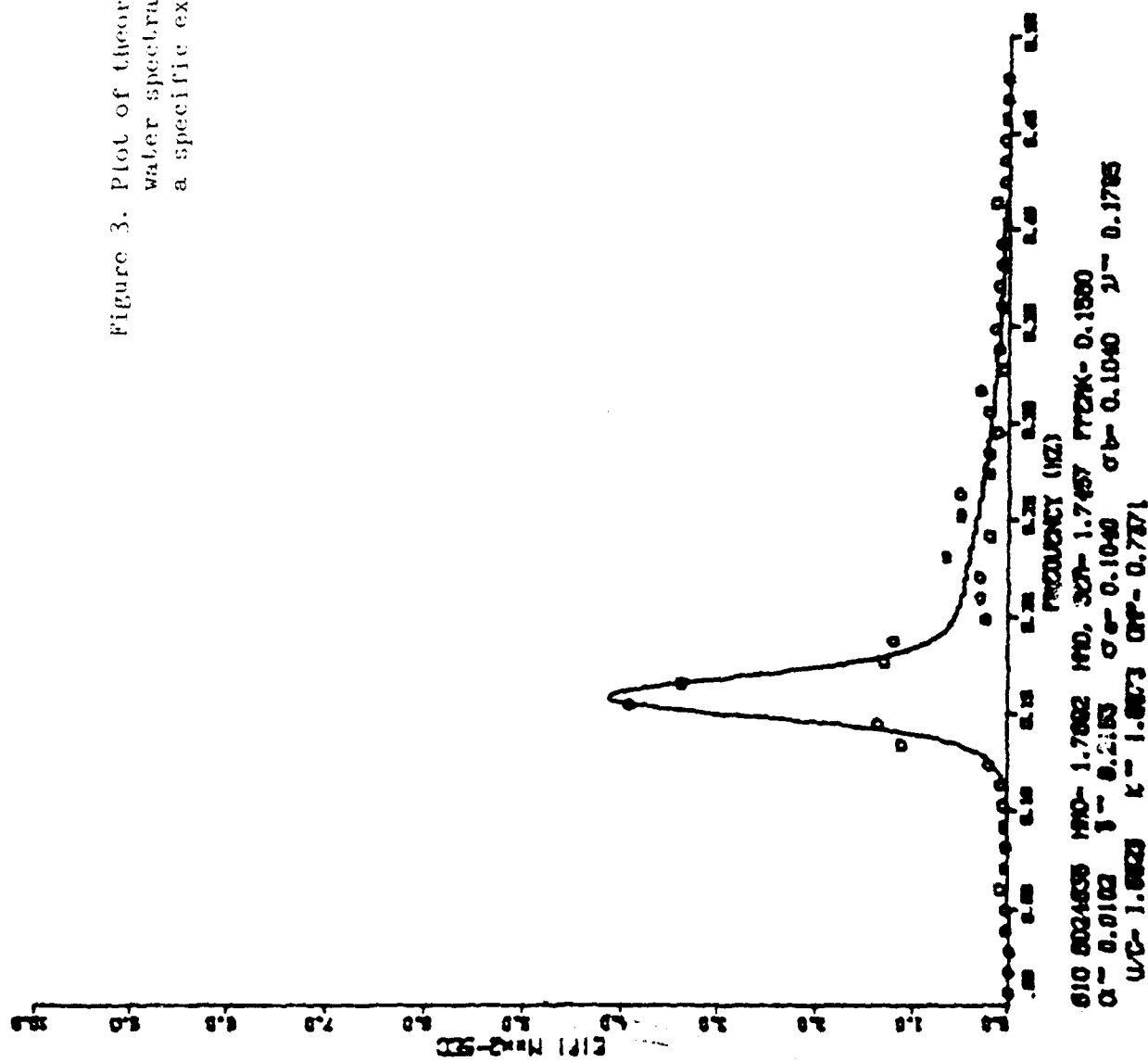


Figure 2B. Wave Growth With Duration

Figure 3. Plot of theoretical shallow water spectral shape fit for a specific example.



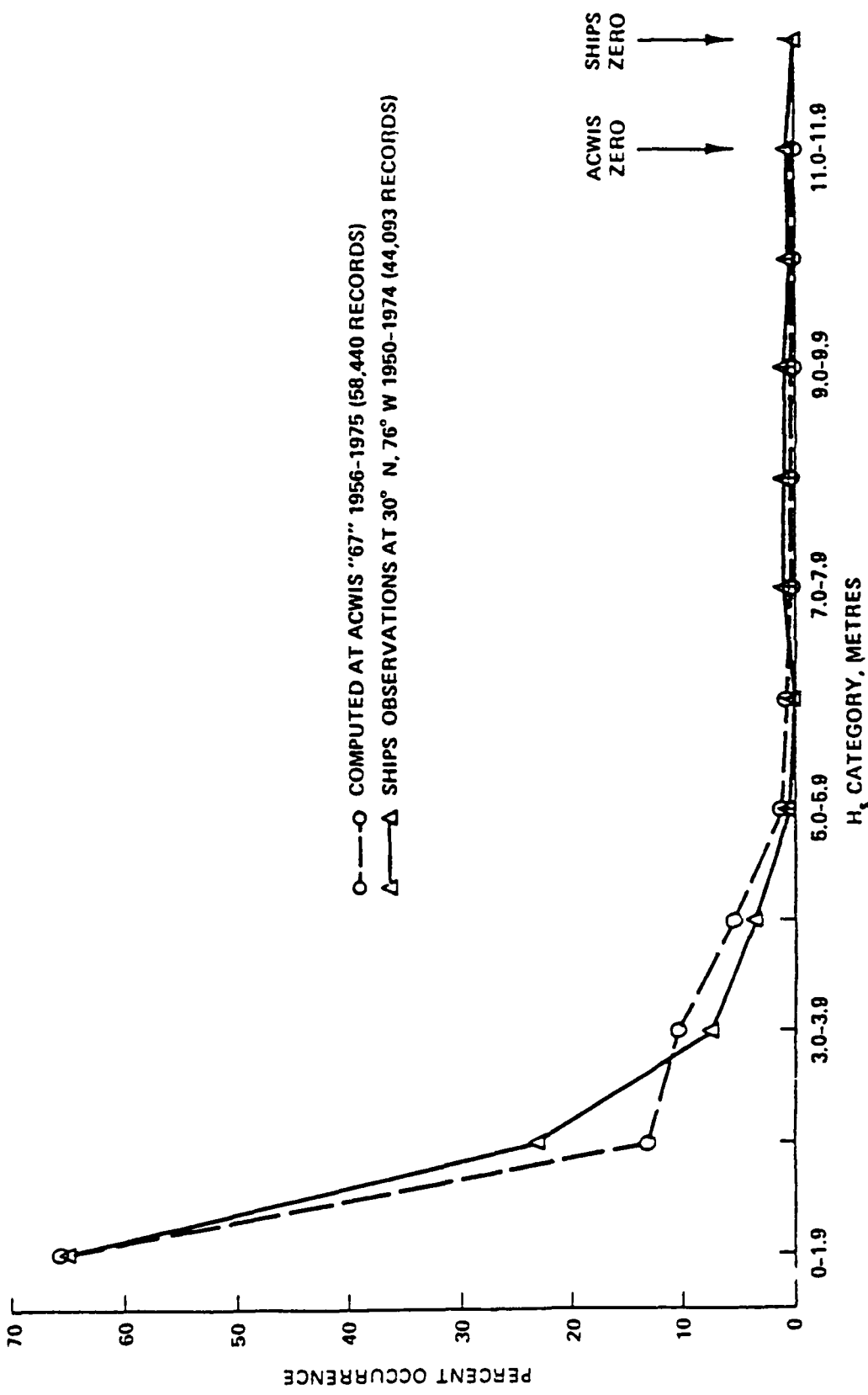


Figure 4. Plot of percent occurrence versus H_s for ships records and computed data. Notice both data sets "zero-out" (no waves recorded in the category or greater) at nearly the same category

ENVIRONMENTAL FORCES ON OCEAN PLATFORMS

by

Robert T. Hudspeth
Department of Civil Engineering
Ocean Engineering Program
Oregon State University
Corvallis, OR 97331

ABSTRACT

Methods for estimating environmental loadings are reviewed for jacket type fixed and compliant platforms; for guyed towers; for articulated towers; for tension leg platforms (TLP); and for submersible buoys. Emphasis is placed on the uncertainties that exist in the current methods and procedures used to estimate hydrodynamic pressure forces on both small members (Morison regime) and large displacement members (diffraction regime). Special attention is given in the application of the Morison equation to the effects of wake-interaction, of the eccentricity in water particle orbits, and of the condition of the data for selecting the force coefficients. In the applications of diffraction theory, special attention is given to the numerical evaluation of principal value integrals and to the advantages of the finite element method (FEM). In addition, the effects of interference and interaction between large and small members in complex structures are reviewed. Geotechnical, wind and ice loadings are also noted.

INTRODUCTION

The purpose of this review of environmental forces is to identify certain features in the state of the art methods used to estimate environmental loads which contain uncertainties that are deserving of further research by NCEL. An in-depth review of all features is not attempted here since several review papers of this nature have recently appeared. In particular, Leonard, et al. (1978) and Garrison (1982) have reviewed deterministic fluid forces while Sarpkaya and Isaacson (1981) have reviewed both deterministic and nondeterministic environmental loadings.

External loadings on offshore structures may be divided into two categories: 1) nonhydrodynamic and 2) hydrodynamic. In addition, hydrodynamic loadings may also be divided into two categories: 1) nonwave-induced and 2) wave-induced. The sources of these external loadings on offshore structures will first be described in these two categories.

NONHYDRODYNAMIC LOADING SOURCES

Two types of loads which are not transmitted by hydrodynamic fluid pressure are: 1) geotechnical forces and 2) surface forces.

Geotechnical Forces

Loads that are transmitted to a bottom-fixed structure by the motion of the benthos. Large vertical or lateral structural motions beneath the benthic interface may be caused by sources such as seismic events, internal waves, storm waves in shallow water, slope destabilization following extensive erosion or scour, and geothermal or other types of subsidence. In the case of seismic loads, it is usually the stiffer structures in relatively shallow water with relatively higher natural frequencies (>0.5 Hz) which are more susceptible to damage. For deeper water structures and/or platforms with smaller restraints to lateral motion, earthquake loads are usually of secondary interest. In a seismic analysis (quasi-static or dynamic) one must include the effects of both added mass and hydrodynamic radiation or viscous damping on the structural motions, as these two parameters significantly affect the structural mass and damping matrices such that lower natural frequencies are obtained. (Tanaka and Hudspeth, 1983).

Surface Forces

Loads that are applied to structural components on or above the ocean surface by loads from ice or wind. For fixed structures sized to resist hydrodynamic loads, wind loads will usually be of a secondary nature. For compliant platforms, however, the wind loading may lead to critical conditions either by wind heeling or by overstressing of the mooring lines. Additionally, with reduced wave effects on compliant structures, wind loads will be of increased importance in the design (Vickery, 1982). Loadings due to floating sea ice are severe and will usually govern the design of a surface structure if they are anticipated. In shallow water, the attachment of the platform restraint system to the benthos may be subjected to ice scour if thick ice or icebergs are present.

HYDRODYNAMIC LOADING SOURCES

These dynamic loads are due to pressure fluctuations normal to immersed surfaces and are caused by the relative motion between the fluid medium and the structural surfaces. Hydrodynamic loading sources may be divided into two categories: 1) nonwave-induced and 2) wave-induced.

Nonwave-Induced Hydrodynamic Loadings

Hydrodynamic pressure force loadings that are due to nonwave-induced currents and to fluid entrained spray. Current profiles must be described by both their temporal and spatial variations. In relatively deep water, rotational variations of current profiles over depth are common. In addition, complex interactions between currents and waves which may be either collinear or oblique result in hydrodynamic loadings with extremely complex spatial variations. These interactions are relatively weakly nonlinear in deeper water but may be significant for platforms in water less than 100 feet. The characteristic temporal and spatial scales which govern the temporal and spatial variations of real currents are further complicated by the relatively large number of physical variables which control these variations (Thomas, 1979). For example, horizontal spatial variations may be controlled by bathymetry while vertical spatial variations and temporal variations may be controlled by weather or tides. Currents may be classified as (Peregrine, 1976): 1) large scale; 2) coastal and tidal; and 3) wind generated. The temporal scales of the interactions between currents and waves are extremely broad and span the spectrum of frequencies from tidal periods to turbulent fluctuations.

Fluid entrained spray loadings occur at the air-sea interface. They are especially significant during intense storm conditions when a substantial increase in the barometric tide increases the mean sea level and exposes to spray loadings those elevated members that are not normally loaded hydrodynamically.

Wave-Induced Hydrodynamic Loadings

Hydrodynamic pressure forces that are due to tidal, surface gravity and internal wave propagation. Complex interactions between these different categories of waves and between complex currents result in dynamic loadings which cover a broad spectrum of excitation frequencies. Even simple approximations to these complex interactions which may be made in order to obtain numerical algorithms that are analytically tractable are frequently still too complex to apply to design methods. This may be readily observed by comparing existing standards and guidelines with recently published analytical treatments of these interactions (Peregrine, 1976 and Thomas, 1979).

DESCRIPTION OF HYDRODYNAMIC LOADS

There are two generally accepted methods for representing the maximum wave-induced loads which will occur during the lifetime of an offshore structure. These are referred to as the deterministic method and the probabilistic method. Both methods are based on a probabilistic analysis of the wave climate at the location of the structure; but in the case of the deterministic method the probability analysis is used only to specify a **design wave**. The wave-induced loads on the structure are then computed using some deterministic wave theory to define either the water particle kinematics for the Morison equation or the hydrodynamic pressures for diffraction analyses associated with the **design wave**. The probabilistic method, on the other hand, refers to a procedure in which the structure is subjected to a random wave system and a probability analysis of the resulting loads is carried out.

Due to the random nature of real ocean waves, it is necessary to consider the dynamic response of ocean structures to these stochastic wave forces in a probabilistic manner. A major distinction between static-deterministic design methods and dynamic-stochastic design methods is the possibility of dynamic amplification of the response of the structure in one of its natural modes. A deterministic dynamic analysis of the response to a single periodic wave would not demonstrate this dynamic amplification. Even a nonlinear periodic wave would not suffice since only the harmonics of the fundamental period would contribute to the structural response. In the stochastic analysis of a truly random sea, the ocean surface and its corresponding wave forces are synthesized from an infinite number of sinusoids of all frequencies with random phase angles.

The major assumptions of the stochastic methods for the description of waves are that the free surface fluctuations are linear and that the linear approximation of the ocean surface has some spectral representation which may be related directly to a Gaussian probability distribution. The amplitude of each sinusoid in the spectral representation is then uniquely related to the frequency of that sinusoid. Because the linear sea is assumed to represent a Gaussian process, the spectral representation of the sea yields not only the frequency dependence of the amplitudes; but it is also directly proportional to the only statistic required to construct the entire probability distribution of a zero-mean Gaussian process; viz., the variance. In the linear deterministic boundary value problem for surface gravity waves in an ocean of constant depth, the method of separation of variables yields a well-posed Sturm-Liouville problem with eigenfunction solutions and arbitrary multiplicative coefficients; viz., the wave amplitudes. Additional physical constraints must be applied in order to quantify the maximum wave height possible, but any other arbitrary value for a wave height which is

less than this maximum value is equally probable. The wave amplitude spectrum, therefore, quantifies the arbitrary multiplicative coefficients (i.e., the wave heights) for the Stieltjes integrals in the case of the nondeterministic wave problem in an analogous manner to the design wave specification in the case of the deterministic problem.

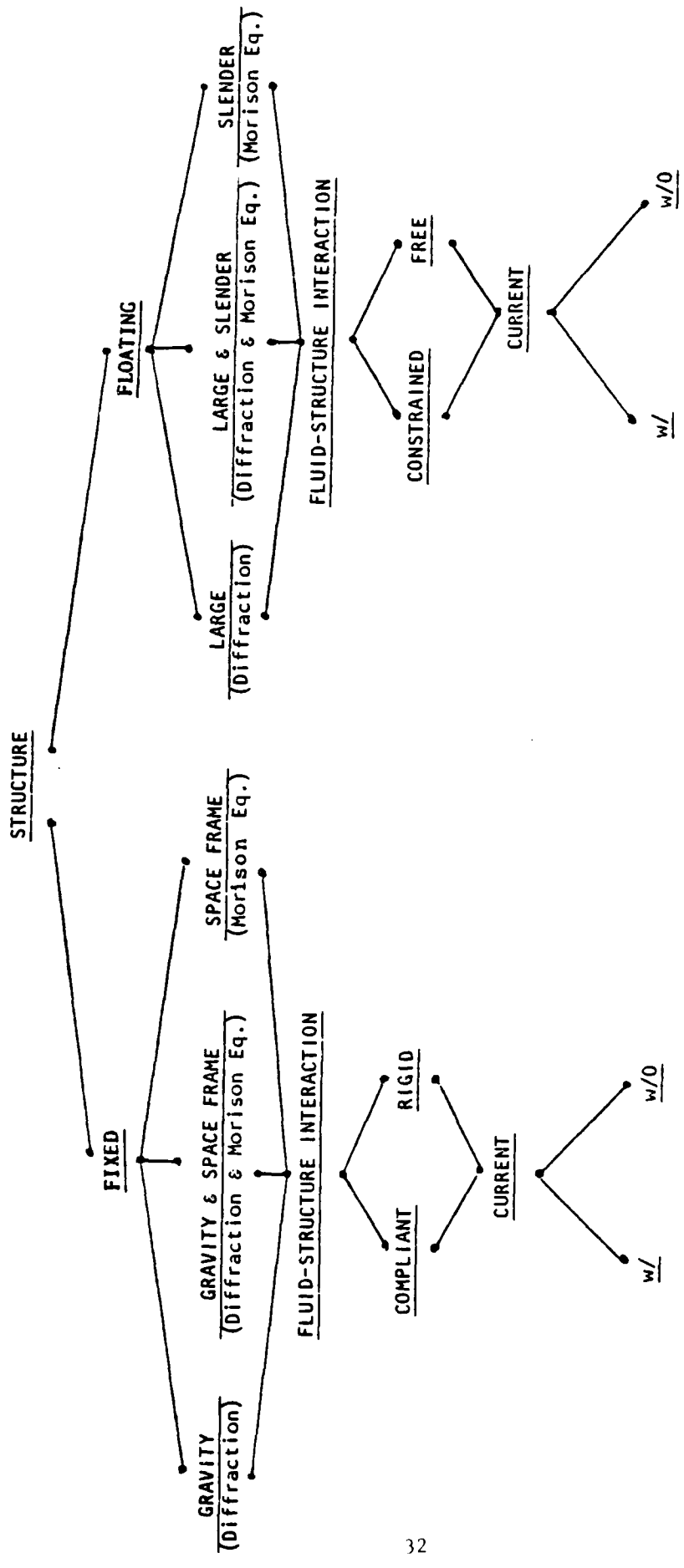
The primary reason for requiring dynamic analyses of a design by stochastic methods is to determine the possibility of a resonant response of the structure in one of its natural modes of vibration. In order to determine this response, it is necessary to synthesize the wave forcing function from an infinite sum of sinusoids whose arbitrary amplitudes must be specified by a spectral representation for a linear Gaussian sea. The effect of the stochastic wave forces on the dynamic response of ocean structures depends not only on the magnitude of this force spectrum but also on whether the force is determined by the Morison equation (for small members) or by the diffraction method (for large members).

DETERMINATION OF LOADS ACCORDING TO MEMBER SIZE

The first step in the computation of magnitudes of wave-induced forces on structures due to hydrodynamic pressures is the estimation of the effect of the structure on the wave field. The two extremes of the effect of this wave-structure interaction are: 1) the structure exhibits no sensible effect on the wave field and waves passing the structure remain essentially unmodified by the presence of the structure; or 2) the structure exhibits significant effects on the incident wave field and a new wave field may be observed radiating away from the structure. For a **fixed** structure, i.e., a structure rigidly connected to its foundation, the generation of this new wave field may be due to either **scattering** of the incident wave or due to dynamic motions of the structure which **radiate** waves away from the structure, much like a classical wavemaker. For **floating**, or **compliant** structures which are large compared to the incident wave length, both scattered and radiated waves may be observed.

Figure 1 illustrates these two extreme possibilities as well as the possibility of a complex structure which may simultaneously include both effects. Since there is at present no single **unified** wave force field theory for computing the entire spectrum of wave force possibilities between these two extremes, only the effects based on the two extreme member sizes will be reviewed. The first effect to be reviewed will be the **small body** or Froude-Kriloff theory in which the structure makes no sensible modification to the incident wave field. The second effect to be reviewed will be the **large body** or diffraction theory which will also include the wave radiation

Fig. 1 WAVE-STRUCTURE INTERACTION CLASSIFICATION



possibility for compliant or for semiconstrained floating bodies. Figure 2 illustrates the three methods used to estimate each of these two extreme loads.

Figure 3 compares both large and small vertical circular cylinders in deep and finite-depth water. Figures 4 and 5 summarize conditions required for the application of the Morison equation to vertical piles extending from the ocean bottom up through the still water level. The Morison equation applies if the pile diameter, D , is both less than 20% of the wave length, L , and less than the wave height, H . As the pile diameter becomes an appreciable fraction of the wave length, the wave is modified to the extent that a boundary value problem must be solved to account for the presence of the pile. Diffraction theory is used to solve for the reflected or scattered waves and for the radiated waves including both propagating and evanescent modes. The resulting pressure field from both the scattered and radiated waves are integrated over the submerged surface of the pile to quantify the unsteady force and moment.

Dimensional Analysis

Dimensional analysis is helpful in illuminating the parametric dependency of the two force calculation method. Assume that the pressure force on a member, F , depends upon the following variables:

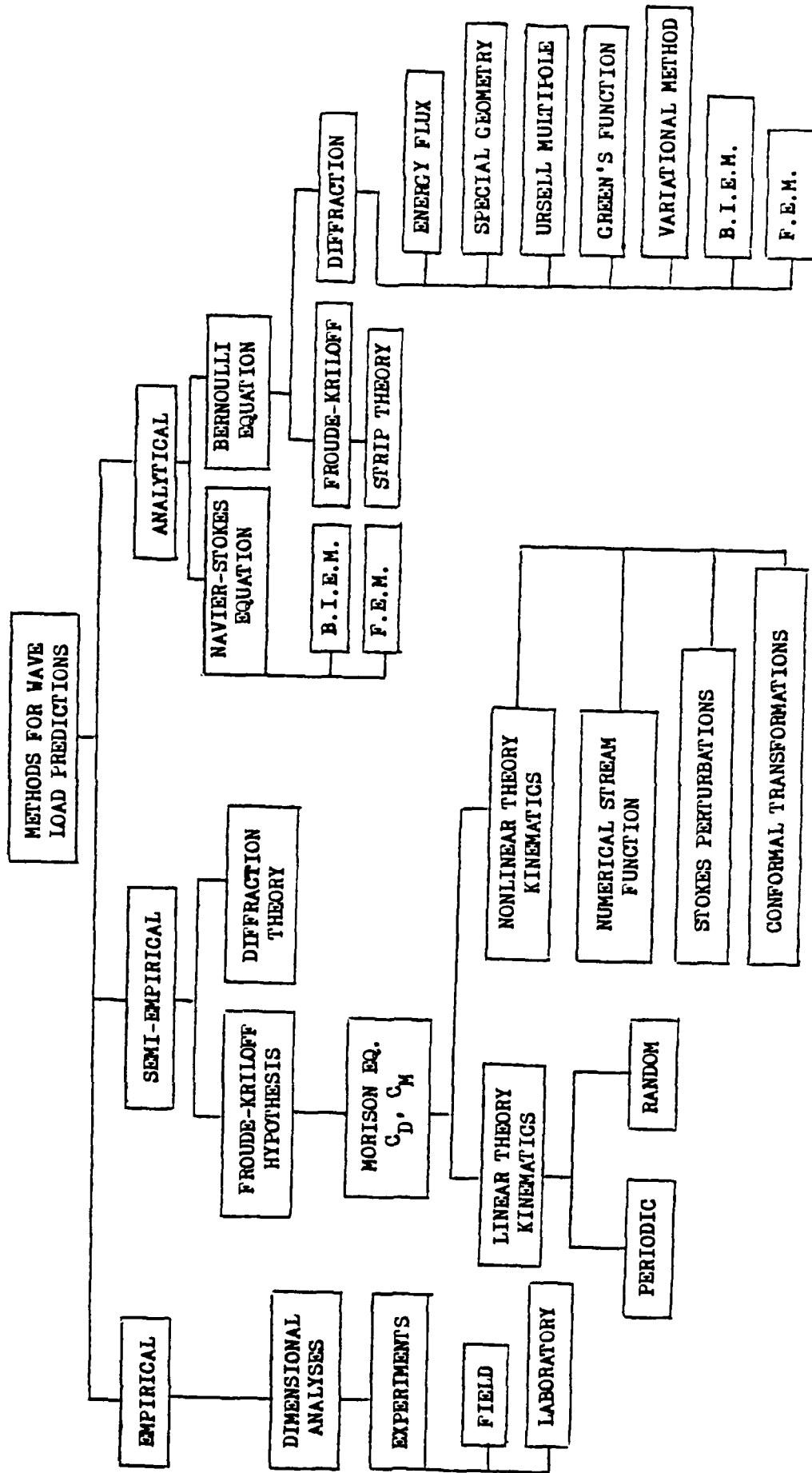
$$F = f_1 \{ h, H, L, T ; g; b; \epsilon; \rho, \mu \} \quad (1)$$

in which the **wave field** variables are: h = water depth, H = wave height, L = wave length, and T = wave period; the **structural** variables are: g = gravitational constant, b = linear dimension of the body, ϵ = surface roughness; and the **fluid** variables are: ρ = fluid density and μ = dynamic viscosity of the fluid. The Ursell parameter $\{U = \frac{H}{L} \left(\frac{L}{h}\right)^3\}$ [or Stokes parameter] which is a measure of both **amplitude** dispersion $[H/L]$ and **frequency** dispersion $(L/h)^3$ indicates that the parametric dependence upon wave period, T , need not be considered explicitly.

Choosing ρ , g and b as the repeating variables gives the following dimensionless wave force representation:

$$\frac{F}{\rho g b^3} = f_2 \left\{ \frac{h}{b}, \frac{H}{b}, \frac{L}{b}, T \left(\frac{g}{b} \right)^{1/2}, \frac{\mu}{\rho \sqrt{gb^3}}, \frac{\epsilon}{b} \right\} \quad (2)$$

FIG. 2 LOAD PREDICTOR METHODS FOR NON-BREAKING WAVES



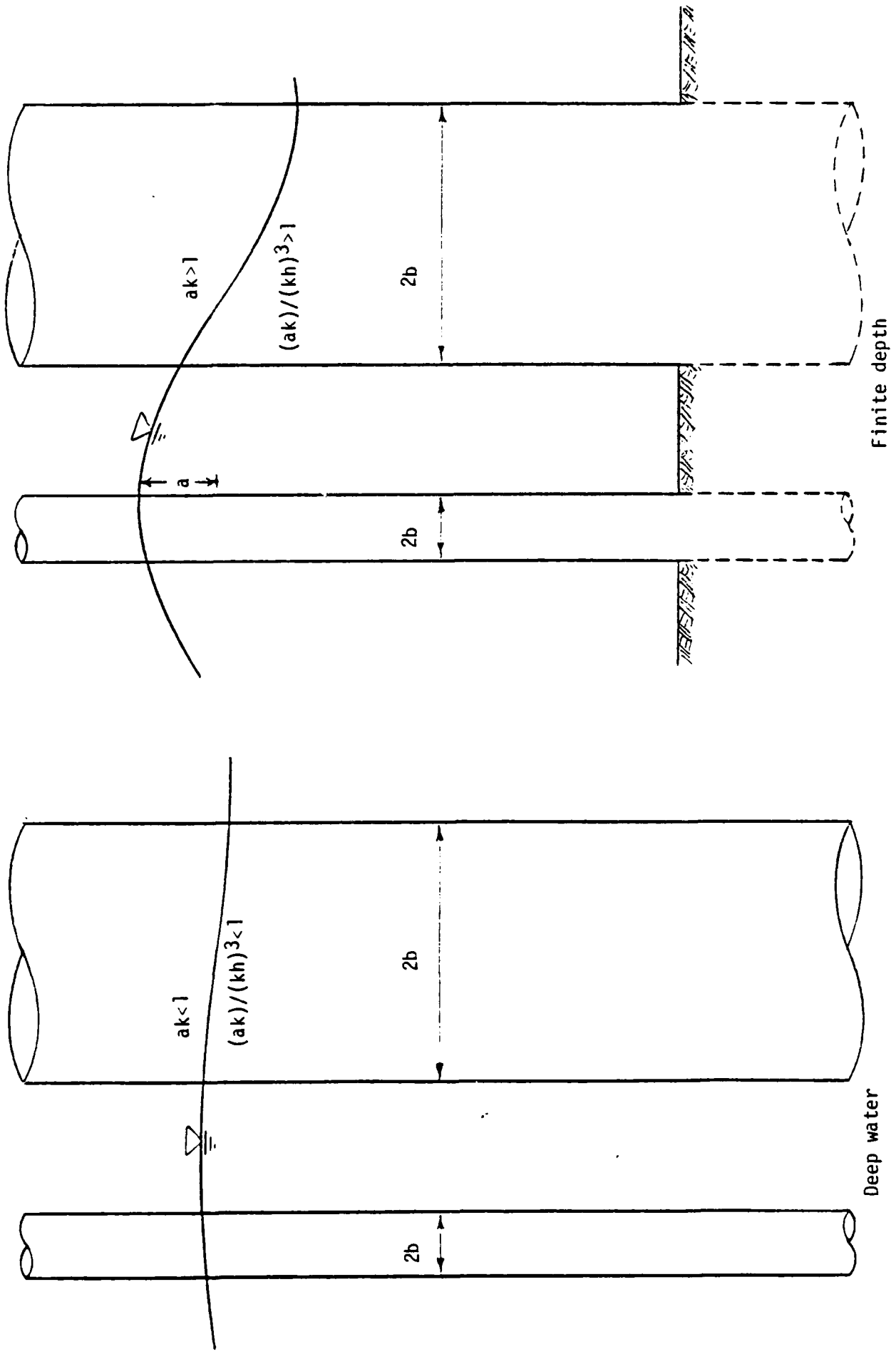


FIG. 3 COMPARISON BETWEEN LARGE AND SMALL MEMBER STRUCTURES IN DEEP AND FINITE-DEPTH WATER

FIG. 4 WAVE FORCE CALCULATION METHODS
FOR VERTICAL CYLINDER
(Sarpkaya and Isaacson, 1981)

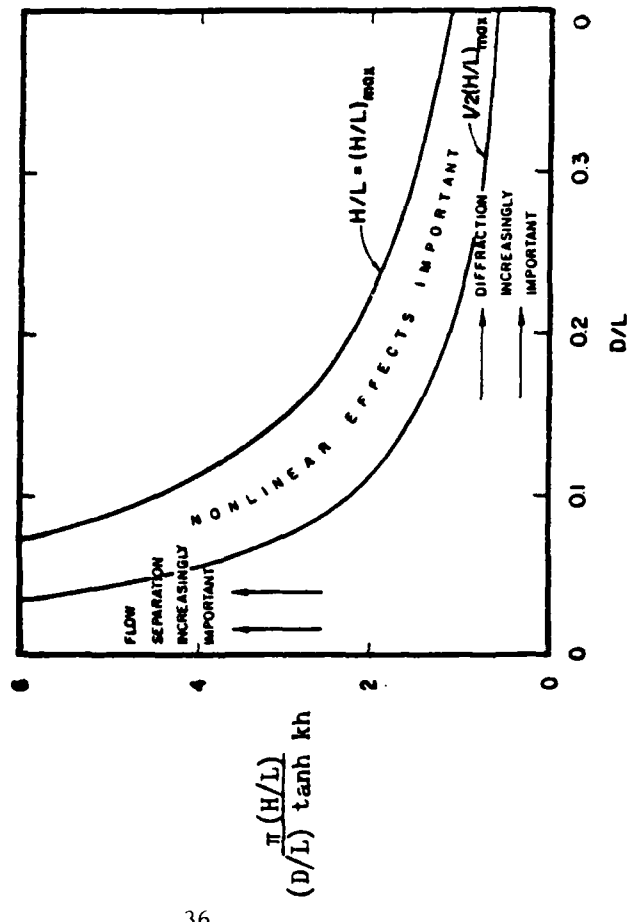
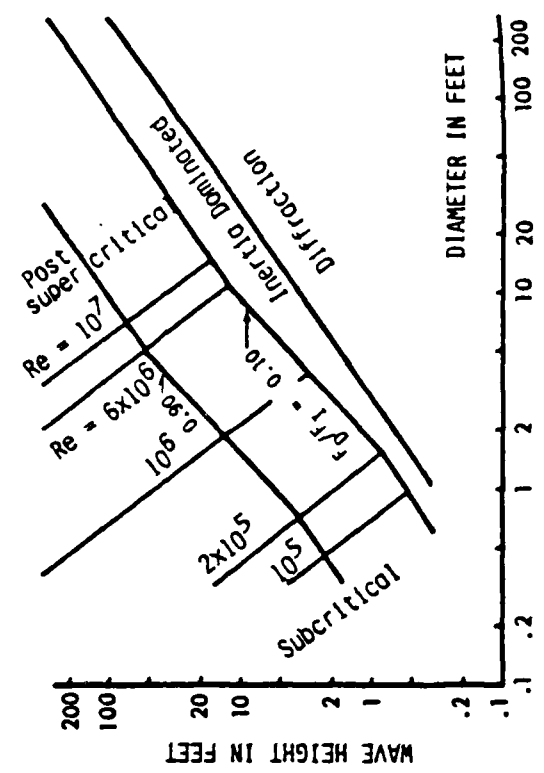


FIG. 5 COMPARATIVE IMPORTANCE OF LOADING
REGIMES AT $z = 0$
(Sarpkaya and Isaacson, 1981)



If the classical dimensionless hydrodynamic parameters given by the Froude number, F , and Reynolds number, R , are defined as $F = u/\sqrt{gb}$ and $R = \rho u^2 D / \mu$ in which u = water particle velocity, then

it is easy to show that $F/R = u/\rho\sqrt{gb}^3$. The only restriction involved up to now is that the waves must be strictly periodic. These results, however, are not restricted to simple linear sinusoids.

Keulegan and Carpenter (1958) identified the following variables for a wave force/unit length in their laboratory experiments using standing waves:

$$F = f_3 \{t, T, U_m, D, \nu\} \quad (3)$$

in which the variables t = time; U_m = semiamplitude of an oscillatory current measured at the node of a standing wave; D = cylinder diameter; and ν = kinematic fluid viscosity. They obtained by dimensional analysis a dimensionless force/unit length expressed by

$$\frac{F}{\rho U_m^2 D} = f_4 \left\{ \frac{t}{T}, \frac{U_m T}{D}, \frac{U_m D}{\nu} \right\} \quad (4)$$

They found no dependence on Reynolds number, $R = U_m D / \nu$ in their experiments; but they did find a dependence on a **period parameter** = $U_m T / D$ (also called the Keulegan-Carpenter parameter, K).

Sarpkaya (1975) in his U tube experiments reached a similar conclusion that harmonic forces correlate with the Keulegan-Carpenter **period parameter**, K , and not with the Reynolds number, R . A subsequent reevaluation of these results by Miller (1977) and by Garrison (1982) as well as by Sarpkaya, himself (1977) eventually illuminated the true Reynolds number dependency of these data.

HYDRODYNAMIC LOADS ON SMALL MEMBERS

A semi-intuitive equation was introduced by Morison, et al (1950) to compute wave forces on immersed objects having characteristic dimensions which are small compared to the wave length of the incident wave. This equation has been extended to three-dimensional analyses of arbitrarily-oriented members of offshore structures. The Morison equation in vector form is

$$\vec{F} = \vec{F}_D + \vec{F}_I \quad (5)$$

in which \vec{F} = hydrodynamic force per unit axial length acting normal to the axis of the member, \vec{F}_D = drag force, and \vec{F}_I = inertia force. The drag force term per unit length is taken (as in the case of steady unidirectional flow) as

$$\vec{F}_D = \frac{1}{2} \rho b C_D | \vec{U}_n - \vec{U}'_n | | \vec{U}_n - \vec{U}'_n | \quad (6)$$

in which ρ = fluid mass density, b = projected width of member in the direction of the cross-flow component of velocity, C_D = dimensionless drag coefficient, \vec{U}_n = component of fluid velocity vector normal to the member axis, and \vec{U}'_n = component of member velocity vector normal to the member axis. Drag forces are predominantly due to flow separations of the velocity field as it passes the member.

The inertia force vector per unit length is due to the pressure gradient associated with the relative acceleration of the member and fluid and is given by

$$\vec{F}_I = \rho A \vec{a}_n + \rho A C_m (\vec{a}_n - \vec{a}'_n) \quad (7)$$

in which A = cross-sectional area of the member, C_m = dimensionless added mass coefficient, \vec{a}_n = component of the total fluid acceleration vector normal to the member axis, and \vec{a}'_n = component of the member acceleration vector normal to the member axis. The fluid acceleration \vec{a}_n denotes the total acceleration which includes both the local and the convective parts. Often the inertia coefficient $C_I = 1 + C_m$ is reported rather than the added mass coefficient C_m .

In wave action, the velocity and acceleration vectors are generally not collinear and, therefore, the drag, \vec{F}_D , and inertia, \vec{F}_I , forces act in different directions. The three-dimensional form given above assumes that the drag and inertia forces are independent and that the **strip theory** principle applies; viz., the forces are based on normal components of velocity and acceleration. The generally accepted limit (MacCamy and Fuchs, 1954) of member size for applications of the Morison equation is $D/L < 0.2$, in which L = the wave length of the incident wave.

In addition to the in-line drag and inertia forces, there is also a force component normal to the incident velocity vector called the lift force. It is due to the formation of eddies which are shed alternately on each side of the member and may be expressed by:

$$F_L = \frac{1}{2} \rho D C_L (U_n - U'_n)^2 \quad (8)$$

in which C_L = dimensionless lift coefficient.

The use of the Morison equation requires an estimation of drag, C_D , and added mass, C_m , coefficients and an estimation from a wave theory of the fluid velocity and acceleration fields.

Effects of Currents on Wave Forces

In the evaluation of fluid forces acting on offshore structures, it is necessary to consider the effects of currents as well as waves. Currents can have a rather significant effect on the total hydrodynamic loads and, therefore, should be accounted for properly.

Currents may be classified into three major subdivisions: 1) those caused by density differences over large scales, 2) those caused by tides, and 3) those caused by wind. However, large scale density currents are normally not significant in the design of offshore structures.

Tide and wind generated currents frequently affect the design of offshore structures. Tidal currents are generally small in the open ocean but in inlets or estuaries where the boundaries constrict the flow, the velocities can become significant. Current profiles developed by tides tend to have boundary layer type velocity profiles. Probably the most common representation of the fully developed current profile is the logarithmic profile first described by Prandtl (cf. Peregrine, 1976 or Thomas, 1979).

Wind generated currents are presumably nearly always present during storm conditions and are normally the major source of current present. Wind currents caused by wind shear tend to have their greatest magnitude at the free surface where the wave forces also tend to be greatest and decrease with depth.

Reid (1957) developed wind generated current profiles based on Prandtl's mixing length concept. The mixing lengths were assumed to increase with distance from both the bottom and the free surface, resulting in current profiles which are dependent on the surface and bottom shear stress. Various other models have been developed to predict the nearshore currents due to extreme winds or hurricanes. In particular, a three-dimensional, time-dependent current model developed by Forristall (1974) represents hurricane generated currents quite well.

Having specified the magnitude of the design current and its direction, it is necessary to include this component of velocity in the wave force calculations. It has been common practice to simply add the current-induced velocity to the wave-induced velocity before squaring the result in the drag term in the Morison equation rather than sum the separately computed drag forces. If drag forces due to wave velocity and current velocity are computed separately and the resulting forces summed, the total force is in error on the low side. Thus, it is important that the current-induced velocity be added vectorially to the wave-induced velocity before the sum is squared.

Assuming that both the wave amplitude and the current magnitude are small, the concept of superposition as described above is valid. The two components act independently and may be simply superimposed. However, this superposition is strictly valid only for small waves and currents so that only the magnitude of the interaction process is of interest. Dalrymple (1973, 1974) has carried out a numerical investigation of the nonlinear interaction of shear currents and waves. His numerical results indicate that the nonlinear interaction effect is rather minor for typical practical applications. The error resulting from the superposition of the wave and current magnitudes tends to be somewhat greater at the wave trough than crest; but this is not of much practical importance because the drag component is greatest at the crest. As a general conclusion, it appears that the nonlinear interaction effect of the current and wave motion is of minor importance in most practical applications; and the simple vector addition of wave-induced and current-induced velocities represents a valid assumption. Peregrine (1976) reviews other more complicated alternative methods for modeling wave-current interaction. Criteria are still lacking, however, for the selection of the appropriate drag force coefficients to use with this wave-current model.

Impact Loads in Splash Zone

Impact or wave slamming loads can occur on members of a structure located near the free surface and may result in large local stresses. Such loads are normally not used to design the complete structure but rather to check the design of critical members or parts of the structure near the free surface which are subjected to wave slamming. Typically, damage occurs because of repeated wave slamming on a given member and, therefore, these wave slamming loads may be used in a fatigue analysis wherein a longterm counting process is used.

Recent experience in the North Sea has emphasized the need to consider the impact loading and varying buoyancy forces acting on horizontal members in the splash zone. As a horizontal member with

axis parallel to the wave crest passes in and out of the water surface, the buoyant force rapidly varies between zero and its fully submerged value. At the same time, an impact load occurs due to water entry of the member. Repeated loading of this type can result in fatigue damage and eventual failure of the member.

The most complete formula for the vertical force on a member was given by Kaplan and Silbert (1976) as

$$F = \rho g A_i + \rho A_i \ddot{\eta} + \frac{\partial}{\partial t} [\eta_3 (\dot{\eta} - w)] \quad (9)$$

in which ρ = mass density of water, A_i = time dependent immersed cross-sectional area of the member, g = acceleration of gravity, $\ddot{\eta}$ = vertical acceleration of the water surface, $\dot{\eta}$ = vertical velocity of the water surface, η_3 = the vertical added mass coefficient which is appropriate to the immersed or semi-immersed member at the free surface, and w = the vertical velocity of the member.

Based on experimental results obtained in a wave tank, Dalton and Nash (1976) proposed a formula for the wave slamming force of the form

$$\bar{F} = \frac{1}{2} \rho A C_S U^2 \quad (10)$$

in which A = projected area normal to plane of wave impact, U = local wave particle velocity, and C_S = dimensionless slam coefficient. Experimental values for C_S show considerable scatter with values ranging between 1 and 5.

Because of the impulsive nature of the loading and of the elastic properties of the member, the resulting stresses in the member must be computed through application of a dynamic/elastic analysis which takes into consideration the mass distribution and the end connections of the member. The integration of the equations describing this system results in a stress history versus time during a given impact.

Determination of Force Coefficients

To aid in evaluating the parametric dependency of the empirical force coefficients, C_D and C_I , note that there have been the following two basic types of empirical evaluations used to obtain these coefficients:

<u>TEST TYPE</u>	<u>KINEMATICS</u>	<u>METHOD OF ANALYSIS</u>
1. LABORATORY		
a. Standing Wave Node	Linear Wave Theory	Fourier
b. U Tube	Measured	Fourier
c. Oscillating Cylinder	Measured & Theoretical	Least Squares & Fourier
2. OCEAN	Measured & Theoretical	Least Squares

Figure 6 from Garrison (1982) compares portions of the results for the drag, C_D , and inertia, C_I , coefficients from the standing wave tests of Keulegan and Carpenter (1958); the U-tube tests of Sarpkaya (1977); and the oscillating cylinder tests of Yamamoto and Nath (1976), and of Garrison, et al. (1977). The Reynolds number range shown extends beyond the transition region and it appears that the post-critical region lies well beyond $Re = 10^6$ for a smooth cylinder. Sarpkaya (1977) used cylinders ranging from 2.0 - 6.5 inches in diameter. Yamamoto and Nath (1976) oscillated horizontally a 1.0 foot diameter cylinder in a wave channel filled to 13.0 foot depth. Garrison et al. (1977) oscillated horizontally 2.0 and 3.0 inch diameter cylinders in a channel 2.0 feet wide, 16.0 feet long and 42 inches deep.

Although exact correlation does not exist between results of the three independent experiments shown in Figure 6, it is noteworthy that trends of the data are all very similar and the agreement is actually as good as exists for equivalent steady flow experiments. However, a certain amount of disagreement should be expected in the transition region because the drag coefficient is fairly sensitive to free stream turbulence (Garrison, 1982). Some variations in the rate of dissipation of the turbulence level and vibration of the test cylinder no doubt existed. At the high-Reynolds numbers the disagreement appears to decrease and the results appear to converge with the asymptotic values of C_D increasing with decreasing values of the displacement ratio (Garrison, 1982).

It is significant that relatively good agreement exists between these different experiments. This may have been unexpected compared to the large degree of scatter that characterizes the drag and inertia coefficient data obtained from ocean test platforms and from small scale wave tank tests (Heiderman, et al., 1979). Since these results cover the transition region where the coefficients are sensitive to a number of different effects, it appears that a correct answer does not exist from the view point of practical applications. However, the post-critical Reynolds number region is generally of more interest in design and, although data in this range

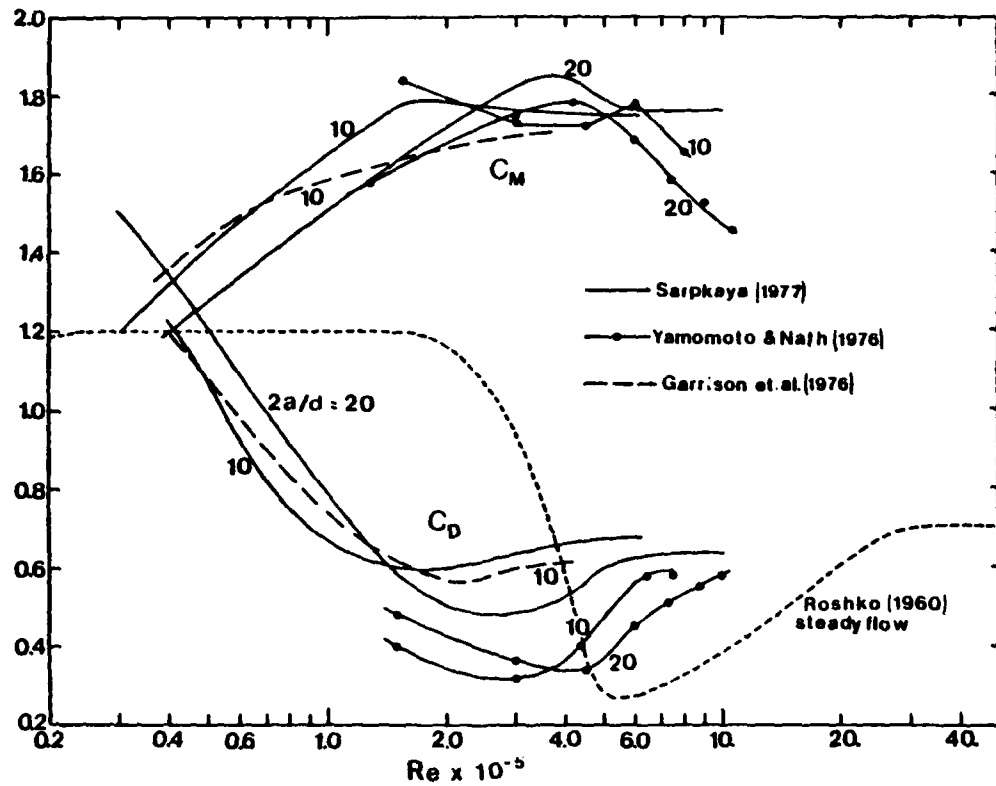


FIG. 6 DRAG AND INERTIA COEFFICIENT IN OSCILLATORY FLOW PAST SMOOTH CIRCULAR CYLINDERS (Garrison, 1982)

for smooth cylinders is still somewhat lacking, it appears that the data in Fig. 6 tend to converge at high Reynolds numbers (Garrison, 1982).

Evaluation of C_I and C_D From Experimental Data

The method of evaluating C_I and C_D from measured force traces depends somewhat on the intended application of the results (Garrison, 1982). For maximum wave forces it seems reasonable to reduce the data in a manner similar to the method used by Kim and Hibbard (1975) where C_D was evaluated using short segments of the measured force trace where the velocity was maximum and C_I was evaluated over short segments where the acceleration was maximum. An alternative to this method which is adaptable to truly periodic motion is to use a least squares fit of the measured force trace to the Morison equation using the complete cycle of the motion. For periodic motion, this method gives

$$C_D = (8/3\pi)/(\rho D U_m^2 L) \int_0^{2\pi} F_m \cos(\theta) |\cos(\theta)| d\theta \quad (11a)$$

$$C_I = (2U_m T/\pi^3 D)/(\rho D U_m^2 L) \int_0^{2\pi} F_m \sin(\theta) d\theta \quad (11b)$$

where F_m/L = measured force per unit length, $C_I = 1+C_m$, C_m being the added mass coefficient and T = the period of the motion.

Keulegan and Carpenter (1958) and Sarpkaya (1975) used a slightly different form. They used the first term of a Fourier series representation and obtained the following alternative expression for the drag coefficient:

$$C_D = (3/4)/(\rho D U_m L) \int_0^{2\pi} F_m \cos(\theta) d\theta \quad (12)$$

The corresponding expression for the inertia coefficient remained the same as for the least squares method.

Both of these methods have been applied in the past with the intention of providing a good fit between the Morison equation and a measured force trace for predicting wave forces. However, an equally important aspect of this same type of flow is the evaluation of the added mass and damping coefficients associated with the motion of compliant structures. While C_m should still be evaluated in such cases, the emphasis in the case of the damping coefficient is quite different (Garrison, 1982).

In the case of damping there is no real need to accurately represent the force versus time relationship. It is of much greater importance to properly represent energy or work done during a cycle of the motion. Thus, equating work done by the measured force to that done by the velocity-squared term in the Morison equation gives a definition of C_D which is appropriate to damping, or wave excitation, of compliant structures. This result is identical to the Fourier method; i.e., the Fourier average drag coefficient defines C_D such as to preserve energy dissipation over a complete cycle of the motion. (Garrison, 1982)

This is consistent with the assumption of a linearized form for the drag term where the drag force is represented by

$$F_D = .5DLC_{DL}U_m \quad (13)$$

in which C_{DL} = the linear drag coefficient. That is, equating the work done by a linear drag force to the work done by the measured force gives

$$C_{DL} = (2/\pi)/(\rho DU_m L) \int_0^{2\pi} F_m \cos(\theta) d\theta \quad (14)$$

If C_{DL} is defined in terms of the C_D in the nonlinear drag force term in the Morison equation, the equality of work done over a complete cycle gives $C_D = (3\pi/8U_m) C_{DL}$ and the expression for C_D given by the Fourier method is again recovered (Garrison, 1982).

The Fourier definition for C_D is most appropriate for use with compliant structures while the least squares definition is most appropriate for repeating the wave force trace (Garrison, 1982). Garrison (1982) has compared the values of C_D computed by both of these methods for the three types of laboratory tests previously described. Garrison (1982) showed that the Fourier method gave slightly higher values than the least squares method. It does not appear to be of any significant value to distinguish between coefficients computed by the two methods for practical design purposes (Garrison, 1982).

Sarpkaya (1975) used an oscillating U tube and Fourier analysis to obtain drag and inertia coefficients on horizontal cylinders in harmonic flow without a free surface. He concluded that these two force coefficients were reasonably well-correlated with the period parameter ($K = U_m T/D$); but that absolutely no correlation was found between these two force coefficients and the Reynolds number ($R = U_m D/v$).

Miller (1977) replotted both the original standing wave data from Keulegan and Carpenter (1958) and the oscillating U tube data from Sarpkaya (1975) and demonstrated that both of these data showed a clear Reynolds number dependence.

Sarpkaya (1977) then re-examined both the original Keulegan and Carpenter (1958) data as well as his own (1975) and determined that a frequency parameter ($\beta = D^2/vT$) and roughness Reynolds number ($Re = U_m \epsilon / v$) could explain the earlier incorrect interpretation regarding no Reynolds number dependence. The frequency parameter, $\beta = D^2/vT$, represents a ratio of Reynolds number, R , to period parameter, K .

Laboratory U Tube Tests. In U tube laboratory tests, oscillatory flow past test cylinders have been obtained by sinusoidal current flow represented by $U = U_m \cos \omega t$ in which $U_m = H\pi/T$. Substituting for the Keulegan-Carpenter number, K , (or period parameter) gives $K = H\pi/D$ which is called the **relative amplitude parameter** and provides a measure of the wake effects in oscillatory flows. The Keulegan-Carpenter number differs from the relative amplitude parameter by π , a constant for harmonic laboratory flows. The effects of relative amplitude on relative roughness in steady flow past smooth cylinders are to elevate the value of the drag coefficient in the high Reynolds number region. Assuming that the drag coefficient in oscillatory flow past smooth cylinders is similar to these steady flow conditions, Fig. 7 demonstrates that C_D decreases from a value of approximately 1.2 for $R < 10^4$ to 0.6 for $R > 10^6$. For $R > 10^5$, the relative roughness parameter, ϵ/D , and the relative amplitude parameter, H/D , tend to increase the value of C_D .

Analyses of the strictly periodic U tube data to obtain C_D and C_I values have been by Fourier methods.

Ocean Wave Data. Dean and Aagaard (1969) used measured pressure forces from a prototype offshore oil platform and a least-squares regression analysis with theoretical nonlinear water particle kinematics computed by the stream function theory to compute C_D , C_I . They found that the drag coefficient varied with Reynolds number and that the inertia coefficient was essentially a constant. The Dean and Aagaard regression analysis illustrates the parametric dependence of the coefficients and explains some of the scatter observed by various investigators.

Dean and Aagaard (1969) computed C_D , C_I from a least squares fit to the measured forces by minimizing the following mean square error:

$$\epsilon^2 = \frac{1}{N} \sum_{n=1}^N \{F_m(n) - F_p(n)\}^2 \quad (15)$$

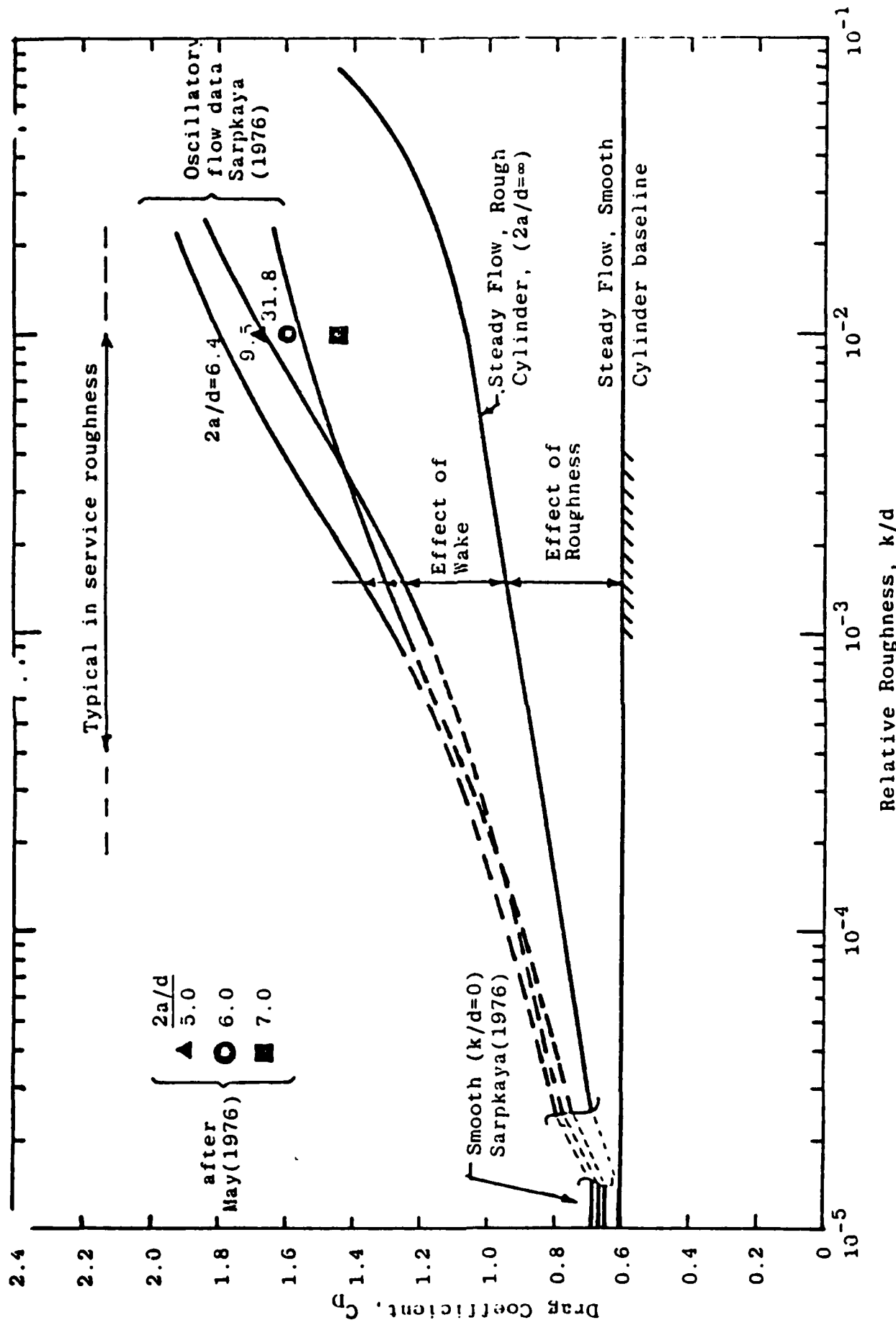


FIG. 7 DRAG COEFFICIENT AT SUPERCRITICAL REYNOLDS NUMBER SHOWING THE EFFECT OF ROUGHNESS AND THE WAKE
(Garrison, 1982)

Minimizing this mean square error requires that

$$\frac{\partial \epsilon^2}{\partial C_I} = 0 \quad \text{and} \quad \frac{\partial \epsilon^2}{\partial C_D} = 0 \quad (16)$$

Equation 15 for the mean square error may be expanded into a general equation for a quadratic surface of second-degree with an origin which has been translated and rotated. The coefficients of the independent variables include products of the wave field kinematics and measured forces and determine whether or not the data are well-conditioned or ill-conditioned for determining true minima (Dean, 1976).

Expanding the mean square error yields the following equation for a quadratic error surface:

$$\epsilon^2 = \left(\frac{C_D \rho}{2}\right) \langle u^4 \rangle + \left(C_I \frac{\rho \pi D}{4}\right)^2 \langle u^2 \rangle + 2\left(\frac{C_D \rho}{2}\right) \left(C_I \frac{\rho \pi D}{4}\right) \langle u | u | \dot{u} \rangle - 2\left(\frac{C_D \rho}{2}\right) \langle F_m u | u | \rangle - 2(C_I \frac{\rho \pi D}{4}) \langle F_m \dot{u} \rangle + \langle F_m^2 \rangle \quad (17)$$

in which the temporal averaging operator $\langle \cdot \rangle$ is defined by $\langle \cdot \rangle = \frac{1}{N} \sum_{n=1}^N (\cdot)_n$. This equation is the general equation for an ellipse whose origin has been translated and rotated. For data which are simple harmonic oscillations, the coordinates of the origin (x_0, y_0) are given by

$$x_0 = \left(\frac{16}{3\rho}\right) \frac{\langle F_m u | u | \rangle}{\langle u_m^4 \rangle} \quad (18a)$$

$$y_0 = \left(\frac{2}{\rho \pi^3}\right) \left(\frac{T}{U_m D}\right)^2 D \langle F_m \dot{u} \rangle \quad (18b)$$

To determine the suitability of the data to resolve the regression coefficients C_D , C_I , changes in the minimum values of these coefficients for a given mean square error are minimized.

For $C_I = \text{constant}$, it may be shown that this minimization of the changes in the minimum values gives

$$\delta C_D = \frac{\sqrt{2}}{\rho} \frac{[\epsilon_i^2 - (\epsilon_i^2)_{\min}]^{1/2}}{[\langle u^4 \rangle]^{1/2}} \quad (19a)$$

and for $C_D = \text{constant}$:

$$\delta C_I = \frac{4}{\rho \pi D} \frac{1}{\sqrt{2}} \frac{[\epsilon_i^2 - (\epsilon_i^2)_{\min}]^{1/2}}{[\langle \dot{u}^2 \rangle]^{1/2}} \quad (19b)$$

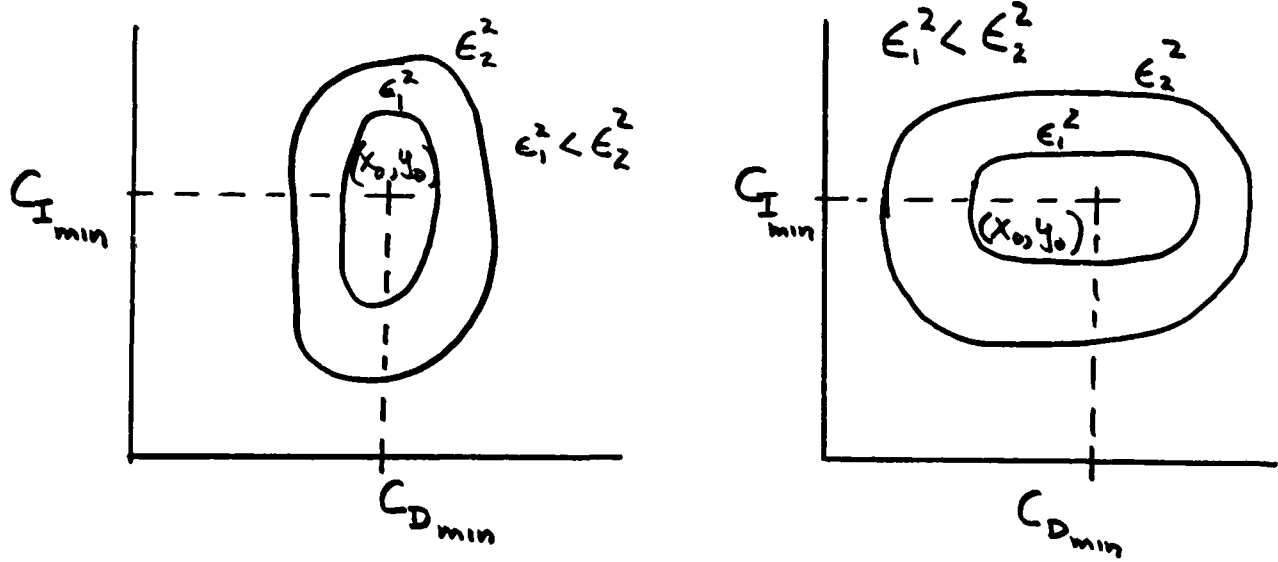
The ratio of the axes of the error ellipse (eccentricity) is given by

$$E = \frac{\delta C_I}{\delta C_D} = \frac{2}{\pi D} \frac{[\langle u^4 \rangle]^{1/2}}{\langle \dot{u}^2 \rangle} \quad (20)$$

For simple harmonic oscillations, this reduces to

$$E = \frac{2}{\pi D} \left[\frac{3}{4} \right]^{1/2} \frac{U_m}{\omega} \quad (21a)$$

$$= \left[\frac{3}{4} \right]^{1/2} \frac{C_I}{C_D} \frac{(F_D)_{\max}}{(F_I)_{\max}} \quad (21b)$$



The error surface for simple harmonic oscillations in dimensionless form is

$$\frac{\epsilon_i^2 - (\epsilon_i^2)_{\min}}{(F_D)^2_{\max}} = \frac{3}{8} \left(\frac{\delta C_D}{\delta C_I} \right)^2 + \frac{1}{2} \left(\frac{F_I}{F_D} \right)^2_{\max} \left(\frac{\delta C_I}{\delta C_D} \right)^2 \quad (22)$$

Dean (1976) gives the following criteria for estimating the suitability of the data for determining C_D , C_I :

<u>E</u>	<u>Relatively Well-Conditioned to Determine</u>
0.25	C_D and C_I
0.25 - 4.0	
4.0	C_D

DIFFRACTION THEORY FOR LARGE MEMBERS

The Morison equation represents a simple procedure for computing wave loads on cylindrical members of offshore platforms whose diameters, D , are less than about $0.2L$ in which L = the wave length of the incident wave. For caissons or other large displacement components of a structure, it is necessary to apply a more fundamental approach to the evaluation of the wave loading. A procedure which may be applied to bodies of arbitrary shape and which may be used to compute all components of forces and moments is often referred to as **diffraction theory** (cf. Garrison, 1978, and Hogben and Standing, 1975).

In the linear diffraction theory, the fluid is assumed to be incompressible and inviscid; and a linear wave is assumed to interact with the immersed surface of a fixed structure. This interaction gives rise to a scattered wave so that the total wave potential may be represented by a linear sum of the **incident** and the **scattered** wave potentials.

The hydrodynamic wave-induced pressure acting on the immersed surface of the structure is computed from a linearized form of the Bernoulli equation. The net forces and moments are computed by integration of the pressure over the total immersed surface. Two components of this pressure (and resulting force) may be identified. The first contribution to the net force results from the pressure component associated with the incident wave alone and is called the Froude-Kriloff force. A second component is due to the diffraction of the incident wave which is caused by the presence of the structure.

Yue, et al. (1978) have developed a procedure based on a hybrid finite element procedure which also appears to be a promising method for practical application. A review is given by Mei (1978).

Although the numerical diffraction theory as applied to offshore structures has been in common usage for only a few years, the recent interest in North Sea gravity platforms has given considerable impetus to its development and acceptance for practical design. There are currently several examples which show excellent agreement between predictions and large-scale wave channel tests both for the simple geometric shapes reported by Hogben and Standing (1975), and for models of actual designs of offshore gravity structures (Garrison, 1978). In the case of the calculations presented by Garrison (1978), the structure was composed of a large displacement caisson with a super-structure composed of smaller diameter members. This procedure described for the first time an interaction method in which the loads on the caisson were computed by use of a

diffraction analysis and the loads on the superstructure by use of the Morison equation.

Limitations of Linear Diffraction Theory

The linear diffraction theory has proved to be useful well beyond its original expectations. There are, of course, limitations which must be taken into consideration in practical applications. Firstly, the analysis is based on linear wave theory. Consequently, as the wave height increases, a point will eventually be reached where the theory will no longer give satisfactory results. Arctic gravity platforms and ship loader caissons (Apelt and McKnight, 1976) represent examples where non-linear effects tend to become pronounced. In these examples, caissons are placed in rather shallow water and are acted upon by fairly large-amplitude design waves. Secondly, in shallow water, the nonlinearities in the incident wave itself tend to be pronounced and these nonlinearities are reflected in the wave loads on the caisson. In cases where the incident wave is nonlinear, the linear diffraction analysis underpredicts the force and, therefore, is non-conservative. Thus, it is necessary to establish the limits of a linear diffraction theory.

Available data which can be used to indicate the limits of linear diffraction analysis are not extensive. However, available data indicate that, in general, when the water depth to wave length ratio becomes less than about $h/L < 0.04$, nonlinear effects in the wave loads begin to become apparent (cf. Apelt and McKnight, 1976, Garrison, et al., 1975, Hafskjold, et al., 1973, and Hogben and Standing, 1975). Because the nonlinear effects in waves tend to die out with increasing depth, the nonlinear effects tend to be less pronounced on deeply submerged caissons than on surface-piercing caissons. In the case of surface piercing caissons where the nonlinear effects tend to be most pronounced, the loads can become substantially greater than predicted by the linear theory as noted by Apelt and McKnight (1976) in the case of the ship loader caisson.

Presently, only linear diffraction analysis is commonly used in practice. A few attempts to develop nonlinear analyses have been made (cf. Chakrabarti, 1975, Garrison, 1976, Isaacson, 1978 and 1982 and Hunt and Baddour, 1981); but the value of such nonlinear analyses is uncertain at present. For this reason, when nonlinear effects become significant, the present state-of-the-art dictates that a properly designed model test should be conducted to evaluate the wave loads. In most model tests of large displacement caissons where drag or other viscous effects are expected to be minor, geometric and Froude scaling is appropriate.

MULTIPLE BODY WAVE INTERFERENCE BY FEM

When large structures adjoin each other, the incident wave train is disturbed by each of the structures. Wave sheltering by, and reflection from, neighboring structures disturb the incident wave field further. For floating structures, the radiating waves due to the forced motions of the structure are diffracted and reflected by the neighboring structures. Their hydrodynamic forces and responses will be affected by such wave interference phenomena (Van Oortmerssen, 1979).

The calculation of wave forces on large offshore structures of arbitrary shape is often performed using linear wave diffraction theory. In general, there are three major classes of solution techniques applied to the corresponding boundary value problems; 1) analytical Eigenseries Expansion Method; 2) Integral Equation Method; and 3) Finite Element Method (FEM).

Only a few **analytical eigenseries** solutions are available and are limited to problems with special structural geometries. These include the eigenseries solutions of MacCamy and Fuchs (1954), Garrett (1971), Spring and Monkmyer (1975) Chakrabarti (1978), Ohkusu (1974), and the 2-D strip theory of Ohkusu (1976).

Numerical **integral equation** solutions for wave interference between two neighboring vertical cylinders have been treated by Lebreton and Cormault (1969) and by Isaacson (1978) using 3- and 2-D wave source representations, respectively. The studies of multiple horizontal cylinders originated from the need to determine the hydrodynamics of catamarans and other multi-hull vessels and have been given by Wang and Wahab (1971), Ohkusu (1974), and Maeda (1974). Sayer and Spencer (1981) have applied a multipole method to calculate the interference problems between two floating cylinders. The interference effects between an impermeable wall and large floating structures have been investigated by Ho and Harten (1975) using a fundamental singularity discretized over the entire boundary. Van Oortmerssen (1979) applied a 3-D Green's function numerical model to calculate the hydrodynamic interference effects between two floating vertical cylinders. Matsui and Tamaki (1981) have investigated the interference effects between groups of vertical axisymmetric bodies.

In general, there are four areas where the most common integral equation formulations have shown potential deficiencies: viz. 1) at irregular frequencies; 2) for modeling complex structural geometries; 3) by underestimating structural volumes or areas and, consequently, the hydrodynamic forces; and 4) in numerical instabilities which result from the numerical evaluation of Cauchy principal value integrals.

Applications of the finite element method (FEM) to wave diffraction and radiation problems have been reviewed by Mei (1978) and by Zienkiewicz, et al. (1978). Techniques that have been adopted in the finite element method to model the radiation condition at infinity in a 3-D fluid domain include: 1) boundary dampers (Huang, 1983 and Zienkiewicz, et al., 1977); matching analytical boundary series solutions (BSM), (Mei, 1978 and Yue, et al., 1978); matching boundary integral equation solutions (BIM), (Zienkiewicz, et al., 1977 and 1978); and infinite elements (Bettess and Zienkiewicz, 1977 and Zienkiewicz, et al., 1977 and 1978).

Techniques for matching finite element inner domains with boundary solutions always involve a broad front linking between the two domains and often result in an inconveniently large bandwidth for the equations. The boundary matching required in the BSM needs to be extended in the full vertical direction. Therefore, extensive finite element modeling is required and prohibits its application to multiple structures system in deep water. In the BIM, a Green's function satisfying a permeable boundary condition has not been developed and, therefore, its application to wave interference problems is limited to impermeable structure and boundaries.

The use of infinite elements leads to errors since an exponential decay function is used to approximate the scattered wave and a Newton-Coates type integration formula is employed in the infinite direction to achieve computing economy (Bettess and Zienkiewicz, 1977). However, such integration does not exhibit a well-behaved monotonic convergence property in the approximation of the harmonic term in the shape function.

To date, only Eatock-Taylor and Zietsman (1981) have used a BIM finite element algorithm to study the interference problem between multiple structures. No irregular frequencies result from an FEM algorithm and, therefore, the same meshes can be used for a broad spectrum of wave frequencies.

The interference effects between multiple floating vessels and an adjacent wharf (part impermeable and part permeable) used as a loading/unloading facility have demonstrated that the effects of permeable wharfs are easily incorporated in a finite element formulation. The heave resonance between two vessels adjacent to a permeable wharf is suppressed; while the sway resonance is strongly excited but at a higher frequency as a result of the interference.

Numerical Examples of Wave Interference Effects

Numerical examples of wave interference effects computed by the FEM are presented for: 1) a 3-D catamaran hull and 2) a ship loading/unloading facility. The numerical values were computed from

a 3-D FEM algorithm using the more computationally efficient radiation boundary dampers (Huang, et al., 1983).

Three-Dimensional Catamaran: The interference effects between the two hulls of a catamaran have been calculated by Leonard, et al. (1983), using a 2-D approximation. A strong heave resonance phenomenon at $va=0.65$ was shown where a = radius of one hull. For the 3-D end effects, a length of $5a$ and infinite water depth were assumed. Finite element solutions used the meshes shown in Fig. 8, where plane dampers and a fictitious bottom were applied at $r_D = 3a$ and $d_f = 2a$, respectively. Numerical solutions have been calculated for the case of beam seas only, and compared with the 2-D solutions to illustrate the end effects of a 3-D catamaran. Numerical results of the sway and heave exciting forces (non-dimensionalized by the hydrostatic restoring force $4\rho g H a b$, where $2b$ = catamaran length) are shown in Figure 9, together with the results from the 2-D approximation. The end effects are again illustrated by a sharp decrease of the heave forces near the 2-D resonance frequency and by an increase of the 3-D resonance frequency. The dimensionless hydrodynamic coefficients in the sway mode are shown in Fig. 10, where end effects are seen to be small. The dimensionless heave added mass and damping coefficients are shown in Fig. 11 where the end effects are clearly demonstrated. These added mass and damping coefficients are nondimensionalized by $2\rho A b$ and $2\omega_p A b$, respectively, where A = submerged section area of catamaran and b = unit length in the 2-D formulation. The standing waves between the two hulls become smaller as a result of the flow around the ends of the catamaran. The heave resonance frequency also increases to approximately $va = 0.9$. Similar results have been calculated recently by Eatock-Taylor and Zietsman (1981) by using the boundary integral method (BIM).

Ship Loading/Unloading Facilities: One concept for ship loading/unloading operations under consideration by engineers is that of a floating derrick barge moored between a vessel and wharf connected by a long causeway to shore. The wharf and causeway could be supported by piles or some other permeable structures. An understanding of the wave interference phenomena between the two floating vessels, the wharf and the supporting structures are essential to the design of the moorings and other forms of interstructural constraints.

For purposes of illustration, the interference phenomena in such a system have been calculated for the case shown in Fig. 12. A permeability of 0.75 was assumed for the supporting pile structure. The geometries and spacing of the two vessels are identical to the 3-D catamaran previously analyzed. Numerical solutions have been calculated for the case of beam seas using the meshes shown in Fig. 12. The predictions of the dimensionless sway and heave exciting forces nondimensionalized by the hydrodynamic force $2\rho g H a b$ are illustrated in Fig. 13. Sharp variations in the exciting forces in

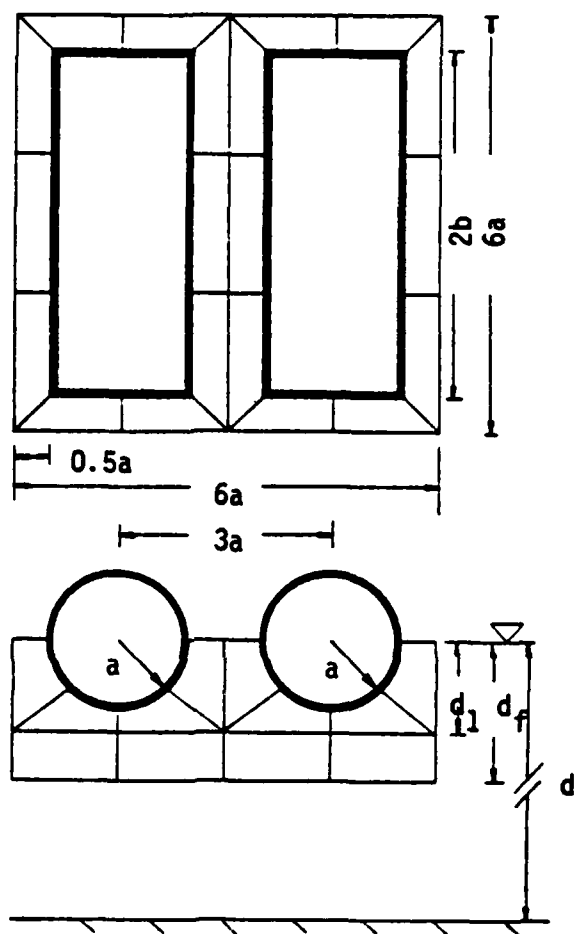


FIG. 8 MESH FOR THREE-DIMENSIONAL CATAMARAN

$$(d/a = \infty, d_1/a = 4/3, d_f/a = 2, 2b/a = 5)$$

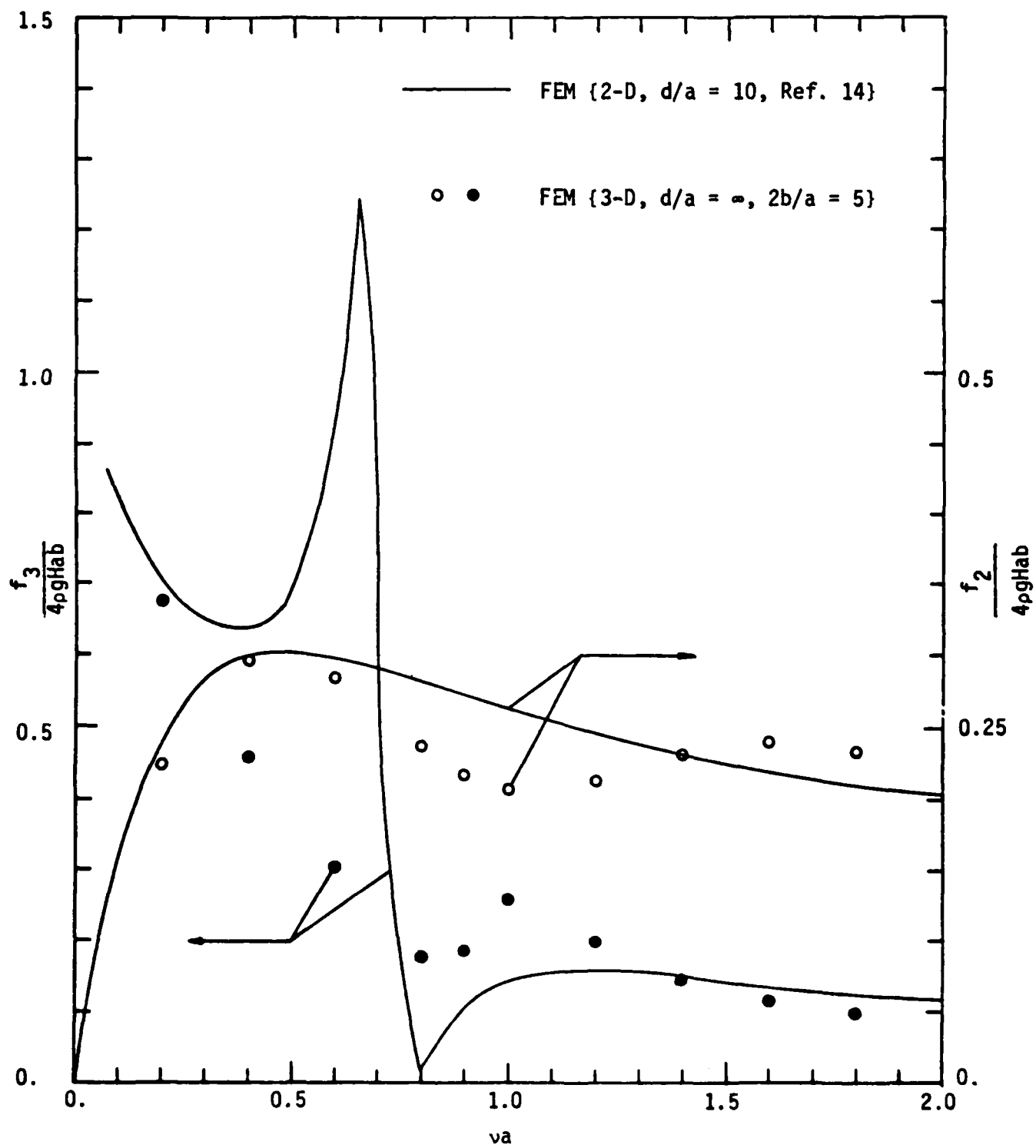


FIG. 9 EXCITING FORCES FOR A CATAMARAN

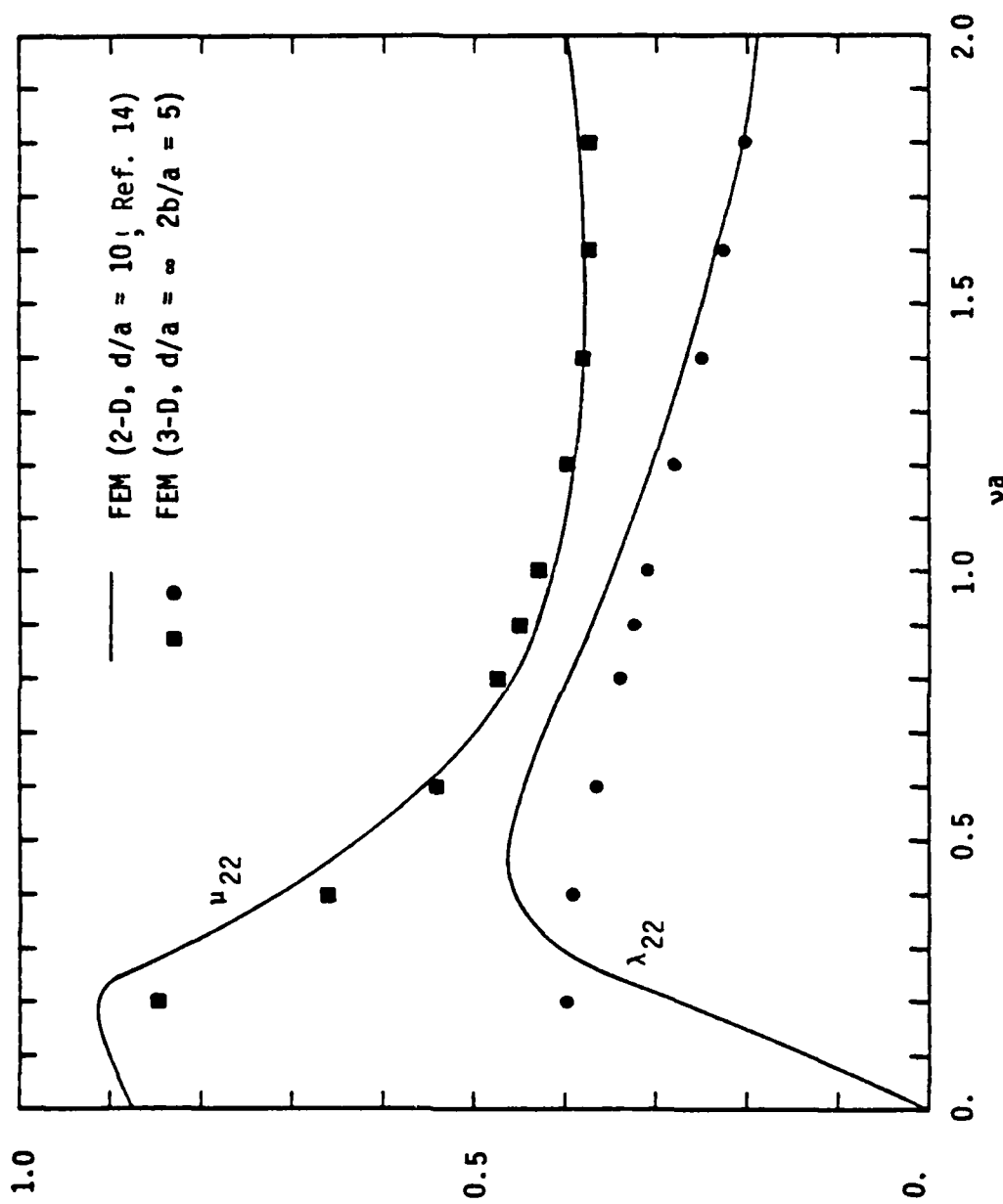


FIG. 10 SWAY ADDED MASS AND DAMPING COEFFICIENTS FOR A CATAMARAN

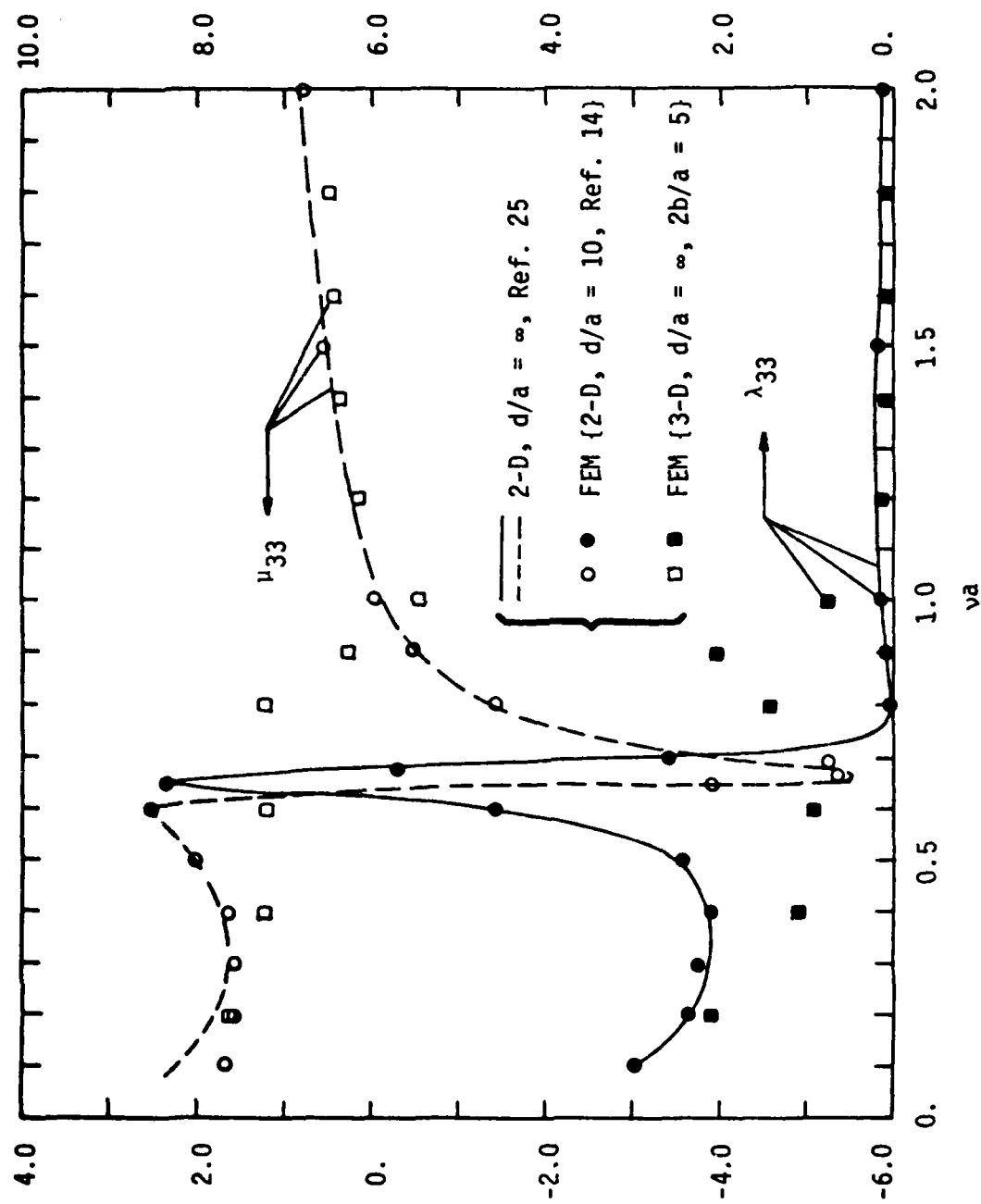


FIG. 11 HEAVE ADDED MASS AND DAMPING COEFFICIENTS FOR A CATAMARAN

both vessels and in both modes are predicted near $va = 0.9$ which corresponds to the resonance frequency of the 3-D catamaran. As would be expected, large exciting forces are exerted on vessel 1 near the resonance frequency since vessel 1 is stationed in the standing wave system between the wharf and vessel 2. An important interference phenomenon noted was that the sway resonance is more pronounced than the heave resonance due to the effect of the permeable supporting structure under the wharf. A preliminary study using a 2-D formulation has shown that: (1) the heave and sway resonance phenomena are strongly suppressed by increasing the permeability of the wall and (2) the resonance frequency increases with increasing permeability of the wharf. For this particular case of a highly permeable supporting structure under the wharf, the transmitted waves provide a suction effect on both vessels which contributed to the large sway response.

Some of the dimensionless hydrodynamic coefficients calculated from the radiation problems are illustrated in Fig. 14. The added mass and damping coefficients are nondimensionalized by $2\rho Ab$ and $2\rho Ab$, respectively, where A now stands for submerged section area of each vessel. The resonance phenomena near $va = 0.9$ are also clearly demonstrated. An important interference phenomenon noted for this case is the negative added mass and the very small damping coefficients predicted in the range of $va > 1.2$, especially in the sway mode. This is in contrast to the catamaran results previously analyzed. The hydrodynamic responses of the vessels are strongly affected by these coefficients. Large responses are associated with both small fluid resistance (small damping) and small water pressure forces acting in the same direction as the vessel's motion (i.e., negative added mass). These responses are shown in Fig. 15 & 16. Large sway responses are predicted near $va = 1.3 \sim 1.4$ for both vessels. The relative sway motions between the two vessels are also seen to have a resonance peak at $va = 1.4$ where the motions are 180 degrees out-of-phase. The relative heave response is also seen to have a small resonance peak near $va = 1.3$.

Summary of FEM Analyses of Wave Interference. The diffraction and radiation of linear waves by multiple 3-D structures may be efficiently analyzed by a finite element method (FEM) algorithm which incorporates both radiation and permeable boundary dampers plus a fictitious bottom boundary that is required for applications in infinitely deep water. The validity and versatility of the finite element model for analyzing wave interference effects has been demonstrated for a variety of multiple structures (Huang, et al. 1983, and Leonard, et al., 1983). Included in the examples analyzed by Huang, et al (1983) were structures floating in deep water by incorporating a fictitious bottom in the diffraction and radiation functionals. In numerical experiments on different choices of the distance of this fictitious bottom below the structure, it was found that its effects on the numerical solutions are very small, except in

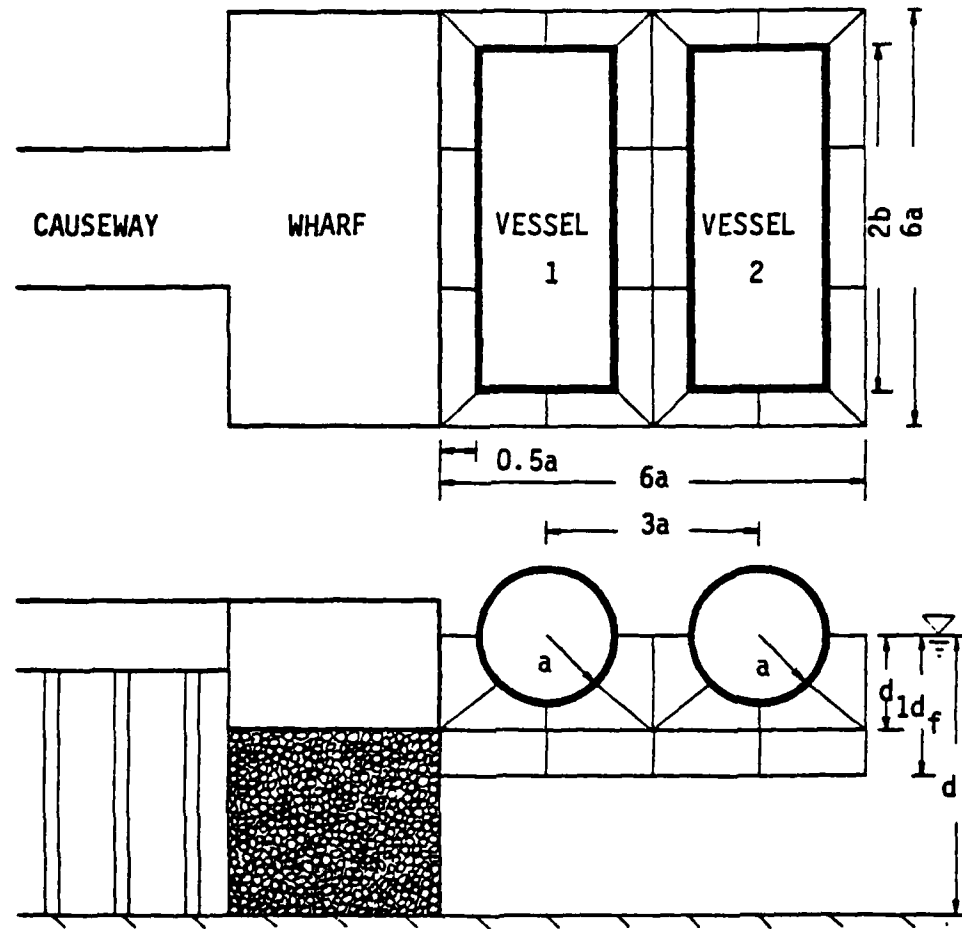


FIG. 12 DEFINITION SKETCH FOR LOADING/UNLOADING FACILITIES

$$(d/a = 4, d_1/a = 4/3, d_f/a = 2, 2b/a = 5)$$

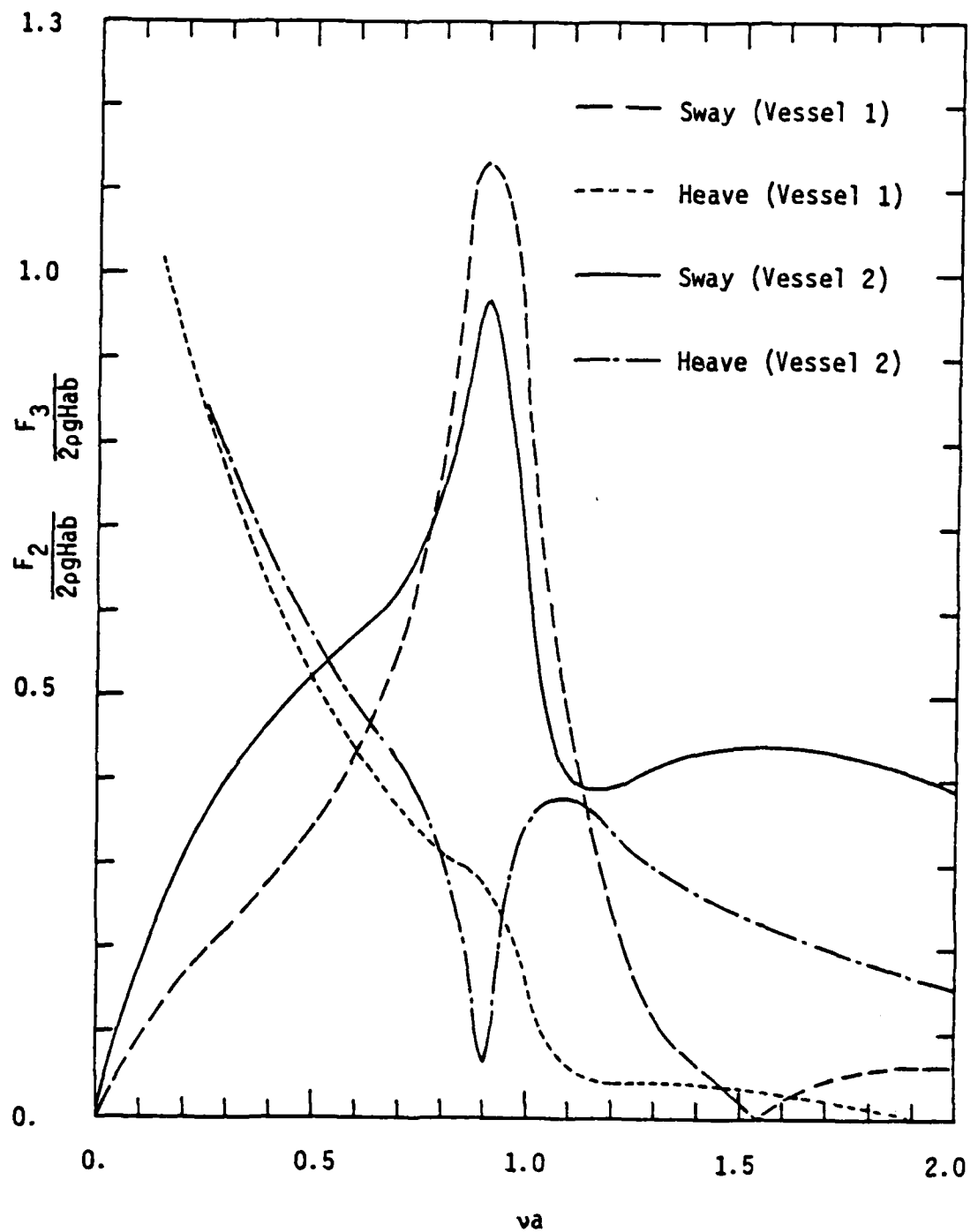


FIG. 13 EXCITING FORCES ON THE TWO VESSELS IN LOADING/UNLOADING FACILITIES
IN BEAM SEAS

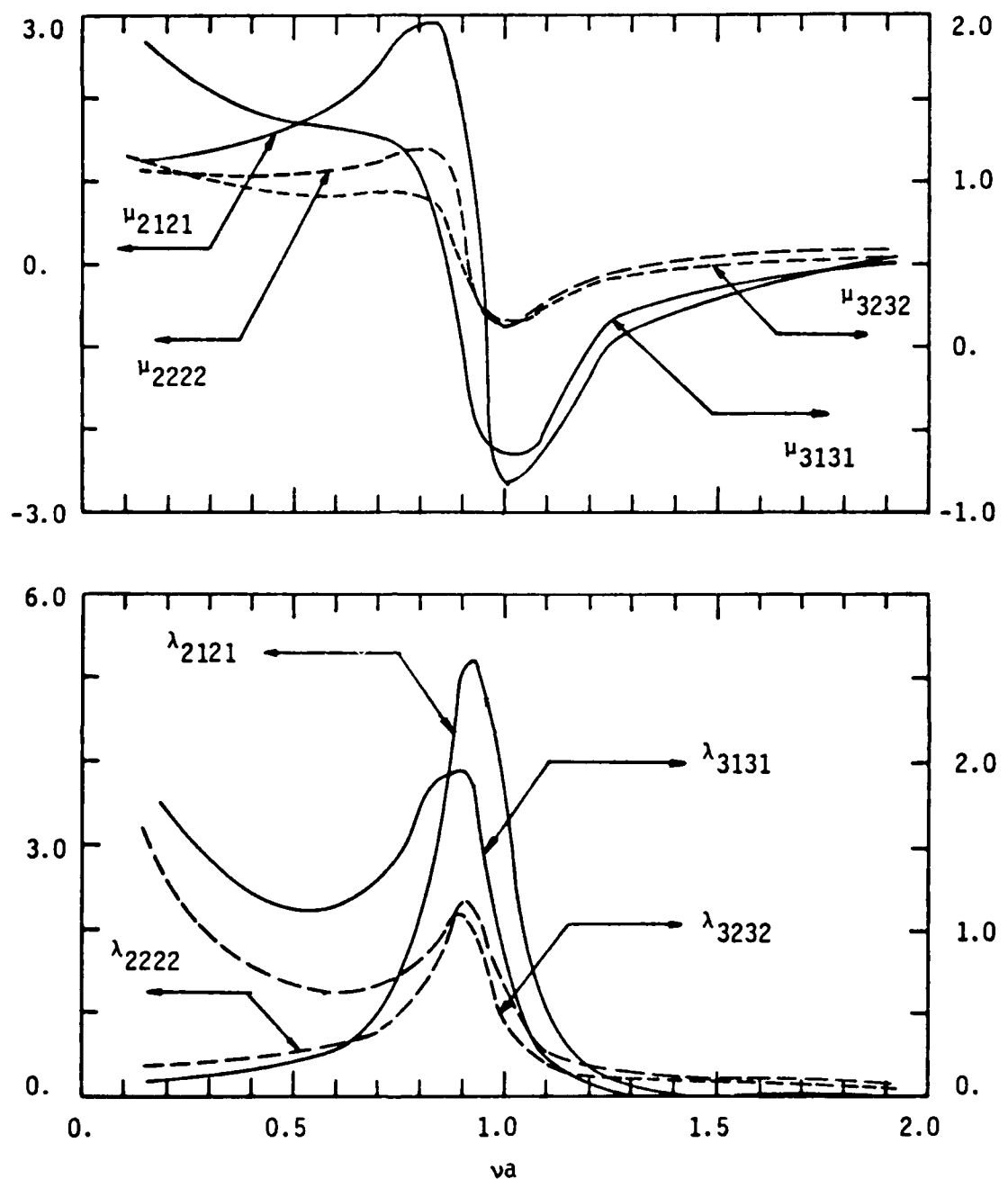


FIG. 14 HYDRODYNAMIC COEFFICIENTS OF THE TWO VESSELS IN
LOADING/UNLOADING FACILITIES

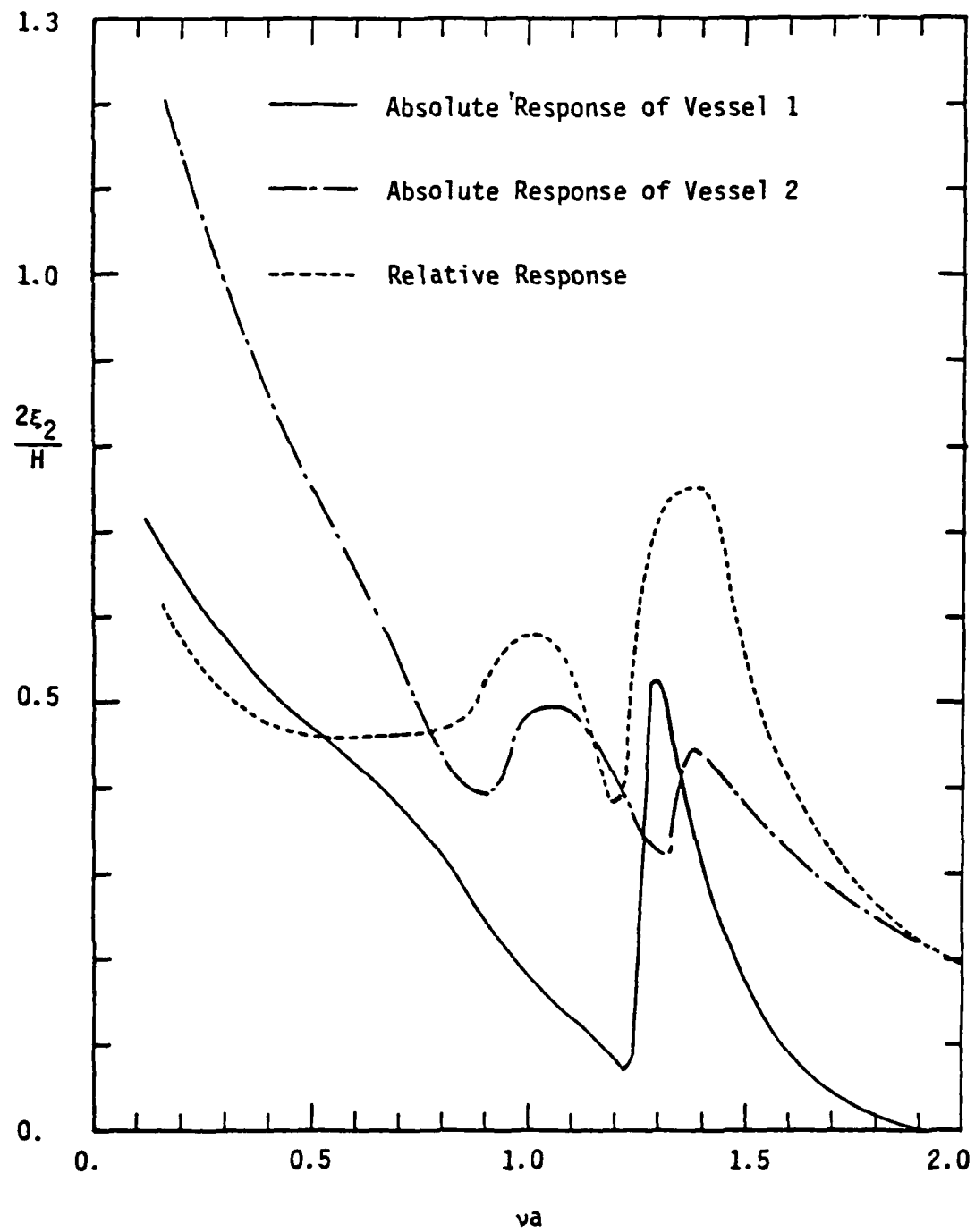


FIG. 15 SWAY RESPONSES FOR THE TWO VESSELS IN LOADING/UNLOADING FACILITIES IN BEAM SEAS

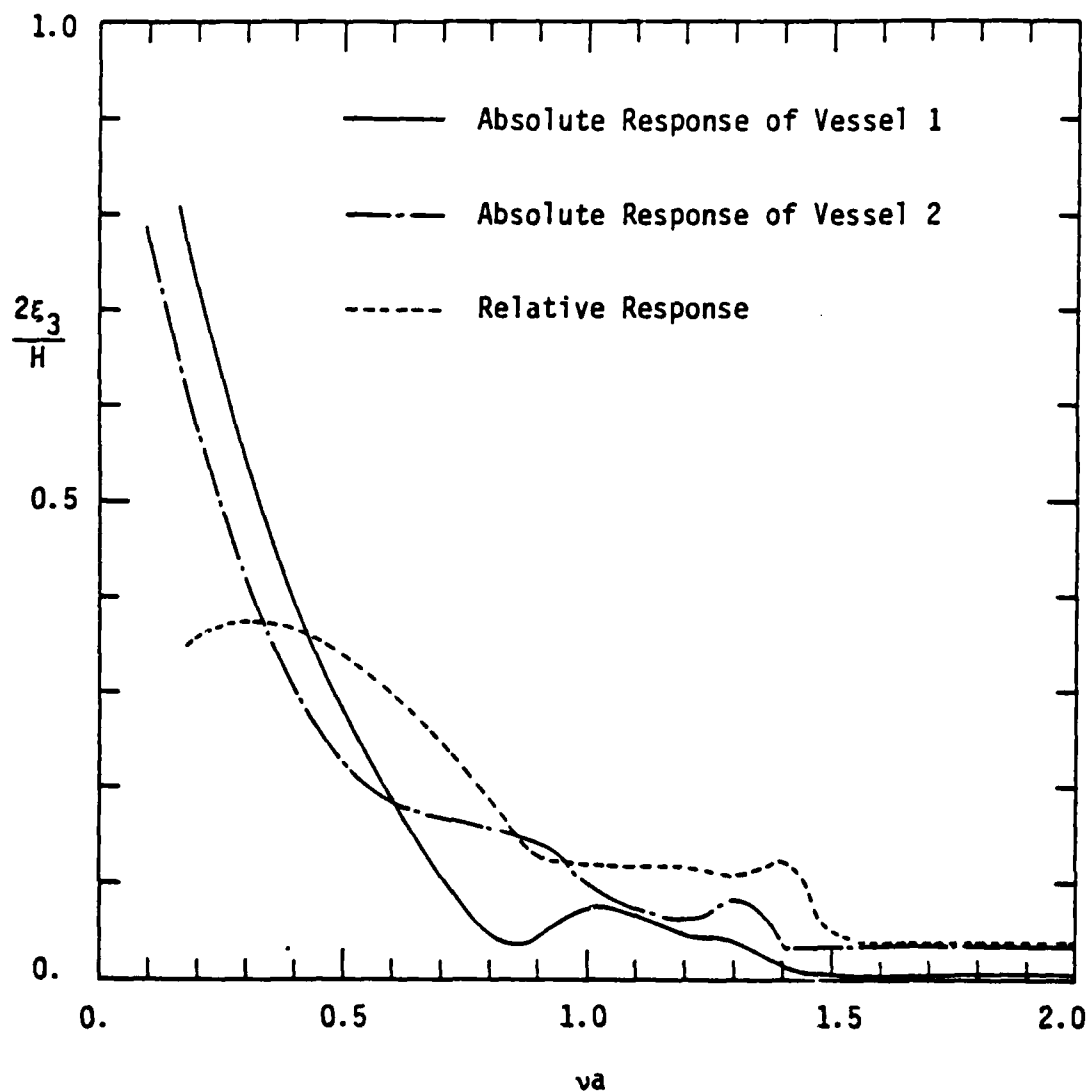


FIG. 16 HEAVE RESPONSES FOR THE TWO VESSELS IN LOADING/UNLOADING FACILITIES IN BEAM SEAS

the range of very long deep water waves. In this range, the solution accuracy was more dominated by the extent of the fluid domain in the radial directions. It was also demonstrated for a 3-D catamaran that the 3-D end effects increased the heave resonance frequency but decreased sharply the amplitude of the standing wave system between the two hulls. Good agreement was obtained between the finite element algorithm using boundary dampers and the Boundary Integral Method (BIM) where extensive use of explicit integration on the boundary is required in order to achieve equivalent computational efficiency. Some discrepancies between the two formulations of the finite element method were found to exist in the low frequency range. However, these discrepancies in the hydrodynamic exciting forces and restoring force coefficients are relatively unimportant in the computation of first order responses. No irregular frequencies were encountered using the FEM algorithm and, therefore, the same meshes could be used for a broad spectrum of wave frequencies. In analyzing the interference effects between multiple floating vessels and an adjacent wharf (part impermeable and part permeable) used as a ship loading/unloading facility, the effects of the permeable wharf were easily incorporated in the finite element formulation. The heave resonance between two vessels moored to the wharf was suppressed; while the sway resonance was strongly excited but at a higher frequency. These examples for wave interferences effects demonstrate the advantages of the FEM over the other two methods used for diffraction analyses. Still other examples in oblique waves have been given by Leonard, et al. (1983).

COMPARISONS OF TLP ANALYSES

Garrison (1982) analyzed by three different methods a typical TLP structure having four 50.0 ft. diameter legs with a draft of 110.0 ft. each and spaced 200.0 ft. apart. His comparisons included analyses by: 1) 3-D Green's function; 2) extended MacCamy-Fuchs (propagating mode only); and 3) Morison equation (slender body theory). His results are summarized in Figures 17-27. Since the 3-D Green's function is widely used for diffraction problems, the results of Garrison's (1982) comparisons are illustrative of the state-of-the-art applications.

Figures 17 and 18 show a comparison of the magnitude of the horizontal excitation force and moment computed for a single leg by MacCamy-Fuchs theory, by the Morison equation ($C_I = 2.0$, $C_D = .8$) and by the 3-D Green's function method. The results indicate that for $T > 8.0$ seconds the Morison equation gives good agreement with the 3-D Green's function but is grossly in error in the small period range. The MacCamy-Fuchs analysis gives excellent agreement for the small wave periods but gives results which are slightly high for the longer wave periods. The difference for large wave periods is a result of the flow around the lower truncated end of the cylinder which is not

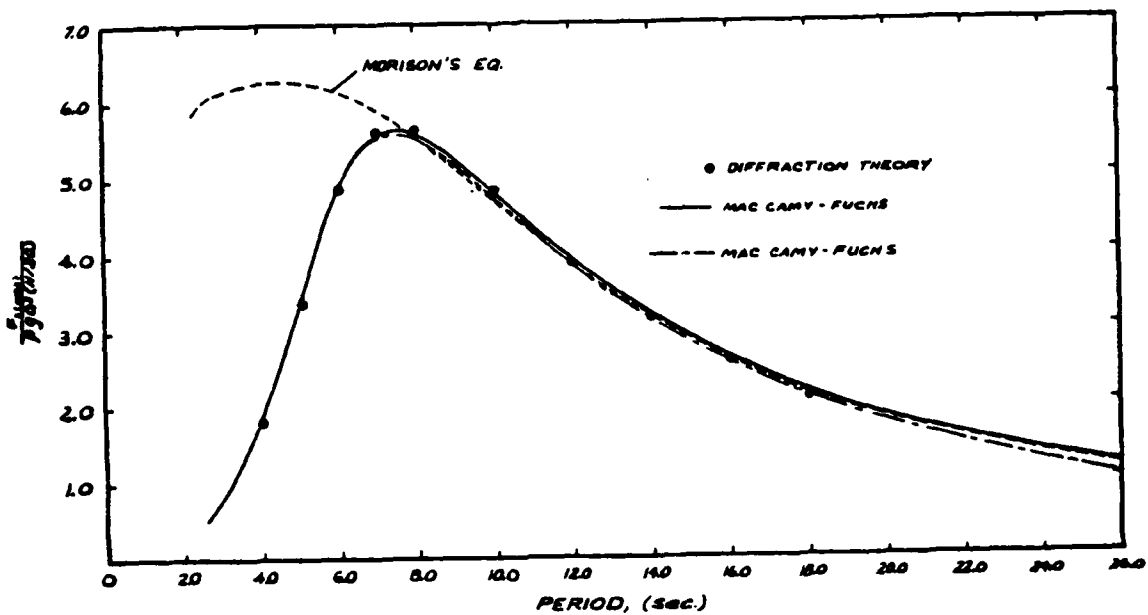


FIG. 17 HORIZONTAL FORCE COEFFICIENT FOR ONE LEG (Garrison, 1982)

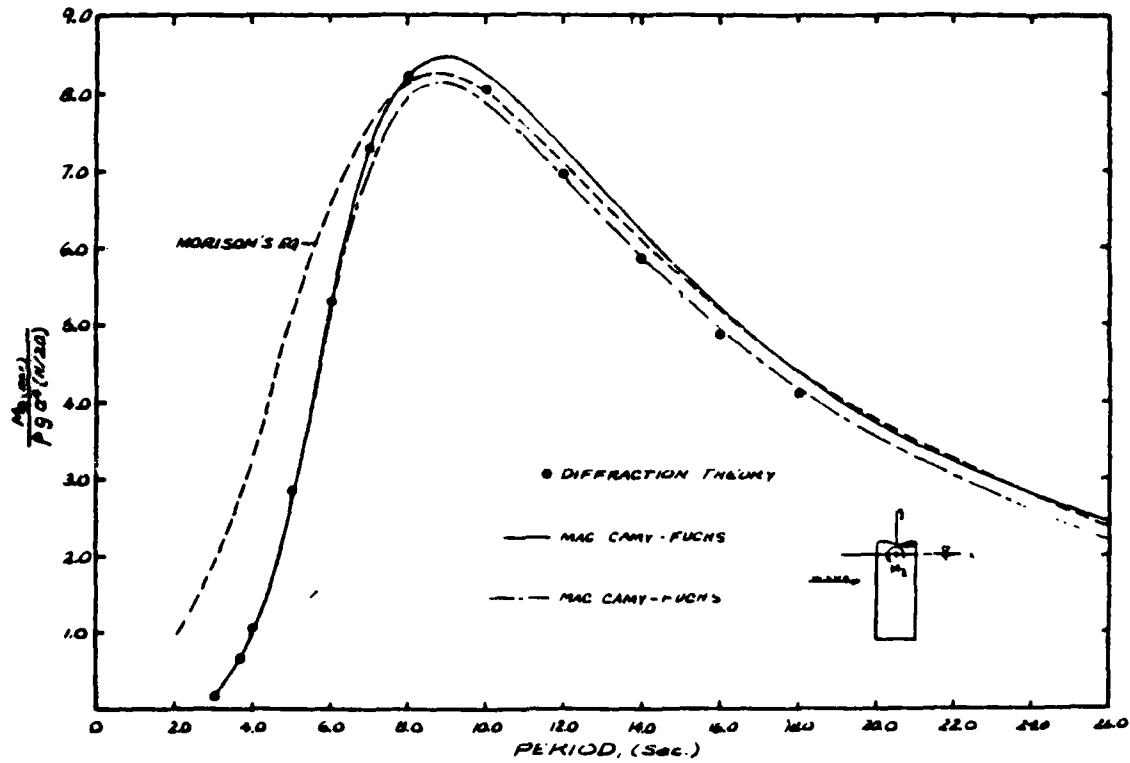


FIG. 18 MOMENT COEFFICIENT FOR ONE LEG (Garrison, 1982)

accounted for properly in the extended MacCamy-Fuchs theory which only uses the propagating-wave mode (Garrison, 1982).

Although the error is rather minor, an improvement can be made by reducing the inertia coefficient near the lower end of the cylinder to compensate for the three-dimensional flow effects. Garrison (1982) demonstrated that this correction makes the results agree almost exactly with the 3-D Green's function method throughout the entire wave period range.

Figure 19 shows the phase angle for the horizontal exciting force and moment. For a single cylinder, the phase angle is not particularly important; but in the analyses of structures having a number of members, the net excitation force is dependent on the relative phase angles of the individual members and, therefore, the phase angle is an important parameter. While the phase angle associated with Morison equation agrees with diffraction theory only for $T > 10.0$ seconds, the MacCamy-Fuchs theory shows good agreement at all frequencies (Garrison, 1982).

Garrison (1982) computed local sectional added mass and damping coefficients by the extended MacCamy-Fuchs theory. His results are compared with similar results computed by the 3-D Green's function method in Figures 20 and 21. These figures demonstrate that the added mass and radiation damping coefficients computed by the extended MacCamy-Fuchs theory (propagating mode only) compared very well with coefficients computed by the 3-D Green's function method. The linear surge mode radiation damping coefficients shown in Figure 20 are nearly identical.

Garrison's comparisons (1982) of the surge, heave and pitch mode hydrodynamic coefficients are shown in Figures 21 - 25. These figures show that all of the hydrodynamic coefficients computed by the MacCamy-Fuchs extended theory (propagating mode only) agree very well with the 3-D Green's function method for all wave periods. The results labeled Morison equation refer to coefficients based on a local sectional added mass coefficient of $C_m = 1.0$. This gives results for inertia coefficients which tend toward agreement with the 3-D Green's function method for large wave periods but which are, in general, too high due to neglecting the 3-D flow effects at the bottom of the leg (Garrison, 1982).

The damping coefficients for a single leg are shown in Figures 24 and 25. Again, the results labeled MacCamy-Fuchs agree well with the results labeled diffraction theory. Also shown in these figures is viscous damping computed by the linearized Morison equation with $C_D = 0.8$. The viscous damping is, of course, nonlinear and, therefore, the coefficients depend on the amplitude of the relative motion between the water and the member. These results indicate that the surge response of the TLP would have to become rather large

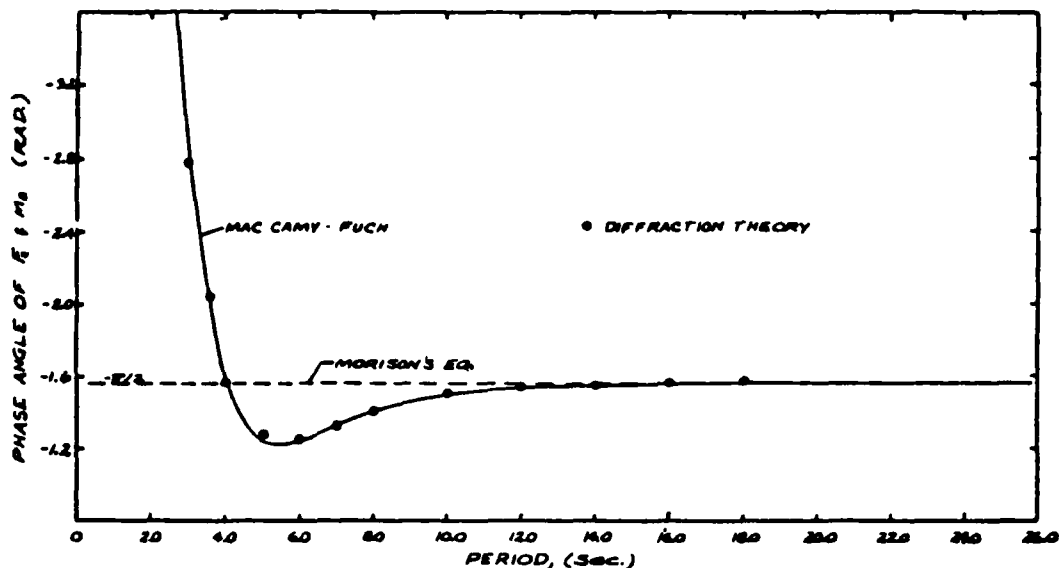


FIG. 19 PHASE ANGLE OF THE HORIZONTAL FORCE AND MOMENT (Garrison, 1982)

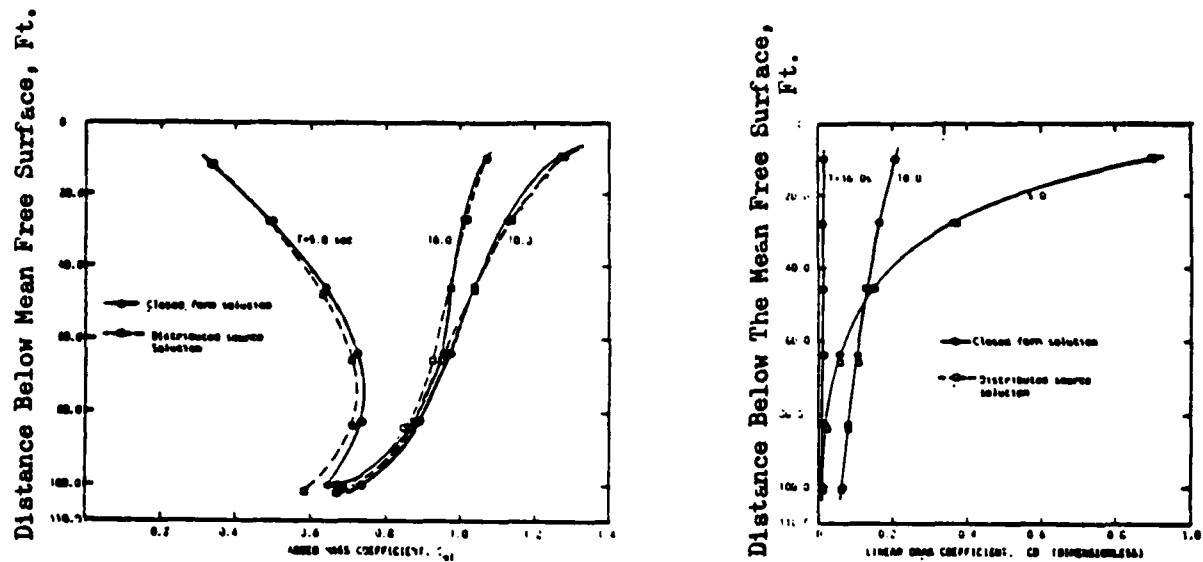


FIG. 20 ADDED MASS AND LINEAR RADIATION DRAG COEFFICIENT ON A TLP LEG IN SURGE (Garrison, 1982)

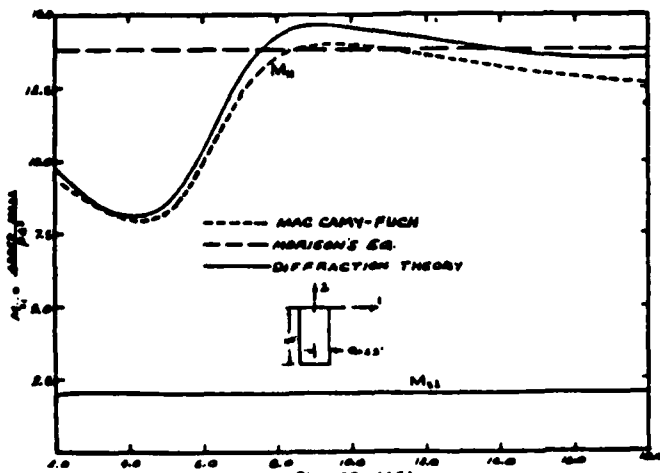


FIG. 21 HEAVE AND SURGE ADDED MASS COEFFICIENT (Garrison, 1982)

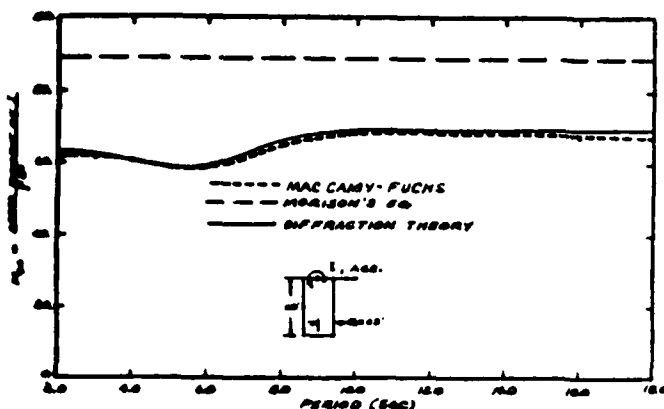


FIG. 22 ADDED MOMENT OF INERTIA IN PITCH:
A DIFFRACTION THEORY (Garrison, 1982)

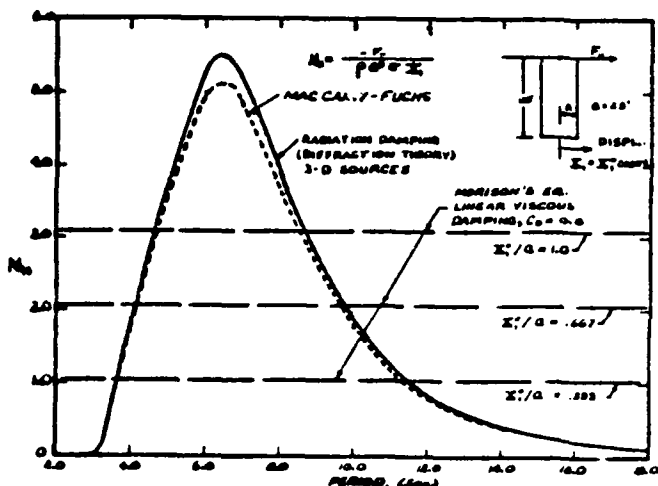


FIG. 24 RADIATION AND VISCOS SURGE DAMPING
FOR ONE LEG (Garrison, 1982)

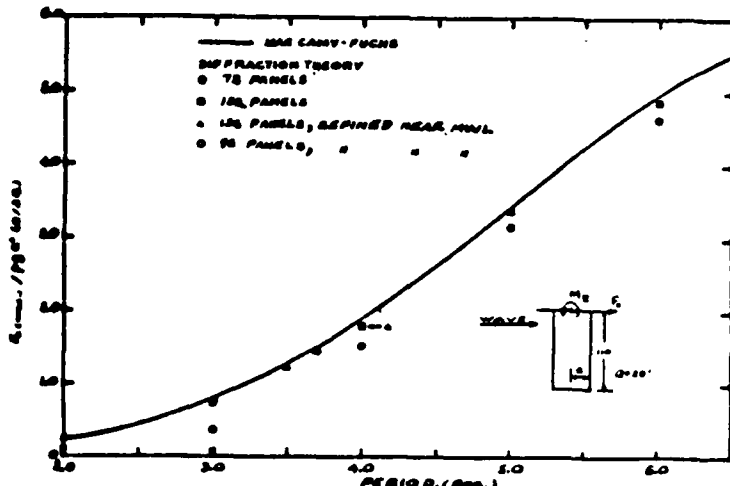


FIG. 26 HORIZONTAL FORCE COEFFICIENT FOR ONE
LEG AT SMALL PERIOD (Garrison, 1982)

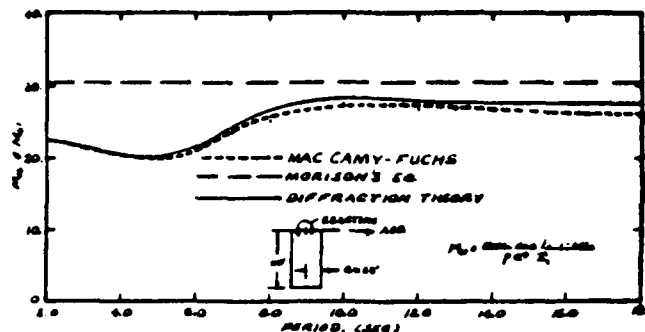


FIG. 23 PITCH-SURGE ADDED MASS COUPLING
COEFFICIENT (Garrison, 1982)

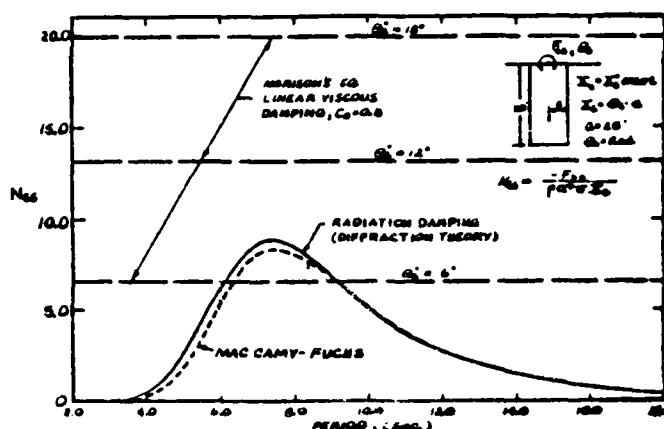


FIG. 25 RADIATION AND VISCOS PITCH
DAMPING FOR ONE LEG (Garrison, 1982)

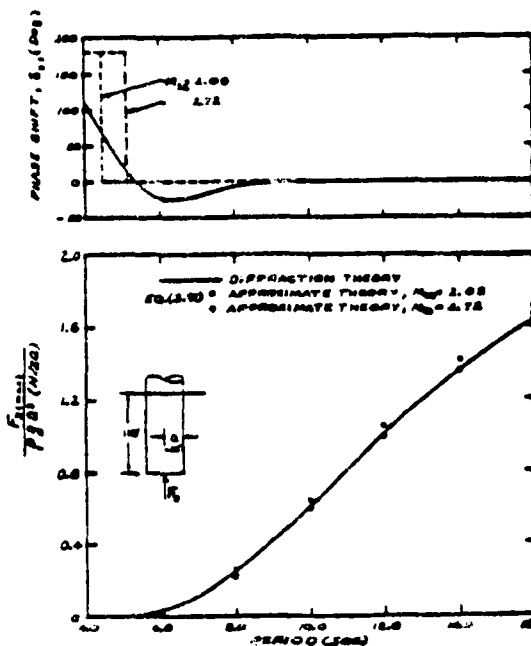


FIG. 27 COMPARISON OF AN APPROX.
FORMULA FOR VERTICAL FORCE ON
A LEG WITH DIFFRACTION THEORY
(Garrison, 1982)

before viscous damping would become comparable to radiation damping (Garrison, 1982).

Figure 26 demonstrates an important result that the extended MacCamy-Fuchs theory (propagating mode only) gives essentially an exact solution for the excitation loads at high-frequency. This is because the wave action does not penetrate down to the lower end of the cylinder. The 3-D Green's function analysis on the other hand requires some care in the discretization of the leg near the water-line in order to model this sharp decay of the wave action with depth.

In Figure 27, Garrison (1982) compares the approximate vertical exciting force with the results of the 3-D Green's function method. The value of $M_{22} = 2.05$ which was obtained from Figure 21 appears to give results which are slightly too high. Figure 27 shows that a value of $M_{22} = 2.72$ gives a better fit to the results computed by the 3-D Green's function.

Results for Four Legs: Interaction Effects (Garrison, 1982).

The computing effort required to evaluate hydrodynamic coefficients for four legs, including interaction effects between legs, is much greater than evaluating coefficients for a single leg; i.e., disregarding the interaction effects. Garrison (1982) has evaluated the magnitude of these interaction effects for a typical TLP. A similar analysis has been given by Paulling (1981).

The horizontal excitation force, moment and vertical excitation force are shown in Figures 28-30 for four legs. These figures compare diffraction theory both with and without interaction and the Morison equation ($C_I = 2.0$ and $C_D = 0.8$). The results indicate that, in general, interaction effects are rather minor and become essentially zero in the small wave period range. The results also show that the Morison equation gives very poor results in the small wave period range. The vertical force computed using heave mode added mass $M_{22} = 2.72$ agrees well with the 3-D Green's function theory because interaction effects are negligible (Garrison, 1982).

Garrison's comparisons (1982) for the added mass coefficients including the effects of interaction are presented in Figures 31-33. In his example, interaction effects on the added mass coefficients are relatively small in general. Moreover, since the total mass matrix is the sum of the added mass plus the structural mass, the error in the total mass matrix resulting from disregarding interaction effects tends to be less important than might be expected from Figures 31-33 alone.

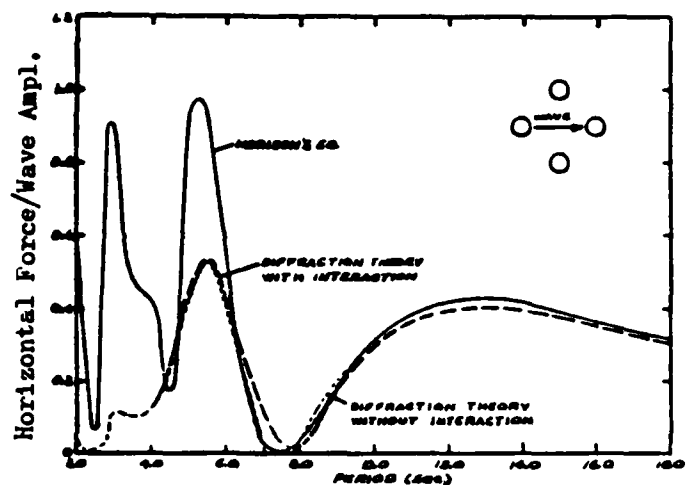


FIG. 28 HORIZONTAL WAVE FORCE ACTING ON FOUR LEGS (Garrison, 1982)

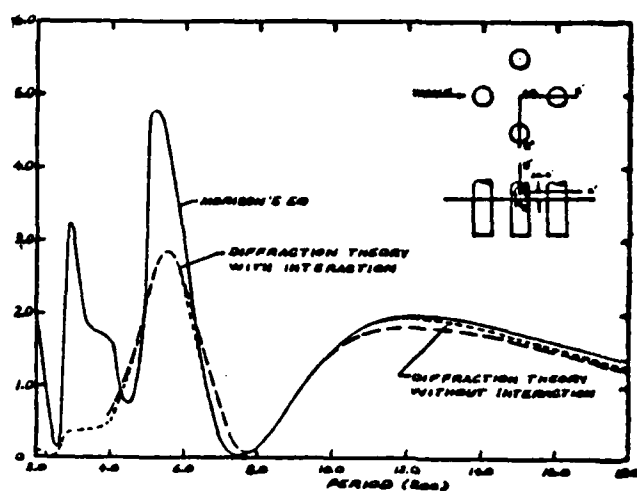


FIG. 29 WAVE INDUCED MOMENT ACTING ON FOUR LEGS (Garrison, 1982)

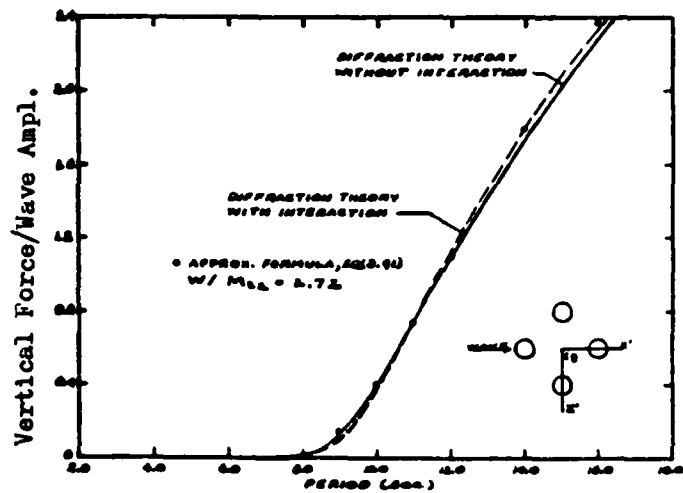


FIG. 30 VERTICAL WAVE FORCE ACTING ON FOUR LEGS (Garrison, 1982)

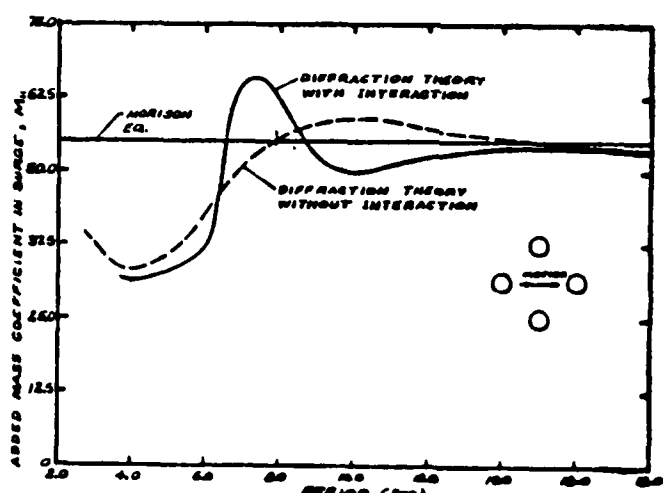


FIG. 31 SURGE ADDED MASS COEFFICIENT FOR FOUR LEGS (Garrison, 1982)

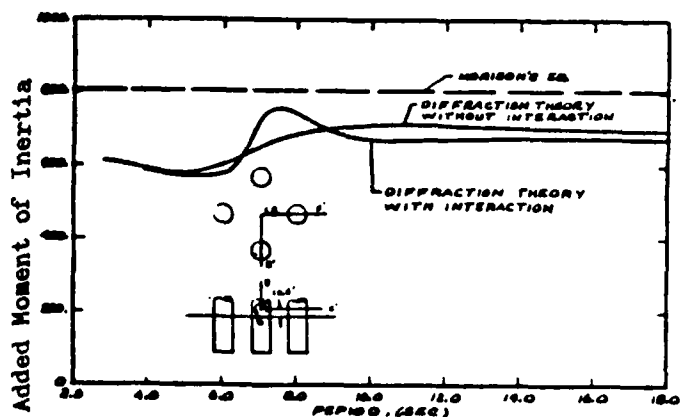


FIG. 32 ADDED MOMENT OF INERTIA COEFFICIENT FOR FOUR LEGS (Garrison, 1982)

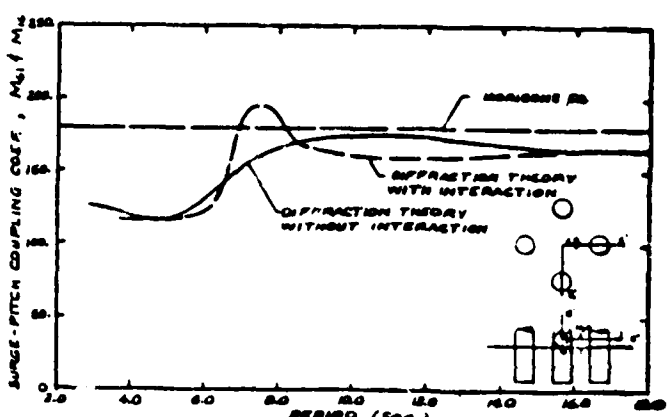


FIG. 33 SURGE-PITCH ADDED MASS COUPLING COEFFICIENT FOR FOUR LEGS (Garrison, 1982)

Garrison's comparisons (1982) of the interaction effects on the damping coefficients are shown in Figures 34-36. These figures show that interaction effects play a major role in damping over the complete wave period range. However, damping does not play a major role in the motion response of TLPs so that disregarding interaction effects on damping may not be as important as might appear from these figures.

Garrison's comparisons (1982) also included the dynamic response of the TLP shown schematically in Figure 37 in order to compare the Morison equation with the 3-D Green's function theory and to determine the effects of interaction between legs. Garrison (1982) analyzed the small-diameter members using the Morison equation (or slender body theory) with $C_m = 1.0$, $C_D = 0.8$. A design wave height of $H = 10.0$ feet was used and a linear drag coefficient was computed by iteration. His results, however, indicated essentially no wave amplitude effects. Results computed on the basis of the MacCamy-Fuchs theory were not given because the previous analysis showed that these results would be almost identical to the results of the 3-D Green's function theory without including interaction effects.

Figure 38 shows the surge response for two different mooring conditions. Due to the small stiffness of the platform in the surge direction, the response at wave periods less than 9.0 seconds is quite small. It is also only in this wave period range that significant differences exist between the two methods (Garrison, 1982).

The heave response is shown in Figure 39 in which resonance occurred at a wave period of about $T = 2.8$ seconds. There is essentially no difference between the Morison equation and the 3-D Green's function method due to the negligible free surface effects on the vertical hydrodynamic coefficients.

The pitch response is shown in Figure 40 where a resonance peak occurred at about $T = 3.4$ seconds. Garrison's results (1982) showed a difference between the various methods of dealing with the legs in the intermediate wave period range. It would appear that both the heave and pitch resonance which occurred at high-frequency could be excited both by high-frequency linear forces or by second-order forces arising from longer period waves.

Figure 41 shows calculations for the dynamic tendon tension corresponding to the three different methods of dealing with the legs. In the 4-8 second wave period range, the three methods give very different results. A great deal of long-term wave action occurs in this wave period range which makes these differences significant from the viewpoint of the platform motions and of fatigue analyses.

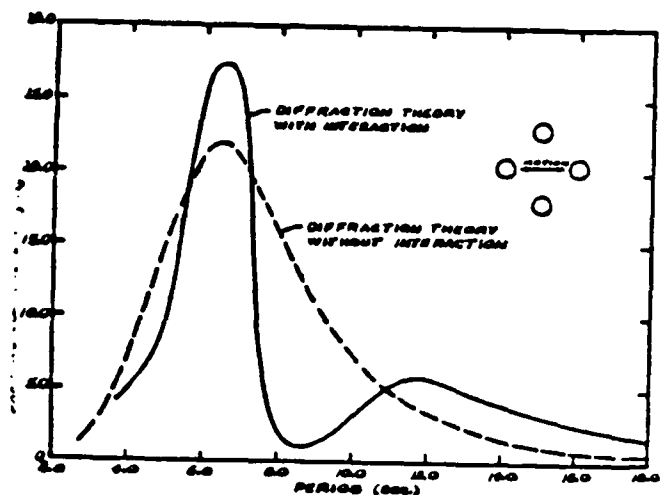


FIG. 34 SURGE DAMPING COEFFICIENT FOR
FOUR LEGS (Garrison, 1982)

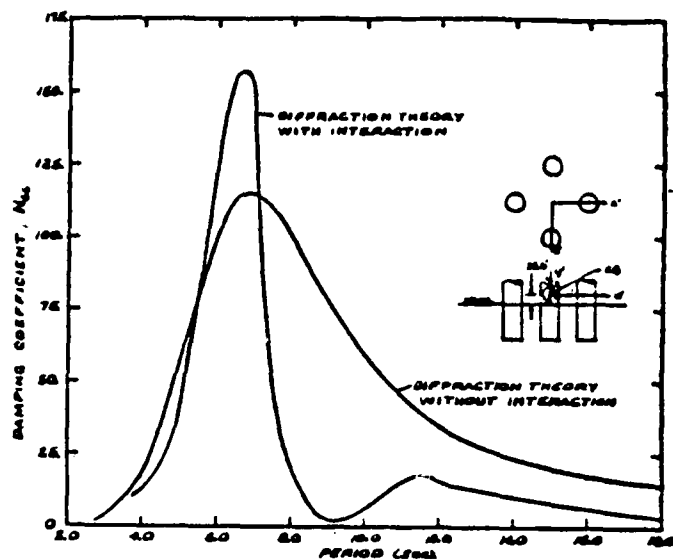


FIG. 35 PITCH DAMPING COEFFICIENT FOR FOUR LEGS (Garrison, 1982)

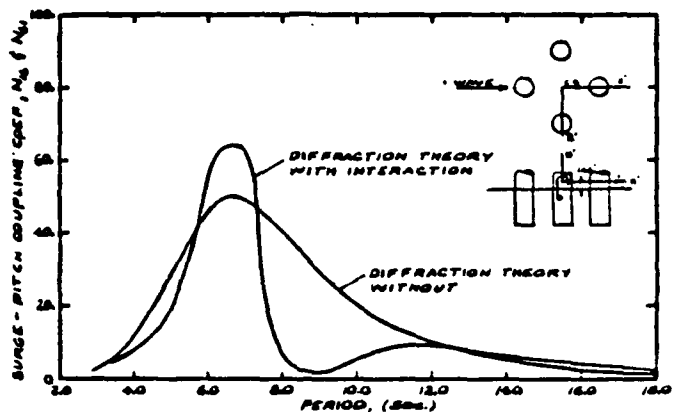


FIG. 36 SURGE-PITCH DAMPING COEFFICIENT FOR FOUR LEGS (Garrison, 1982)

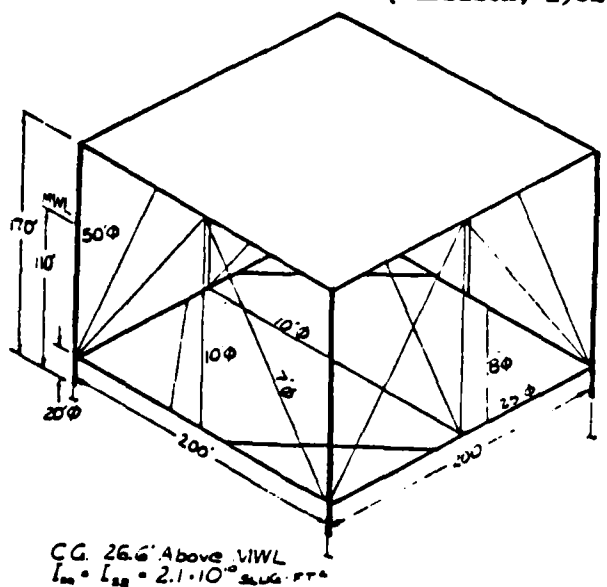


FIG. 37 SCHEMATIC DIAGRAM OF TLP
(Garrison, 1982)

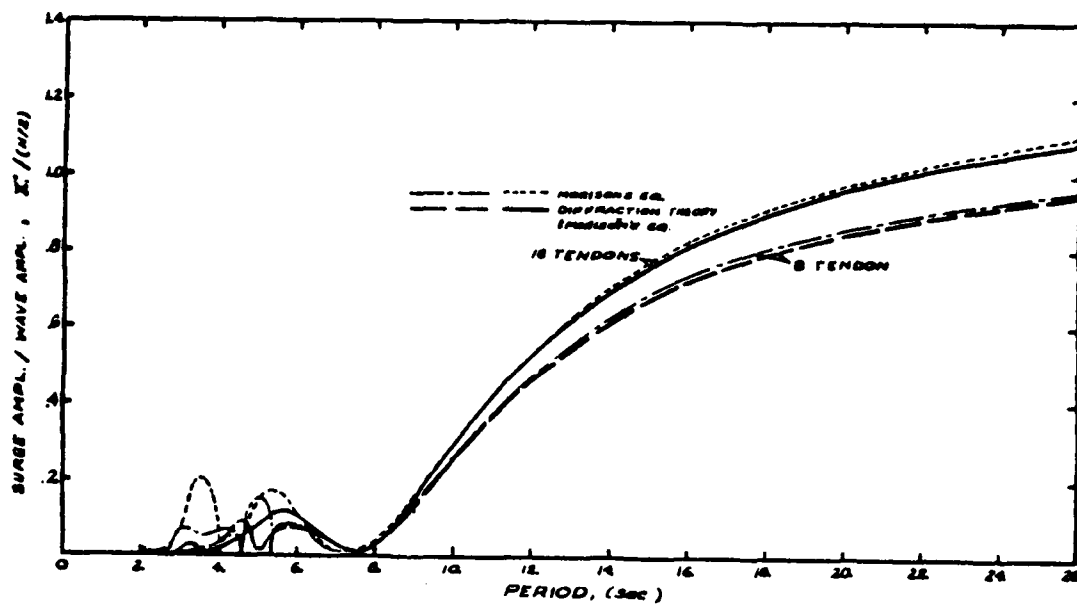


FIG. 38 RESPONSE OF TLP IN SURGE
(Garrison, 1982)

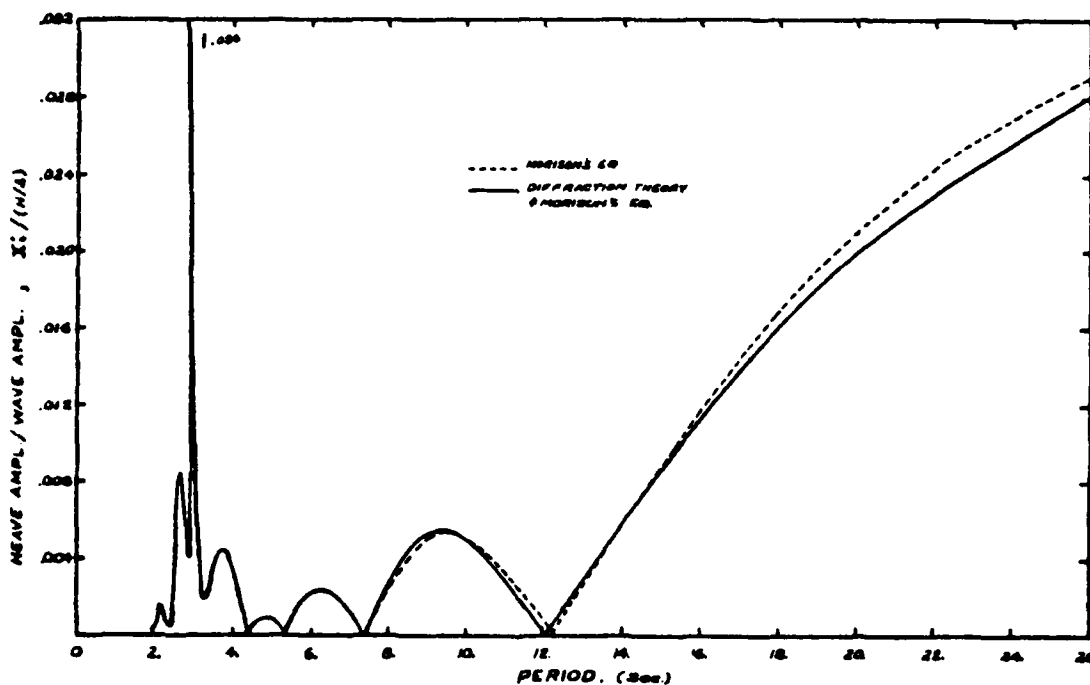


FIG. 39 RESPONSE OF TLP IN HEAVE
(Garrison, 1982)

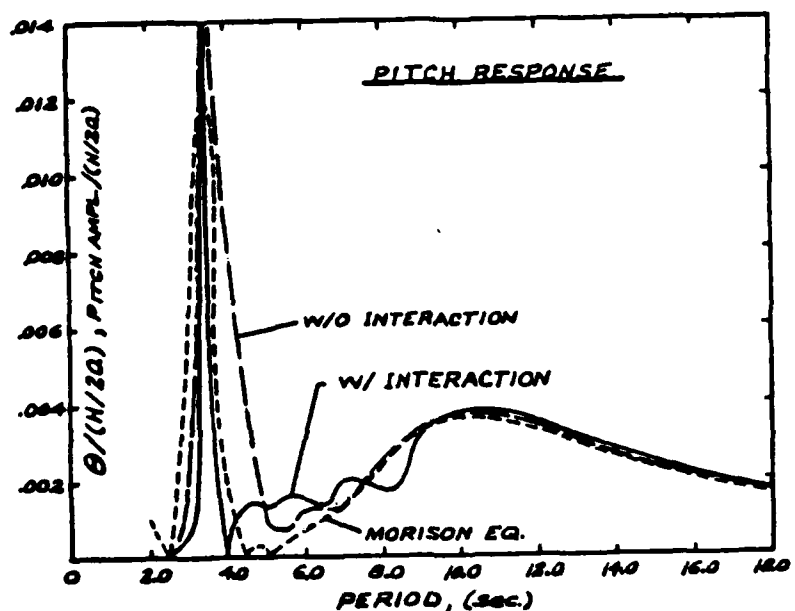


FIG. 40 RESPONSE OF TLP
(Garrison, 1982)

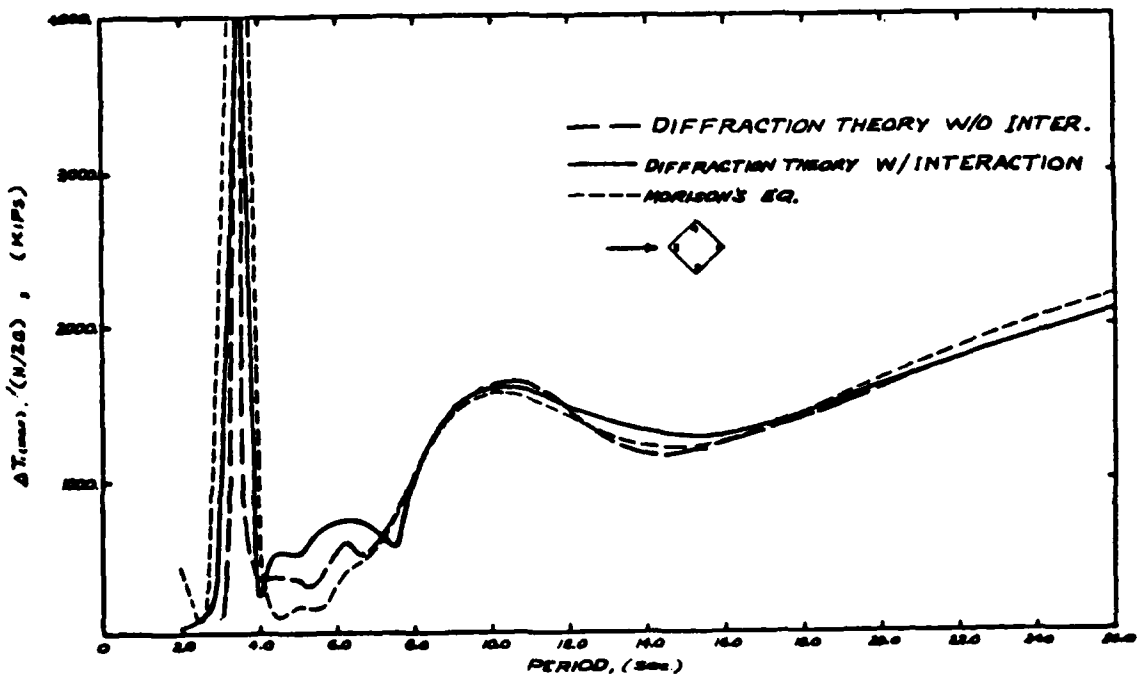


FIG. 41 DYNAMIC TENDON TENSION
(Garrison, 1982)

Figure 42 shows the mean drift-force computed for the legs only. These results indicate that it is only the short period waves which produce drift forces due to radiation of waves. The results in Figure 42 were computed by the 3-D Green's function method including interaction effects (Garrison, 1982).

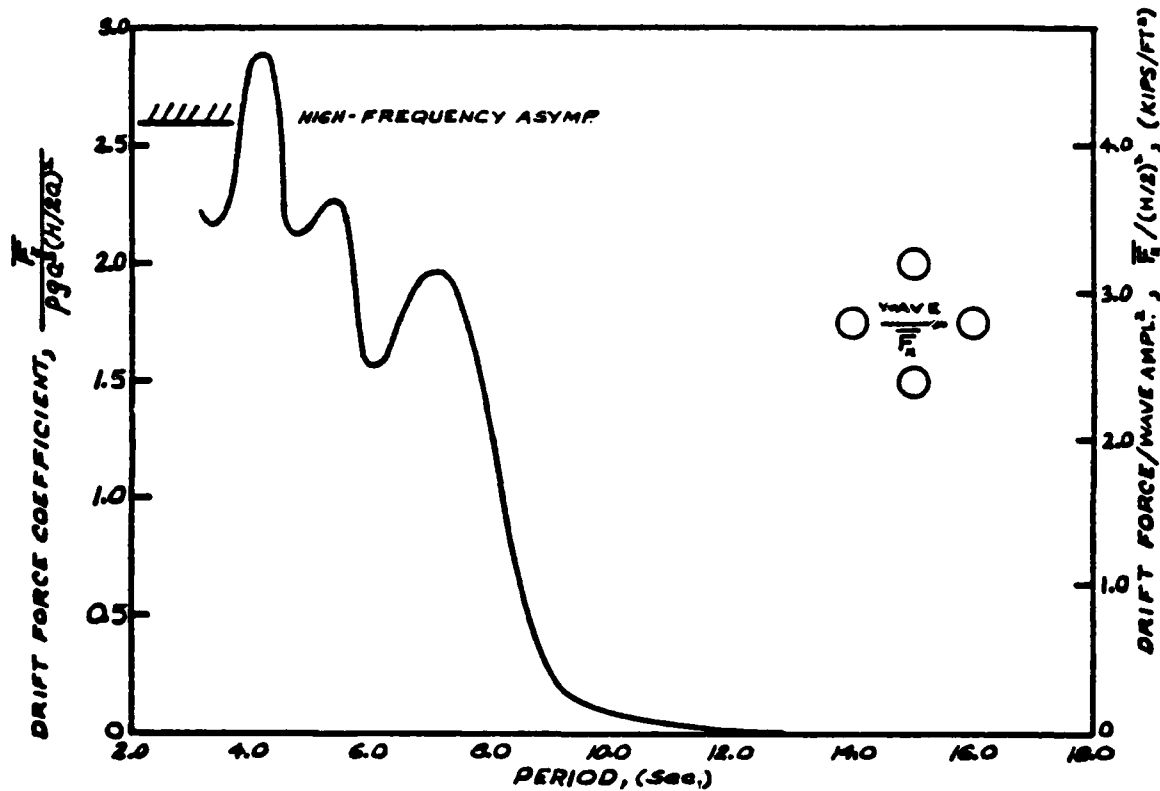


FIG. 42 MEAN DRIFT-FORCE
(Garrison, 1982)

SUMMARY

Morison Equation (slender members)

The effects of wake interaction and marine roughness significantly influence the drag force coefficients. The condition of the data significantly affect the inertia and drag coefficients computed from measured data. Wave-current interaction and relative-motion structural responses influence inertia and drag force coefficients in a manner that is not presently well-understood. All of the topics deserve in-depth research for the NCEL platform program.

Diffraction Theory (large members)

The finite element method (FEM) using boundary dampers is computationally efficient and avoids some of the problems found in 3-D Green's function algorithm (e.g. numerically evaluating Cauchy principal value singular integrals and the irregular John's frequencies). Interaction between large members and small members deserves further research and experimental verification.

REFERENCES

Apelt, C.J. and McKnight, A., 1976, "Wave Action on Large Off-Shore Structures," Proc., 15th Coastal Engineering Conference, Honolulu, Hawaii.

Bettess, P. and Zienkiewicz, O.C., 1977, "Diffraction and Refraction of Surface Waves Using Finite and Infinite Elements," International Journal for Numerical Methods in Engineering, Vol. 11, pp. 1271-1290.

Chakrabarti, S.K., 1975, "Second-Order Wave Force on Large Vertical Cylinder," Journal of the Waterways, Harbors and Coastal Engineering Div., ASCE, Vol. 101, No. WW3, August, pp. 311-317.

Chakrabarti, S.K., 1978, "Wave Forces on Multiple Vertical Cylinders," Journal of Waterway, Port, Coastal and Ocean Div., ASCE, Vol. 104, No. WW2, Proc. Paper 13727, pp. 147-161.

Dalrymple, R.A., 1973, "Water Wave Models and Wave Forces with Shear Currents," Univ. of Florida, Gainesville, Coastal Engineering Laboratory, Tech. Report 20.

Dalrymple, R.A., 1974, "Models for Nonlinear Water Waves on Shear Currents," Proc., Offshore Technology Conference, Paper No. OTC 2114, Vol. II, pp. 843-856.

Dalton, C. and Nash, J.M., 1976, "Wave Slam on Horizontal Members of an Offshore Platform," Proc., Offshore Technology Conference, Paper No. 2500, Vol. 1, pp. 769-780.

Dean, R.G. and Aagaard, P.M., 1970, "Wave Forces: Data Analysis and Engineering Calculation Method," Journal Petroleum Technology, March, pp. 368-375.

Dean, R.G., 1976, "Methodology for Evaluating Suitability of Wave and Wave Force Data for Determining Drag and Inertia Coefficients," Proceedings BOSS '76, Vol. 2, Trondheim, Norway, pp. 40-64.

Eatoek-Taylor, R. and Zietsman, J., 1981, "A Comparison of Localized Finite Element Formulations for Two-Dimensional Wave Diffraction and Radiation Problems," International Journal for Numerical Methods in Engineering, Vol. 17, pp. 1355-1384.

Forristall, G. Z., 1974, "Three-Dimensional Structure of Storm-Generated Currents," Journal of Geophysical Research, Vol. 79, No. 18, June 20, pp. 2721-2729.

Forristall, G.Z., Ward, E.G., Borgman, L.E. and Cardone, V.J., 1978, "Storm Wave Kinematics," Proc., Offshore Technology Conference, Vol. III, pp. 1503-1514.

Garrett, C.J.R., 1971, "Wave Forces on a Circular Dock," Journal of Fluid Mechanics, Vol. 46, Pt. 1, pp. 129-139.

Garrison, C.J., Gehrmann, F.H., and Perkinson, B.T., 1975, "Wave Forces on Bottom-Mounted Large-Diameter Cylinder," Journal of the Waterways, Harbors and Coastal Engineering Div., ASCE, Vol. 101, No. WW4, November, pp. 343-356.

Garrison, C.J., 1976, "Consistent Second-Order Diffraction Theory," Abstract, 15th Coastal Engineering Conference, Honolulu, Hawaii.

Garrison, C.J., Fields, J.B., and May, M.D., 1977, "Drag and Inertia Forces on a Cylinder in Periodic Flow," ASCE, Journal of Waterways, Port, Coastal and Ocean Div., Vol. 103, WW2, May.

Garrison, C.J., 1978, "Hydrodynamic Loading of Large Offshore Structures," Ch. 3 in Numerical Methods in Offshore Engineering, editors O.C. Zienkiewicz, R.W. Lewis, and K.G. Stagg, John Wiley and Sons, pp. 87-140.

Garrison, C.J., 1982, "Forces on Semi-Submerged Structures," Proceedings Ocean Structural Dynamics Symposium '82, Corvallis, OR, Oregon State University, Sept. 8-10, pp. 28-54.

Hafskjold, P.S., Torum, A. and Eie, J., 1973, "Submerged Offshore Concrete Tanks," International Navigation Congress, Ottawa.

Heideman, J.C., Olsen, O.A., and Johansson, P.I., 1979, "Local Wave Force Coefficients," Proceedings Civil Engineering in the Ocean, IV, ASCE, Vol. II, Sept. 10-12, pp. 684-699.

Ho, R.T. and Harten, A., 1975, "Green's Function Techniques for Solutions of Floating Body Problems," Proceedings Civil Engineering in the Ocean III, ASCE, Univ. of Delaware, Vol. 3, pp. 939-958.

Hogben, N. and Standing, R.G., 1975, "Experience in Computing Wave Loads on Large Bodies," Proc., Offshore Technology Conference, Paper No. OTC 2189, Vol. I, pp. 413-437.

Huang, M-C, 1983, "Finite Element Analysis of Wave Interference Effects Between Large Structures," Thesis presented to the Oregon State University, Corvallis, OR, in partial fulfillment of the requirements for the degree of Doctor of Philosophy.

Huang, M-C, Leonard, J.W., and Hudspeth, R.T., 1983, "FEM Solution of 3-D Wave Interference Problems," ASCE, Journal of Waterways, Port, Coastal and Ocean Engineering Division, (in review).

Hudspeth, R.T. and Leonard, J.W., 1982, "Dynamic Wave-Platform-Restraint Interaction for Tension Leg Platforms," Proceedings Ocean Structural Dynamics Symposium, 1982, Corvallis, OR, Oregon State University, Sept. 8-10, pp. 604-631.

Hunt, J.N. and Baddour, R.E., 1981, "The Diffraction of Nonlinear Progressive Waves by a Vertical Cylinder," Quarterly Journal of Applied Mathematics, Vol. XXXIV, Pt. 1, pp. 69-87.

Isaacson, M., 1977, "Shallow Wave Diffraction Around Large Cylinders," Journal of the Waterways, Port, Coastal and Ocean Div., ASCE, Vol. 103, No. WW1, February, pp. 69-82.

Isaacson, M., 1978, "Vertical Cylinders of Arbitrary Section in Waves," Journal of Waterways, Port, Coastal and Ocean Div., ASCE, Vol. 104, No. WW4, Proc. Paper 13973, pp. 309-324.

Isaacson, M., 1982, "Nonlinear Wave Effects on Fixed and Floating Bodies," Journal of Fluid Mechanics, Vol. 120, pp. 267-281.

Kaplan, P. and Silbert, M.N., 1976, "Impact Forces on Platform Horizontal Members in the Splash Zone," Proc. I, Offshore Technology Conference, Paper No. 2498, Vol. 1, pp. 751-768.

Keulegan, G.H. and Carpenter, L.H., 1958, "Forces on Cylinders and Plates in Oscillating Fluids," Journal of Research of the National Bureau of Standards, Vol. 60, No. 5, pp. 423-440.

Kim, Y.Y. and Hibbard, H.C., 1975, "Analysis of Simultaneous Wave Force and Water Particle Velocity Measurements," Offshore Technology Conference, OTC Paper 2192.

Lebreton, J.C. and Cormault, P., 1969, "Wave Action on Slightly Immersed Structures, Some Theoretical and Experimental Considerations," Proceedings of the Symposium Research on Wave Action, Delft, Netherlands.

Leonard, J.W., Garrison, C.J., and Hudspeth, R.T., 1981, "Deterministic Fluid Forces on Structures: A Review," ASCE Jour. Structural Div., v. 107, ST6, pp. 1041-1057.

Leonard, J.W., Huang, M-C., and Hudspeth, R.T., 1983, "Hydrodynamic Interference Between Floating Cylinders in Oblique Seas," Applied Ocean Research, (in press).

MacCamy, R.C. and Fuchs, R.A., 1954, "Wave Forces on Piles: A Diffraction Theory," U.S. Army Corps of Engineers, Beach Erosion Board, Technical Memo, No. 69.

Maeda, H., 1974, "Hydrodynamical Forces on a Cross-Section of a Stationary Structure," Proceedings International Symposium on the Dynamics of Marine Vehicles and Structures, Univ. College, London, pp. 80-90.

Matsui, T. and Tamaki, T., 1981, "Hydrodynamic Interaction Between Groups of Vertical Axisymmetric Bodies Floating in Waves," International Symposium on Hydrodynamics in Ocean Engineering, The Norwegian Inst. of Tech., Trondheim, Norway, pp. 817-836.

Mei, C.C., 1978, "Numerical Methods in Water-Wave Diffraction and Radiation," Annual Review Fluid Mechanics, Vol 10, pp. 393-416.

Miller, B.L., 1977, "The Hydrodynamic Drag of Roughened Circular Cylinders," Journal of the Royal Inst. of Naval Architects, Vol. 119, March.

Morison, J.R., O'Brien, M.P., Johnson, J.W. and Schaaf, S.A., 1950, "The Force Exerted by Surface Waves on Piles," Petroleum Transactions, Vol. 189, TP 2846, pp. 149-154.

Nath, J.H. and Wankmuller, R.N., 1982, "Wave Forces on Kelp Covered Horizontal Cylinders," Proceedings, Ocean Structural Dynamics Symposium '82, Oregon State University, Corvallis, OR., pp. 259-277.

Nath, J.H., 1982, "Heavily Roughened Horizontal Cylinders in Waves," BOSS '82, M.I.T.

Ohkusu, M., 1974, "Hydrodynamic Forces on Multiple Cylinders in Waves," Proceedings International Symposium on the Dynamics of Marine Vehicles and Structures, Univ. College, London, pp. 107-112.

Ohkusu, M., 1976, "Ship Motions in Vicinity of a Structure," Proceedings of the First Conference on the Behavior of Offshore Structures, BOSS' 76, Trondheim, Norway, Vol. I, pp. 284-306.

Paulling, J.R., 1981, "The Sensitivity of Predicted Loads and Responses of Floating Platforms to Computational Methods," Proceedings of the Second International Symposium on Integrity of Offshore Structures, Glasgow, Scotland.

Peregrine, D.H., 1976, "Interaction of Water Waves and Currents," Advances in Applied Mechanics, Vol. 16, pp. 9-117.

Reid, R.O., 1957, "Modification of the Quadratic Bottom - Stress Law for Turbulent Channel Flow in the Presence of Surface Wind Stress," U.S. Army B.E.B., T.M. 93, February.

Sarpkaya, T., 1975, "Focus on Cylinders and Spheres in an Oscillating Fluid," ASME, Journal of Applied Mechanics, Vol. 42, pp. 32-37.

Sarpkaya, T., 1977, "In-Line and Transverse Forces on Cylinders in Oscillatory Flow at High Reynolds Numbers," Journal of Ship Research, Vol. 21, No. 4, pp. 200-216.

Sarpkaya, T. and Isaacson, M. St. Q., 1981, Mechanics of Wave Forces on Offshore Structures, Von Nostrand Reinhold Co., New York, N.Y.

Sayer, P. and Spencer, R., 1981, "The Wave-Induced Motions of Adjacent Vessels," Proceedings International Symposium in Hydrodynamics on Ocean Engineering, The Norwegian Inst. of Tech., Trondheim, Norway, pp. 781-798.

Spring, B.H. and Monkmyer, P.L., 1975, "Interaction of Plane Waves with a Row of Cylinders," Proceedings of the 3rd Specialty Conference on Civil Engineering in the Oceans, ASCE, Univ. of Delaware, Vol. III, pp. 979-998.

Tanaka, Y. and Hudspeth, R.T., 1983, "Earthquake Response of Circular Cylindrical Structures in Water," Journal of Earthquake Engineering and Structural Dynamics (in review).

Thomas, G.P., 1979, "Water Wave-Current Interactions: A Review," Mechanics of Wave-Induced Forces on Cylinders, T.L. Shaw (ed.), Fearon Pitman Publishers, Inc., Belmont, CA, pp. 179-203.

Tuah, H. and Hudspeth, R.T., 1982, "Comparisons of Numerical Random Sea Simulations," ASCE, Journal of the Waterways, Port, Coastal and Ocean Div. Vol. 108, WW4, Nov., pp. 569-584.

van Oortmerssen, G., 1979, "Hydrodynamic Interaction Between Two Structures, Floating in Waves," Proceedings of the 2nd Conference on the Behavior of Offshore Structures, BOSS '79, London, Vol I, pp. 339-356.

Vickery, B.J., 1982, "Wind Loads on Compliant Offshore Structures," Proceedings, Ocean Structural Dynamics Symposium '82, Oregon State University, Corvallis, OR., Sept. 8-10, pp. 632-642.

Wang, S. and Wahab, R., 1971, "Heaving Oscillations of Twin Cylinders in a Free Surface" Journal of Ship Research, Vol. 15, No. 1, pp. 33-48.

Yamamoto, T. and J.H. Nath, 1976, "High-Reynolds Number Oscillating Flow by Cylinders," Proceedings 15th International Conference on Coastal Engineering.

Yue, D.K.P., Chen, H.S. and Mei, C.C., 1978, "A Hybrid Element Method for Diffraction of Water Waves by Three-Dimensional Bodies," International Journal for Numerical Methods in Engineering, Vol. 12, pp. 245-266.

Zienkiewicz, O.C., Kelly, D.W. and Bettess, P., 1977, "The Coupling of the Finite Element Method and Boundary Solution Procedures," International Journal for Numerical Methods in Engineering, Vol. 11, pp. 355-375.

Zienkiewicz, O.C., Bettess, P. and Kelly, D.W., 1978, "The Finite Element Method for Determining Fluid Loading on Rigid Structures, Two- and Three-Dimensional Formulations," in Numerical Methods in Offshore Engineering, ed. O.C. Zienkiewicz, et al., Wiley, Chichester, England, pp. 141-183.

Civil Engineering Laboratory, Port Hueneme, California
Ocean Platform Seminar, January 11-12, 1982

FIXED AND GUYED TOWER PLATFORMS
STATE-OF-THE-ART

by

L. D. Finn
Sr. Research Associate
Exxon Production Research Company

INTRODUCTION

Offshore platforms, from a structural behavior viewpoint, can be divided into two classes; fixed-base platforms which are secured to the ocean bottom and "rigidly" resist environmental forces, and compliant platforms which are permitted to move in compliance with dynamic environmental forces. There are two main types of fixed-base platforms: pile-founded steel jackets and gravity-based structures. Most of the gravity-base structures have been made of reinforced concrete although a few employ an all-steel construction. The guyed tower, buoyant tower, and tension leg platform are example of compliant platforms.

Pile-founded steel jacket structures have been used very successfully for many years as oil and gas producing platforms. More recently, gravity based concrete structures have been successfully employed in the North Sea. When discussing the state-of-the-art for these fixed-base platforms it seems logical to also discuss the guyed tower and the buoyant tower platforms since these concepts represent only modest extensions to fixed-base platform technology. Other compliant platforms will be covered by other presenters. This paper will concentrate on discussing the extensions that are being made to fixed-base platform technology to allow these structures to be used in deeper water and more hostile environments.

FIXED-BASE PLATFORMS

PILE-FOUNDED JACKETS

Experience - The pile-founded jacket type platforms (Fig. 1) were developed in the Gulf of Mexico[1] where over a thousand have been installed. Typically, these structures are constructed from steel tubular members with eight legs. The space frame is referred to as a jacket or template because it laterally supports the piles and guides them as they are driven through the legs. Additional support is usually provided by skirt piles driven through sleeves located around the perimeter of the jacket's base. These structures are fabricated onshore and then skidded onto a barge, transported offshore, launched from the barge, upended, and secured to the bottom with piles. The center two legs on the wider side of the jacket run parallel to each other to facilitate the load-out and launch. A whole industry has been built around this structural geometry and many important details have been worked out over the years resulting in an economic and nearly optimum design. Any deviation from this standard design will require considerably more engineering and the installed cost could rise appreciably.

Offshore platforms are generally designed to resist some rare environmental event. The two most common design events are storms and earthquakes. Less common events are mud slides, high currents, and ice flows. The pile-founded jacket type structures are best suited for storm event areas such as the Gulf of Mexico and the North Sea and earthquake event areas such as Santa Barbara Channel and offshore Japan and New Zealand.

The challenge for platform designers is to extend the applicability of this very successful jacket concept into deeper water. Shell's Cognac platform standing in 1025 ft of water in the Gulf of Mexico[2,3] holds the present water depth record. Cognac was built in three pieces

onshore. The pieces were joined in-place by lowering them down into the water. The platform was primarily designed to resist wind, wave, and current forces generated by a Gulf of Mexico hurricane.

The water depth record in an earthquake environment is held by Exxon's Hondo platform standing in 850 ft of water in the Santa Barbara Channel[4,5]. The jacket was built in two pieces onshore. The pieces were joined offshore as they floated horizontally in the water. In the harsh North Sea environment, British Petroleum's Magnus platform standing in 610' of water[6] holds the water depth record. This platform deviates considerably from the typical Gulf of Mexico jacket. Magnus has only four large diameter legs. The piles are grouted to sleeves clustered around each of the legs. The structure was built on its side in a graving dock and towed to the offshore installation site using the buoyancy of the two lower legs.

Two recent platforms installed in the Gulf of Mexico by Union Oil Co. set the trend of things to come for deepwater jacket-type platforms. Both Cerveza and the Cerveza Ligera platforms[7] were launched in one piece and installed in 935 ft and 925 ft of water respectively in a manner similar to their shallower water cousins. This was made possible principally because of the development of a new class of very large launch barges. How far this single piece launch concept can economically be extended has not been determined. Several cooperative industry studies now underway are aimed at providing some answers. Some platform designers believe that jackets for 1500 ft of water in the GOM and 1000 ft in the North Sea are achievable using present technology.

Technical Challenges - Conquering these greater water depths will not be accomplished by simply using brute force. Numerous deviations from the present practice will be required. As is the case in most engineering fields, commonly used design practices are successful because years of experience have demonstrated that they work. These deepwater platforms typically employ higher strength steels to help

reduce the weight of steel required. The tubulars used are larger in diameter and thicker. In addition, it is generally required that steels in deeper water jackets be strong and more fatigue resistant. There is a need for a better understanding of the material characteristics, particularly the fatigue resistances and ductility of welded tubular joints of these thicker and high strength steels. A number of major platform projects have encountered fabrication problems. The end result is a substantial increase in the unit fabrication costs for these larger and more complex platform projects.

A second challenge facing deepwater platform designers is to predict the fatigue life of these large diameter tubular joints. Excessive conservatism needs to be removed from the presently used procedures, if jacket platforms are to be economically extended to deeper water. Wave spreading and wave direction need to be properly considered when predicting stress history for a hot spot. Better data is needed on the fatigue life of these thick walled fabricated tubular joints.

GRAVITY BASE STRUCTURES

Experience - The concrete gravity base structure (Fig. 2) has only recently been used as an oil and gas producing platforms. Much of the technology employed, however, had been proven for many years in such structures as wharfs and lighthouses. Because these structures use their weight to resist overturning and sliding, they are, of necessity, relatively large and massive. As a result, the gravity base structures are best suited to resist severe storm environmental events and ice forces.

The Statfjord B platform is the largest gravity platform standing in 476 ft of water in the North Sea[8]. The 440-ft diameter base is formed from 24 intersecting cylindrical cells. Four of these 75-ft diameter cylinders extend up from the base to the deck. The bottom portion of the base was fabricated in a graving dock and subsequently

towed to a deeper water site in a fjord where the rest of the base and the legs were constructed using slipforming techniques. The steel deck was fabricated in one unit and, using barges, mated to the legs by ballasting the concrete tower down into the fjord.[9] The structure was raised up for tow to the site and installed by ballasting.

Advantages - One of the main advantages of the gravity structure is that the platform, complete with a preinstalled deck, can be installed very rapidly offshore. This is especially important in the rough North Sea where construction barge down time can be a big factor in the total cost. This advantage has been somewhat negated by the development of the big semisubmersible derrick barges now being used in the North Sea.

The reinforced concrete gravity structures do not require highly skilled labor to construct. They do not require high strength steel with difficult welding procedures. The materials needed are readily available at many locations around the world.

Technical Challenges - The main challenge facing the concrete gravity structure designer is to extend its applicability to areas outside the North Sea. The Norwegian fjords provide an ideal protected deepwater site for slipforming the legs and mating the deck. Even in this rather ideal location, the towing draft to the installation site may be a problem for deeper water gravity structures[10].

The gravity structure uses the strength of the supporting soil to provide vertical, lateral, and overturning stability. The over-consolidated, near-surface soils typically found in the northern North Sea are an order of magnitude stronger than those near the surface in the Gulf of Mexico and many other areas of the world. Extending the gravity concept to soft soil areas will require innovative engineering. The lateral stability of the gravity structure in an earthquake prone area is also a concern presently being investigated.

COMPLIANT STRUCTURES

GUYED TOWER

Experience - The first full-scale guyed tower platform will be installed this summer in 1000 ft of water in the Gulf of Mexico[11]. The Lena tower (Fig. 3) has slots for 58 wells and supports a three-level deck with space for twin rig drilling. The tower is supported laterally at the upper end by an array of twenty guylines. The net vertical load of the platform is transmitted to the soil by eight main piles located near the center of the tower. Twelve buoyancy tanks located near the upper end of the structure help reduce the net load on the piles and also provide reserve overturning stability. Six perimeter piles located at the base of the tower help the conductors and main piles provide the required torsional and lateral strength.

The structure is being fabricated onshore and will be skidded onto a barge and launched sideways in one piece. It will then be upended, positioned over the site, and secured with four preinstalled guylines. The piles will be driven and the remaining guylines installed. The deck packages will then be installed in a conventional manner.

Projected Applicability - The guyed tower is classified as a compliant structure because it is designed to move (or comply) with the waves instead of rigidly resisting wave forces as with fixed-base platforms. This compliancy is achieved by allowing the tower to effectively pivot about its base. The oscillatory wave loads are resisted principally by the inertia of the platform, provided the sway period of the tower is somewhat greater than the dominant period of the sea. As a result, the guyed tower has a shallow water limit in the neighborhood of 1000 ft, depending on the period of the extreme sea state and the size (mass) of the tower.

Because the compliant guyed tower uses its own inertia to resist cyclic loadings, it is ideally suited to resist wave loadings[12]. If the tower acts compliantly, the maximum force induced in the guying system will be only a fraction of the peak wave loading. However, any steady or long period loadings such as current and wind loads must be resisted in total by the guylines and base support system.

In deeper water, the tower stiffness must be increased in order to keep the first bending period sufficiently low to minimize structural vibrations and possible fatigue damage. The tower stiffness can be increased most effectively by increasing the cross-sectional width of the tower. This increased tower width, however, results in an increase in the tower weight per unit depth. Thus, somewhere between 2000 and 3000 ft of water, it probably becomes uneconomical to consider a guyed tower for oil and gas producing operations even under the most favorable of reservoir conditions.

Technical Challenges - With the installation of the Lena guyed tower this summer 1000 to 1500 ft-guyed towers will effectively move over into the proven concept category. The challenge for guyed tower designers will be to improve upon this first of a kind design and to extend the usefulness of the concept to deeper waters.

In deeper water, tower installation will present numerous technical challenges. Present schemes call for multiple tower segments to be joined while they float horizontally in the water. Finding a sufficiently calm 150 - 200 ft of water assembly-site will be very difficult if not impossible in some regions of the world. It will become increasingly more difficult to moor construction vessels at the installation site. Significant revisions in the methods for installing the anchor piles will be required. Perhaps, explosively imbedded or suction anchors will prove to be feasible.

As mentioned previously, a guyed tower becomes more susceptible to fatigue damage in deeper water. Fatigue life prediction procedures that better address guyed tower loading conditions will have to be developed before the concept can economically move into deeper water. Modifications to the guying system design will also be required to move into water deeper than about 2000 ft. where steel cable guying systems become very heavy, cumbersome, and ineffective. Kevlar lines appear to offer an excellent solution to this self-weight problem.

BUOYANT TOWER

Experience - A buoyant tower (Fig. 4) has not been used as an oil and gas producing platform although one tower in the North Sea[13] will be used to assist a subsea gas production system. Other potential applications are still being pursued[14]. Smaller versions of the concept have been used in the North Sea as flare towers and tanker loading structures. The buoyant tower, in many respects, is very similar to the guyed tower. It is a compliant structure that pivots about its base and employs buoyancy at the upper end to remain upright. Because the buoyancy supplied restoring moments are generally much smaller than guyline restoring forces per degree of tilt, the buoyant tower tilts considerably more than a guyed tower. This larger tilt angle necessitates using a mechanical pivot at the base. Also the well conductors are subjected to higher bending stresses at the base of the buoyant tower.

Technical Challenges - The main challenge for buoyant tower designers is to engineer a reliable mechanical pivot. Pivot design is made more difficult because of the relatively large vertical and torsional loads that must be resisted. The vertical load transmitted to the pivot is minimized by placing ballast material in a compartment at the lower end of the tower above the pivot. This weight counteracts the buoyancy of the tower. Standard universal joint designs for a production platform size buoyant tower require very massive bearing components which have no redundancy. Recently proposed innovative pivot designs[15] separate the

RD-A139 419

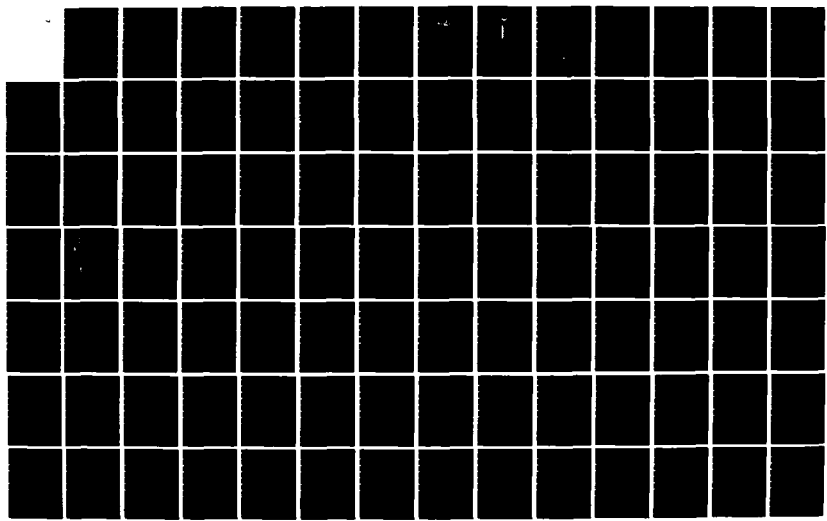
NCEL (NAVAL CIVIL ENGINEERING LAB) OCEAN PLATFORMS
SEMINAR(U) NAVAL CIVIL ENGINEERING LAB PORT HUENEME CA
D R SHIELDS NOV 83 NCEL-TN-1681

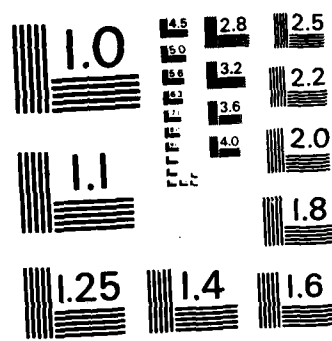
2/4

UNCLASSIFIED

F/G 13/13

NL





MICROCOPY RESOLUTION TEST CHART
NATIONAL BUREAU OF STANDARDS - 1963 - A

torsional restraint mechanism from the vertical restraint mechanism and also provide some component redundancy.

A second challenge for the buoyant tower designers relates to installing the base. Installing piles in a pile-founded base probably can best be achieved by using an underwater hammer. However, if the tower is tilted due to wind and current loads, it may be very difficult to reach all the pile locations. Some of the smaller buoyant tower designs employ a gravity base concept. These base designs are rather massive and require fairly competent near-surface soils.

Attachment of the buoyancy chambers to the structural tower members is a third area needing further study. If large diameter ring-stiffened, cylindrical buoyancy chambers are attached to small diameter structural members, an innovative joining detail will be required to avoid major fatigue failures. One recently proposed design employs a larger diameter concrete cylinder for buoyancy at the upper end. The connection detail between the concrete segment and the steel tubular space frame is an area needing very careful study.

CONCLUDING REMARKS

Much of the technology that has been developed over the years concerning the design and construction of fixed base and guyed tower platforms is publicly available. However, I am not aware of any single reference document or even collection of documents that effectively describe the finer points of the technology that has evolved. As in many industries, this knowledge, in effect, is housed within the people skilled in platform design and construction. Numerous consulting firms are capable of designing fixed-base jackets and a few can handle guyed and buoyant towers. Several contractors can design, fabricate, and install both the fixed-base and compliant towers. Gravity structure design and construction technology is primarily located with European contractors.

Many industry cooperative studies have been conducted in the past and a number of very interesting programs are presently in progress. After the confidentiality period expires, this type of information generally becomes available in the literature. Of course, any organization can elect to participate in a study or purchase the information for a participation fee plus a modest late fee. Much of the data developed by individual firms can generally also be purchased for a reasonable price.

References

1. Lee, G. C., Design and Construction of Deep Water Jacket Platforms, Third International Conference on Behavior of Offshore Structures, Massachusetts Institute of Technology, August 1982.
2. Cox, B. E., G. H. Sterling, R. M. Warrington, Design of the Cognac Platform for 1025 feet Water Depth, Gulf of Mexico, Offshore Technology Conference (OTC-3494), 1979, Houston.
3. Leblanc, L., Cognac Weathers Odds, Tops all Expectations, Offshore V 38, No. 12, pp 43-48, November, 1978.
4. Delflache, M. L., M. S. Glasscock, D. A. Hayes, W. J. Ruez, A. W. Wildenstein, Design of the Hondo Platform for 850-ft Water Depth in the Santa Barbara Channel, Journal of Petroleum Technology, V 31, No. 4, pp 407-414, April 1979.
5. Bardgette, J. J., J. T. Irick, Construction of the Hondo Platform in 850 Feet of Water in the Santa Barbara Channel, Offshore Technology Conference (OTC-2959), 1977, Houston.
6. Magnus Jacket Takes Heavy Honors, Offshore V 42, No. 5, pp 189, 191-193, May 1982.
7. Tannahill, C. A, W. M. Eisenhower, D. D. Engle, Cerveza - A Project Overview of a Deep-Water Platform for the East Breaks 160 Field, Offshore Technology Conference (OTC-4185), 1982, Houston.
8. Tondberg, S., L. Hayling, Statfjord B Posed Fabrication Challenges, Offshore V 42, No. 6, pp 110, 113-116, June 1982.
9. Mating Operations on Statfjord-B Steeldeck, Ocean Industry V 15, No. 2, pp 61-62, February 1980.

10. Huslid, J. M., O. T. Gudmestad, A. Alm-Paulsen, Alternate Deep Water Concepts for Northern North Sea Extreme Conditions, Third International Conference on Behavior of Offshore Structures, Massachusetts Institute of Technology, August 1982.
11. Glasscock, M. S., L. D. Finn, Design of a Guyed Tower for 1000 Feet of Water in the Gulf of Mexico, ASCE 1982 Annual Convention, October 25-27, 1982, New Orleans.
12. Finn, L. D., A New Deepwater Offshore Platform - The Guyed Tower, Offshore Technology Conference (OTC-2688), 1976, Houston.
13. First-of-a-kind Production Scheme, Ocean Industry V 17, No. 4, pp 374-375, April 1982.
14. New Concept: Deepwater Gravity Tower, Ocean Industry V 15, No. 6, p 65, June 1980.
15. Sedillot, F., A. Stevenson, Laminated Rubber Articulated Joint for the Deep-Water Gravity Tower, Offshore Technology Conference (OTC-4195), 1982, Houston.

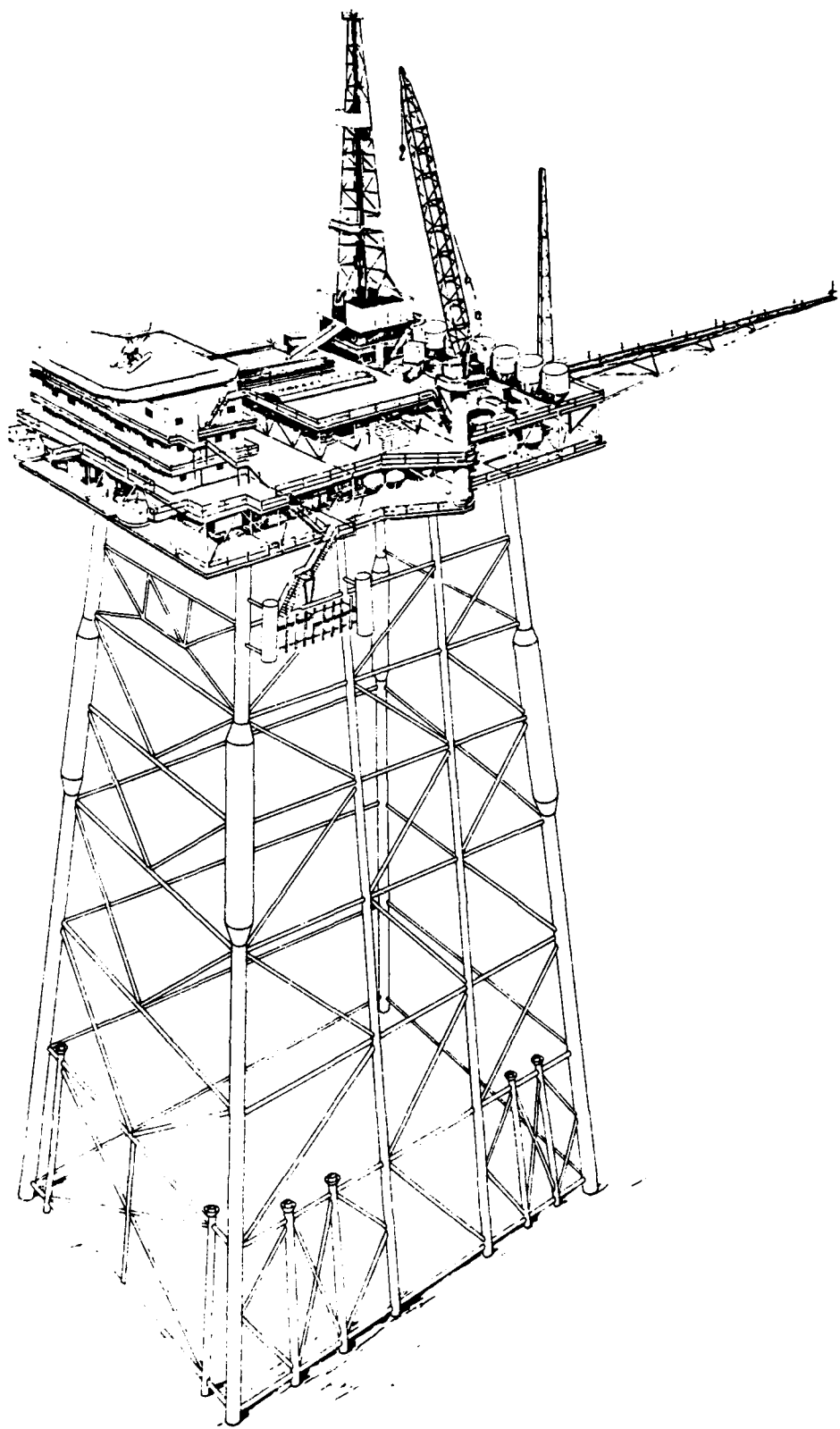


Figure 1. Typical pile-founded steel template offshore producing platform.

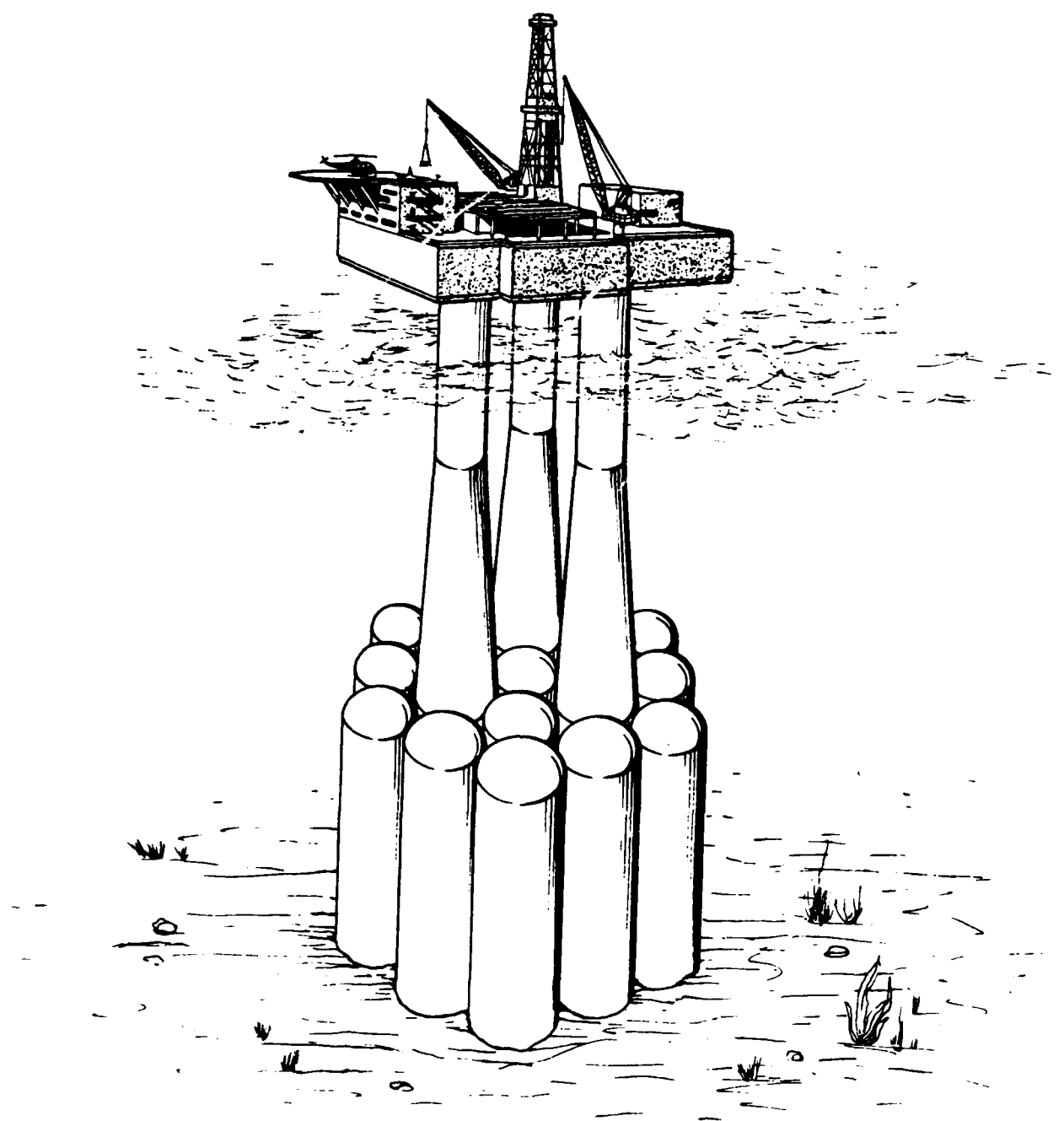


Figure 2. Concrete gravity structure typical of the North Sea.

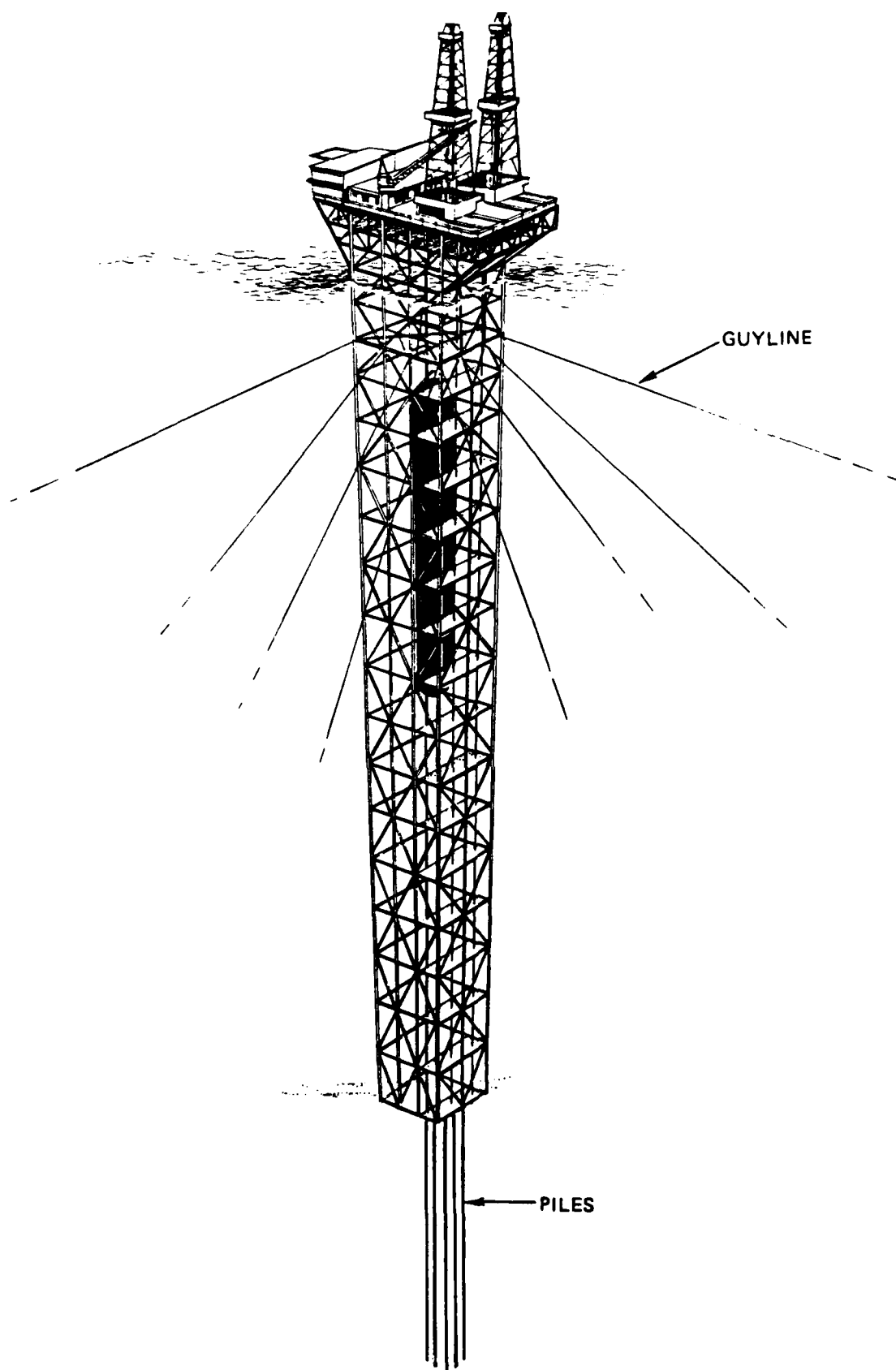
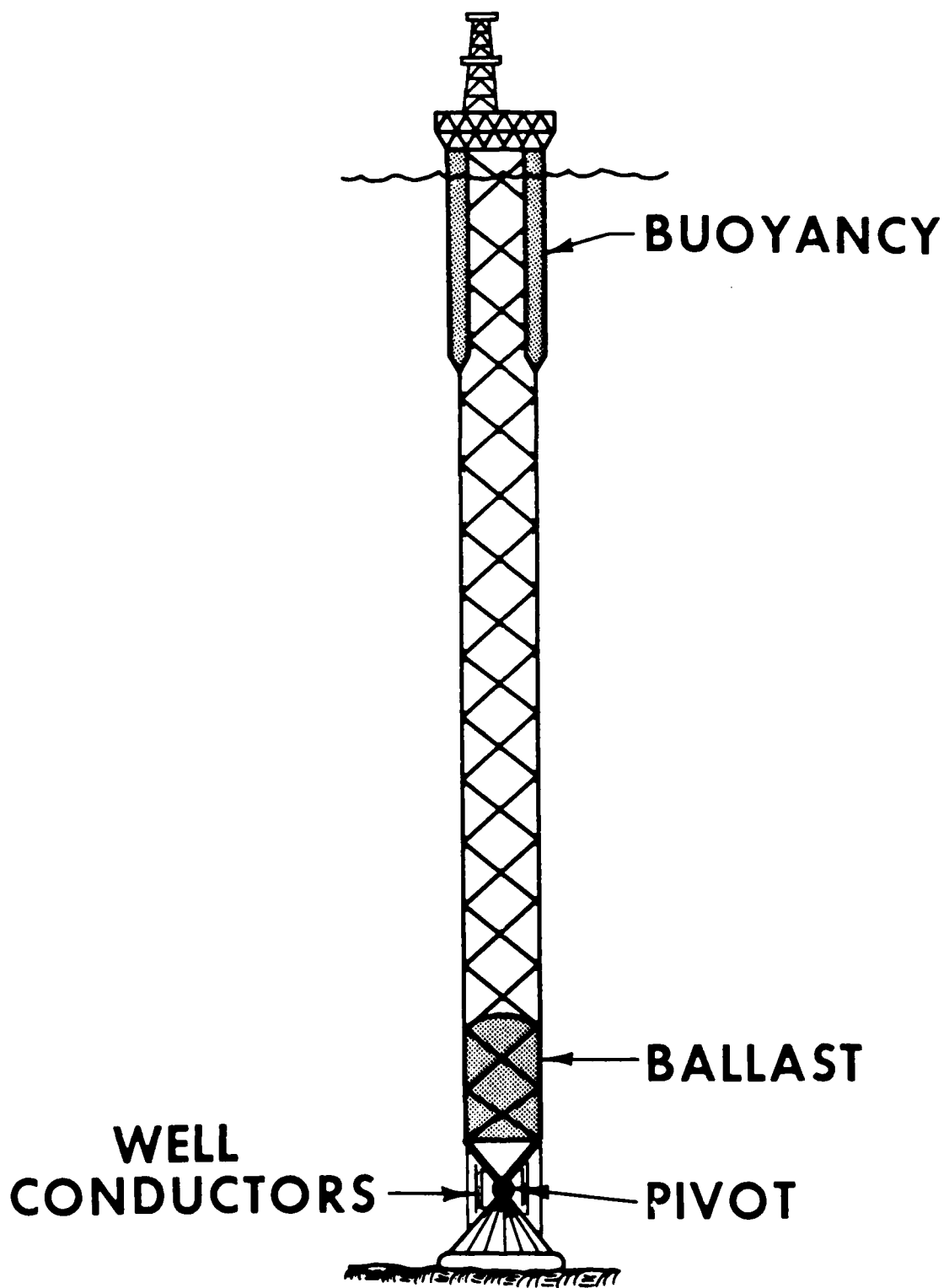


Figure 3. Compliant guyed tower producing platform



BUOYANT TOWER
FIGURE 4

SEMISUBMERSIBLE AND TENSION LEG PLATFORMS

by

J. R. Paulling
Professor of Naval Architecture
University of California, Berkeley

Prepared for

Ocean Platform Seminar
Naval Civil Engineering Laboratory

January 11-12, 1983

TABLE OF CONTENTS

	Page
I. INTRODUCTION	103
II. WAVE LOADS AND MOTION CHARACTERISTICS	106
CHARACTERISTICS OF THE WAVE-INDUCED FORCES	107
HYDRODYNAMIC FORCE COEFFICIENTS	110
HEAVE MOTION RESPONSE	112
TLP FORCES AND RESPONSE	113
ADDITIONAL MOTION RESPONSE EFFECTS	116
III. DESIGN CONSIDERATIONS	118
HEAVE MOTION OPTIMIZATION - SEMISUBMERSIBLE	118
TENSION OPTIMIZATION - TLP	119
IV. CONCLUDING OBSERVATIONS	121
REFERENCES	124

I. INTRODUCTION

In their general appearance and in some of their response characteristics, the semisubmersible platform and the tension leg platform (TLP) bear a certain resemblance to one another. There are some significant differences, however, in the load-carrying capabilities, and in those response characteristics which are closely related to the mooring system.

The mooring system, of course, represents the principal difference between the two platform types. The semisubmersible is usually moored by means of an array of conventional anchors attached to the platform by chain or wire and chain having a scope of several times the water depth. This provides relatively soft restraint to the platform in all directions, sufficient to offset the mean disturbing effects such as wind and current, but providing virtually no restraint on the higher frequency wave-induced disturbances. The TLP is moored by a system of vertical taut lines, either wire or tubular members, which substantially restrict the heave, roll and pitch motions, meanwhile providing weak restraint against surge, yaw and sway to about the same degree as the semisubmersible's catenary mooring.

There have been proposals for a TLP moored by a spread array of taut lines which would thereby be restrained in the lateral motions to about the same extent as the vertical. The redundant nature of such a mooring system causes great difficulty in insuring that all members remain under tension at all times, and the concept has not been developed to as high a degree as the vertically-moored TLP. It should be

noted that the insurance of tautness is a prime design constraint for a TLP since the impact loads which would follow a momentary slackening would be impractical to design against.

The purpose of this paper will be first, to discuss the principal response characteristics of the two types of platforms as these characteristics are related to size and configuration; second, to discuss the state of the art in design of each type of platform; third, to discuss some of the important characteristics as they are expected to affect the suitability of each type of platform for the perceived needs of the navy; and finally, to point out some of the areas in which it is felt that research and engineering development is needed, again with particular reference to the needs of the navy.

The most common geometric configuration for both the semisubmersible and the TLP consists of a space-frame arrangement of tubular members of circular or oval cross-section. Platforms of somewhat simplified geometry but having proportions typical of modern offshore oil field drilling and production applications are shown in Figures 1 and 6. The twin hull arrangement has become, by far, the most widely used arrangement for the semisubmersible, dictated largely by considerations of low resistance to forward motion when in transit. The first full scale working TLP is only now under construction so typical practice has not been firmly established. The TLP shown in Figure 6 is a composite of several conceptual designs which have been developed by various oil companies. Since most of these have been intended for oil production rather than exploratory drilling, mobility has not influenced the arrangement to the same extent as in the case of the semisubmersible. Considerations of optimum mooring tension response have

resulted in somewhat larger vertical members in relation to the horizontal members as compared to the semisubmersible.

Some important characteristic of both of these platforms are the following:

Much of the volume is deeply submerged and the waterplane area is relatively small in relation to the total volume.

Most of the tubular members are relatively small in cross section compared to the length.

The spacing between members is large compared to the member cross section.

The first of the above characteristics gives the platform its "wave transparency" properties. The second and third may be utilized in deriving an analysis of the wave-induced forces and resultant motions which, although greatly simplified, nevertheless is quite accurate and informative in developing understanding of the principles upon which the two types of platforms may be designed. This is taken up in the next section.

II. WAVE LOADS AND MOTION CHARACTERISTICS

In computing the motion response of either type of platform to wave excitation, we solve the equations of rigid body motion based upon Newton's second law. In the case of moderate wave motion and correspondingly small platform motion, we may linearize the equation, in the form of Equation (1)

$$(m + m')\ddot{x} + b\dot{x} + cx = fe^{-i\omega t} \quad (1)$$

In this equation, it has been assumed, following standard practice, that the external force system acting on the platform can be written as the sum of four terms. The first is proportional to the acceleration of the platform, the second proportional to the velocity, the third proportional to the displacement from the mean position, and the last independent of the platform motion but depending only on the wave motion. This last term, the wave exciting force, is therefore computed as though the platform remains stationary in its mean position.

Equation (1) has been written for a simple sinusoidal wave of constant frequency. For a realistic random seaway composed of many wave components, the response may be obtained by superimposing such elementary solutions corresponding to all of the component elementary waves, and this superposition process forms one of the most powerful applications of the simple linear analysis.

In Equation (1), the mooring system is contained principally in the static restoring term which may also

include effects coming from changes in the buoyancy of the platform with change of position. It is through this mooring term that the principal differences arise in the response of the two types of platforms.

The response to waves depends upon two quantities: The magnitude of the exciting force and the tuning factor or relation of the wave frequency to the natural frequency of the platform's motion. We shall next examine both of these for the two types of platforms.

CHARACTERISTICS OF THE WAVE-INDUCED FORCES. Consider first the heave force exerted by waves on the platform. This force is of considerable importance in both cases. For the semisubmersible, the heave motion is one of the most important motions limiting the ability of the platform to perform the drilling operation. For the TLP, the heave force causes a variation with time in the mooring member tension, and as noted earlier, it is usually required that the net tension, which equals the sum of this variation and the mean tension, must always remain positive.

A good estimate of the heave force on platforms similar to those depicted in Figures 1 and 6 may be obtained by considering just the wave-induced pressure and acceleration field around the individual cylindrical members of the platform, thus neglecting the drag forces. For the assumed members of small cross section sparsely distributed throughout the structure, we may compute these forces on each member as though the other members were not present. Furthermore, if we assume the wave length to be large compared to the member cross section, fluid flow quantities computed at the position of the member centerline may be used as approximations of the average values around the member periphery. Under these assumptions, and assuming deep water

waves approaching the platform of Figure 1 from abeam, the vertical force on a horizontal circular cylindrical member representing one of the lower pontoons is given by Equation (2)

$$F_H = -2\rho A_H L \omega^2 e^{-kd} \cos(kb - \omega t) \quad (2)$$

Here

A_H = Cross sectional area of one horizontal member,

L = Length of member,

$2b$ = Horizontal spacing of the members.

d = depth of the member.

The force given by Equation (2) includes the integral of the undisturbed pressure over the surface of the member (the Froude-Krylov force), and a correction term, assumed proportional to the wave-induced acceleration of the water about the member. For a circular cross section deeply submerged in the water, these two terms are equal to each other.

The force on the vertical surface-piercing members is given by Equation (3).

$$F_V = \rho g A_V a e^{-kd} \cos(kb - \omega t) \quad (3)$$

Here,

A_V = Cross sectional area of all vertical members on one side of the platform.

d = depth of bottom of member (assumed approximately the same as depth of the horizontal member.)

The total force may be expressed as in Equation (4).

$$2\sigma g a e^{-kd} (A_v - 2kLA_H) \cos kb \cos \omega t$$
$$= F_o e^{-kd} (1 - kbA_o) \cos kb \cos \omega t \quad (4)$$

Here,

$$F_o = 2\sigma g a A_v$$

$$A_o = 2 \frac{L}{b} \frac{A_H}{A_v}$$

$$k = \frac{\omega^2}{g}$$

Note that this total heave force consists of the product of four terms, the last of which is sinusoidal in time. The amplitude of the force is the product of three terms which differ from each other in the manner in which they vary with wave frequency. It is of considerable interest to examine this behavior since it has important implications for the heave motion of the semisubmersible and for the mooring member tension of the TLP.

The three terms of Equation (4) are plotted in the upper part of Figure 2 and their product in the lower part. The following characteristics should be noted:

The force vanishes at the zeros of the $\cos kb$ term and also at the values of kb for which the term containing the ratio of areas of horizontal and vertical members crosses the axis.

The area ratio term increases in value with increasing

k_b while the exponential term decreases. The limiting value of the product for high k_b is zero.

For high values of k_b , the wave length is no longer large compared to the member cross sectional dimensions, therefore, a basic assumption underlying the simplified force calculation does not apply in this range of k_b . The computed force is meaningful for values of k_b up to about $\frac{3\pi}{2}$.

Several effects which are neglected in the simplified analysis are expected to make the actual heave force differ from the values shown in Figure 2 and some of these effects are:

The finite dimensions of the members as well as the interaction or proximity effects of one member on another.

Frequency-dependence in the added mass term which was represented by a simple constant multiplied by the wave-induced acceleration at the horizontal member location.

Fluid viscous damping forces.

Fluid damping due to wave radiation. This is strongly frequency-dependent.

Effects of finite wave and platform motion amplitude.

HYDRODYNAMIC FORCE COEFFICIENTS. Several of these effects are examined in Figures 3, 4 and 5. In Figure 3 are shown the damping force for the example twin hull semisubmersible, including both wave radiation and viscous effects. The curve

labelled "strip method" utilizes a variation on a procedure which is frequently used for surface ship motion computations, in this case extended to treat the twin hull configuration. Effects included here are the finite member dimensions and interaction between the two lower hulls. The latter is seen to result in a cancellation/reinforcement effect which varies with wave frequency in a manner somewhat similar to the effect shown in Figure 2. In this case, the humps or hollows can be shown to occur at wave lengths which are integral multiples of the hull half-spacing.

Also shown on this figure is the damping due to viscosity, computed by assuming a quadratic relationship between the force and the relative velocity between member and water, and then expressing the result as an equivalent linear damping coefficient. Since the relative velocity depends upon both wave and member motion, the linearized damping force per unit velocity depicted here will vary with the severity of motion, therefore the sea state. This term is, therefore, shown for several different levels of the sea state.

The upper curve in Figure 3 is the heave added mass term, which, for short waves, is seen to vary substantially with wave period or frequency. For comparison, the constant added mass coefficient used in the simplified slender member computation is also shown.

Figure 4 presents the heave exciting force amplitude which is analogous to the quantity shown in Figure 2. As indicated by the key to this figure, results are given for the lower hulls alone and for the lower hulls plus the surface-piercing columns. Both the strip method and the slender member methods were used. For the slender member computation, an additional term was included representing

viscous drag on the member. This term is not contained in Equation (4) but is found to slightly round off the minima in the force so we do not obtain complete cancellation. Two minima appear in this figure at wave periods of about 9 and 25 seconds. These correspond to the force zeroes in Figure 2 at k_b values of approximately $\frac{\pi}{2}$ and 0.5, although there is a slight difference in the former because the results given in Figure 4 were computed for the oval cross section while a circular section was used in Figure 2.

HEAVE MOTION RESPONSE. The typical heave response characteristics of a semisubmersible are shown in Figure 5. The heave motion amplitude is determined by both the resonance properties of the spring-mass-damper model of the platform, and by the amplitude of the exciting force due to waves. A good approximation to the natural frequency in heave may easily be derived. The restoring force coefficient (spring constant) in heave is equal to the product of the specific weight of water and the total waterplane area, $2A_v$. We may assume an added mass in heave equal to the displaced mass of the two pontoons, or $2\rho A_H L$. The total weight of the platform equals the total displacement, $2\rho g(dA_v + LA_H)$, and the total effective mass in heave is the sum of the added mass and the physical mass of the platform. The natural frequency is then equal to the square root of the spring constant divided by the effective mass, with the result given in equation (5).

$$\omega_n = \frac{2\pi}{T_n} = \sqrt{\frac{g}{d + 2L \frac{A_H}{A_v}}} \quad (5)$$

In Figure 5 we observe a peak in the response at a wave period of 28 seconds resulting from heave resonance, and minima in the response at about 9 and 25 seconds corresponding to the force minima which are apparent in the previous figure. The three computed responses correspond to

different damping values. The highest resonance peak is obtained using only the wave radiation damping predicted by the strip computation. The two lower peaks, whose amplitudes are typical of observed responses of models and prototype platforms, include viscous damping modelled by a quadratic dependence upon relative velocity between member and water. As a result of the quadratic term, the procedure is seen to predict a higher effective damping, and therefore, a lower normalized response in the higher sea state.

TLP FORCES AND RESPONSE. In most essential respects, the heave forces exerted by waves on the TLP will exhibit the same cancellation and reinforcement characteristics which were observed for the semisubmersible. Since the TLP is highly restrained in heave, the motion in heave will not, in general, be of serious concern. Of greatest importance in most TLPs will be the surge motion response and the tension fluctuations in the mooring members.

We will first examine the surge forces and hydrodynamic characteristics for the four-column TLP shown in Figure 6. The surge damping and added mass for this platform are shown in Figures 7 and 8. In this case, a three-dimensional diffraction theory was used in addition to the simplified slender member procedure. The diffraction procedure takes into consideration effects due to finite member dimensions and interaction between the members of the structure.

The wave radiation damping coefficients by diffraction procedure are shown for the complete four column platform as well as for a single column, and from these results, the effect of wave interaction between the members of the platform may be clearly seen. Viscous damping is again given in the form of an equivalent linear coefficient for three different sea states. Note that, although the viscous

damping coefficient is much smaller than the peak of the radiation damping, it is much larger than the radiation damping in the long waves. The natural period of surge of a typical TLP is in the range of 50 to 200 seconds, depending primarily on water depth, and thus we see that viscous effects will provide the only damping of any importance in the vicinity of resonance.

The added mass coefficients depicted in Figure 8 display a behavior similar to those for the semisubmersible in that they decrease in the shorter waves and in the longer waves the more exact values are somewhat lower than the constant value used in the slender member procedure.

Of greatest interest, perhaps, are the surge exciting forces shown in Figure 9. As in the case of the heave force, the hump-hollow characteristic is much in evidence and, for the longer waves, the slender member method gives results which are substantially in agreement with the three-dimensional diffraction computations. In the shorter waves, however, the slender member method overestimates the forces, and a modification to the procedure may be introduced which somewhat improves the force prediction. In this modified slender member procedure, average values of the wave-induced velocities and other properties are computed over the member cross section, and used in place of the single value computed on the member centerline. Figure 9 shows that results obtained in this way are in somewhat closer agreement with the diffraction procedure results. The modified slender member results shown in Figure 9 contain viscous drag effects which are not included in the ideal fluid results, but as in the case of the damping coefficients, these viscous wave force effects are relatively unimportant in the shorter wave periods.

An approximate expression for the natural frequency in surge may be derived in the following way. By reference to the sketch in the upper right hand part of Figure 6, it is seen that the surge restoring force coefficient is given by Equation (6). Here l is the length of the mooring line and the mean tension = $\Delta - w$, where w is the weight, and Δ is the displacement of the platform. For very deep water, l is approximately equal to the water depth d , and we have, therefore,

$$C = \frac{T}{l} \approx \frac{\Delta - w}{d} \quad (6)$$

The added mass is equal to or slightly less than the displaced mass and, as for the semisubmersible, the total effective mass is the sum of the physical mass and the added mass. The natural frequency, equal to the square root of the ratio of the spring constant to the effective mass, is then given by Equation (7).

$$\omega_n = \sqrt{\frac{g}{d} \left(\frac{1 - w/\Delta}{1 + w/\Delta} \right)} \quad (7)$$

The natural frequency is seen to be depth dependent, and, for typical TLP configurations, is usually much smaller than any of the wave frequencies having significant energy.

Two responses of the TLP are shown in Figures 10 and 11 are the wave-frequency surge motion and the tension fluctuations in the mooring members. In Figure 10 it is seen that the slender member method is equal to the diffraction procedure in predicting the surge motion. The mooring tensions, however, are very responsive to resonance in pitch and heave of the platform. Recall that these motions are almost completely restrained by the extensionally very stiff mooring members, and, consequently, their natural frequencies

will be quite high. The highest tension response occurs in the frequency range for which we observe the greatest discrepancy between the diffraction and slender member methods. Since these large, high-frequency tensions play an important role in the fatigue behavior of the mooring members, there is an obvious necessity of accurately predicting the hydrodynamic terms in the high frequency range even though the motion responses are quite small.

ADDITIONAL MOTION RESPONSE EFFECTS. In the foregoing sections, we have concentrated upon the wave-frequency forces and responses of both semisubmersibles and TLPs. There are several additional effects which may be present in the responses of one or the other of these platforms which may be incapable of analysis by linear hydrodynamic procedures yet which may be extremely important in some situations. We will illustrate one and describe others of these.

For both the TLP and the semisubmersible, there will be some effects due to waves reflecting from the platform which result in a small but nevertheless significant mean force. If the waves are random rather than regular, the reflection force will vary slowly with time having a frequency distribution similar to the envelope of the wave train. These forces may be substantially smaller than the basic wave frequency forces, yet because of their lower frequency, they may excite resonant response in the lightly restored surge, sway and yaw modes of motion.

A second type of nonzero mean or slowly-varying force acts only on the surface-piercing members and is caused by viscous effects. If we consider the vertical member shown in Figure 12, we observe that the immersed length in a wave crest will be greater than the immersed length of member in a wave trough. Also, note that the direction of the fluid

velocity will be in the direction of wave motion in the crest but in the opposite direction in the trough. As a result, the force in the direction of wave motion which acts on a member in a wave crest will be greater than the force in the opposite direction when the member is in a trough. The time history of the total force, therefore, consists of an oscillatory part superimposed on a steady mean value in the downwave direction. In random waves, this nonzero mean viscous force will again vary in a manner related to the envelope of the wave train. Figure 13 illustrates the effect of this force on the surge motion of a TLF in regular waves. The mean offset due to the steady part of the force is clearly discernable and is similar in magnitude to the wave-frequency surge motion.

Other steady or slowly varying disturbances are caused by wind and by the combined action of waves and current. At the present time, totally satisfactory analytic methods for their prediction are lacking. Model experiments, which offer an alternative method, sometimes suffer from scale effects which render their results less than satisfactory as well.

III. DESIGN CONSIDERATIONS

The foregoing sections have given a brief introduction to the principal response characteristics of semisubmersibles and TLPs and the means for their prediction. In the present section, we will outline the application of some of these considerations to the selection of platform proportions in a design situation.

The reinforcement-cancellation nature of the vertical forces depicted in figures 2 and 4, and their relationship to the size and distribution of members as expressed in Equation (4), suggest the possibility of optimizing platform response through proper choice of member proportions.

HEAVE MOTION OPTIMIZATION - SEMISUBMERSIBLE. In the case of the twin hulled semisubmersible, a typical design objective might be to require that the proportions be selected so as to result in minimum heave motion in a certain prescribed seastate. The seastate would typically be described by a specified spectral density function.

Several possible means of obtaining minimum response may be thought of in view of the heave response characteristics illustrated in Figures 2 and 5.

- (a) We might select the proportions of horizontal and vertical members such that the heave natural frequency coincides with a frequency at which the heave force is zero due to the cancellation effect. This could be expected to reduce or eliminate the resonance peak in the heave response.

- (b) The proportions might be selected to result in a heave force minimum at the frequency of the peak of the wave spectrum, thus reducing the response at the frequency of strongest excitation.
- (c) The proportions might be selected so as to shift the heave natural frequency away from the vicinity of the spectral peak by a substantial margin.

These three procedures have been utilized in the case of a hypothetical platform having dimensions of 400 feet long by 100 feet depth and a total weight of 22.78 million pounds. Characteristics of platforms meeting the three criteria listed above are given in Table 1 and summaries of their responses to random waves in Table 2. The reason for the superior behavior of candidate (c) is apparent from Figure 14 which contains the response functions for the three platforms. It is seen that the two platforms which rely upon cancellation effects have substantially higher average response within the range of appreciable wave energy than does the platform which relies on detuning for motion optimization. Not surprisingly, it is this latter procedure which is usually employed in the design of oil drilling semisubmersibles to achieve minimum motion. It has, presumably, been arrived at through a combination of experience, model testing and reasoning somewhat similar to that which is employed here.

TENSION OPTIMIZATION - TLP. As noted previously, the distribution of buoyancy between vertical and horizontal members also affects the varying tension in the mooring members of the TLP. Since this tension is an important design parameter in the TLP, we might consider selecting the member proportions so as to minimize the variable tension.

As an example, consider a small TLP of triangular planform having three vertical surface-piercing members and three horizontal pontoons at the base. Computations of the amplitude of mooring tension variations have been performed for a range of regular wave periods and are plotted in Figure 15 versus the ratio of volume of horizontal members to total buoyant volume. For each wave period, there is clearly an optimum volume ratio, but there is also considerable variation in this ratio with wave period. The computations have, therefore, been repeated for random seas in order to determine if an optimum may be defined in the presence of a collection of waves of different frequencies. The results for several sea states are given in Figure 16, and here we observe that the minimum in the response is still obtained, but it is less sharply defined than in the regular wave.

Reasoning similar to the above forms a suitable basis for the selection of member proportions, and has been used in several of the presently active TLP design projects.

IV. CONCLUDING OBSERVATIONS

The preceding sections have outlined the principal characteristics and some design considerations for semisubmersibles and TLPs. It should be borne in mind that most of the literature and experience with such platforms deal with offshore oil drilling and production applications, and navy needs may differ in important respects regarding size, payload capacity, longevity, mode of operation and others.

Let us consider payload. Semisubmersible platforms currently being designed and used for drilling have dimensions similar to or slightly larger than those shown in Figure 1. The deck load (payload) is in the range of 3000 to 6000 long tons and the total displacement ranges from 25000 to 45000 long tons. Most of the current generation of semisubmersibles are self-propelled and the installed power, which serves the drilling and dynamic positioning function as well, is from 15000 to 35000 horsepower. Such platforms are now equipped to drill in water depths of up to 6000 feet and will normally rely on dynamic positioning in depths of over approximately 1000 feet.

The Hutton Field TLP depicted in Figure 17 is currently under construction. This is intended as a production platform and is designed for a working life on one station of approximately 20 years. This is a relatively heavy platform and will be installed in a water depth less than that for which a TLP would normally be considered economical in comparison to a fixed platform. The Deep Oil X-1 depicted in Figure 18 was built as a large scale model and would perhaps

be more nearly in the size range of navy sensor platform needs. In developing such a small platform for very deep water, the weight of the mooring members may become a large part of the total system weight, and some special provision such as distributed buoyancy or nonmetallic material must be considered. In this regard it should be noted that current thinking holds that the TLP in oil production service may be limited to water depths of not more than about 5000 feet because of the weight of the mooring members.

The purpose of the above enumeration of current practice is to emphasize the point that, in designing a navy sensor platform, current oil field practice and experience must be used with full understanding of the effects of scale. For example, consider the problem of selecting the optimum proportions for a semisubmersible platform. Since there are interactions between the different modes of response, we cannot focus attention solely upon achieving a desired value of the natural heave frequency, but must also consider the effect of the choice of dimensions on other factors such as static stability and the angular motion responses. The final choice invariably involves compromises between several requirements. In the case of a small sensor platform the result of a preliminary design study may be a set of member dimensions whose proportions differ appreciably from those of a large oil drilling platform. The motion, strength and stability, in such a case may not be simply scaled from nor evaluated and judged using the same criteria that are used for a large oil drilling platform.

Finally, some of the simplifications and assumptions which go into the analysis and design process for a large platform may not be so readily applicable to a smaller platform. An example here is the assumption concerning sea state severity. Since the sea is the same for large and

small platforms, the small platform is exposed to relatively more severe conditions, and simplifications such as those underlying the linear motion analysis may not yield results of sufficient accuracy for the designer's needs. On the other hand, the navy sensor platform, as a result of its unmanned mode or possibly a shorter designed lifetime may be designed using less severe structural design criteria.

In conclusion, we list below some of the areas in which some research or engineering development attention may be necessary in light of perceived navy sensor platform design needs.

Survey of the applicability of the current design practices, criteria, standards, computational methods and software to platforms whose proportions and size differ appreciably from typical offshore oil applications.

Investigation of certain subtle or nonlinear motions and loads effects, some of which are still incompletely understood, for their influence on platforms of unusual proportions and size. Such effects include wave drift forces, viscous drift forces caused by simultaneous wave-current action, autoparametrically-induced motions of TLPs, interaction between platform and mooring system dynamics, steady-heel phenomena in semisubmersibles, and stability and survivability in extreme wave conditions.

Wind effects, especially unsteady wind forces and heeling moments in the presence of high waves.

Long term structural effects such as cumulative fatigue damage as they may affect design procedures or may be incorporated into design criteria.

REFERENCES

J. R. Paulling and E. E. Horton
"Analysis of the Tension Leg Platform", OTC 1263, 1970.

J. R. Paulling
"Wave-induced Forces and Motions of Tubular Structures", 8th ONR Hydrodynamics Symposium, Pasadena 1970.

E. E. Horton, L. B. McCammon, J. P. Murtha, J. R. Paulling
"Optimization of Stable Platform Characteristics", OTC 1553, 1972.

J. R. Paulling
"Time-Domain Simulation of Semisubmersible Platform Motion with Application to the Tension-Leg Platform", SNAME Spring Meeting/STP Symposium, San Francisco, 1977.

J. R. Paulling
"The Sensitivity of Predicted Loads and Responses of Floating Platforms to Computational Methods", PROC. Conf. on Integrity of Offshore Structures, Glasgow, 1981, (Pub. by Applied Science Publishers, Essex, U. K., 1981)

J. R. Paulling
"Mathieu Instabilities in TLP Response", PROC. OSDS '82, Oregon State Univ., Corvallis, 1982.

N. Salvesen, et. al.
"Computations of Nonlinear Surge Motions of Tension Leg Platforms", OTC 4394, 1982.

E. Numata, W. H. Michel, A. C. McClure
"Assessment of Stability Requirements for Semisubmersible Units" TRANS, SNAME, v84, 1976.

J. T. Dillingham
"Recent Experience in Model Scale Simulation of Tension Leg Platform Performance", No. Calif. Section SNAME, Nov. 1982.

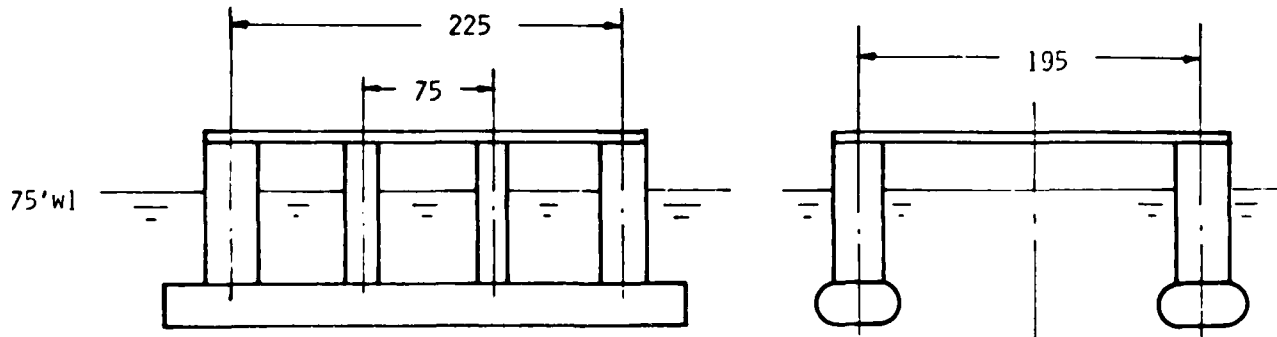
TABLE 1 - FOUR-COLUMN PLATFORM FAMILY

$L = 400$ feet, $h = 100$ feet,
 $\beta = 4$, Disp = 22780 kips

Platform Number	Design Criterion	R_H feet	R_V feet	α	Natural Period in Heave-Sec.	Period of Heave Force Cancellation sec.
Ia	(a)	5.41	15.00	0.130	13.6	13.6
Ib	(b)	6.92	13.65	0.257	15.8	14.9
Ic	(c)	9.25	10.55	0.768	22.4	—

TABLE 2 - FOUR-COLUMN PLATFORM FAMILY RESPONSE TO RANDOM SEAWAY

	Wave Height (Pk-to-Pk) Feet	Heave Motion (Pk-to-Pk) Feet		
CASE		Ia	Ib	Ic
Average	18.5	10.84	11.18	6.16
Significant	29.7	17.34	17.90	9.84
Average of Highest 1/10	37.8	22.10	22.82	12.56



Main hulls 21 x 50 x 300 ft.
 Main columns 30 ft. dia.
 Intermediate columns 15 ft. dia.
 Weight 48×10^6 lbs.

Figure 1 Twin Hull Semisubmersible

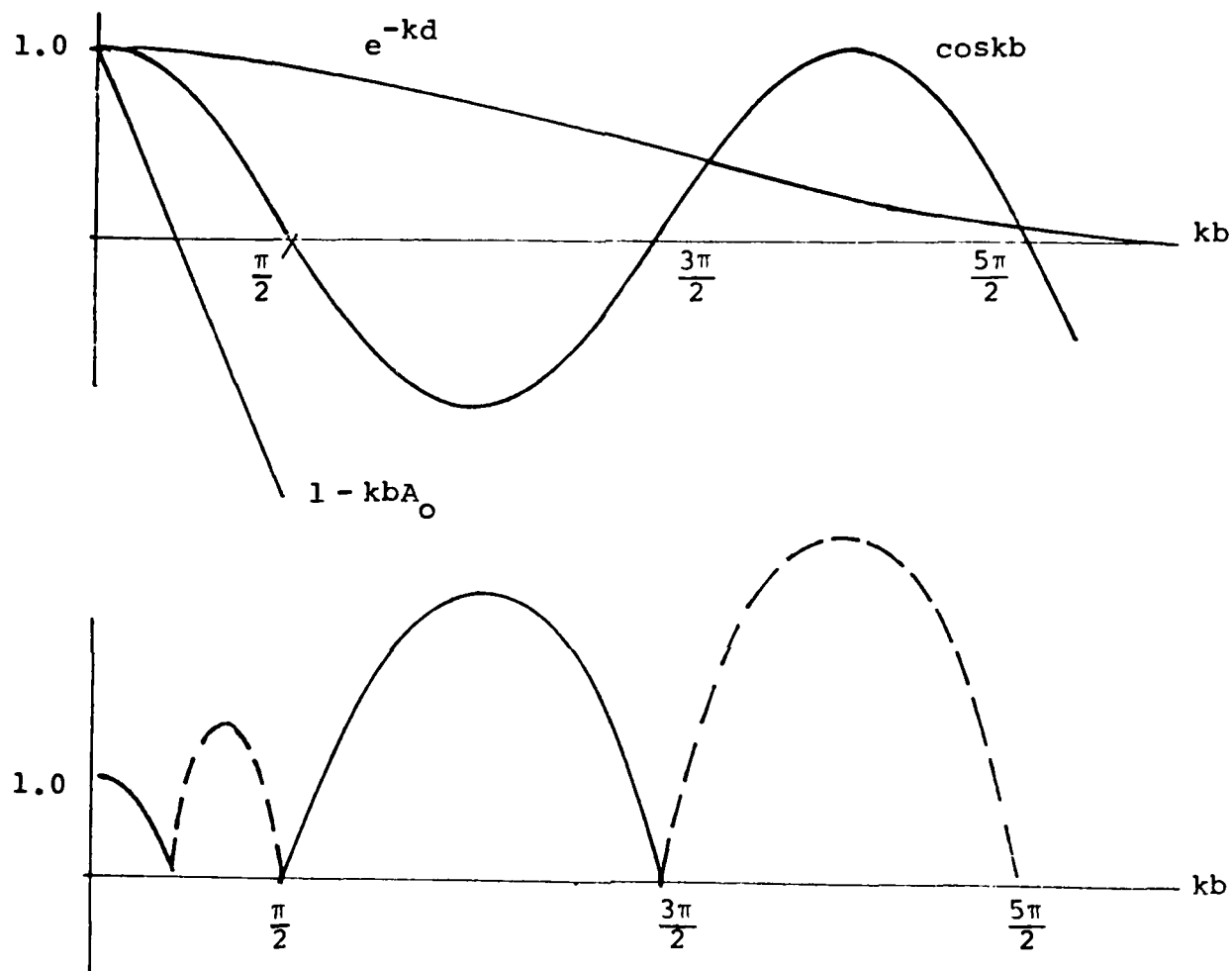


Figure 2. Components of Heave Force--Twin Hull Semisubmersible

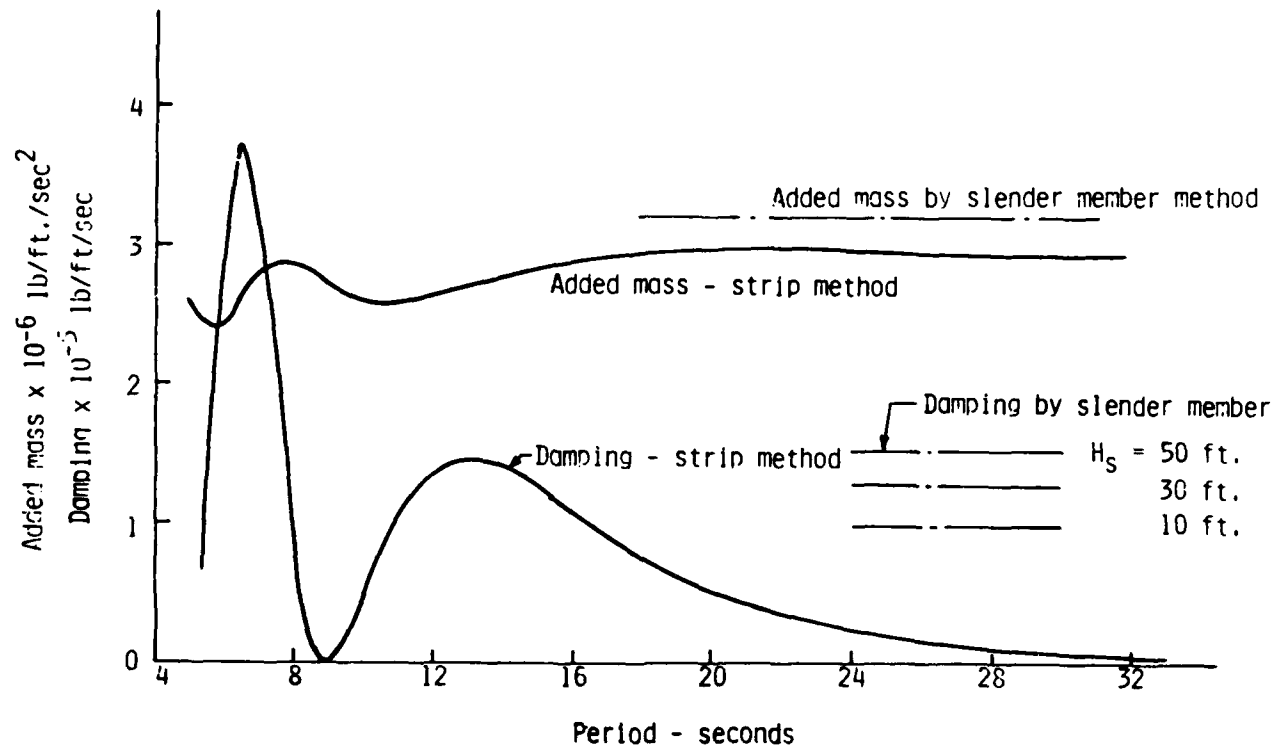


Figure 5 Twin Hull Semisubmersible - Heave damping and added mass

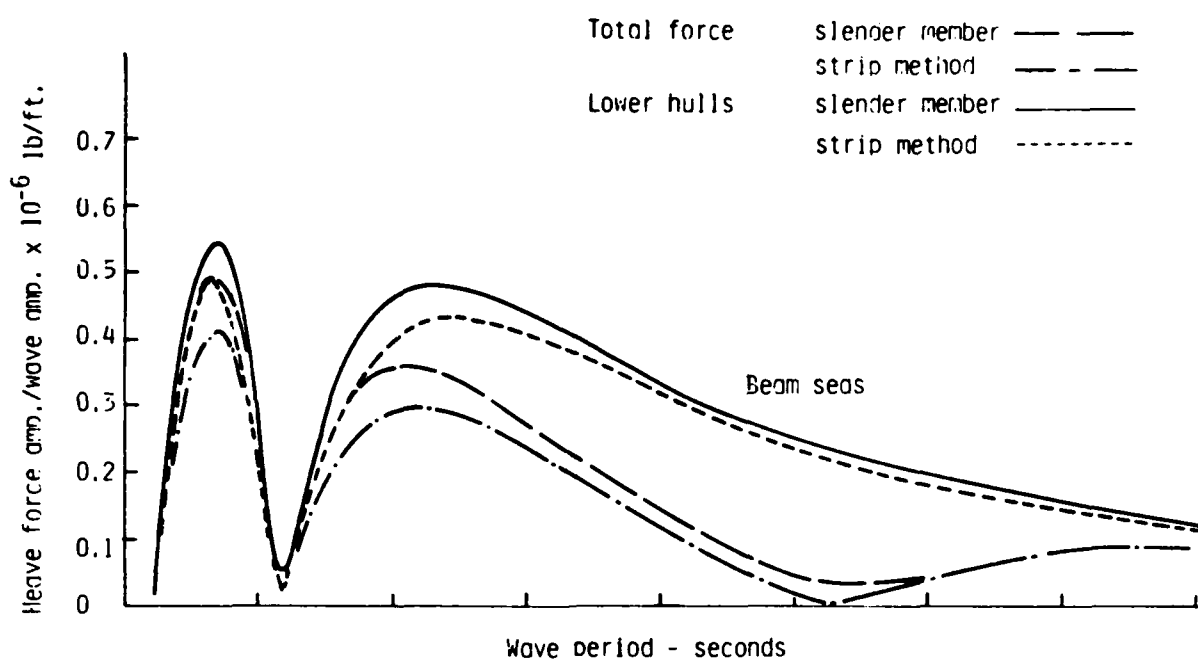


Figure 4 Twin Hull Semisubmersible Heave Exciting Force

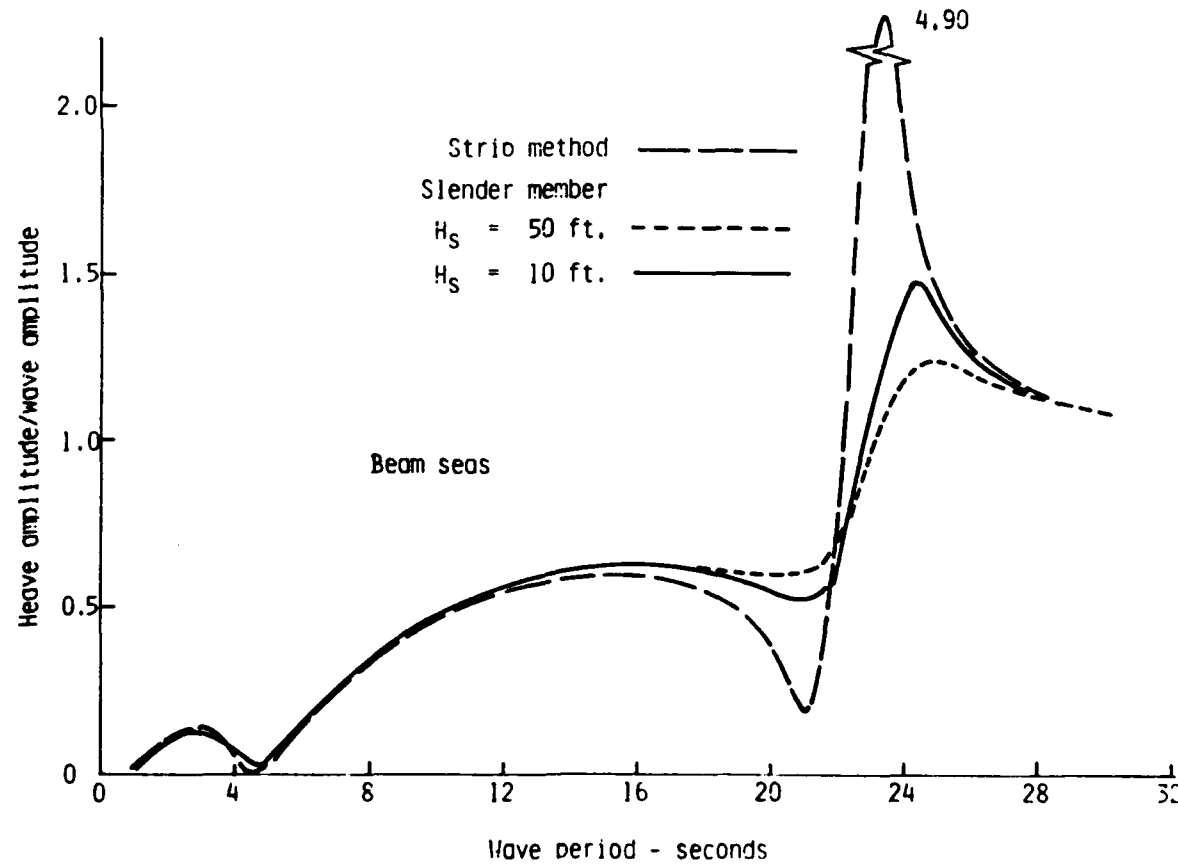


Figure 5 Twin Hull Semisubmersible Heave Response Function

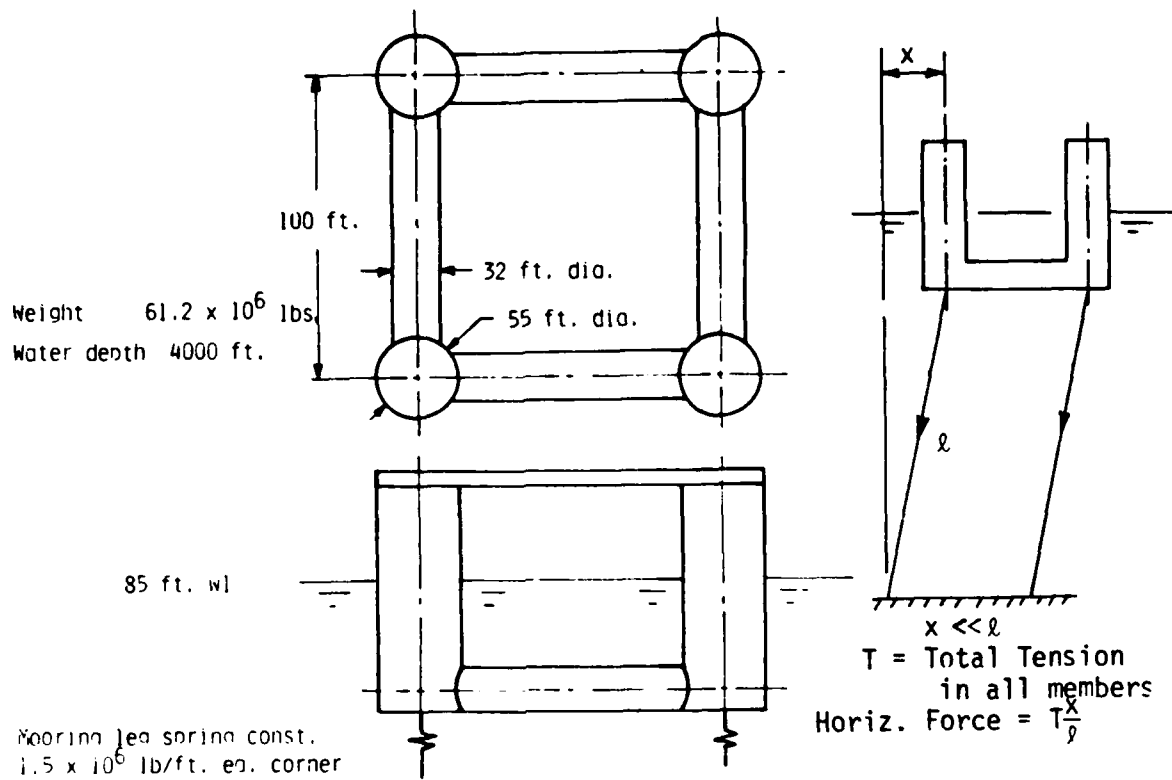


Figure 6 Four Column Example TLP

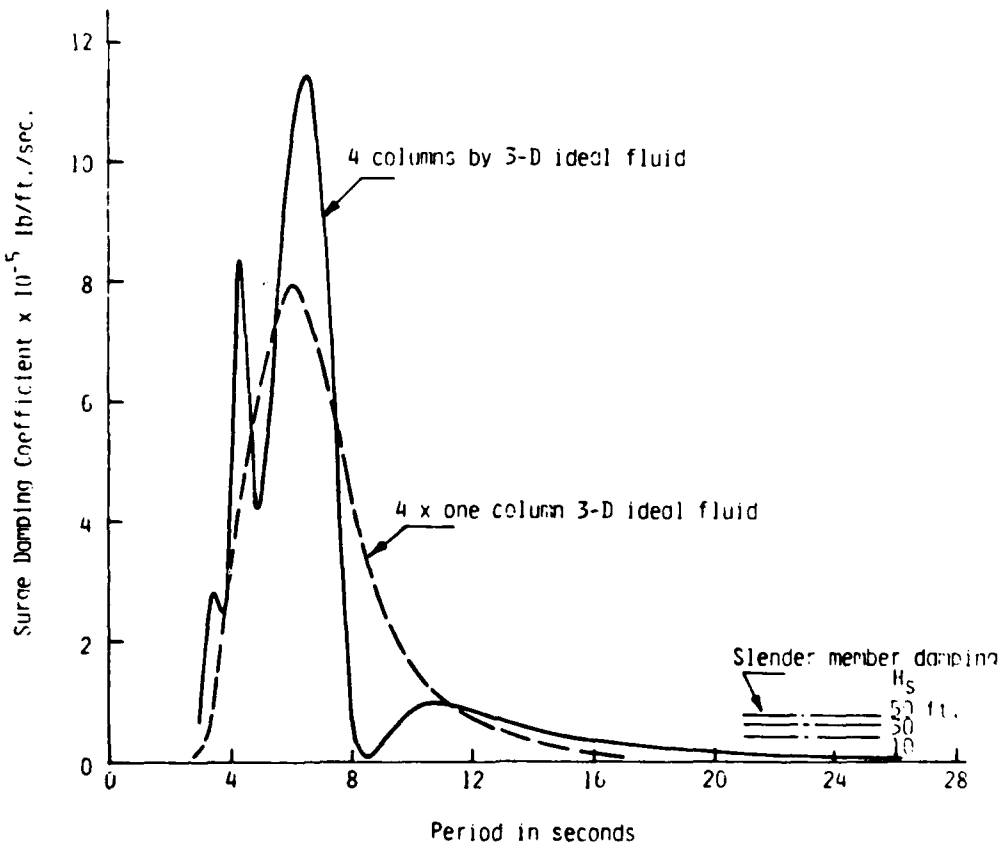


Figure 7 Four Column TLP Surge Damping

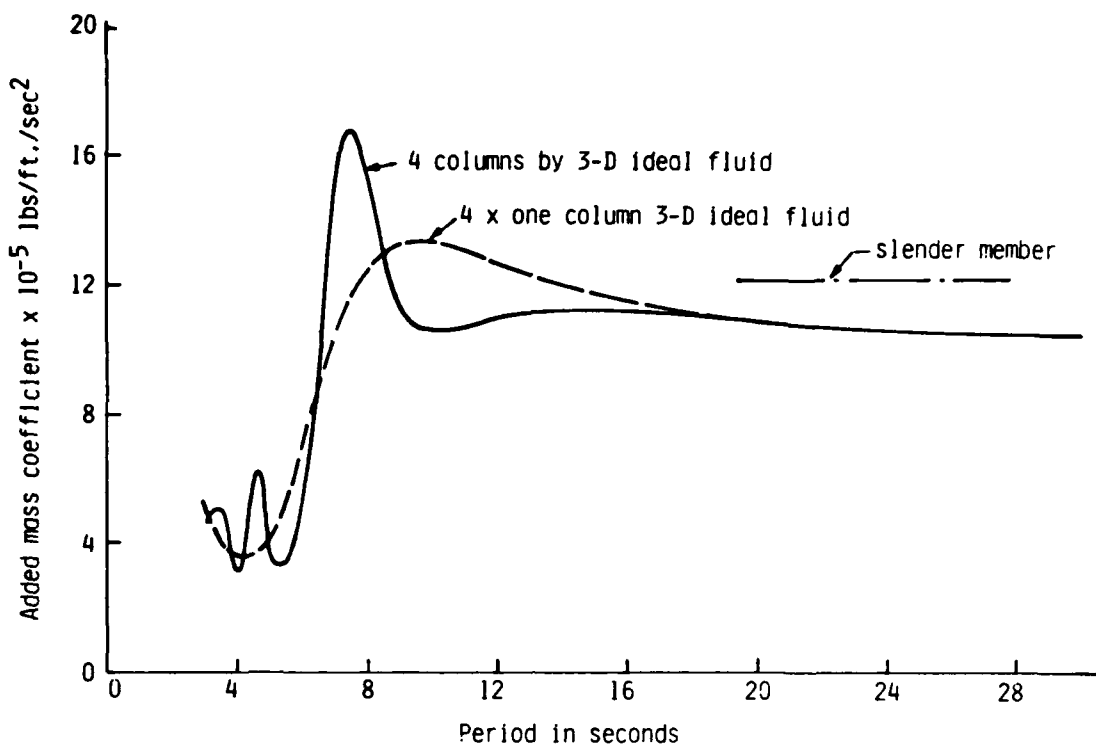


Figure 8 Four Column TLP Added Mass in Surge

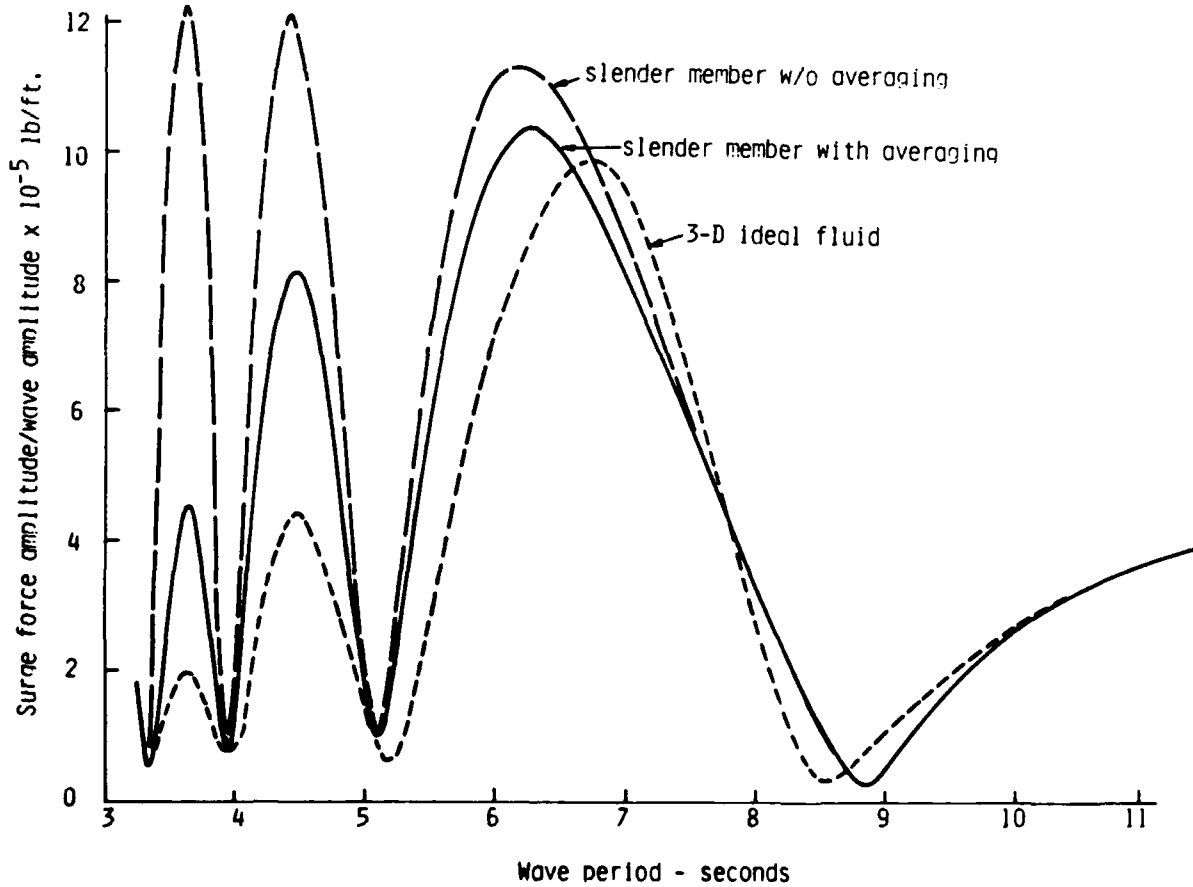


Figure 9 Four Column TLP Surge Force

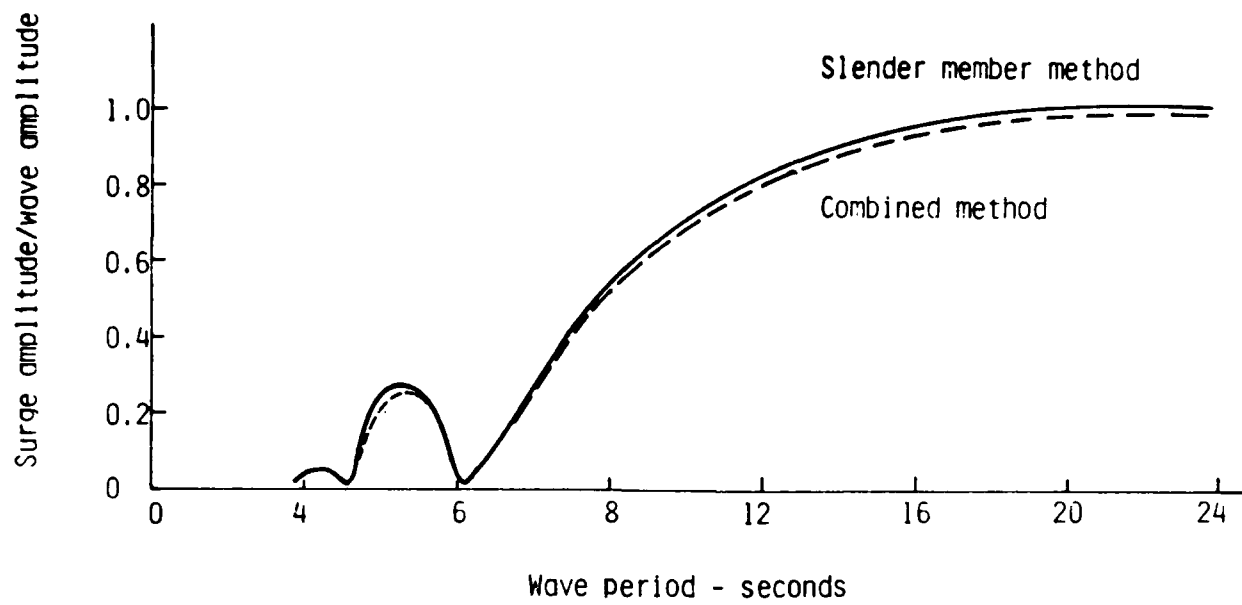


Figure 10 Four Column TLP Surge Motion Response Amplitude

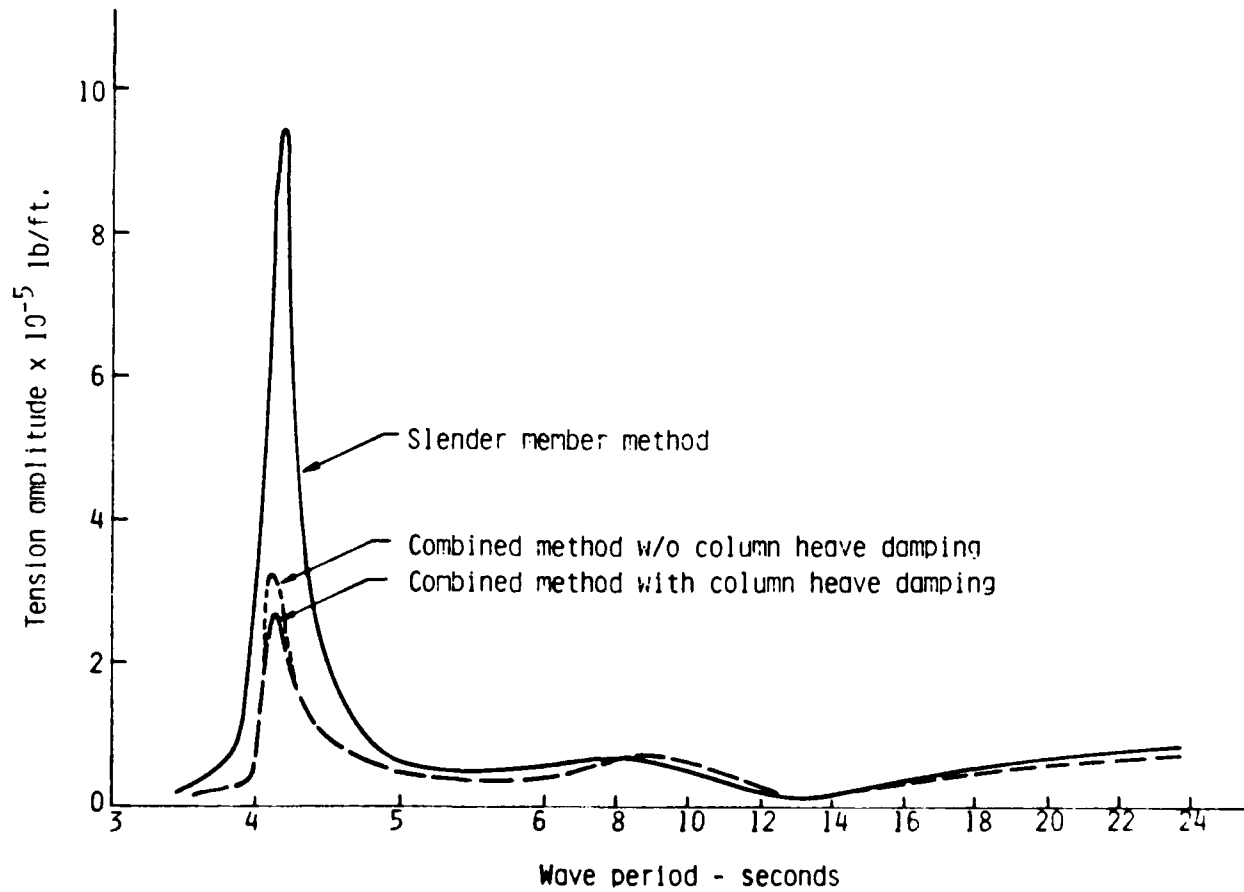


Figure 11 Mooring Leg Tension Response Amplitude

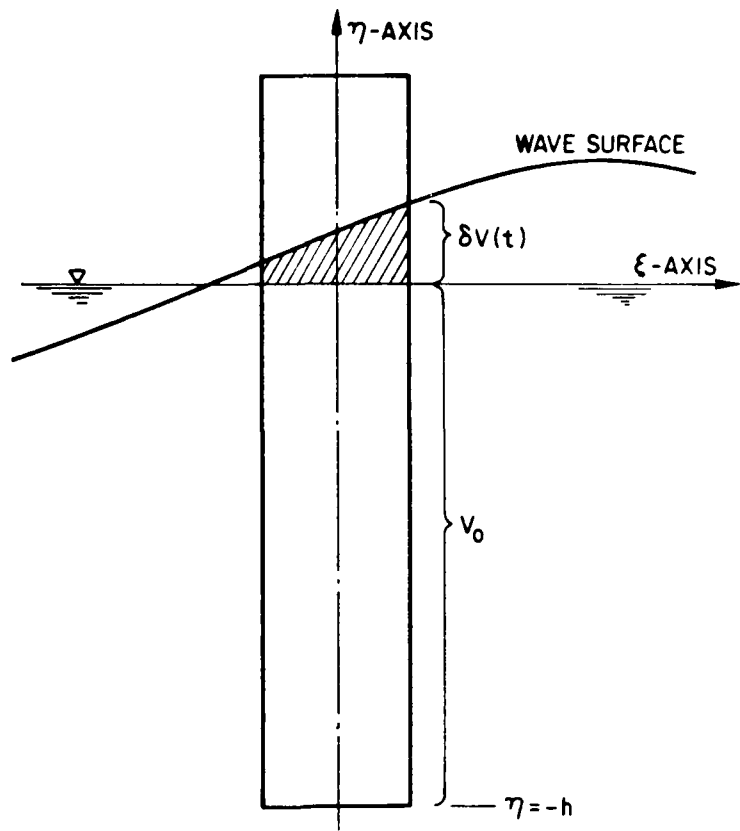


Figure 12. Surface piercing member.

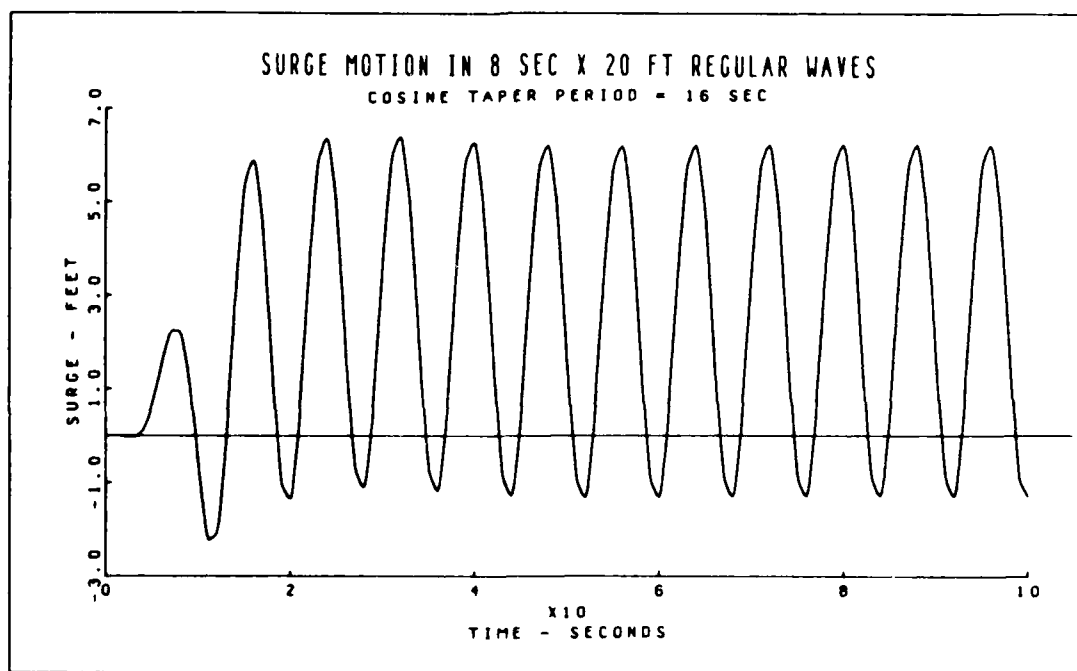


Figure 13. Illustration of nonzero mean offset caused by varying immersed length.

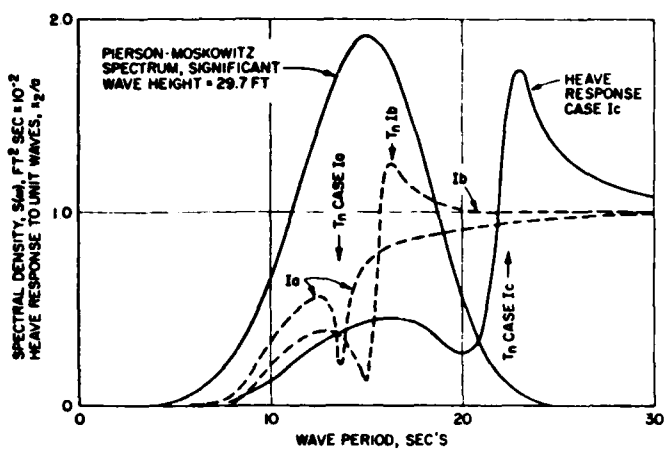


Fig. 14 - Heave response functions for four column platforms.

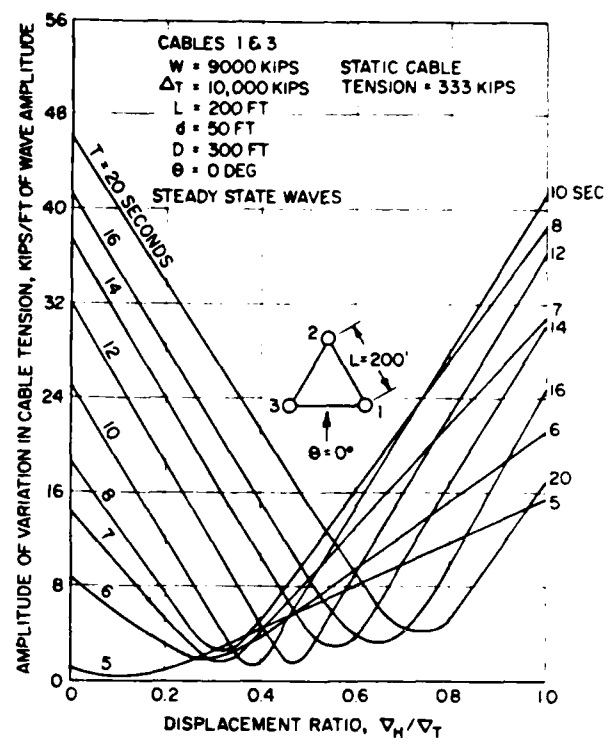


Fig. 15 - Tension variation vs volume ratio.

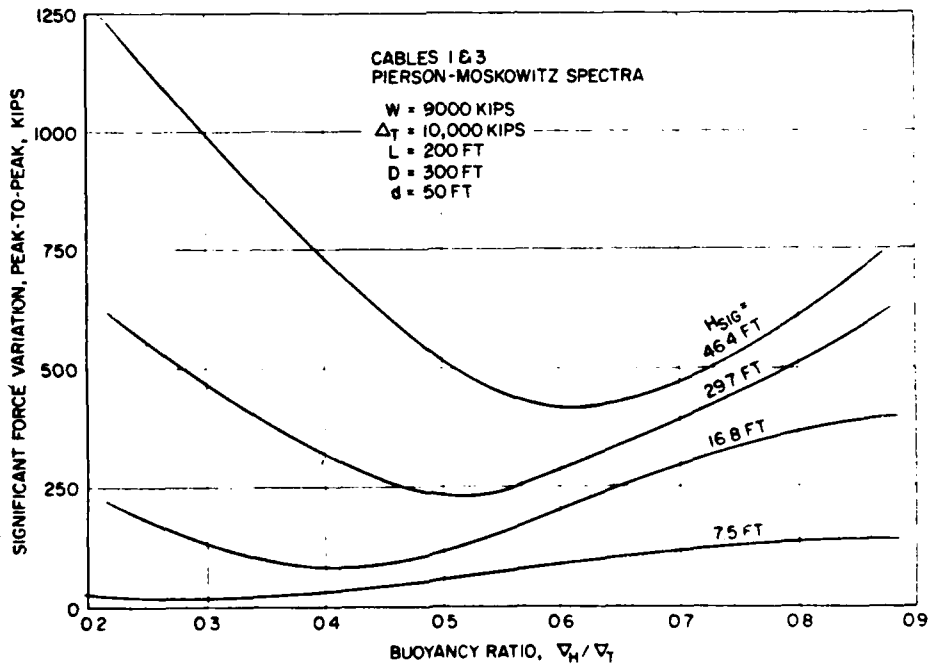
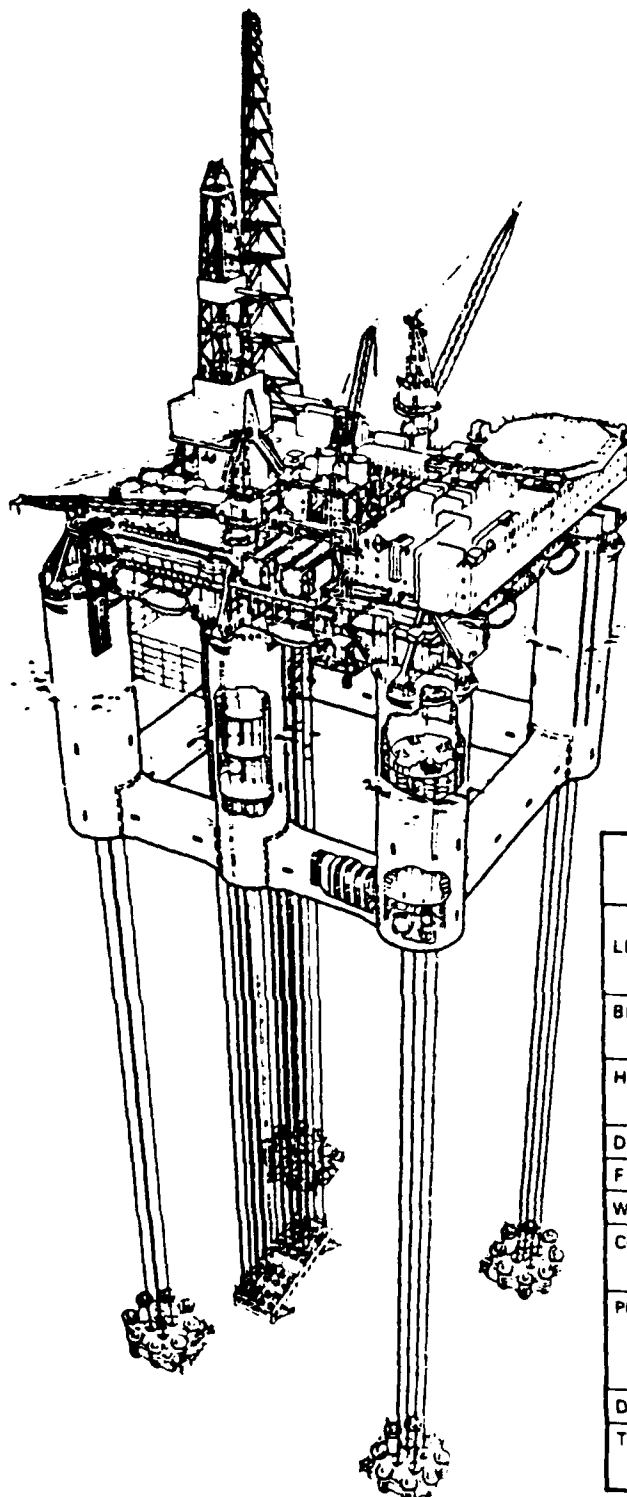


Fig. 16 - Tension leg platform, significant anchor line variations in random seas.



HUTTON FIELD
TENSION LEG PLATFORM

GEOMETRY (All dimension to moulded lines)		
LENGTH	Between column centres	78.00 M
	Overall	95.70 M
BREADTH	Between column centres	74.00 M
	Overall	91.70 M
HEIGHT	Keel to main deck	57.70 M
	Main deck to weather deck	11.25 M
DRAUGHT	Operating	32.00 M at LAT
FREEBOARD	To underside of main deck	24.50 M at LAT
WATER PLANE	Area	1324.00 M ²
COLUMNS	4 Corners	17.70 M Dia
	2 Centre	14.50 M Dia
PONTOONS	Height	10.80 M
	Width	8.00 M
	Corner radius	1.50 M
DISPLACEMENT	Approx	61500 Tonnes
TOTAL WEIGHT	Including riser tension (Approx)	48500 Tonnes

Figure 17. Overall view on TLP with key dimensions.

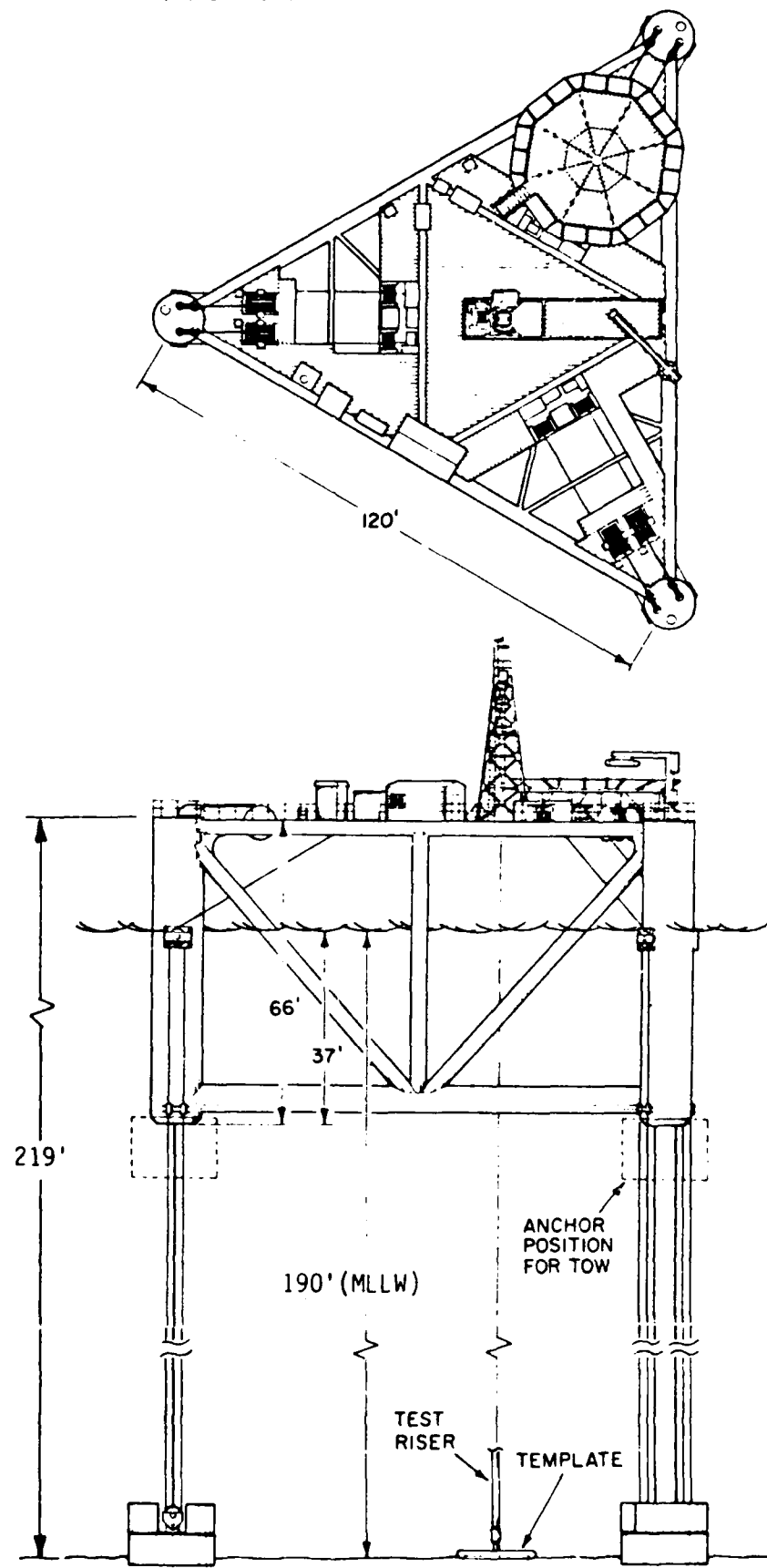


Figure 18. Deep Oil X-1.

NOTES ON DISC AND SPAR BUOYS

by

H.O. Berteaux

January 10, 1983

1. INTRODUCTION

A considerable number of surface buoys are each year deployed in the oceans for a variety of purposes.

A short list of applications using surface buoys could include the following:

- o Aid to navigation markers (U.S.C.G.)
- o Harbor and offshore ship moorings (NCEL)
- o Offshore loading of tankers (SPM)
- o Meteorological/weather buoys (NOAA)
- o Oceanographic/research buoys (WHOI)
- o Telemetry/relays (TACTS)

Surface buoys vary markedly both in size and shape.

Mission purpose (WHAT) and environmental constraints (WHERE) often dictate buoy type and dimensions.

This paper first describes the generic buoy forms most commonly encountered. It then reviews the reasons and the methods for predicting the dynamic response of DISC and SPAR buoys. A comparison is then made of the respective advantages and drawbacks of these two types of buoys.

Maintaining these buoys on station as depth and currents increase deserves as much attention as buoy response to wave excitation. The second part of the paper reviews the mooring schemes commonly used to moor DISC and SPAR buoys, again pointing advantages and drawbacks. The paper concludes with a conceptual case study illustrating the practical difficulties and limits inherent to the deployment of large surface buoys in 7400 feet of water depth.

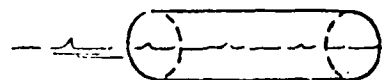
2. GENERIC BUOY FORMS

Buoy shapes usually fall within one of the basic generic forms shown in Figure 1.

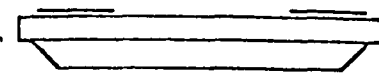
Disc buoys (1-a) having large water plane areas but small displacements tend to follow the waves both in heave and slope. Spar buoys (1-d) on the contrary have small water plane areas combined with large displacements. This makes wave excitation difficult and as a result spar buoys tend to be surface decoupled.

Intermediate buoys (1-b) combine relatively large water planes and considerable displacement. As a result these buoys will follow the wave amplitude but not the slope. They heave considerably but roll only a little. Boat shape hulls (1-c) when moored will point into the wind and the waves. They will provide ample buoyancy with minimum drag, but will heave and pitch considerably.

Typical DISC and SPAR buoys are shown in Figures 2 to 5.

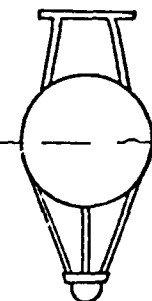


TOROID

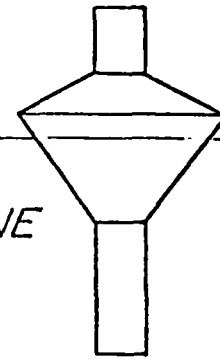


FLAT DISC

a. DISC

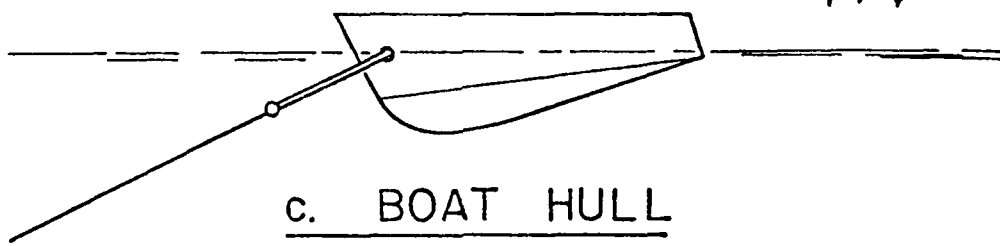


SPHERE



CONE

b. INTERMEDIATE



c. BOAT HULL

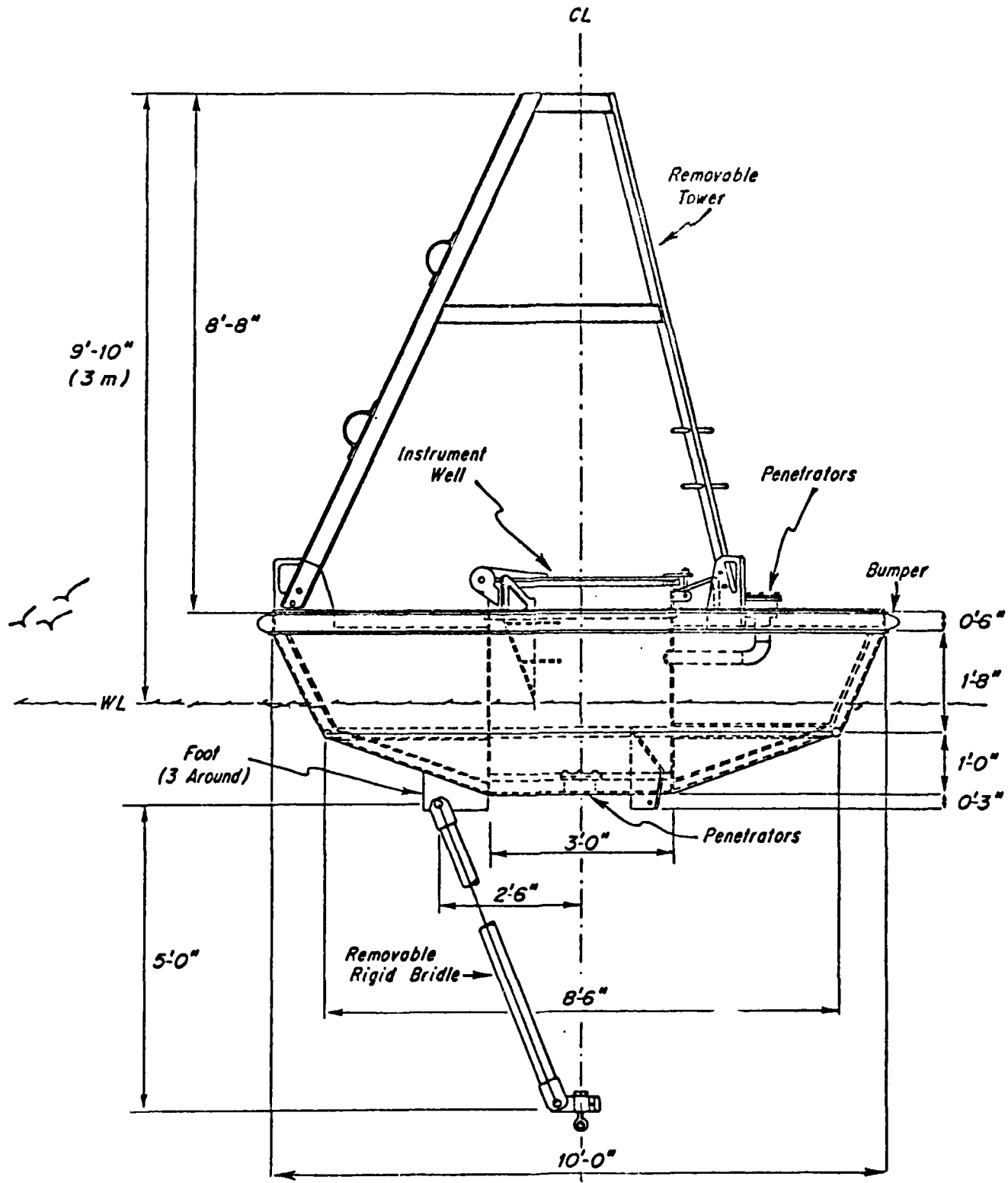


POLE

BALLAST

d. SPAR

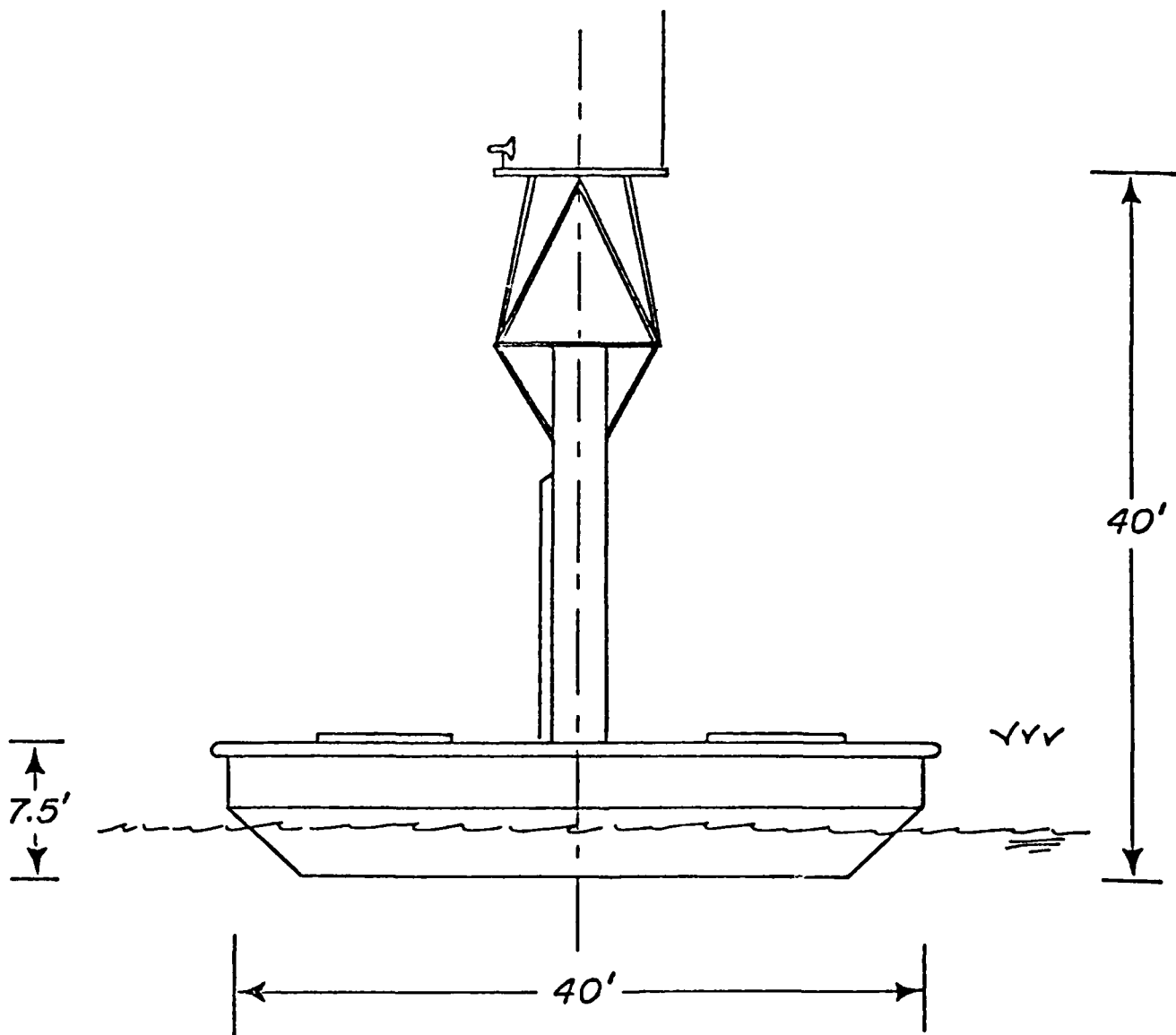
GENERIC BUOY FORMS



10 FT. WHOI DISCUS BUOY

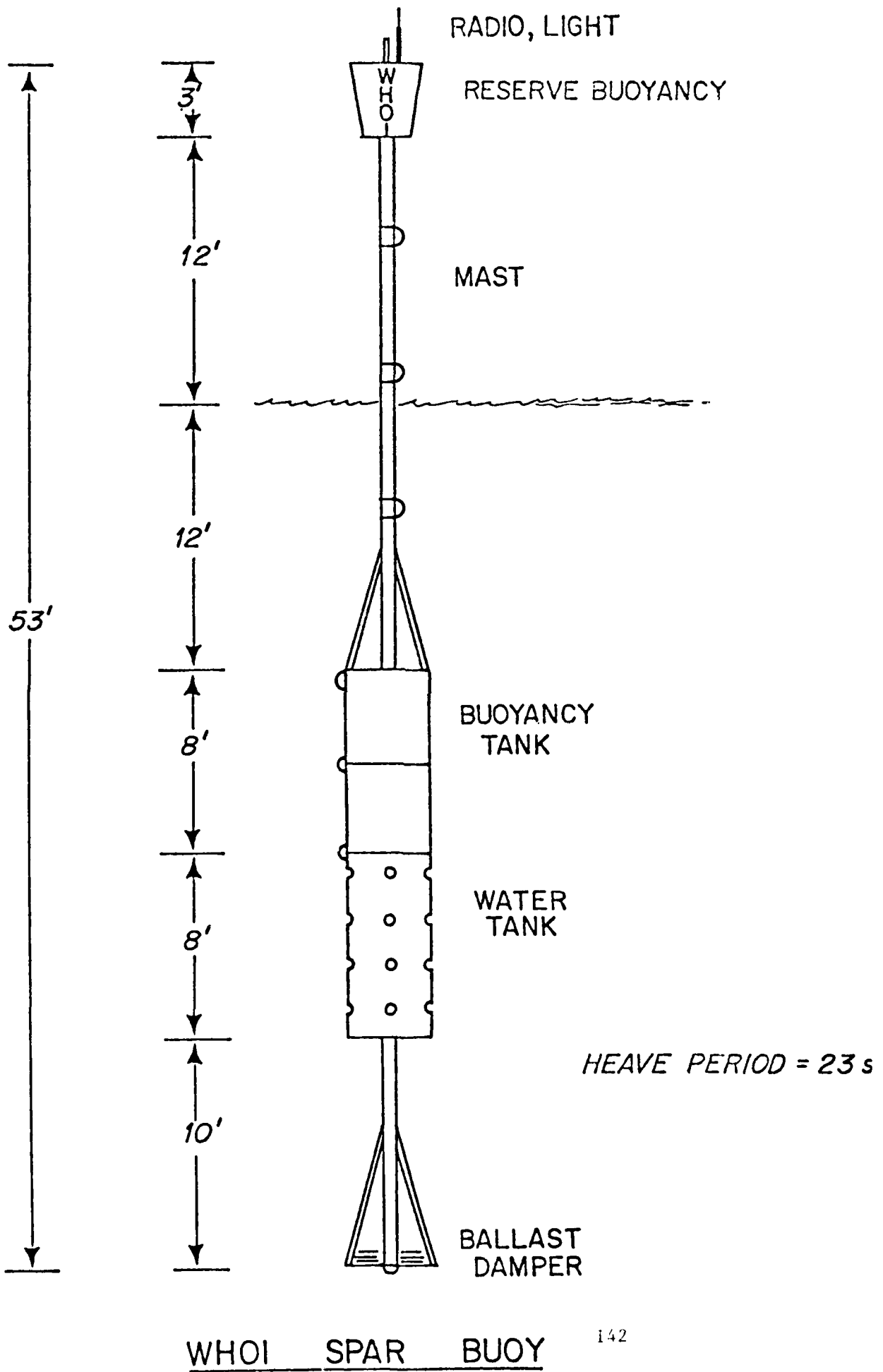
140

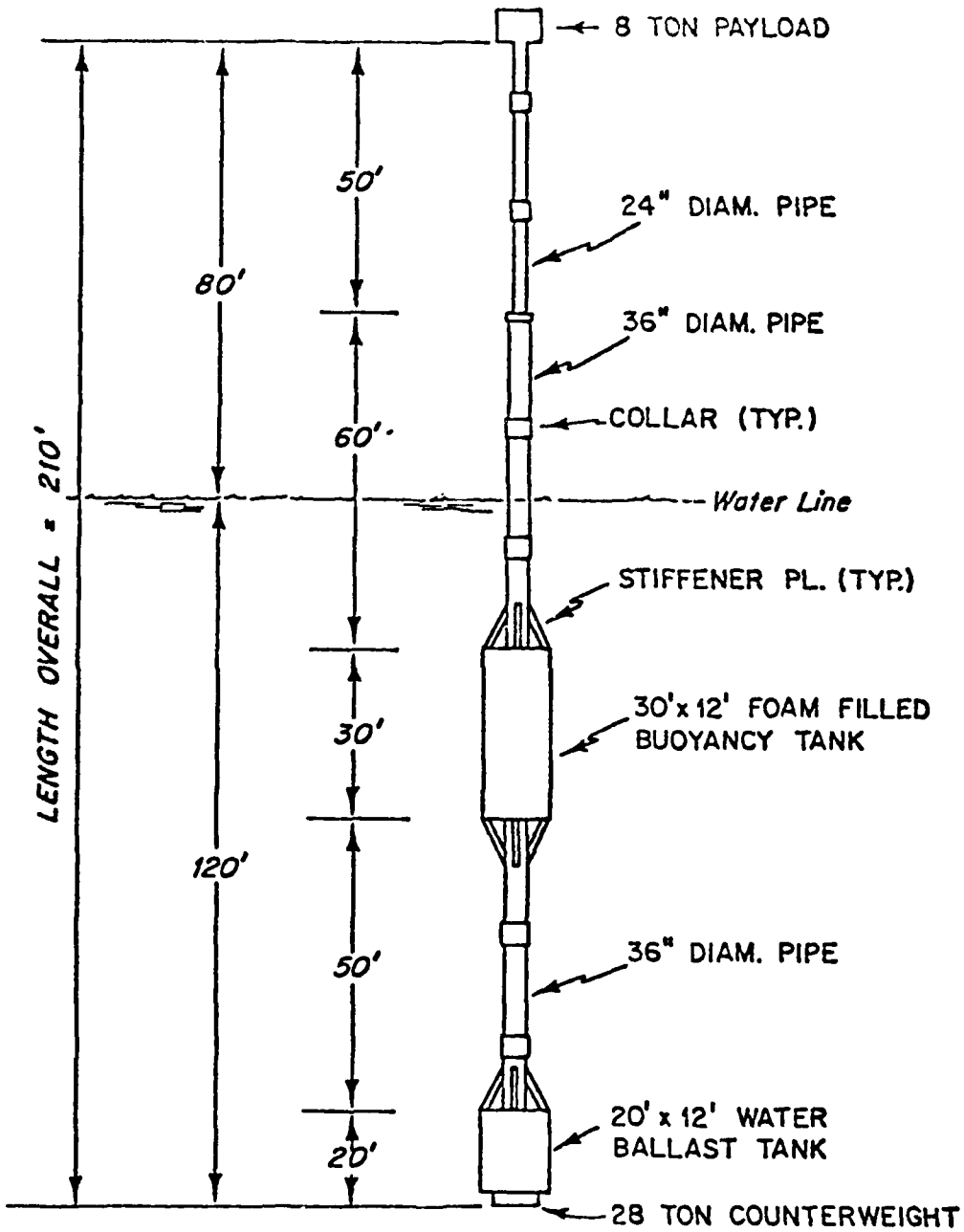
Figure 2



LARGE DISC BUOY (NDBO)

Figure 3





TOTAL WEIGHT = 118 tons
 NATURAL ROLL PERIOD = 29 secs.
 NATURAL HEAVE PERIOD = 34 secs.

LARGE SPAR BUOY

Figure 5

3. PREDICTION OF HEAVE AND ROLL BUOY RESPONSE

The analysis of buoy response to wave action follows the principles and the techniques used in ship dynamics theory (Ref. 1). The fact that most buoys are axisymmetrical and moored - as opposed to propelled - permit to greatly reduce the number and the complexity of the equations describing the motion of a ship sailing in a sea way (Ref. 2). Most buoy models ignore motion coupling terms and evaluate heave and roll separately.

The pedestrian approach of considering the forces at play and of deriving and integrating the equations of buoy heave and roll motion has considerable merit. It can help understand the physics of the problem, it permits to point out some practical aspects of buoy design, and to a certain extent it is a measure of the state-of-the-art of buoy dynamics analysis.

The response of disc and spar buoys can be described by similar equations. For the purpose at hand, a study of spar buoy response might be more enlightening.

HEAVE AND ROLL RESPONSE TO SINGLE HARMONIC WAVE

Assumptions. Simple models of buoy response to harmonic waves usually make the following assumptions:

- The water particles move in circular orbits of exponentially decreasing amplitude, the parametric equations of their motion being:

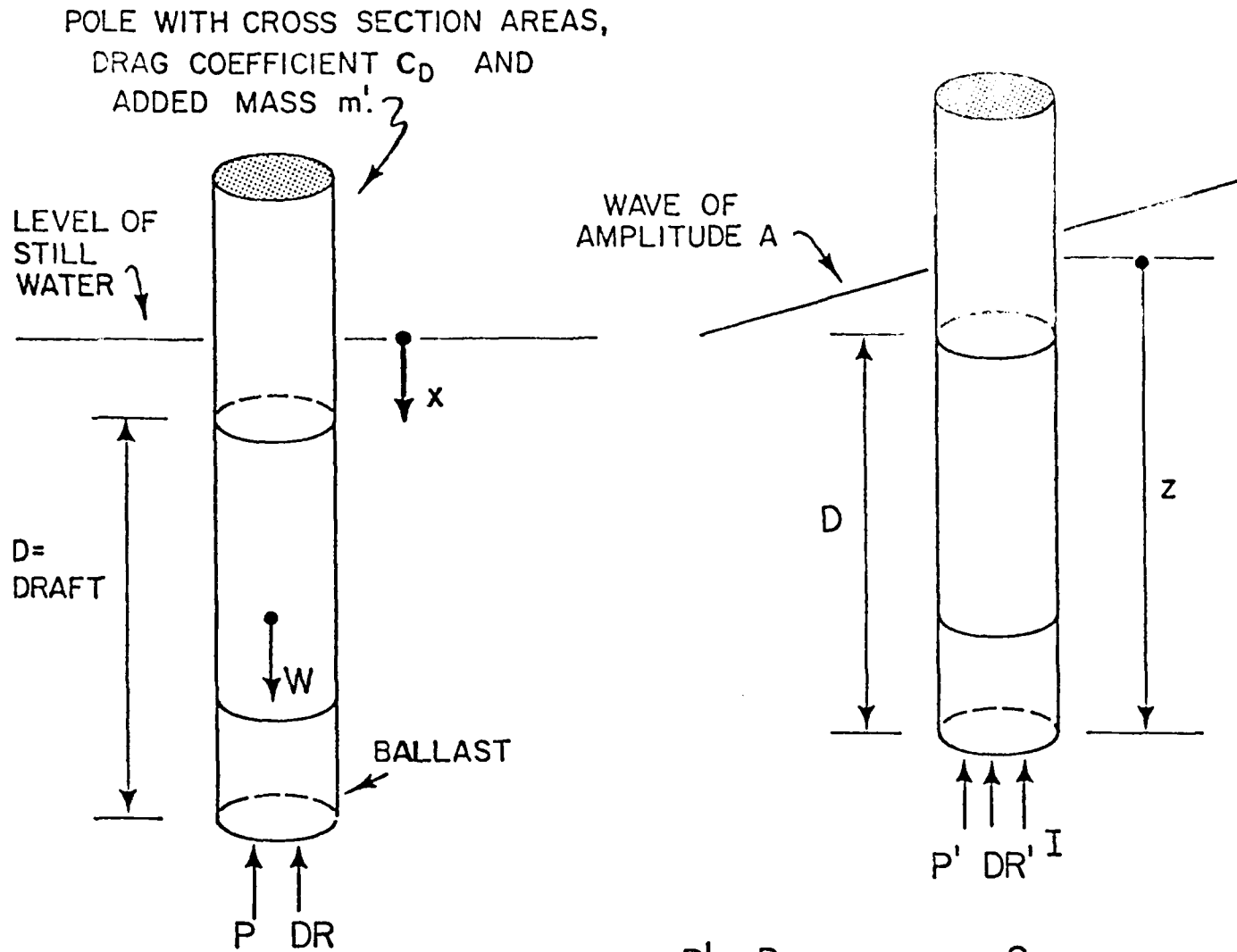
$$\xi = Ae^{-kz} \sin \omega t \quad (3.1)$$

$$\eta = Ae^{-kz} \cos \omega t \quad (3.2)$$

where A is the wave amplitude, ω the wave angular frequency, k the wave number ($k = \omega^2/g$, g being the gravity acceleration) and z the depth below the mean water level.

- The diameter of the buoy is small compared to the wave length, and it is assumed that the presence of the buoy does not alter the shape of the wave.
- The center of roll is at the buoy center of gravity.

Heave motion. The telephone pole. The spar buoy of simplest geometry is the "traditional" ballasted telephone pole. As the pole heaves in a "regular" sea way the forces acting on the pole can be considered as made of two parts: those resulting from the motion of the pole in still water and those resulting from the wave acting on a fixed pole. These forces and their expression are shown in Figure 6.



$$P = \text{Pressure} = \rho g S (x+d)$$

$$DR = \text{Drag} = 1/2 \rho C_D S I \dot{x} \dot{x}$$

$$W = \text{Weight} = \rho g S D$$

$$P' = \text{Pressure} = \rho g S \eta$$

$$DR' = \text{Drag} = 1/2 \rho C_D S I \dot{\eta} \dot{\eta}$$

$$I = \text{Inertia} = m' \ddot{\eta}$$

$$\eta = \text{Water Particle Vertical Motion}$$

$$= A e^{-Kz} \cos \omega t$$

a. BUOY HEAVING IN STILL
WATER

b. WAVE INDUCED FORCES
ON FIXED BUOY

Figure 6
HEAVE MOTION OF A TELEPHONE POLE

When combined these forces yield the following equation:

$$(\rho g S)x + \frac{1}{2} \rho C_D S |\dot{x}| \dot{x} + (m + m') \ddot{x} = \{ \rho g S \eta + \frac{1}{2} \rho C_D S |\dot{\eta}| \dot{\eta} e^{-kz} + m' \eta \} e^{-kz} \quad (3.3)$$

The "x" terms refer to buoy motion, the "η" terms to water particle motion.

This equation can be computer integrated to yield a time domain solution of the buoy heave response to the particular wave considered. The integration technique is not difficult, but the results are not very rewarding when one wants to investigate the response of the buoy to different waves or to a random sea way.

If one assumes that most of the wave induced forces act at the pole lower end ($z = \text{Draft} = D$), and that somehow the drag forces can be linearized then equation (3.3) takes the more palatable and useful form:

$$cx + b\dot{x} + m_y \ddot{x} = (c\eta + d\dot{\eta} + m' \eta) e^{-kD} \quad (3.4)$$

Where $c = \rho g S$ is the restoring constant

b is the linear coefficient of heave damping

d is the linear coefficient of wave induced drag

and $m_y = m + m'$ is the buoy virtual mass, m' being the added mass.

Assuming the passing wave to have a unit amplitude ($A = 1$), equation (3.4) can be further reduced to:

$$cx + b\dot{x} + m_y \ddot{x} = F \cos(\omega t + \sigma) \quad (3.5)$$

where F , the exciting force, is given by:

$$F = e^{-\frac{\omega^2 D}{g}} \sqrt{(c - m' \omega^2)^2 + (d\omega)^2} \quad (3.6)$$

and σ the phase angle between force and wave by:

$$\sigma = \tan^{-1} \frac{b\omega}{c - m' \omega^2} \quad (3.7)$$

Using equation (3.5) with $b = F = 0$, the natural period of heave T_H is found to be

$$T_H = 2\pi \sqrt{\frac{m_y}{c}} \quad (3.8)$$

In the case of a pole of constant cross sections S

$$m_y \approx \rho g S D$$

$$c = \rho g S$$

and thus

$$T_H = \frac{2\pi}{\sqrt{g}} \sqrt{D} \quad (3.9)$$

Thus like penduli of equal length, telephone poles of equal draft have equal periods of free oscillations. Furthermore, they require considerable draft to oscillate slowly. As an example the draft needed for a pole to have a natural period of 20 seconds would be an astonishing 100 meters!

Leaving these factual remarks aside, let us return to our linearized equation of heave (3.5). One may well at this time ask what kind of subterfuge was used to linearize the equation. A linearization technique commonly used is based on the assumption that linear and nonlinear cyclic drag forces dissipate the same amount of energy per cycle. Using this rationale the linear coefficients b and d of drag equivalence are found to be:

$$b = \frac{4}{3\pi} \omega \rho C_D S x = b(x, \omega) \quad (3.10)$$

$$d = \frac{4}{3\pi} \omega \rho C_D S = d(\omega) \quad (\text{assuming } A = 1) \quad (3.11)$$

This unfortunate result stipulates that one must know the answer before he can attempt to calculate it with the help of equation (3.5). This, however, is not as big a predicament as it may seem. One, for example, can always guess a value of heave "x" to compute $b(x, \omega)$ and upgrade this value by iterative computations.

Thus, in principle, at least, the integration of (3.5) may now proceed. The result (steady state) is:

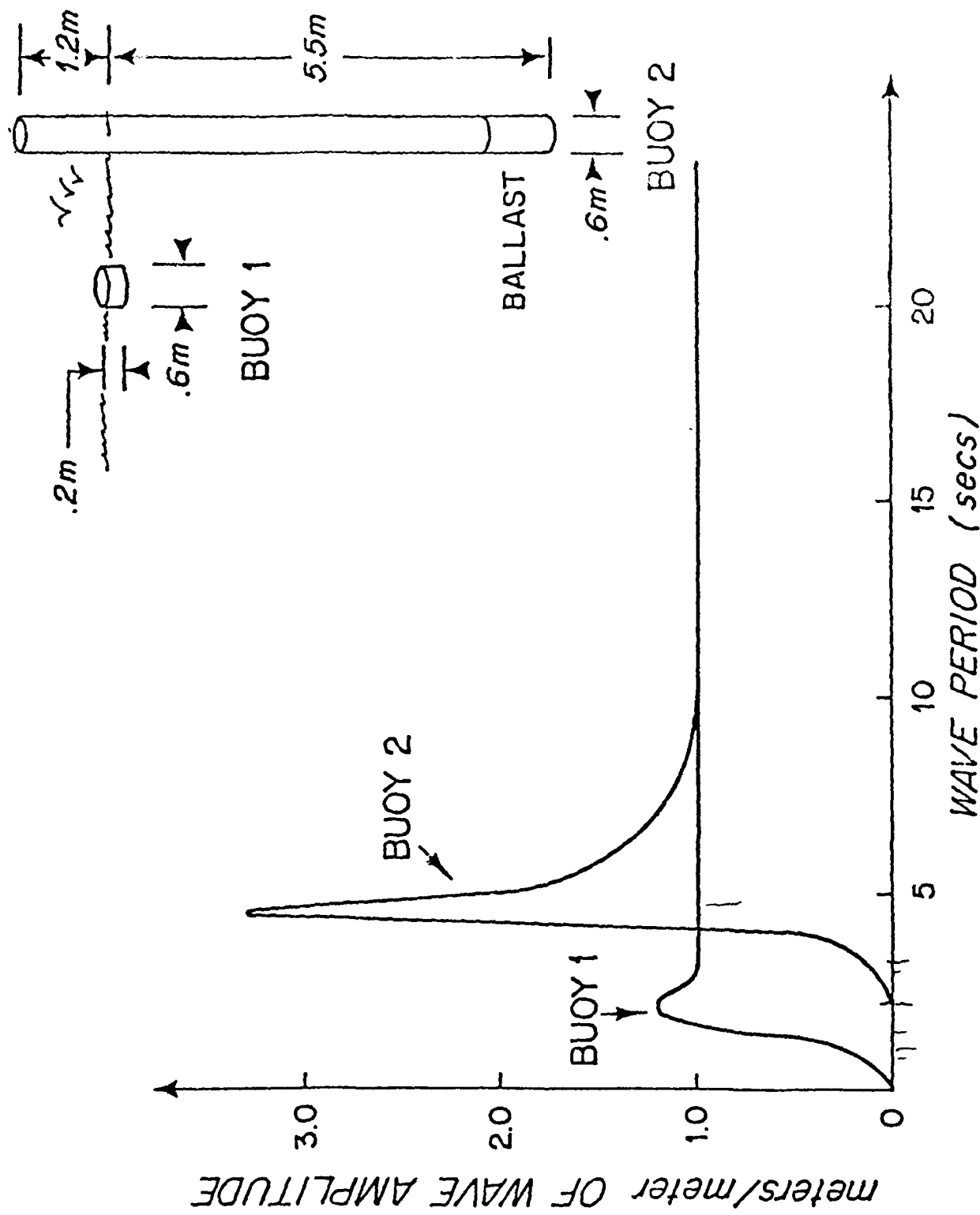
$$x = \frac{e^{\frac{-\omega^2 D}{g}} \sqrt{(c - m' \omega^2)^2 + (d\omega)^2}}{\sqrt{(c - m' \omega^2)^2 + (b\omega)^2}} \cos(\omega t + \theta + \sigma) \quad (3.12)$$

θ , the phase angle between the force and the heave response is given by

$$\theta = \tan^{-1} \frac{-\omega b}{c - m' \omega^2} \quad (3.13)$$

Expression (3.12) is known as the heave transfer function $H(\omega)$. It describes the buoy heave response, both in amplitude and phase, to waves of unit amplitude and frequency ω . The amplitude of the transfer function $|H(\omega)|$ is known as the heave response amplitude operator (RAO).

The immediate usefulness of RAOs is to present a clear and concise picture of the buoy predicted behavior as a function of wave period. Fig. 7 shows the RAOs of a disc and a spar buoy of same cross section. As expected the RAO of the flat disc has a value of one over most wave periods. On the other hand, the spar buoy magnifies the amplitude of the wave with periods between 4 and 10 seconds at which time it becomes itself a wave follower. Using these RAOs, the heave amplitude produced by a wave of one meter amplitude and 5 seconds period is found to be one meter for the disc and 3.3 meters for the pole.



HEAVE RESPONSE AMPLITUDE OPERATORS
OF TWO CYLINDRICAL BUOYS

Figure 7

Heave motion. Buoys of complex geometry. Formula (3.8), i.e.

$$T_H = \sqrt{\frac{m_v}{c}}$$

stipulates that a buoy with a large mass and a small neck sticking through the surface could yield large heave periods without necessarily resorting to extreme buoy drafts.

Furthermore if damping plates could be added the heave at resonance would be reduced and the spar buoy would not jump out of the water as the bare pole does.

With these considerations in mind, spar buoys of the type shown in Fig. 4 have been designed and built.

The method to derive the heave RAO of buoys of complex shape is similar to the one just described. First the forces due to buoy vertical motion and wave vertical speed and acceleration acting on the different buoy components must be evaluated at their respective depth and linearized. The sum of these forces yield the equation of motion. The buoy heave transfer function is then obtained by integration. The ensuing RAO will again have the familiar form:

$$|H(\omega)| = \frac{\sqrt{(M-\omega^2 Q)^2 + (N\omega)^2}}{\sqrt{(c-m_v \omega^2)^2 + (\omega B)^2}} \quad (3.14)$$

It may be instructive to give the expression of the buoy physical parameters as they appear in the RAO.

- $M = \rho g \sum_i S_i e^{\frac{-\omega^2 h_i}{g}}$ is the wave pressure parameter,
with S_i being the area of the component i subjected to pressure at the depth h_i .
- $Q = \rho \sum_i C_{m_i} V_i e^{\frac{-\omega^2 h_i}{g}}$ is the buoy added mass parameter,
 V_i is the water of volume displaced by the component i at depth h_i , C_{m_i} being the added mass coefficient in vertical motion.
- $N = \omega \sum_i \frac{4}{3\pi} \rho C_{D_i} S_i e^{\frac{-\omega^2 h_i}{g}}$ is the linearizing coefficient of wave drag,
 S_i is the area of the component i , drag coefficient C_{D_i} at depth h_i .

m_v is the buoy virtual mass in vertical motion, and

$$B = \omega \sum_i \frac{4}{3\pi} \rho C_{D_i} S_i x \quad \text{is the linearizing coefficient of buoy drag.}$$

Before leaving the heave subject the following comments should be made. Damping plates if placed too close to the surface, will enhance heave motion. Tanks filled with water after deployment greatly increase the buoy mass. Finally a "good" spar buoy does not heave! This means that the length of its "neck" should be long enough to permit most waves to climb up and down without swamping the top end or exposing the lower end of the neck.

Roll motion. Any spar buoy. The literature certainly encourages the readers to develop their own equation of roll. Following the hint and again starting from basic principles, let us derive a detailed expression of roll RAO for any type of spar buoy.

The equation of buoy roll can be obtained from Newton's law for rotating bodies, namely:

$$\sum_i M_i = (I + I')\ddot{\theta} \quad (3.15)$$

where $\sum_i M_i$ is the sum of the moments applied to the buoy

I is the moment of inertia with respect to the instantaneous center of roll

I' is the moment of inertia of the entrained water and

θ is the angle of roll, assumed to be small

The resultant moment can again be considered as the sum of the moments due to the buoy free rolling in still water and of the moments induced by the passing wave. These moments are:

- The righting moment $M_r = W\overline{gm} \theta = C\theta$

where

W is the buoy "air" weight

\overline{gm} is the distance between the buoy c.g. and the metacenter.

and $C = W\overline{gm}$

- The damping moment M_D which also opposes roll motion. The expression of M_D can be obtained by integration over the entire buoy submerged length of the damping forces opposing free rolling. Let us consider, as shown in Fig. 8, an elementary section of the buoy located at a distance r from the c.g. Let $d(r)$ be the diameter of the buoy at that section.

The damping force acting on this elementary section is:

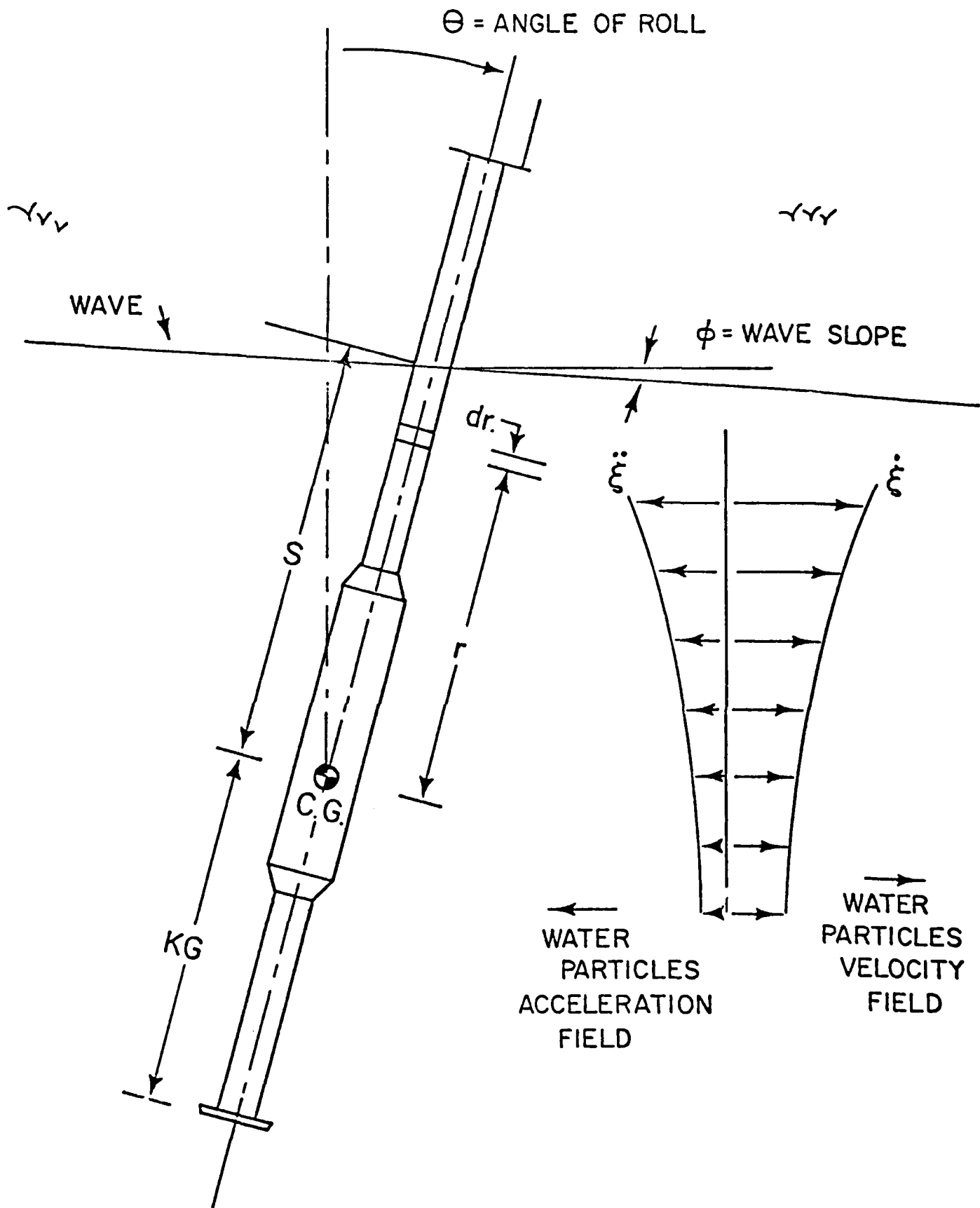
$$dF_D = \frac{1}{2} \rho C_D d(r) |r\dot{\theta}| r dr$$

which can be linearized to

$$dF_D = b(r) r \dot{\theta} dr$$

$$\text{with } b(r) = \frac{4}{3\pi} \rho C_D(r) d(r) \omega \overline{r}$$

where $C_D(r)$ is the drag coefficient at that location



ROLL MOTION OF A SPAR BUOY

151

and $\bar{\theta}$ is an averaged or guessed angle of roll.
The moment of this elementary force is

$$dM_D = rdF_D$$

and the total moment is found by integrating from the buoy keel to the buoy water line.

Thus

$$M_D = \left(\frac{4\omega}{3\pi} \rho \bar{\theta} \int_{KG}^S C_D(r) d(r) r^3 dr \right) \dot{\theta}$$

or $M_D = E\dot{\theta}$

- The capsizing moment M_C due to wave slope ϕ , simply given by

$$M_C = \overline{Wgm} \phi = C \frac{\omega^2}{g} \sin \omega t$$

- The wave drag moment M_F due to water particles impinging on the buoy with speed

$$\dot{\xi} = \omega e^{-kz} \cos \omega t$$

Above the c.g. these forces tend to capsize the buoy. Below the c.g. they tend to upright the buoy (see Fig. 8). The wave induced drag forces acting on the elementary buoy section previously considered will again be assumed to be of the form

$$dF_F = c(r) \dot{\xi}$$

with

$$c(r) = \frac{4}{3\pi} \omega \rho C_D(r) d(r) X(r) dr$$

where $X(r)$ is the amplitude of water particle horizontal cyclic motion at depth z . For a wave of unit amplitude

$$X(r) = e^{-kz}$$

The moment of this elementary force is

$$dM_F = rdF_F = rc(r) \dot{\xi}$$

Expressing z as a function of r , the integration yielding the wave drag moment M_F is

$$M_F = \left(\frac{4\omega}{3\pi} \rho \int_{KG}^S C_D(r) d(r) e^{-2kz} r dr \right) \omega \cos \omega t$$

$$M_F = F \omega \cos \omega t$$

The wave induced inertia Moment due to the water particles horizontal acceleration

$$\ddot{\xi} = -\omega^2 e^{-kz} \sin \omega t.$$

Inertia forces acting above the c.g. tend to upright the buoy, the others will tend to capsize it.

The elementary inertia force dI acting on an elementary buoy volume dV

$$dV = \frac{\pi}{4} d(r)^2 dr$$

is of the form

$$dI = Cm(r) \frac{\pi}{4} d(r)^2 \ddot{\xi} dr$$

where $Cm(r)$ is the added mass coefficient in horizontal motion for the particular dV .

The corresponding elementary moment is

$$dM_I = r dI$$

and the total moment is found from

$$M_I = \left(\frac{-\pi \rho}{4} \int_{KG}^S Cm(r) d(r)^2 e^{-kz} r dr \right) \omega^2 \sin \omega t$$

or

$$M_I = G \omega^2 \sin \omega t.$$

Inserting the values of the external moments into equation (3.15) yields

$$(I + I') \theta + E \theta + C \sigma = M \cos(\omega t + \sigma) \quad (3.16)$$

where

$$M = \sqrt{\left(\frac{C \omega^2 + G \omega^2}{g} \right)^2 + (F \omega)^2} \quad (3.17)$$

is the exciting Moment and σ

$$\sigma = -\tan^{-1} \frac{\left(\frac{C \omega^2 + G \omega^2}{g} \right)}{F \omega} \quad (3.18)$$

is the phase angle between wave and exciting moment.

Before integrating the equation of roll, the added moment of inertia I' must be evaluated.

By definition

$$I' = \int r^2 dm' = \rho \int r^2 Cm(r) dV$$

where dm' is the added mass of a buoy elementary volume dV , with an added mass coefficient $Cm(r)$. The integral is to be evaluated over the entire immersed buoy volume.

Thus

$$I' = \left(\frac{\pi \rho}{4} \int_{KG}^S Cm(r) d(r)^2 r^2 dr \right)$$

If the buoy is of cylindrical shape, then $C_m(r) = 1$. The added moment of inertia is then simply

$$I' = \rho \int r^2 dV \quad (3.19)$$

which happens to be the moment of inertia of the water displaced with respect to the buoy c.g.

Integrating the linearized equation of roll (3.16) yields the roll transfer function $R(\omega)$. The roll R.A.O. $|R(\omega)|$ is then expressed by:

$$|R(\omega)| = \frac{\sqrt{\frac{(C\omega^2 + G\omega^2)^2 + (F\omega)^2}{g}}}{\sqrt{(C - I_v\omega^2)^2 + (\omega E)^2}} \quad (3.20)$$

Here $I_v = I + I'$ is the buoy virtual moment of inertia.

A graph of the roll response operator for the WHOI spar buoy shown in Fig. 4 is shown in Fig. 9.

The free rolling period of roll T_R is given by

$$T_R = 2\pi\sqrt{\frac{I_v}{C}} \quad (3.21)$$

Response of moored buoys. To evaluate the heave and roll response of moored buoys one must introduce the mooring tension force in the equations of motion previously derived. This force is usually expressed as the sum of a static and a dynamic component, i.e.

$$T = T_s + T(x, \theta, t) \quad (3.22)$$

The static component T_s is best obtained from a computer solution of the equilibrium trajectory of the mooring line when subjected to a known current profile. In absence of currents the static tension is simply the immersed weight of the mooring line supported by the buoy, plus, in the case of a taut moor, the tension resulting from the stretch of the compliant mooring part.

As the buoy heaves and rolls in the sea way it imparts dynamic stresses which must be added to the static mean. Modeling the dynamic response of mooring lines goes beyond the scope of this paper. This broad subject is comprehensively reviewed in Reference 3.

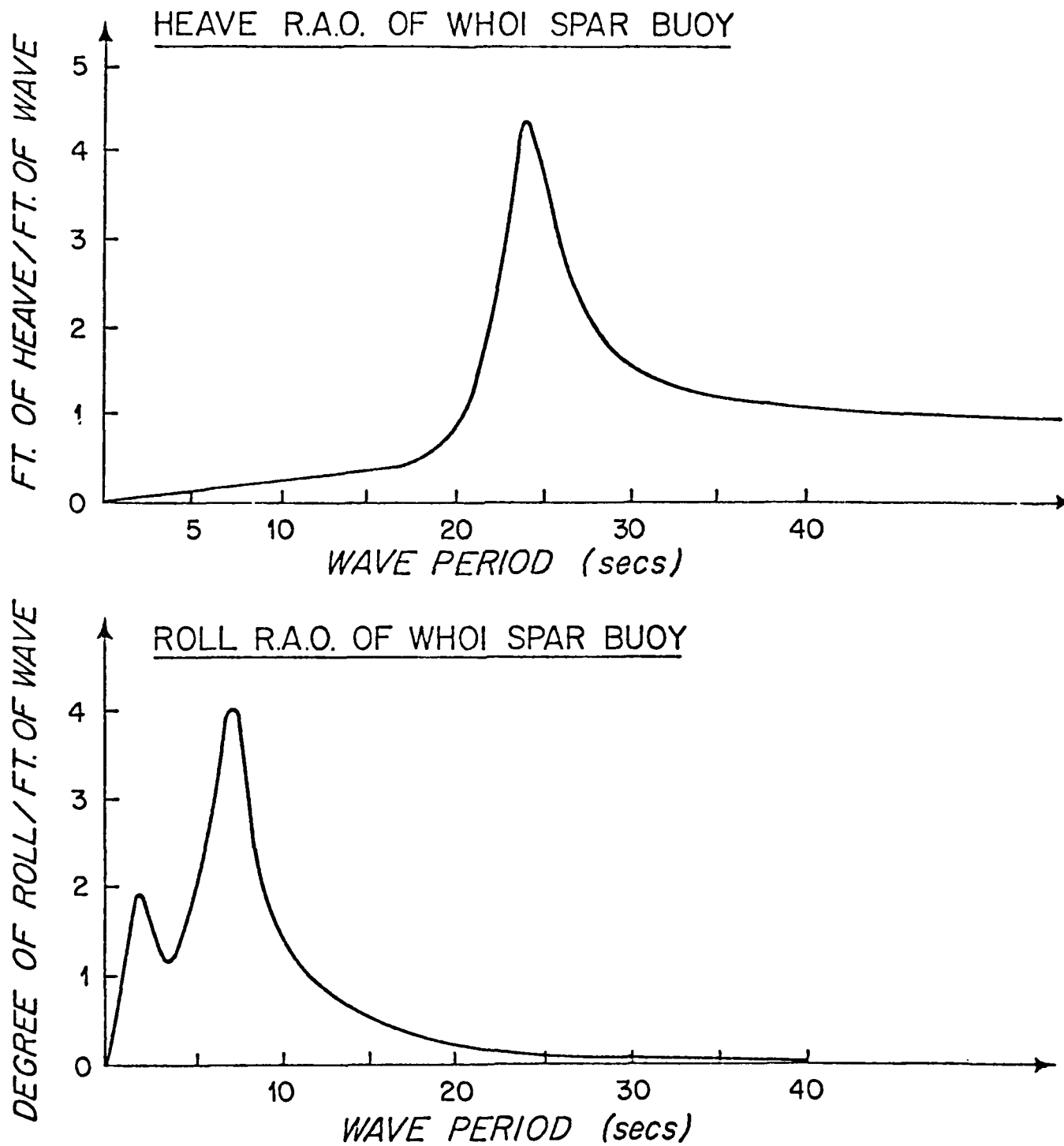


Figure 9

Of practical value for our purpose are the limiting cases where 1) the static component is much greater than the dynamic one 2) the dynamic component is assumed to be directly proportional to heave motion.

In the first case the vertical component of the static tension will increase the draft of the free buoy. Buoy heave and roll RAOs parameters previously defined should then be evaluated accordingly. The horizontal component of the tension, if any, must equal the current induced drag on the buoy. This couple produces a constant tilt easily found from equilibrium considerations. Predicted buoy inclinations would then be the sum of the computed roll angles and of the constant tilt angle.

In the second case the vertical component of the tension T_v will be

$$T_v = T_s \cos\theta + kx$$

where θ is the mooring line angle with the vertical and
k is the mooring line spring constant.

Introducing this force in the heave equation (3.4) will only result in a change of the restoring constant c from $c = \rho g S$ to $c' = c + k$. The heave RAO of the moored buoy will be of the same form as the one given by (3.14).

On the other hand, the introduction of a heave dependent tension force will produce nonlinear terms in the roll equation. Under these conditions, one can resort to computer integration techniques to sequentially integrate the equation of heave and heave dependent roll. Time domain solutions for regular waves of particular interest could thus be obtained.

STATISTICAL PREDICTION OF BUOY RESPONSE

Simple harmonic waves - or regular swells - are exceptional. The amplitude of actual seaways is usually a random function. Confronted with this randomness, one must resort to statistical analysis to describe the buoy response in terms of means and maxima which are likely to occur. If the amplitudes "r" of the buoy response to a given seaway could be described by an explicit probability density function $p(r)$ then these statistical means and maxima could be directly calculated. For example:

- The mean amplitude \bar{r} would be found from

$$\bar{r} = \int_0^{\infty} rp(r)dr \quad (3.23)$$

- Similarly the significant response $\bar{r}_{1/3}$, that is the average of the one third highest responses, would be found from:

$$\bar{r}_{1/3} = 3 \int_{r_0}^{\infty} rp(r)dr \quad (3.24)$$

where r_0 , the amplitude of the smaller response in that bunch, must be evaluated using

$$\frac{1}{3} = \int_{r_0}^{\infty} p(r)dr \quad (3.25)$$

Under certain restrictive conditions, the amplitude of ship response (heave, pitch, roll) to random seaways has been found (Ref. 4) to follow a probability density function given by:

$$p(r) = \frac{2r}{r^2} e^{-\frac{r^2}{r^2}} \quad (3.26)$$

where \bar{r}^2 is the mean square value of the particular mode of response.

When this Rayleigh probability density function is used to compute means such as those just defined, the results are found to be proportional to the root mean square (RMS) of the response. For example, the significant response will have an amplitude $\bar{r}_{1/3}$ given by

$$\bar{r}_{1/3} = 1.416 \sqrt{\bar{r}^2}$$

When a record exists of response measurements, then the RMS is directly obtained from the record. On the other hand if no measurements have yet been made, then the prediction of response means and maxima will depend on the possibility of hindcasting the RMS response to a given seaway.

The technique used to calculate the RMS amplitude of buoy response is similar to the one used in the probabilistic theory of ship dynamics (Ref. 5). First the assumption is made that the buoy response to a simple harmonic wave is linear. Furthermore the stipulation is made that the random seaway can be reproduced by a summation of elementary sinusoids. The buoy response to any of these being linear, one can safely state that the buoy response to the sum of the sinusoids describing the seaway equals the sum of the responses to the individual sinusoids.

If $S(\omega)$ is the spectral density function describing the particular seaway, then the quantity

$$\lim_{d\omega \rightarrow 0} \sqrt{S(\omega_n) d\omega}$$

represents the amplitude of the elementary sinusoid with angular frequency ω_n .

Now if $X(\omega)$ is the buoy linear response to a wave of unit amplitude, then

$$\lim_{d\omega \rightarrow 0} X(\omega_n) \sqrt{S(\omega_n) d\omega}$$

represents the response of the buoy to this elementary wave. The quantity $X^2(\omega_n) S(\omega_n) d\omega$ represents the mean square value of the response in the frequency band $d\omega$ around ω_n . The mean square value of the response to all component waves is then simply:

$$\bar{r}^2 = \int_0^{\infty} X(\omega)^2 S(\omega) d\omega = \int_0^{\infty} R(\omega) d\omega = R \quad (3.27)$$

where $R(\omega)$ is known as the response spectral density and R is the area under the response spectrum.

The square root $\sqrt{r^2} = \sqrt{R}$ is the RMS amplitude of the response which was to be found.

To summarize, the steps to calculate statistical means and maxima of buoy response are as follows:

- Decide which wave amplitude spectrum $S(\omega)$ best represents the contemplated sea conditions.
- Establish the response amplitude operator $X(\omega)$ for the particular mode of buoy response. To hindcast heave motion one could for example use $|H(\omega)|$ as expressed by (3.14).
- Compute the mean square value of the response by performing the integration suggested in (3.27).
- Compute the RMS.
- Multiply this RMS by the numerical coefficients obtained with the Rayleigh probability density function for calculating specific means and maxima. For example, the significant heave $\bar{h}_{1/3}$ would be found, using

$$\bar{h}_{1/3} = 1.416 \sqrt{r^2}$$

while the maximum heave in 1000 waves could be as high as

$$h_{1000} = 2.78 \sqrt{r^2}$$

Thus, in principle at least, the procedure is straightforward. Values of the Rayleigh probability constants have been widely published (Ref. 4). One must exercise great caution however to properly match the type of spectrum used (amplitude, semi-amplitude, height, double height...) and the published Rayleigh "magic numbers" (Ref. 6).

To illustrate the usefulness of this technique, Table 1 shows the heave and roll amplitudes that the large spar buoy shown in Figure 5 would have if excited by a fully developed sea with the wind blowing at 20 and 40 knots.

TABLE 1
Statistical Expectations of Heave and Roll for the Spar Buoy Shown in Fig. 5.

Wind (kn.)	Average		Significant		Average 1/10 of Highest		MAXIMA					
	20	40	20	40	20	40	20	40	20	40	20	40
Wave Amplitude (Ft)	2.3	9.4	3.7	15	4.8	19	6.0	24	6.9	27	7.3	29
Heave Amplitude (Ft)	.44	3.81	.69	6.09	.88	7.74	1.12	9.81	1.28	11.2	1.36	11.9
Roll Amplitude (Degrees)	.30	2.25	.40	3.58	.52	4.55	.65	5.77	.75	6.60	.80	7.03

The computation approach just reviewed has the merit of simplicity and clarity. It has been extensively followed to calculate "engineering" short term statistics of buoy response. More advanced models of buoy dynamics have been proposed (Ref. 7). Ease of implementation usually decreases as model complexity increases.

4. DISC AND SPAR BUOYS: ADVANTAGES AND DRAWBACKS

Because of their radically different shapes, disc and spar buoys behave quite differently. When attempting to qualitatively compare the two classes of buoys, size, water depth, and methods of anchoring should also be considered. The merit of most buoy conceptual designs is best confirmed by a dynamic analysis based on the theoretical principles just reviewed (Ref. 8).

Disc buoys are relatively easy to design and build. They are easy to handle and cost efficient. They have excellent buoyancy to drag ratios and thus are not difficult to moor. On the negative side, small as well as large disc buoys may capsize in rough seas. Adding a rigid bridle to provide a stronger righting moment has been found helpful to prevent buoy capsizing.

The major drawback of disc buoys remains their natural propensity to follow the waves both in amplitude and slope. They heave and roll forever. This constant motion may impair good radio transmission; it certainly degrades the quality of measurements made from the buoy on its mooring line; and it is the cause of repeated cyclic stresses often leading to mooring failure.

Spar buoys, if of sufficient mass and size, will provide good platform stability. Reduced buoy motion can greatly enhance the quality of measurements made with sensors mounted on the buoy or on the data line hanging from it. It can improve radio transmission capability.

Smaller spars (10 meters or less) have little reserve buoyancy. Thus they are difficult to moor. They will heave in most wave periods but, if properly designed, they will remain fairly stable in roll. They are often used as drifters.

Medium size spars (10 to 20 meters) are designed to "work" up to a certain sea state. As the seas build in period and strength, buoy performance degrade. In storms they do the best they can to survive. They are judged bulky, awkward to handle with standard ship gear. They are difficult to moor. Their usefulness is rather limited.

The best spar buoys are the larger ones. They can be designed to remain relatively stable in most seaways. Their cost is high, their handling not as bad as it may seem. Because of their large cross section they remain difficult to moor in high currents and deep waters.

Communications in support of the TACTS system may require pitch, roll and yaw stability of the platform mounted antennas. Heave motions are probably of less concern. Directive antennas, whether of the disk type or horizontally or vertically spaced arrays will be responsive to these motions. The greater their directivity the more degradation of their performance will be experienced due to motion. Spar buoys, particularly if large, will generally provide a better antenna platform. The problem of yaw (rotation) can be reduced using multiple points of attachment, or alignment vanes.

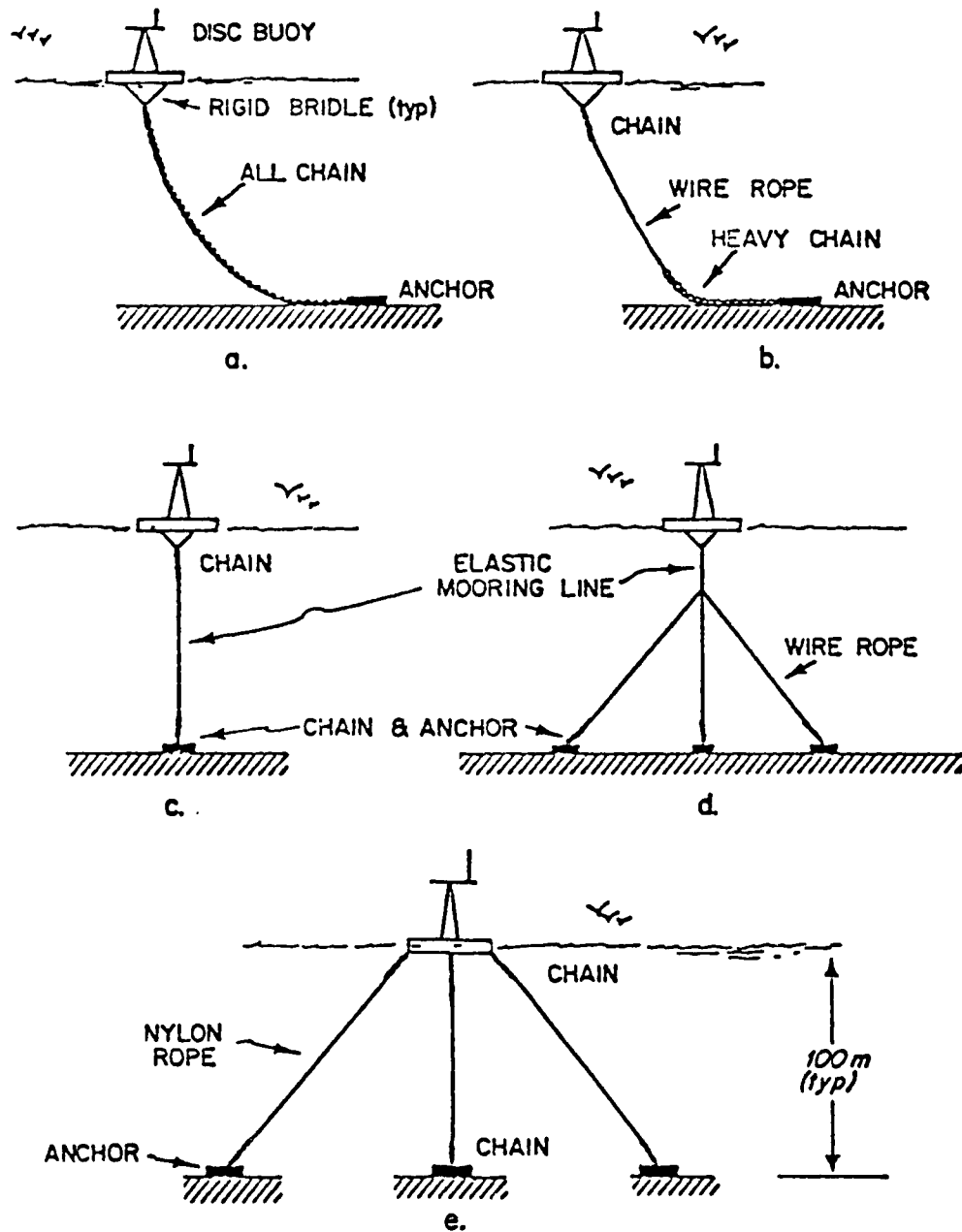
5. DISC AND SPAR BUOY MOORINGS

The techniques commonly used to maintain disc and spar buoys on station are hereafter briefly reviewed together with their advantages and drawbacks.

SHALLOW WATER MOORINGS (100 meters or less)

Disc buoys. Different schemes to anchor disc buoys in shallow waters are depicted in Figure 10. The mooring shown in 10-a is an all chain slack moor. When the depth is larger than 50 meters or so, some of the chain can be replaced, as shown in 10-b, by a length of wire rope to reduce mooring cost. In both cases the weight of the chain supported by the buoy provides substantial and desirable tension at the point of buoy attachment. Chain catenary provides the compliance needed to accommodate for tide and wave action. An all chain or all metal mooring will better resist pilferage, accidental damage due to fishing operations and biological attacks such as shark bites. These very common moorings are highly reliable. Their drawback remain extensive abrasion of the chain on the bottom and relatively large buoy watch circles.

In sketch 10-c the disc buoy is moored by a single taut moor. The compliant part of the mooring line provides the tension needed to maintain the buoy on a tight watch circle and help prevent overturning. It allows the buoy to rise and fall with the waters and tides under continuous tension. As depth increases, a three point moor as shown in 10-d can be used to reduce the buoy watch circle. Synthetic fiber rope or NATSYN rubber can be used as elastic mooring material. A number of buoys using these taut mooring schemes have been successfully deployed. Their susceptibility to cutting damage, at least in certain areas, should remain a cause of concern.



SHALLOW WATER DISC BUOY
MOORING SCHEMES

Figure 10

A taut surface trimoor, as shown in Fig. 10-e, is probably the best scheme to moor a large disc buoy in shallow water. This arrangement provides for minimum watch circle and continuous mooring line tension. It should prevent the buoy from spinning and overturning. Mooring leg vulnerability to dragging operations still remains a problem.

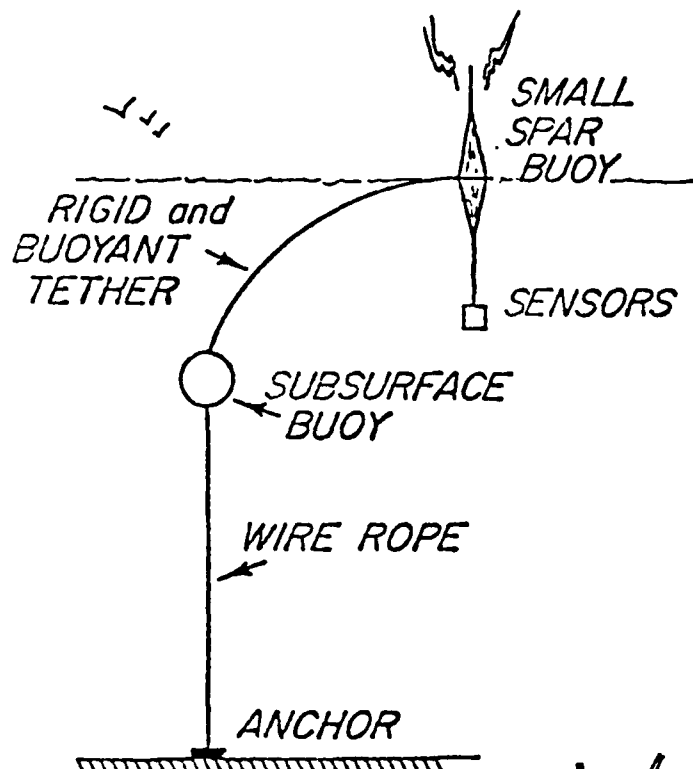
Spar buoys. Because of their small reserve buoyancy, spar buoys designed to free float are difficult to moor. Smaller spars are usually moored with the help of an auxiliary subsurface buoy and a rigid buoyant tether line as depicted in Figure 11-a. Large spars with draft approaching the water depth (Figure 11-b) have been single point moored in protected waters (Ref. 9). Subsurface buoys with towers protruding through the surface are a different breed. If free to float they do not behave like spar nor disc buoys. When moored these semi-submersible structures look and in fact respond like spar buoys. Such a pseudo spar of large dimensions is shown in Figure 11-c. The multileg mooring arrangement shown provides maximum station keeping capability and prevents spinning.

DEEP WATER MOORINGS

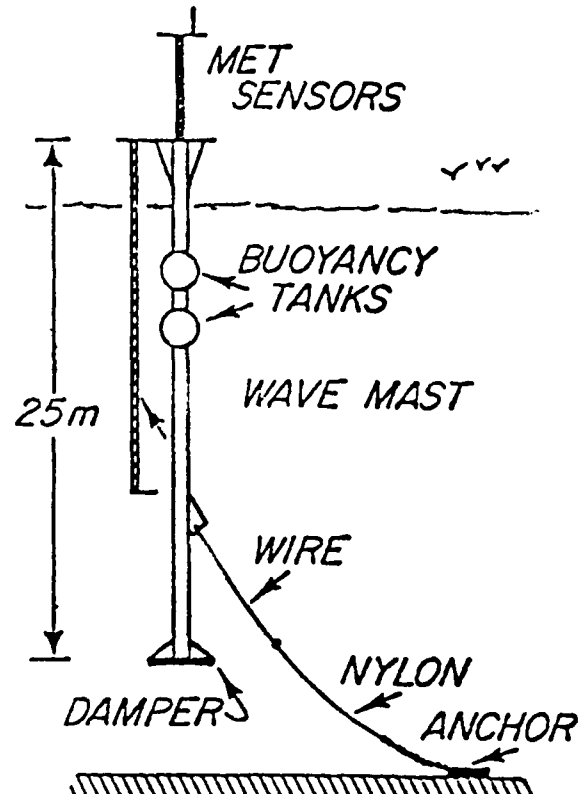
Disc buoys. Taut and slack single point moors have been traditionally used to anchor disc buoys in deep waters. Currents acting on the buoy and the mooring line result in considerable downstream excursions of the surface buoy. Naturally a buoy on a taut moor will have a smaller watch circle. Still, because of mooring compliance, excursions of deep sea taut moored buoys are often measured to be half the water depth or more. In addition to somewhat reduced buoy watch circle, taut moors of the type shown in Figure 12-a will constantly provide the hard pull needed to prevent flat buoys from capsizing during storms.

The disadvantages of taut moors are high dynamic loading of the mooring line due to wave action and high static tension under severe currents. These high stresses, often resulting in mooring losses, are reduced when the scope of the mooring is increased. This is why disc and boat hull buoys are often anchored on S shape slack moors of the type shown in Figure 12-b. The upper part of such a mooring is usually heavy whereas the lower part is buoyant (polypropylene) or supported by glass balls to avoid possible piling on the ocean floor. Occasionally disc buoys moored on slack moorings will overturn.

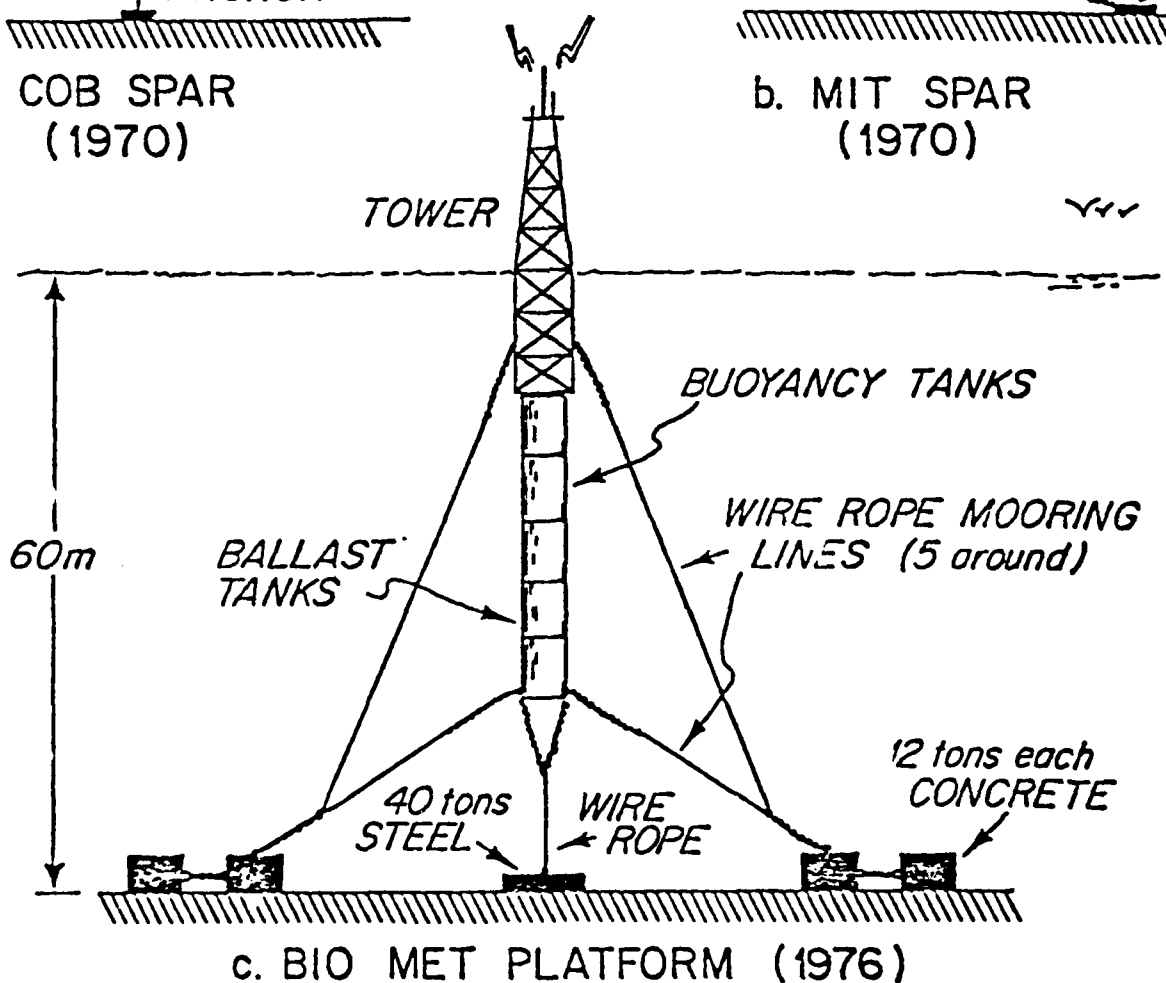
A disc buoy moored on three legs is shown in Figure 12-c. The performance of such deep sea surface trimoors is not well documented. This trimoor arrangement should be effective in reducing buoy watch circle and spin. It is doubtful that it helps reduce buoy heave and roll in severe seas. Such a buoy system is dominated by the response of the mooring legs to prevailing currents. Should one of the legs be in the path of a strong and coherent current, then the two downstream legs would "bow out". The upstream leg would carry the bulk of the current induced forces. The tension in the downstream legs would be greatly reduced, the vertical component of the tension would be small as well as the righting moment of these two legs.



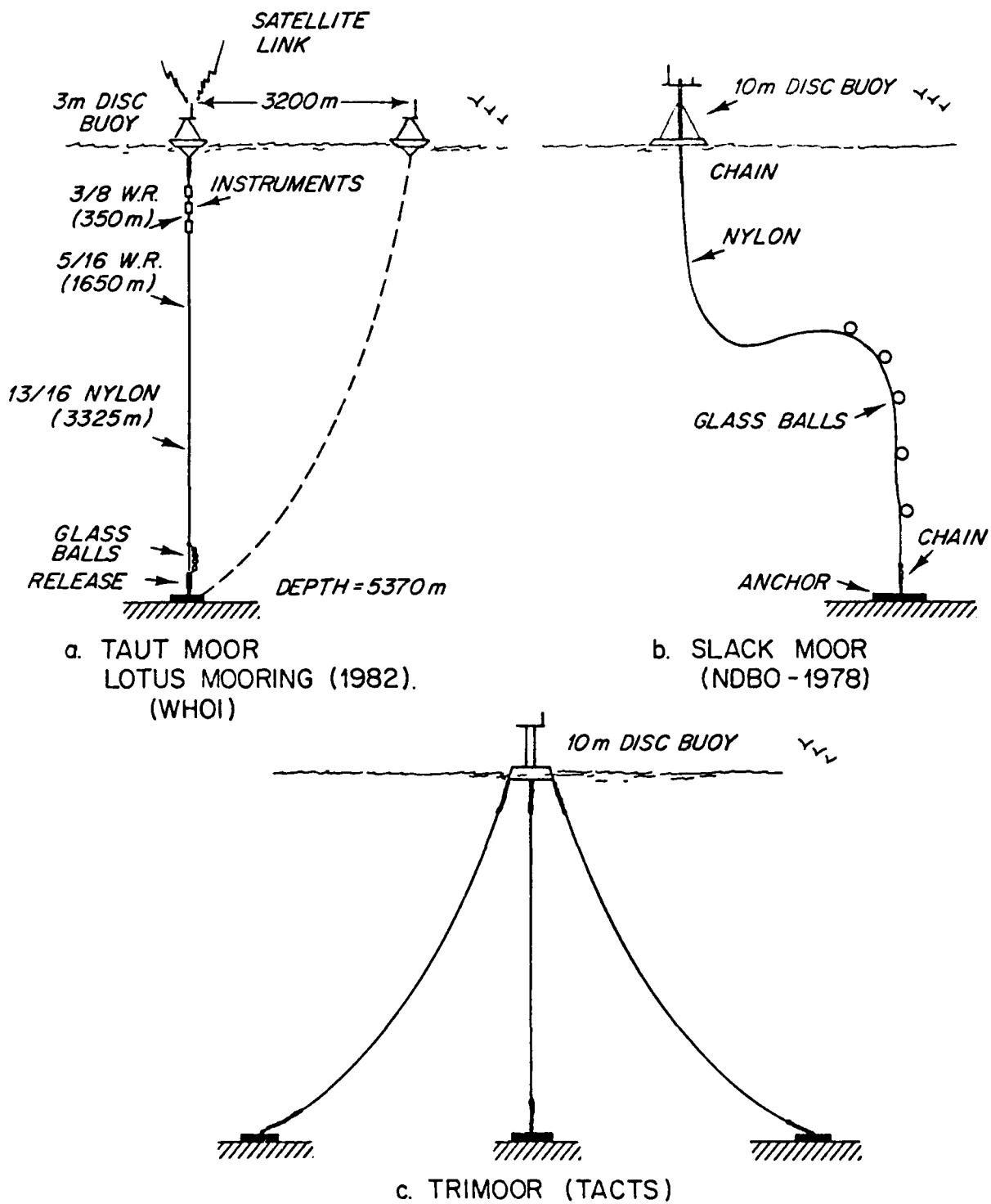
d. COB SPAR
(1970)



b. MIT SPAR
(1970)



SHALLOW WATER SPAR BUOY
MOORING SCHEMES



DEEP WATER DISC BUOY
MOORING SCHEMES

Figure 12

Spar buoys. Currents acting on the mooring line of spar buoys directly moored to the ocean floor would cause the spar buoy to pull under. For this reason spar buoys with little reserve buoyancy are moored with the help of one or two auxiliary subsurface buoys which support the bulk of the mooring weight and drag (Figure 13-a and 13-b). These mooring arrangements will result in relatively large buoy watch circles.

Larger spar buoys such as FLIP and the manned Bouées Laboratoire BOHRA I and BOHRA II have been moored using single point slack moors and trimoors (Figure 13-c and 13-d). Rotation of the buoy on its longitudinal axis - spin - has been observed on the single point moored buoys. The trimoor BOHRA II was moored in the MED off the coast of southern FRANCE in approximately 2500 meters of water depth. Tension in the mooring lines could be adjusted with the help of a winch installed on board the buoy. The buoy, no longer on station, has been found to be a very stable platform. Buoy watch circles were observed and reported to be relatively small (Ref. 10). One mooring leg broke during a storm.

6. CONCLUSION

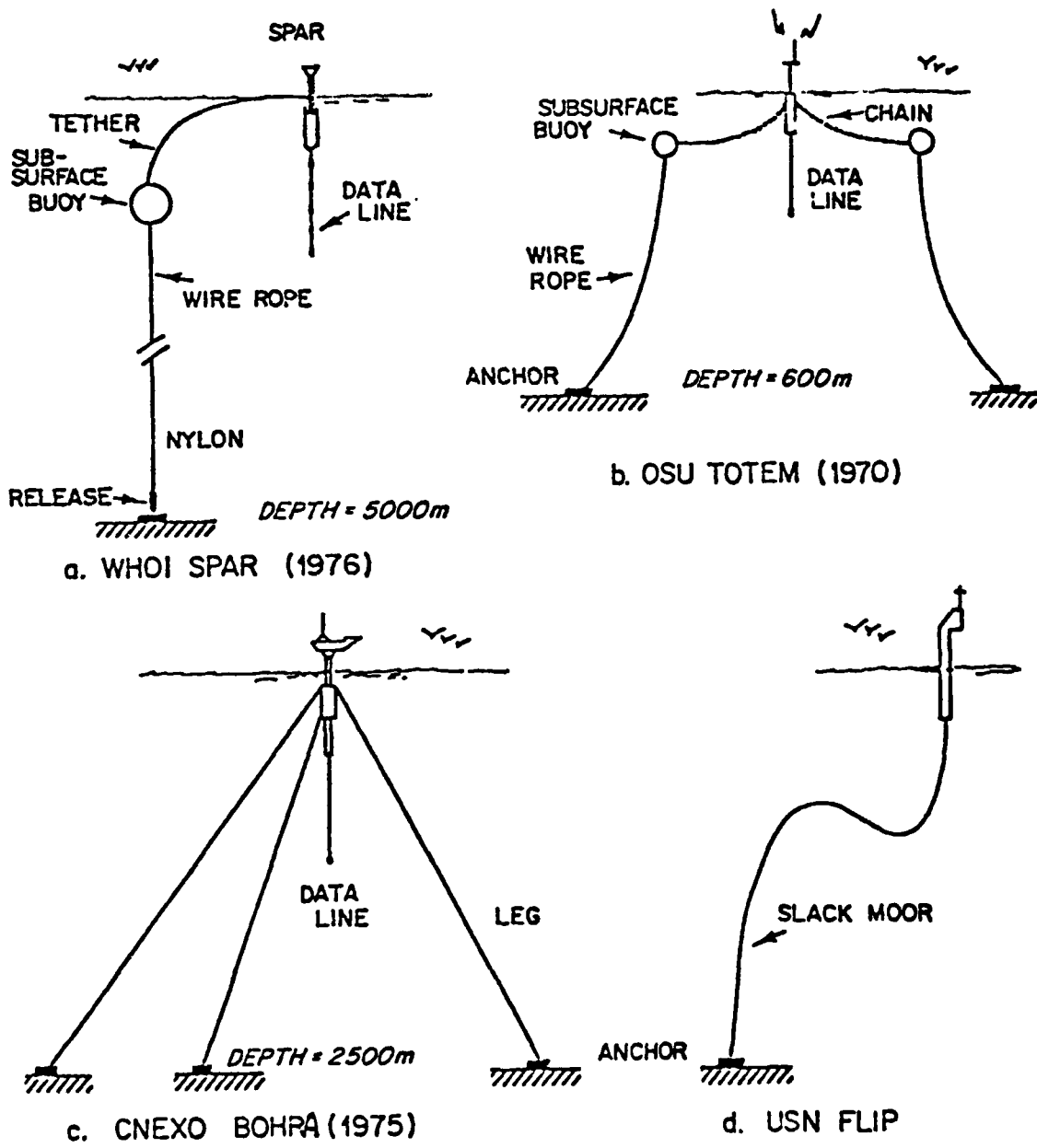
To conclude this general review of disc and spar buoys on a practical note, let us investigate how the mooring scheme depicted in Figure 14 would respond to oceanic currents. Such an exercise could point out the difficulties, perhaps the limits, inherent to such mooring systems.

Assuming platform stability and small watch circle to be desirable objectives, the proposed system consists of a spar buoy of large dimensions attached to a subsurface trimoor.

After some preliminary runs, three candidate systems were retained for the exercise. Trimoor legs size and strength and buoyancy of the surface and subsurface buoys of the three systems are tabulated in the lower half of Figure 14 together with the displacements obtained when the systems are subjected to the mild, the severe, and the extreme current profiles shown on the upper half of the same figure.

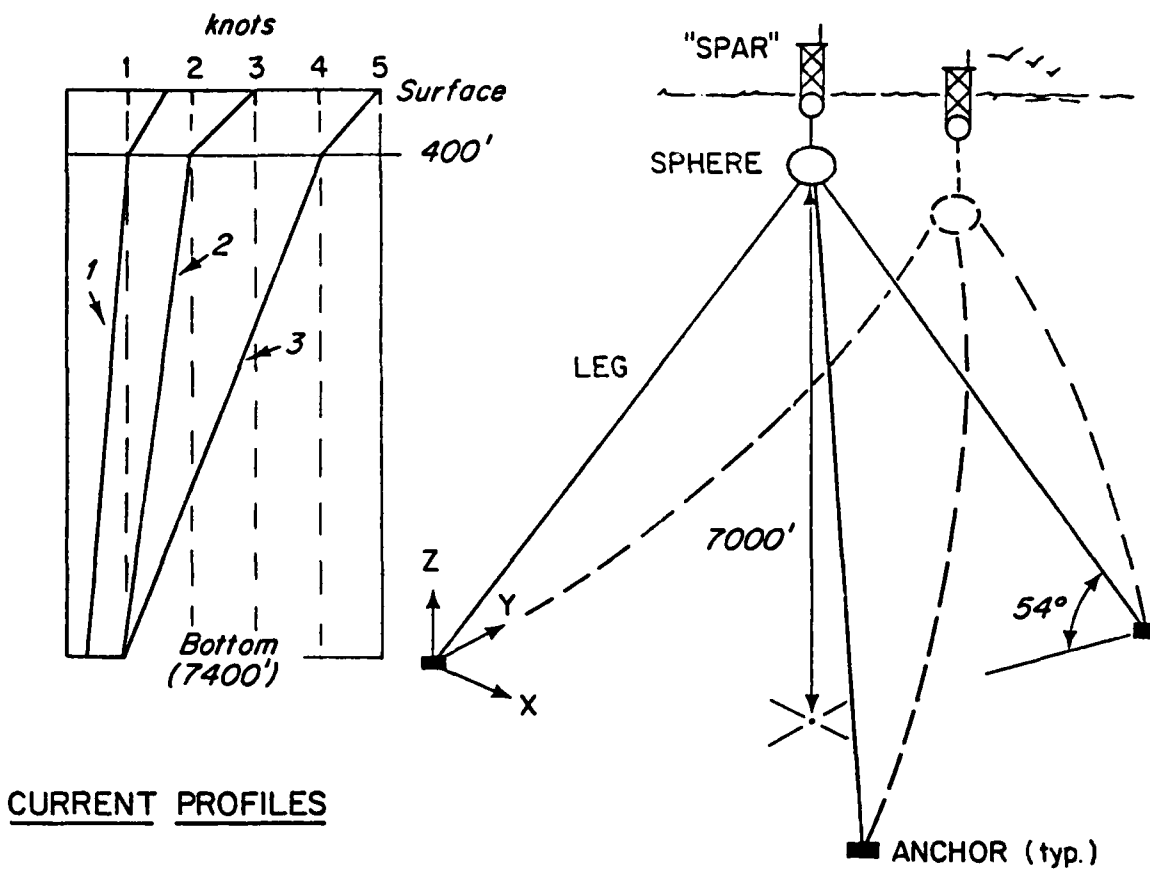
As can be seen from the displacements shown, the three systems would perform equally well under mild current conditions. Under severe current conditions (Profile #2), only the two larger systems can maintain the spar float reasonably close to the surface. Under the full blow of the Gulf Stream, the spar buoy of the two smaller systems sink way under the surface, while the third one dips a tolerable (?) 21 feet.

These results are indicative of the size (and the cost) of the mooring components necessary to maintain some degree of platform static stability at a deep site and under severe to extreme current conditions.



DEEP WATER SPAR BUOY MOORING SCHEMES

Figure 13
166



CURRENT PROFILES

TRIMOOR LEG				BUOYANCY		CURRENT PROFILE NO.	DISPLACEMENTS (ft)				
SIZE (in)	STRENGTH (lbs)	SPHERE (lbs)	SPAR (lbs)	SPHERE			SPAR				
				HORIZ	VERT		HORIZ	VERT			
1	1.0*	100,000	60,000	60,000		1	1	1	28	2	
2						2	23	14	126	27	
3	↓	↓	↓	↓		3	1175	571	1364	620	
4	1.50*	225,000	150,000	100,000		1	1	1	8	1	
5						2	2	4	25	5	
6	↓	↓	↓	↓		3	135	75	210	81	
7	3.0**	500,000	600,000	100,000		1	1	0.5	7	1	
8						2	1	2	24	3	
9	↓	↓	↓	↓		3	15	15	82	21	

* JACKETED STEEL WIRE ROPE

** KEVLAR ROPE

TRIMOOR AND SPAR BUOY

Figure 14

REFERENCES

1. Bhattacharyya, R., Dynamics of Marine Vehicles, Wiley Interscience Publication, John Wiley & Sons (1978).
2. McCormick, M.E., Ocean Engineering Wave Mechanics, Wiley Interscience Publication, John Wiley & Sons (1974).
3. Palo, P.A., "The 1980 CEL Mooring Dynamics Seminar", CEL Technical Note TN No. N-1604 (1981).
4. Marks, W., "The Application of Spectral Analysis and Statistics to Sea Keeping", S.N.A.M.E. Technical Bulletin No 1-24 (1963).
5. Price, W.G. and R.E. Bishop, Probabilistic Theory of Ship Dynamics, John Wiley & Sons (1974).
6. Berteaux, H.O., Buoy Engineering, Wiley Interscience Publication, John Wiley & Sons (1976).
7. Hoffman, D., E.S. Geller, C.S. Niederman, "Mathematical Simulation and Model Tests in the Design of Data Buoys", SNAME Annual Meeting 1973.
8. Berteaux, H.O. and R.G. Walden, "Design of a Stable Floating Platform for Air-Sea Interaction Measurements", W.H.O.I. Technical Report No. 78-88 (1978).
9. Mollo-Christensen, E., "A Buoy System for Air-Sea Interaction Studies", M.I.T./ C.S.D. Report No. 71-4 (1971).
10. Magenham, J.C., "Déplacements de la Bouée Laboratoire BOHRA II dans son Aire d'Evitement" Laboratoire d'Oceanographie Physique, Muséum National d'Histoire Naturelle, Paris, France (1977).
11. Berteaux, H.O. and R.G. Walden, "A Feasibility Study for a Versatile, Deep Sea, Multileg, Stable, Cable Array", W.H.O.I. Technical Report No. 81-13 (1981).
12. Skop, R.A. and J. Mark, "A Fortran Program for Computing the Static Deflections of Structural Cable Arrays", N.R.L. Report No. 7640.

Marine Cable Strumming and Its Prevention

**A Paper Prepared for the
NCEL Ocean Platform Seminar
January 11 and 12, 1983**

OWEN M. GRIFFIN

*Marine Technology Division
Naval Research Laboratory
Washington, DC 20375*

NOMENCLATURE AND LIST OF SYMBOLS

a_1, b_1, c_1, d_1	Coefficients defined in Table 3.
C_D, C_{DO}	Steady drag coefficient on a vibrating (stationary) cylinder or cable.
C_{LE}	Excitation force coefficient; see Table 3.
D	Cable diameter (m or ft).
f_n	Natural frequency (Hz).
f_s	Strouhal frequency (Hz).
I_i	Modal scaling factor; see equation.
k_s	Reduced damping; see equation (2).
L	Cable length (m or ft).
m	Cable physical mass per unit length (kg/m or lb_m/ft).
m_e	Effective mass per unit length (kg/m or lb_m/ft) (physical plus added mass); see equation (1).
m'	Cable virtual mass (physical plus added mass) per unit length (kg/m or lb_m/ft).
Re	Reynolds number, VD/ν .
St	Strouhal number, $f_s D/V$.
T	Cable static tension (N or lb_f)
V	Incident flow velocity (m/s or ft/sec or knots).
V_r	Reduced velocity, $V/f_n D$.
$V_{r,crit}$	Critical reduced velocity; see equation (4).
w_r	Response parameter, $(1 + 2 \bar{Y}/D) (V_r St)^{-1}$; see equation (5).
\bar{y}	Cross flow displacement (m or ft).
\bar{Y}	Cross flow displacement amplitude (m or ft).
Y	Normalized displacement amplitude, \bar{Y}/D .
$Y_{EFF,MAX}$	Normalized displacement amplitude; see equation (8).
z	Coordinate measurement along the cylinder or cable (m or ft).
δ	Log decrement of structural damping; see equation (2).

γ_i	Normalizing factor; see equation (8).
μ	Mass ratio, see equation (3).
ν	Kinematic fluid viscosity (m^2/sec or ft^2/sec).
ρ	Fluid density (kg/m^3 or lb_m/ft^3).
ρ_s	Cable density (kg/m^3 or lb_m/ft^3).
$\psi_i(z)$	Mode shape for i th natural mode; see equation (8).
ζ_s	Structural damping ratio; see equation (3).

MARINE CABLE STRUMMING AND ITS PREVENTION

INTRODUCTION

Background

The oscillations of marine cables caused by vortex shedding, commonly termed *strumming*, result in fatigue, increased steady and unsteady hydrodynamic forces, and amplified acoustic flow noise. They sometimes lead to structural damage and possibly to costly failures. Flow-excited oscillations very often are a critical factor in the reliable and economical design of undersea cable arrays, mooring systems, riser systems, and offshore platforms. Many components of these complex structures usually have bluff cylindrical shapes which are conducive to vortex shedding when water flows past them.

As the state of the ocean engineering art steadily progresses, more and more stringent demands are being placed upon the performance of cable structures and moorings. In particular, displacement tolerances and constraints in response to currents are becoming more stringent; fatigue is becoming an important design consideration; and the sensitivity of acoustic sensors has increased to the point that they cannot differentiate between legitimate acoustic targets and slight variations in their vertical position. All of these are problems that are aggravated by cable strumming. In order for an engineer to be able to design a structure or cable system to meet the constraints imposed by operational and environmental requirements, he or she must be able to assess the effect of strumming on the structure in question.

Scope of this Paper

This paper is limited in scope to the problems caused by vortex shedding from undersea cable structures and moorings, and to the resonant cross flow or strumming oscillations that often are excited by the vortices. A discussion is given of the essential fluid dynamic characteristics of a cable in an incident flow, including the hydrodynamic forces, resonant dynamic response characteristics, and the static deflections caused by the amplified hydrodynamic drag forces. Relevant experimental findings from towing channel experiments, small-scale field experiments and large-scale field experiments also are discussed.

Strumming analysis methods for marine cables are summarized along with the computer codes that are available to implement the various analysis procedures. Available methods and devices for the suppression of cable strumming vibrations are reviewed briefly. Many of these topics are discussed in more detail in a recent NCEL report (1) and a related paper (2).

BASIC CHARACTER OF VORTEX SHEDDING

The frequency f_s of the vortex shedding from a circular cylinder (cable) is related to the other main flow parameters (D , the diameter of the cylinder; V , the flow velocity) through the nondimensional Strouhal number defined as

$$St = \frac{f_s D}{V}.$$

The value of the Strouhal number varies somewhat in different regimes of the Reynolds number and with the shape of the cylinder (circular, D -section, triangular, etc). For the range of the Reynolds number where the Strouhal number remains constant the relation between the shedding frequency and the velocity is linear for a given cylinder, i.e.

$$f_s = KV,$$

where $K = St/D$. If a cylinder or cable immersed in a flowing fluid is free to oscillate in the cross-flow direction, then the latter relation does not hold in the vicinity of the natural frequency of the cylinder. This resonance phenomenon—called "lock-on" or wake capture—is discussed in this paper in the context of strumming.

If the Reynolds number is lower than about 10^5 , then the vortex shedding is predominately periodic and the value of the Strouhal number can be roughly assumed to be 0.2 for a circular cylinder or cable. Measurements of the frequencies, displacement amplitudes and forces which result from vortex-excited oscillations have been obtained by many investigators from experiments both in air and in water. A detailed but somewhat selective review of the basic aspects of the problem of vortex-excited oscillations in general has been made recently by Sarpkaya (3). King (4) and Griffin and Ramberg (5,6,7) have discussed the subject in the context of ocean engineering applications.

3. EXPERIMENTAL CABLE STRUMMING RESULTS

3.1 Hydrodynamic Drag

A most important manifestation of cable strumming is the increased hydrodynamic drag. The measured mean drag coefficients (C_D) for several strumming cables are plotted against the Reynolds

number (Re) in Figure 1. As a basis for comparison the typical drag coefficients for a stationary circular cylinder and several nominally stationary braided and plaited marine cables also are plotted in the figure. It is clear that the drag coefficients C_D for the strumming cables are increased substantially (by as much as a factor of two) for a variety of Kevlar cables over a wide range of towing speeds or Reynolds numbers between $Re = 3(10^3)$ and $3(10^4)$. This increase in the mean drag is typical of structures and cables that vibrate resonantly due to vortex shedding. Some additional discussion of strumming drag is given later in this paper. A thorough treatment of hydrodynamic drag effects and of the other hydrodynamic forces is given by Griffin and Ramberg, and others (1,2,6,7).

Laboratory-Scale Cable Strumming Experiments

The measured frequency and displacement amplitude responses for small-diameter taut cables undergoing cross flow strumming vibrations in water (8) are plotted in Figure 2. In these experiments a 2.5 mm diameter cable, 1.8 m in length, was excited in several modes over the frequency range between 10 and 30 Hz. In a similar experiment (9), Dale and McCandless measured strumming drag coefficients as large as $C_D = 2$. This corresponds to an amplification of the steady drag by a factor of about two, a finding which is in good agreement with the results discussed elsewhere in this paper.

Field Measurements of Cable Strumming

Small scale field experiments. Field studies of the strumming behavior of marine cables were conducted over several summers through 1981 at Castine, Maine by staff members of the Ocean Engineering Department at MIT. The field test layout for the most recent experiments is shown in Figure 3. Sections of faired and unfaired cables, nominally 23 m (76 ft) in length, were positioned normal to a spatially uniform tidal current which ranged in magnitude from 0 to 0.7 m/sec (0 to 1.36 kt). The first experiments have been reported in detail (10). Some more recent experiments, performed during 1976, were concerned with measurements of the strumming response of both unfaired and faired marine cables in an ocean environment (11). The most recent experiments were conducted at Castine during the summer of 1981, and a discussion of these experiments is given in this section and by Vandiver and Griffin (12). The measurements of C_D are consistently between 2 and 3 for time intervals as great as two and one half hours shown when the current velocity is near 0.6 m/s (1.2 kt). The strumming response of the cables usually was in the first six ($n = 1$ to 6) natural modes.

Test runs were conducted at the field site in 1981 with different combinations of locations, numbers, and masses of cylindrical bodies attached to the cable. An example taken from one of the more complex test runs is shown in Figure 4. Six cylindrical masses were attached to the cable: two

light ones ($m = 4.4 \text{ lb}_m$ or 2 kg) at $x = L/8$ and $L/2$; and four heavy ones ($m = 10 \text{ lb}_m$ or 4.5 kg) at $x = L/3$, $5L/8$, $3L/4$ and $7L/8$. The RMS strumming response data shown for a two and one half hour time period in Figure 4 were recorded at $x = 3L/4$, where both one of the attached masses and an accelerometer fair were located.

Several important results of the experiments can be observed from the figure. The vibration level over the time of the test run was approximately $\bar{Y} = \pm 0.3$ diameters (RMS), indicating that in general the attached mass did not act as a node of the strumming vibration pattern. The drag coefficient of the system is $C_D = 2.4$ to 3.2 which again represents a substantial amplification from the stationary cable value of $C_D \approx 1.2$. The relative contributions to the overall drag have not yet been determined. Several segments of the time history in Figure 4 exhibit nearly constant drag and vertical RMS response levels; this is indicative of resonant cable strumming vibrations.

Large scale field experiments. FISHBITE is the name of a marine cable experiment conducted by Softley, Dilley and Rogers in 1976 (13). A wire rope 12 mm (0.47 in.) in diameter and 500 m (1640 ft) long was hung from a ship anchored in 1960 m (6430 ft) of water at the Tongue of the Ocean, located at $77^{\circ} 52' \text{ W}$ and $25^{\circ} 10' \text{ N}$. The tidal flow varied both temporally and spatially from 0.1 to 0.4 m/s (0.2 to 0.8 knots). A current meter was attached at the halfway point, but no other lumped masses were attached to the cable. The cable response was measured at the top end only and the cable parameters resulted in a modal frequency spacing of 0.025 Hz. The response typically included more than one hundred modes between 8 and 12 Hz, with a center frequency of 10 Hz. No lock-on was observed during any of the FISHBITE experiments.

SEACON II was a major undersea construction experiment which had as its goal the measurement of the steady-state response of a complex three-dimensional cable structure to ocean currents. The measured array responses were to be employed in a validation of analytical cable design models and computer codes (14).

The SEACON II structure consisted of a delta-shaped module with three mooring legs. It was implanted in 885 m (2900 ft) of water in the Santa Monica Basin during 1974 and was retrieved during 1976. The top of the cable structure was positioned 137 m (450 ft) below the water surface. The mooring legs were 1244 m (4080 ft) long and each arm of the delta was 305 m (1000 ft) long. An artist's view of the completed structure is shown in Figure 5. The entire cable system was instrumented in order to collect water current and array position data. The data were used to validate the computer code DECEL1 (the original NRL version is called DESADE). This code was developed at NRL and revised at NCEL (15). The delta cables experienced uniform currents over their respective lengths and often were subject to cable strumming. These strumming oscillations led to increased hydrodynamic drag and static deflections.

The drag coefficient C_D of the SEACON II cable was measured in two series of tests conducted for NCEL. These measurements are plotted in Figure 6. The tests conducted at the Naval Postgraduate School utilized a short segment of the cable that was restrained from oscillating. An average value of $C_D = 1.55$ was obtained. The DTNSRDC tests were conducted with a 4.6 m (15 ft) long cable segment. The increase in the drag coefficients in Figure 6 from the stationary cable data was caused by strumming.

Alexander (16) has reported a series of experiments that were conducted with the Scripps Institution of Oceanography's Deep Tow survey system. The system, an oceanographic sensor package, was deployed from a Scripps research vessel by a towing wire 0.68 in (1.72 cm) in diameter at typical depths in excess of 6560 ft (2000 m) and at nominal towing speeds of 1.5 kt (0.75 m/s). In order to investigate suspected strumming vibrations a two-axis accelerometer was attached to the tow wire at a depth of 98 ft (30 m) and its output was recorded in a diver-operated vehicle about 3 ft (1 m) downstream. Both in line and crossflow strumming oscillations were measured. Sharply peaked frequency spectra were obtained that contained frequencies in line at twice the crossflow strumming frequencies. An analysis of the frequency amplitude and phase data by Alexander suggests that the vortex shedding from the tow wire produces strumming oscillations in the form of travelling waves in the wire.

A towing channel fixture was built to reproduce under controlled laboratory conditions the amplitude, frequency and phase conditions of a point on the tow wire using a vibrating cylinder. A constant drag coefficient $C_D = 1.8$ was measured over a range of representative strumming conditions at Reynolds numbers in the range $Re = 7000$ at 12000. Details of the at-sea and laboratory test programs are given by Alexander (16).

METHODS FOR CALCULATING CABLE STRUMMING EFFECTS

Analytical Models

A number of analytical models have been developed to predict the vortex-excited oscillations of general bluff cylindrical structures. Application to cable strumming problems is but one specific example of the utility of the various methods. In general the models that have been developed fall into these categories:

- Nonlinear, or wake oscillator models;
- Empirical models, which are based upon measured fluid dynamic force coefficients;
- Random vibration models;

- Discrete vortex models, which are based upon the insertion of arrays of small vortices to represent the overall features of the vortex shedding;
- Numerical models, which are based upon numerical integration of the governing equations of fluid motion.

The wake oscillator models have been developed because many features of the resonant interaction between the vibrations and the vortex shedding exhibit the characteristics of a nonlinear oscillation. The basic idea has been developed by Skop and Griffin (17), Iwan (18), Blevins (19), and Hartlen and Currie (20), among others. The wake oscillator concept is discussed in more detail in references 1, 17, 18 and 19.

Random vibration models to predict vortex excited oscillations in general and cable strumming in particular have been developed by Blevins and Burton (21), and by Kennedy and Vandiver (22). Some limited success has been achieved with these approaches to the problem. A general model for employing measured force coefficients in an empirical formulation is described by Griffin (23). Measured force coefficients such as those reported by Sarpkaya (3) and by Griffin and Koopmann (24) are used to predict the resonant crossflow oscillations. All of the different classes of predictive models are discussed in detail in a recent NCEL report (1). However, only the first three modeling techniques have proven useful for practical applications.

General Design Procedures

All of the methods developed thus far are in agreement that the following parameters determine whether large-amplitude, vortex-excited oscillations will occur (5):

- the *logarithmic decrement of structural damping*, δ ;
- the reduced velocity, $V/f_n D$;
- the mass ratio, $m_e/\rho D^2$.

Here m_e is the *effective mass* of the structure or cable which is defined as

$$m_e = \frac{\int_0^L m(x) y^2(x) dx}{\int_0^L y^2(x) dx}, \quad (1)$$

where $m(x)$ is the mass per unit length including contributions due to internal water, fluid added mass, joints, sections of different material, etc., $y(x)$ is the modal shape of the structure or cable along its

length, L is the overall length of the structure or cable, measured between its terminations. The effective mass m_e defines an equivalent structure whose vibrational kinetic energy is equal to that of the real structure. In the context of cable strumming, this equation is applicable both to bare cables, to composite cables, and to cables with distributed arrays of attached masses.

As described in several related reports (1,4-7), the mass ratio and the structural damping can be combined in the forms

$$k_s = \frac{2m_e\delta}{\rho D^2} \quad \text{or} \quad \frac{\zeta_s}{\mu} = 2\pi Sf_n^2 k_s, \quad (2.3)$$

both of which are called the reduced damping. The reduced damping k_s is the ratio of the actual damping force (per unit length) and $\rho f_n D^2$, which may be considered as an inertial force (per unit length). The results obtained by several investigators also suggest criteria for determining the critical incident flow velocities for the onset of cable strumming. They are given by the equation

$$V_{crit} = (f_n D) V_{r,crit}, \quad (4)$$

where $V_{r,crit} = 3.5$ for cross flow oscillations at Reynolds numbers greater than about $5(10^5)$. For Reynolds numbers below 10^5 , $V_{r,crit} = 5$ which is a typical value for cable strumming applications.

Step-by-step procedures for determining the deflections that result from vortex-excited oscillations have been developed by Skop, Griffin and Ramberg (25), by King (4), Every et al (26), and by Griffin (5,6,7). The steps to be taken are outlined in Figure 7. They are discussed in detail in the references just cited and generally should follow the sequence given most recently in Ref. 1:

- Compute/measure vibration properties of the structure or cable system (natural frequencies or periods, normal modes, modal scaling factors, etc.)
- Compute Strouhal frequencies and test for critical velocities, V_{crit} (in-line and cross flow), based upon the incident flow environment.
- Test for reduced damping, k_s , based upon the structural damping and mass characteristics of the structure or cable.

If the cable system is vulnerable to vortex-excited strumming oscillations, then

- Determine vortex-excited unsteady displacement amplitudes and corresponding steady-state deflections based upon steady drag augmentation according to the methods given in references 1, 6 and 26, as applicable (see Figure 7);

- Determine new stress distributions based upon the new steady-state deflection and the superimposed forced mode shape caused by the unsteady forces, displacements and accelerations due to vortex shedding.
- Assess the severity of the new stress levels relative to fatigue life, critical stresses, etc.

Practical Design Aids

Several models of varying levels of sophistication have been developed to predict the displacement amplitudes that are excited by vortex shedding. Several empirical predictions of the dependence between the peak cross flow displacement amplitude and the reduced damping have been developed over the past several years. The three most widely used are listed in Table 1. The prediction curve developed by Griffin, Skop and Ramberg is a least-squares fit to those data points in Figure 8 that were available in 1976 (about two-thirds of the points now appearing in the figure). The Iwan and Blevins curve was developed during a study of one wake-oscillator formulation (19) and Sarpkaya's result is based upon a discrete vortex modeling study (3).

All of the equations in Table 1 correctly reproduce the self-limiting displacement amplitude that is shown at small values of reduced damping in Figure 8. It is also important to note that all of these models are based upon *the structural damping ratio*, typically *the still air value*, for whatever mode of the structure or cable is excited. The models in Table 1 tend to overpredict the cross flow displacement amplitude at $\bar{Y}/D < 0.05$ to 0.1 where the vortex shedding is not fully correlated over the length of the cable or cylinder, but these small-amplitude cross flow oscillations are of more concern in air flow rather than in water.

The drag coefficient C_D for a cable or structure vibrating due to vortex shedding is increased as shown in Figure 9. The ratio of C_D and C_{DO} (the latter is the drag coefficient for a cylinder, cable or other flexible bluff structure that is restrained from oscillating) is a function of the displacement amplitude and frequency as given by the response parameter (see Ref. 25)

$$w_r = (1 + 2\bar{Y}/D)(V_r S_t)^{-1}. \quad (5)$$

Here $2\bar{Y}$ is the double amplitude of the displacement, V_r is the reduced velocity and S_t is the Strouhal number. The ratio of the drag coefficients is given by

$$C_D/C_{DO} = 1, \quad w_r < 1 \quad (6a)$$

$$C_D/C_{DO} = 1 + 1.16(w_r - 1)^{0.65}, \quad w_r \geq 1 \quad (6b)$$

which is a least-squares fit to the data in Figure 25. The equation

$$\bar{Y}_{MAX}/D = \frac{1.29\gamma_i}{[1 + 0.43(2\pi St^2 k_s)]^{3.35}} \quad (7)$$

from Table 1 can be combined with equations (5) and (6) to compute the unsteady displacements, the drag amplification and the amplified static deflection that is due to the vortex excited oscillations. The local displacement amplitude along a flexible cylindrical structure (in the *i*th normal mode) is given by

$$\bar{y}(z) = \bar{Y}_i(z) \sin(2\pi f t),$$

where

$$\bar{Y}_i(z) = Y_{EFF,MAX} D \gamma_i = Y_{EFF,MAX} D \psi_i(z) / I_i^{1/2}. \quad (8)$$

These equations can be employed as outlined in Figure 7 to iteratively compute the static deflection of a structure or cable due to the vortex-excited drag amplification.

Several test runs were conducted with a bare cable during the 1981 Castine field tests. A 300 second time history for one such test is shown in Figure 10. The cable was resonantly strumming at 1.9 Hz in the third mode normal to the current and non-resonantly in the fifth mode in line with the flow at 3.8 Hz. Other details and results of the experiment are given by Vandiver and Griffin (12).

The vertical displacement amplitude is approximately $\bar{Y} = \pm 0.6$ to 0.7 diameters (RMS) over the length of the record. The average drag force coefficient on the cable is approximately $C_D \approx 3.2$; this is considerably greater than the drag coefficient $C_D = 1.2$ that would be expected if the cable were restrained from oscillating under these flow conditions. The drag coefficient on a strumming cable with a sinusoidal mode shape can be predicted with the equation

$$C_{D,Avg} = C_{D0} [1 + 1.043 (2\bar{Y}_{RMS}/D)^{0.65}],$$

which is derived from the original equation (6) given above. The strumming drag coefficient predicted using this equation is in the range $C_D = 2.4$ to 2.6 as shown in Figure 10. This is approximately 20 to 25 percent below the drag force coefficient measured at the field site. However, the predicted values are reasonable in view of the limited drag data upon which the model is based.

The coefficients for a cubic fit to the data for the excitation force coefficient C_{LE} have been computed and are given in Table 3. C_{LE} is the unsteady lift force component that transfers energy to the cable and drives the strumming. This cubic equation is given by

$$C_{LE} = a_1 + b_1 Y_{EFF,MAX} + c_1 Y_{EFF,MAX}^2 + d_1 Y_{EFF,MAX}^3. \quad (9)$$

The fitted curve to the data is applicable between $Y_{EFF,MAX} = 0$ and $Y_{EFF,MAX} = 1.25$ ($2Y_{EFF,MAX} = 2.5$). The results in the table can be employed as one input to a predictive model for the strumming oscillations of a flexible cable. For a cable or structure the average value of C_{LE} over a given length L is (1,5)

$$C_{LE} = \frac{\int_0^L C_{LE}(z) \psi_i(z) dz}{\int_0^L \psi_i(z) dz}. \quad (10)$$

It is important to note that the coefficient C_{LE} represents only the excitation force on the structure or cable. For vibrations in water it is necessary to have accurate and precise representations of the coefficients of the added mass, hydrodynamic damping and hydrodynamic inertia forces. Details concerning applications of the force equation in Table 3 are given in Ref. 1.

A handbook and a catalogue of relevant data are available to aid in applying the methods described here. These consist of a survey of steady drag coefficients for cables subjected to cross flow currents (27) and a detailed handbook of hydrodynamic coefficients for moored array components (28). The report by Dalton (27) is a compilation of steady drag coefficients for stranded steel and synthetic fiber cables. These data are tabulated according to the source and in each case a critical assessment is made concerning the reliability of the experimental findings. The report by Pattison, Rispin and Tsai (28) is a lengthy and detailed compilation of hydrodynamic force coefficients for moored array components of various shapes (cylinders, spheres, spheroids, streamlined bodies, etc.) and for cables and cable fairings. The authors also make an assessment of the quality and quantity of the experimental data that they include in their report. Solutions to a number of example problems are given in order to illustrate the application of the data. Most of the results discussed in this section have been applied in ocean engineering practice (29).

NATFREQ, a Strumming Prediction Computer Code

NATFREQ was developed by the California Institute of Technology for the Naval Civil Engineering Laboratory (NCEL) to calculate the natural frequencies, mode shapes, and drag amplification factors for taut cables with attached masses. Drag amplification factors calculated by NATFREQ using the Skop-Griffin strumming model (16,24) are used as inputs to the DECEL1 cable structural analysis code. The DECEL1 code and other available cable array analysis codes are described in Ref. 1. The solution technique is based on a new, efficient iterative algorithm (30). The computed results have been compared to simple laboratory experiments with good agreement. One of the cases analyzed using the algorithm was a 4700 m (15,400 ft) cable with 380 attached bodies. The calculated mode shape for mode

number 162 is shown in Figure 11. This mode is excited by current velocities near one knot and thus is likely to occur in practice. The complexity of the waveform is evident.

A reliable prediction of the strumming-induced drag amplification depends upon accurate knowledge of the natural frequencies and mode shapes of the cables in their higher modes. When the cable system has large numbers of attached masses, the prediction of the cable modes and frequencies must be done numerically. NATFREQ is ideally suited to this type of analysis. NATFREQ presently is being compared with the results from the 1981 Castine Bay cable strumming experiments that are described in Sections 3 and 4. Some initial comparisons have been encouraging (12).

CABLE STRUMMING SUPPRESSION

Oscillations due to vortex shedding can be reduced to tolerable levels by altering the mass (natural frequency) and damping of the structure, or by attaching some device to alter the flow field and thereby to reduce the coherence of the vortex shedding or to suppress the shedding entirely. It is usually costly and time consuming to modify the structure in order to change its damping and natural frequency. Most marine cables are lightly damped and increasing the damping usually is not practical, but sometimes the natural frequency can be changed sufficiently by increasing the tension in the cable. The suppression of strumming oscillations is a complex problem because the slenderness (length/diameter) of most practical cable array segments is very large and many cable vibration modes are present in the oscillations. Many undersea cable systems have very large ratios of length/diameter, have nonuniform currents incident upon them, and often are inclined to the flow. These factors complicate the suppression of strumming oscillations as compared to the suppression of oscillations for a cylindrical beam or other flexible member.

The strumming oscillations of cables are usually reduced by attaching some form of external device to interfere with the vortex shedding sufficiently to reduce the oscillations to acceptable levels. Most strumming suppression devices increase the hydrodynamic damping and, possibly, the cable's added mass and the effective frontal area of the cable that is projected into the flow. The steady hydrodynamic drag force then is increased relative to the drag on a stationary bare cable.

Several studies have been conducted in recent years to categorize the various types of strumming suppression devices and to attempt to understand more completely the mechanics of strumming suppression. A paper by Every, King, and Weaver (31) discusses the vortex excited vibrations of cables and cylinders and compares the effectiveness of various devices which have been developed to suppress the oscillations. Häsen and Meggitt (32) have consolidated the existing data on most available

devices that have been used to deal with strumming oscillations. They suggest criteria for making comparisons among different strumming suppression devices. Vandiver and Pham (11) reported the findings from field tests of four different types of strumming suppression devices. The devices tested included different types and configurations of synthetic fiber helical fringe and "haired" windings of various lengths and linear spacings. Three of the devices completely suppressed the oscillations but they resulted in a substantial drag penalty. Water tunnel flow visualization experiments showed that the devices did not eliminate vortex shedding but instead tended to reduce the spanwise coherence of the vortices.

Kline, Nelligan and Diggs (33) also have studied and have attempted to categorize various devices that have been developed to suppress cable strumming. Meggitt, Kline and Pattison (34) have conducted a series of experiments in one of the DTNSRDC towing channels to provide a data baseline for characterizing the behavior of representative strumming suppression devices in a quantitative manner. Several bare cables of various constructions (Kevlar, steel, nylon) and several cables with attached devices (helical fringe, helical ridge, segmented airfoil) were tested. A neutrally buoyant segmented foil reduced the strumming amplitude to negligible levels and also substantially reduced the drag on the cable. Both the helical fringe and helical wrap reduced the cable strumming to tolerable levels, but the helical fringe increased the steady drag coefficient by a factor of 100 percent.

It is typical of much of the cable strumming suppression literature that considerable scatter is evident in the existing data and that conflicting results often appear. There is little agreement between laboratory and at-sea data. Many devices for cable strumming suppression are Reynolds number dependent in terms of their operating characteristics, and data often are given for a particular device at a Reynolds number different from an intended application. However, the trends that have been identified are now discussed in terms of potential marine cable applications.

Hafen and Meggitt (32) generally have classified the most effective strumming suppression devices into four categories. These include helical ridges (strakes), flexible ribbon fairings, "fringe" fairings and "haired" fairings. Rigid, streamlined airfoil-shaped devices also are used effectively to suppress strumming under some circumstances (31,34). These devices yield relatively low drag coefficients but they are expensive, difficult to handle and can undergo large lateral deflections (kiting) at nonzero angles of attack. Specially designed cable handling equipment is required. Rings and sleeves have been tried but generally these devices have proven to be ineffective as strumming suppressors. The various devices are sketched in Figure 12, from Every, King and Weaver (31). Photographs of two typical "haired fairing" devices studied by Hafen and Meggitt (32) are shown in Figure 13.

With the exception of the airfoil-shaped suppression device, virtually all other strumming suppression devices tend to produce large increases in the steady hydrodynamic drag, as shown by Meggitt, Kline and Pattison (34). The hydrodynamic drag on a helical fringe fairing was as high as $C_D = 4.8$ on a 12.7 mm (0.5 in) Kevlar cable with a 76 mm (3 in) fringe over its entire length. The same cable with four helical wraps over its length had a $C_D = 2.5$. Other measured values of the drag ranged from $C_D = 0.72$ (ballasted airfoil) to $C_D = 2.9$ (helical fringe 25.4 mm (1 in) long over the entire cable). Typically the same bare cable underwent sustained strumming vibrations and $C_D = 2.3$. Thus a drag penalty is paid in most applications and an optimum design for a strumming suppression device must weigh the relative importance of reduced vibration levels against the penalty of increased drag. The drag penalty is an important consideration in the design of deep water cable arrays that are intended for deployment in 1200 m (3900 ft) to 1800 m (5900 ft) depths or greater.

SUMMARY

The dynamic analysis of marine structures and cable systems has become increasingly important and sophisticated in order to accurately predict stress distributions and operational lifetimes in the ocean environment. The strumming vibrations of marine cables have serious consequences because they take place at relatively high frequencies and are a potential cause of fatigue for system components. They also are a cause of increased hydrodynamic drag and steady deflections. Strumming can introduce acoustic noise in sensor components attached to the cable and can cause abrasion and wear of fittings and of the cables themselves. These vibrations usually are caused by a current flowing past the cable. However, they also are caused sometimes by low-frequency wave drift forces and long period swells when the cable extends downward from the vicinity of the ocean surface.

This paper has summarized the present state-of-the-art for predicting the strumming vibrations of marine cables. Reliable data now are in hand for the dynamic response of and hydrodynamic forces on model-scale structures and cables, and based upon these findings empirical and semi-empirical prediction models have been developed and calibrated for use in practice. Many of the recent findings have come from the Navy's marine cable dynamics research program. The results obtained from that program through 1981 are discussed in a recent Naval Civil Engineering Laboratory (NCEL) report (1).

Several outstanding problems have not yet been addressed in sufficient detail. They are:

- The response of long marine cables ($L/D \sim 2000$ and longer) in nonuniform (shear) currents;
- Hydrodynamic drag forces on long cables;

- Reliable design criteria and data (drag coefficients, etc.) for in situ long cables;
- The nonresonant strumming response of marine cables. Nonresonant oscillations typically occur when many cable vibration modes are present in the strumming signature.

REFERENCES

1. O.M. Griffin, R.A. Skop, S.E. Ramberg, D.J. Meggitt and S.S. Sergev, "The Strumming Vibrations of Marine Cables: State of the Art," Naval Civil Engineering Laboratory Technical Note No. N-1608, May 1981.
2. O.M. Griffin, J.K. Vandiver, R.A. Skop, and D.J. Meggitt, "The Strumming Vibrations of Marine Cables," Ocean Science and Engineering, Vol. 8, to appear, 1983.
3. T. Sarpkaya, "Vortex-Induced Oscillations, A Selective Review," Trans. ASME, Series E, J. Applied Mechanics, Vol. 46, 241-258, 1979.
4. R. King, "A Review of Vortex Shedding Research and Its Application," Ocean Engineering, Vol. 4, 141-171, 1977.
5. O.M. Griffin, "OTEC Cold Water Pipe Design for Problems Caused by Vortex-Excited Oscillations," NRL Memorandum Report 4157, March 1980; see also Ocean Engineering, Vol. 8, 129-209, 1981.
6. O.M. Griffin, "Steady Hydrodynamic Loads Due to Vortex Shedding from the OTEC Cold Water Pipe," NRL Memorandum Report 4698, January 1982.
7. O.M. Griffin and S.E. Ramberg, "Some Recent Studies of Vortex Shedding With Application to Marine Tubulars and Risers," Trans. ASME., J. Energy Resources Tech., Vol. 104, 2-13, 1982.
8. J. Dale, H. Menzel and J. McCandless, "Dynamic Characteristics of Underwater Cables: Flow Induced Transverse Vibrations," Naval Air Development Center Report NADC-AE-6620, 1966.
9. J.R. Dale, "Water Drag Effects of Flow Induced Cable Vibrations," Naval Air Development Center Report NADC-AE-6731, 1967.
10. J.K. Vandiver, "A Field Study of Vortex-Excited Vibrations of Marine Cables," Offshore Technology Conference Preprint 2491, May 1976.
11. J.K. Vandiver and T.P. Pham, "Performance Evaluation of Various Strumming Suppression Devices," MIT Ocean Engineering Department Report 77-2, March 1977.
12. J.K. Vandiver and O.M. Griffin, "Measurements of the Vortex-Excited Strumming Vibrations of Marine Cables," Ocean Structural Dynamics Symposium '82 Proceedings, Oregon State University, 325-338, September 1982.
13. E.J. Softley, J.F. Dilley and D.A. Rogers, "An Experiment to Correlate Strumming and Fishbite Events on Deep Ocean Moorings," GE Document 77SDR 2181, General Electric Co.: Re-Entry and Environmental Systems Division, 1977.

14. T.R. Kretschmer, G.A. Edgerton and N.D. Albertsen, "Seafloor Construction Experiment, SEA-CON II: An Instrumented Tri-Moor for Evaluating Undersea Cable Structure Technology," Civil Engineering Laboratory Technical Report R-848, December 1976.
15. R.A. Skop and J. Mark, "A Fortran IV Program for Computing the Static Deflections of Structural Cable Arrays," Naval Research Laboratory Report 7640, August 1973.
16. C.M. Alexander, "The Complex Vibrations and Implied Drag of a Long Oceanographic Wire in Cross-Flow," Ocean Engineering, Vol. 8, 379-406, 1981.
17. R.A. Skop and O.M. Griffin, "On a Theory for the Vortex Excited Oscillations of Flexible Cylindrical Structures," J. Sound and Vib., Vol. 41, 263-274, 1975; see also "The Vortex-Induced Oscillations of Structures," J. Sound and Vib., Vol. 44, 303-305, 1976.
18. W.D. Iwan, "The Vortex-Induced Oscillation of Elastic Structural Elements," Trans. ASME, J. Engrg. Indus., Vol. 97, 1378-1382, 1975.
19. R.D. Blevins, *Flow-Induced Vibration*, Van Nostrand-Reinhold: New York, 1977.
20. R.T. Hartlen and I.G. Currie, "Lift-Oscillator Model of Vortex-Induced Vibrations," Proc. ASCE, J. of Eng. Mech., Vol. 96, 577-591, 1970.
21. R.D. Blevins and T.E. Burton, "Fluid Forces Induced by Vortex Shedding," Trans. ASME, Series I, J. Fluids Engrg., Vol. 98, 19-24, 1976.
22. M.J. Kennedy and J.K. Vandiver, "A Random Vibration Model for Cable Strumming Predictions," CIVIL ENGINEERING IN THE OCEANS IV, Vol. I, 272-293, ASCE: New York, September 1979.
23. F.J. Fischer, W.T. Jones and R. King, "Current-Induced Oscillations of Cognac Piles During Installation—Prediction and Measurement," in Proc. Symp. on Practical Experiences with Flow-Induced Vibrations (Preprints), Karlsruhe, Vol. I, 216-228, September 1979.
24. G. Grimminger, "The Effect of Rigid Guide Vanes on the Vibration and Drag of a Towed Circular Cylinder," David Taylor Model Basin Report 504, April 1945.
25. O.M. Griffin, R.A. Skop and S.E. Ramberg, "Resonant, Vortex-Excited Vibrations of Structures and Cable Systems," Offshore Technology Conference Preprint OTC 2319, 1975.
26. M.J. Every, R. King and O.M. Griffin, "Hydrodynamic Loads on Flexible Marine Structures Due to Vortex Shedding," Trans. ASME, J. Energy Resources Tech., Vol. 104, 330-336, 1982.
27. W.L. Dalton, "A Survey of Available Data on the Normal Drag Coefficient of Cables Subjected to Cross Flow," Naval Civil Engineering Laboratory Report CR 78.001, Port Hueneme, CA, August 1977.
28. J.H. Pattison, P.P. Rispin and N.T. Tsai, "Handbook on Hydrodynamic Characteristics of Moor-Array Components," David Taylor Naval Ship Research and Development Center Report SPID-745-01, March 1977.
29. "Wind and Water-Current-Induced Oscillations in Tubulars," Petroleum Engineer International, Vol. 51, No. 12, 46-62, October 1979.

30. S. Sergev and W.D. Iwan, "The Natural Frequencies and Mode Shapes of Cables with Attached Masses," Naval Civil Engineering Laboratory Technical Note N-1583, August 1980.
31. M.J. Every, R. King and D.S. Weaver, "Vortex Excited Vibrations of Cylinders and Cables and Their Suppression," Ocean Engineering, Vol. 9, 135-158, 1982.
32. B.E. Hafen and D.J. Meggitt, "Cable Strumming Suppression," Naval Civil Engineering Laboratory Technical Note N-1499, September 1977.
33. J.E. Kline, J.J. Nelligan and J.S. Diggs, "A Survey of Recent Investigations into the Nature of Cable Strumming, its Mechanism and Suppression," MAR Inc. Technical Report 210, July 1978.
34. D. Meggitt, J. Kline and J. Pattison, "Suppression of Mooring Cable Strumming" Proceedings of the Eighth Ocean Energy Conference, Paper 1B5, Marine Technology Society: Washington, DC, Vol. 1, 107-116, 1982.

Table I
Predictions of Cross Flow Displacement
Amplitude Due to Resonant Vortex-Excited Oscillations
as a Function of the Reduced Damping

Investigator	Predicted Displacement Amplitude
Skop, Griffin and Ramberg (25)	$\bar{Y}/D = \frac{1.29\gamma}{[1 + 0.43(2\pi St^2 k_s)]^{3.35}}$
Blevins (19)	$\bar{Y}/D = \frac{0.07\gamma}{(1.9 + k_s) St^2} \left[0.3 + \frac{0.72}{(1.9 + k_s) St} \right]^{1/2}$
Sarpkaya (3)	$\bar{Y}/D = \frac{0.32\gamma}{[0.06 + (2\pi St^2 k_s)^2]^{1/2}}$

Legend: \bar{Y} = displacement amplitude; D = cylinder diameter; m = mass or equivalent mass per unit length; St = Strouhal number; k_s = reduced damping; γ = dimensionless mode shape factor, $\gamma = 1$ for a spring-mounted rigid cylinder, $\gamma = 1.3$ for the first mode of a cantilever, and $\gamma = 1.16$ for a sinusoidal mode shape (cable).

Table 1
Vortex-excited Cross Flow Displacement Amplitude
Response of Cylindrical Structures.
Legend for Data Points in Fig. 8

Type of cross-section and mounting; medium	Symbol
Various investigators, from Griffin et al. (1):	
Spring-mounted rigid cylinder; air	*○—○*
Spring-mounted rigid cylinder; water	◆
Cantilevered flexible circular cylinder; air	△
Cantilevered flexible circular cylinder; water	X▽⊕
Pivoted rigid circular rod; air	□▲
Pivoted rigid circular rod; water	●
Spring-mounted rigid cylinder; water	■
Flexible circular cylinder, $L/D = 240$; water	■
Cantilevered flexible circular cylinder, $L/D = 52$ (PVC); water	○
Cantilevered flexible circular cylinder, $L/D = 52$ (stainless steel); water	○

Table 3
Excitation Force Coefficient C_{LE} , equation (8);
data from Figure 2.7, reference (1).

Force coefficient: $C_{LE} = a_1 + b_1 Y_{EFF,MAX} + c_1 Y_{EFF,MAX}^2 + d_1 Y_{EFF,MAX}^3$
where $a_1 = 0.12$, $b_1 = 2.12$, $c_1 = -3.57$, $d_1 = 1.45$
and the standard deviation of the curve $\sigma = 0.1$.

Effective displacement: $Y_{EFF,MAX} = \frac{(\bar{Y}_{MAX}/D)}{\gamma_i}$, $\gamma_i = \frac{|\psi_i(z)|_{MAX}}{I_i^{1/2}}$

In terms of \bar{Y}_{MAX}/D ,

$$C_{LE}|_{\bar{Y}_{MAX}} = a_1 + (b_1/\gamma_i) (\bar{Y}_{MAX}/D) + (c_1/\gamma_i^2) (\bar{Y}_{MAX}/D)^2 + (d_1/\gamma_i^3) (\bar{Y}_{MAX}/D)^3$$

where the factor γ_i is representative of different end fixities, i.e. free-pinned, pinned-pinned, clamped-clamped, etc. Hence \bar{Y}_{MAX}/D is the *peak* displacement along the beam. The factor γ_i can be calculated from the data listed in references 1 and 5.

AD-A139 419

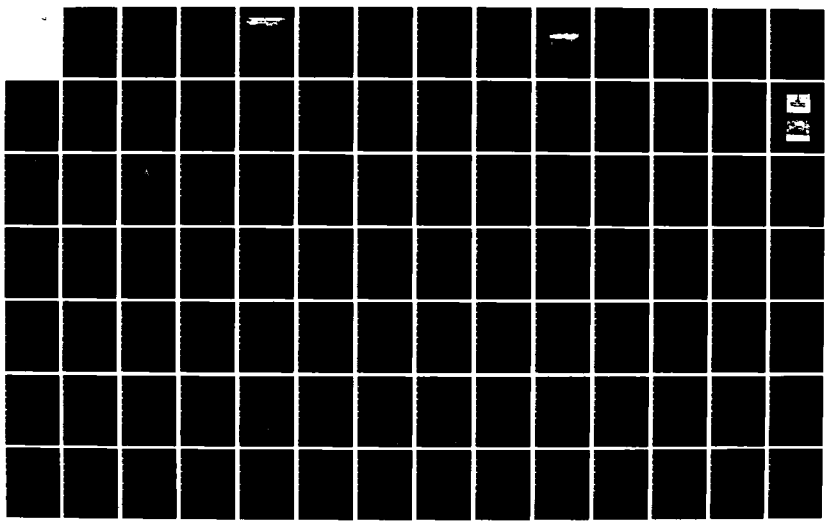
NCEL (NAVAL CIVIL ENGINEERING LAB) OCEAN PLATFORMS
SEMINAR(U) NAVAL CIVIL ENGINEERING LAB PORT HUENEME CA
D R SHIELDS NOV 83 NCEL-TN-1681

3/4

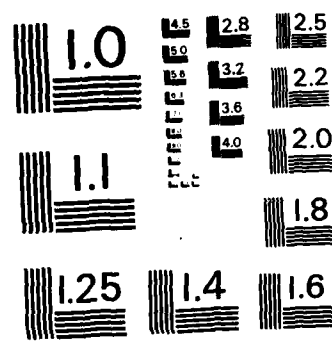
UNCLASSIFIED

F/G 13/13

NL



3/4



MICROCOPY RESOLUTION TEST CHART
NATIONAL BUREAU OF STANDARDS - 1963 - A

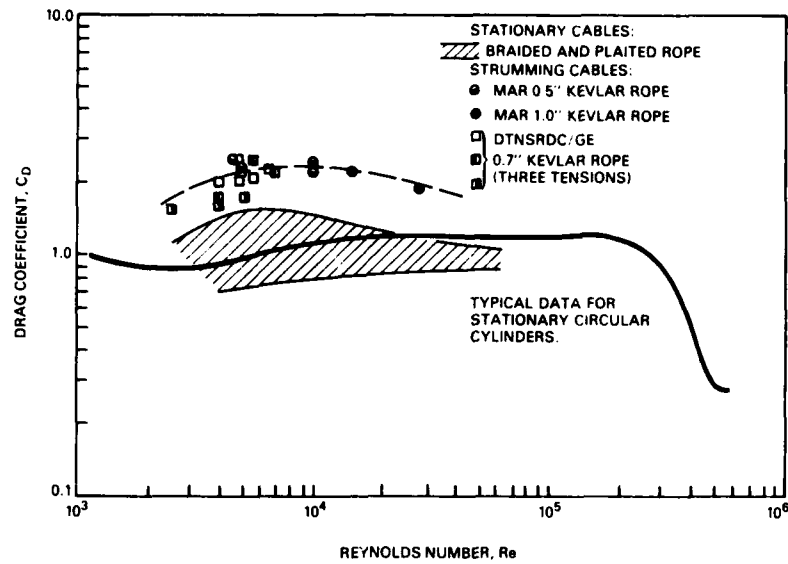


Fig. 1 — The drag coefficient C_D plotted against the Reynolds number Re for several synthetic fiber marine cables. A curve of C_D versus Re for typical stationary cylinders is plotted as a reference. All of the cable strumming experiments were conducted at the David Taylor Naval Ship R&D Center. The original figure was provided by D.J. Meggitt of the Naval Civil Engineering Laboratory.

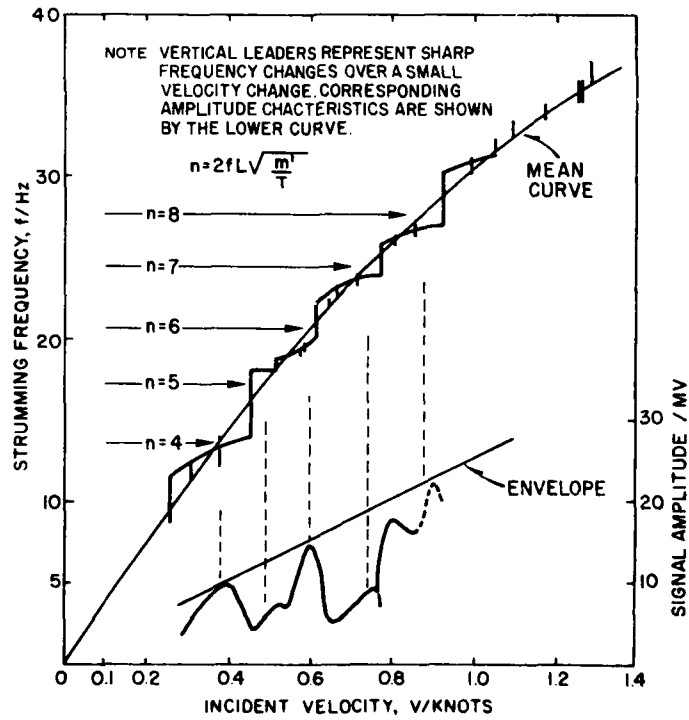


Fig. 2 — Vortex-excited strumming vibrations of a taut marine cable; from Dale, Menzel and McCandless (8)

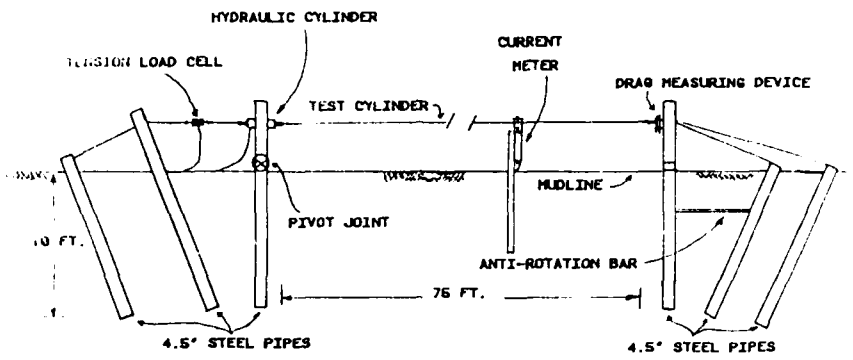


Fig. 3 — Layout of the Castine Bay cable strumming test set-up; from Vandiver and Griffin (12)

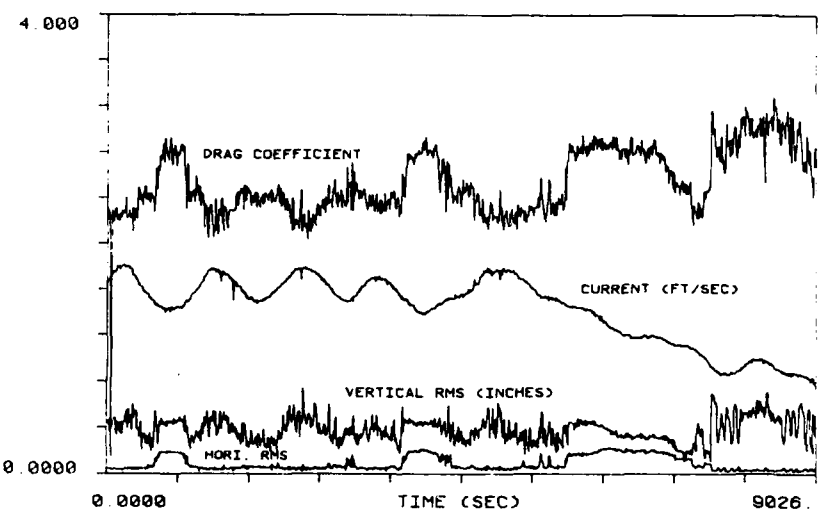


Fig. 4 — The drag coefficient, current, and displacement amplitude for a 22.9m (75 ft) long marine cable with six attached cylindrical masses. The strumming data were recorded at $3L/4$ along the cable; from Vandiver and Griffin (12).

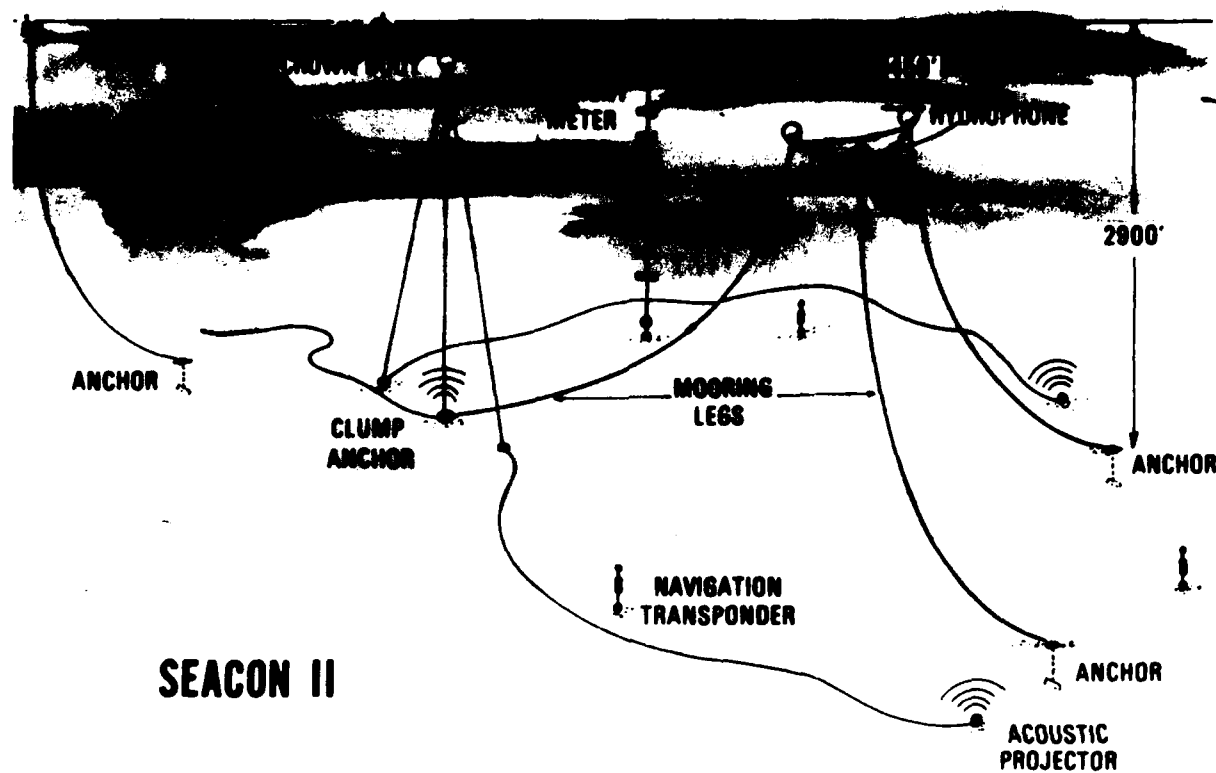


Fig. 5 — A schematic drawing of the SEACON II experimental cable mooring

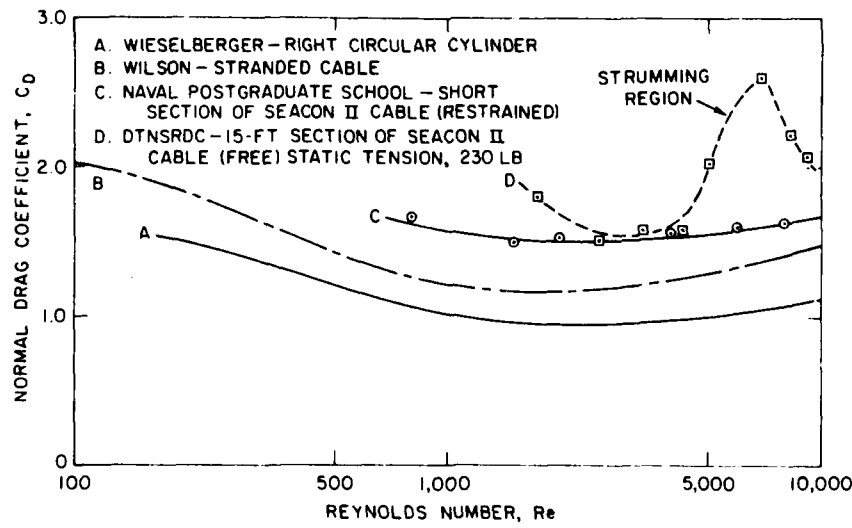


Fig. 6 — Measured drag coefficients for the SEACON II cable, from Kretschmer et al. (14).

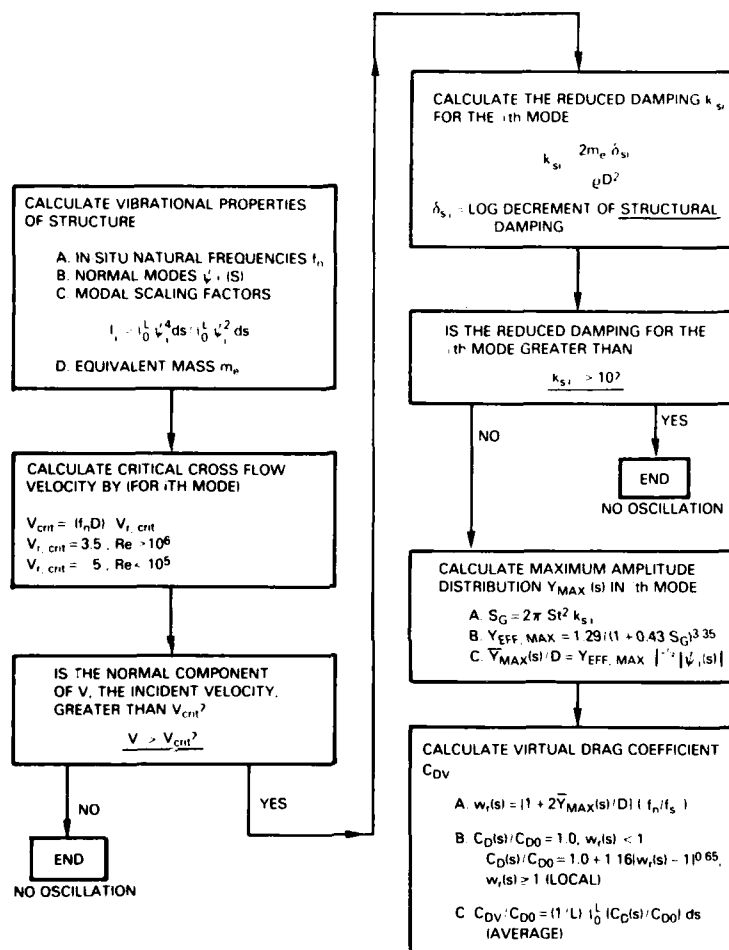


Fig. 7 — Flow diagram of the steps required for the calculation of the steady drag amplification due to vortex-excited oscillations; from Griffin (5).

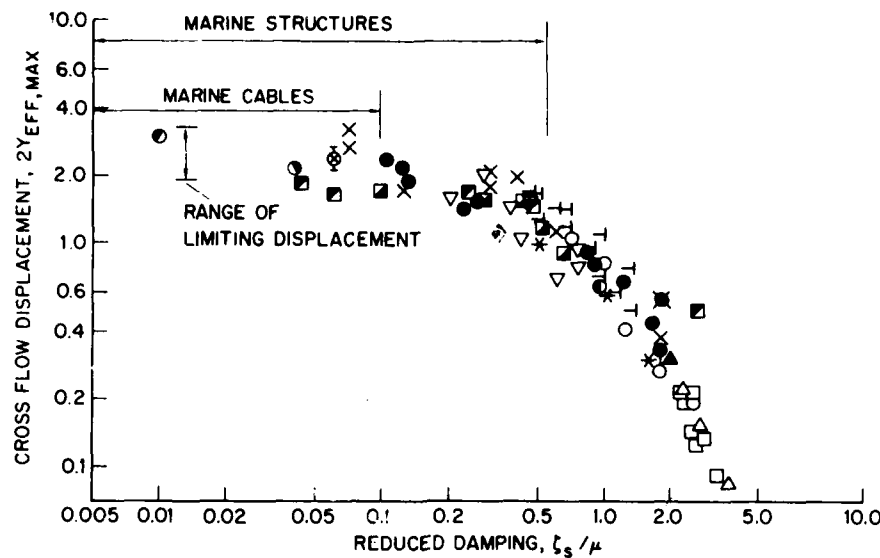


Fig. 8 — Maximum vortex-excited cross flow displacement $2Y_{EFF, MAX}$ of circular cylinders, scaled as in equation (5), as a function of the reduced damping $\zeta_s/\mu = 2\pi St^2 k_s$

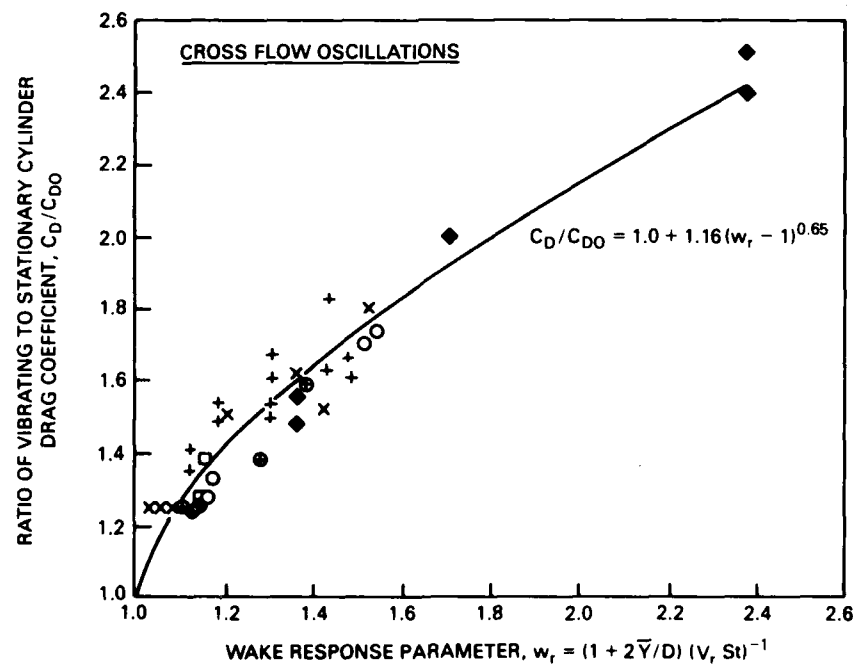


Fig. 9 — The ratio of the steady drag coefficient C_D due to vortex-excited cross flow oscillations and the steady drag coefficient C_{D0} on a stationary circular cylinder plotted against the wake response parameter w_r , from Skop, Griffin and Ramberg (25)

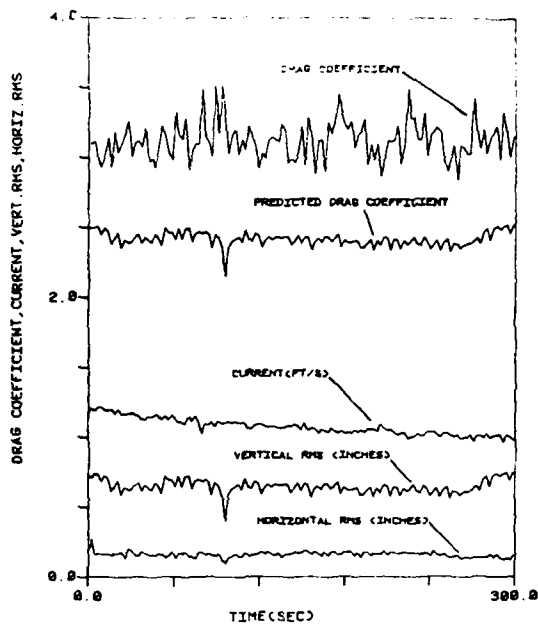


Fig. 10 — The predicted drag coefficient for a time interval during one bare cable test during the 1981 Castine field test program. The strumming data were recorded to $L/6$ along the cable at an antinode of the third mode strumming vibrations; from Vandiver and Griffin (12).

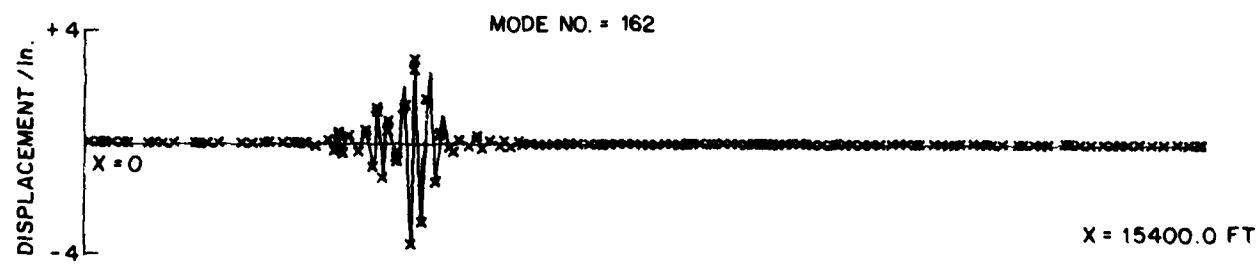


Fig. 11 — The calculated mode shape for a 4700 m (15400 ft) long marine cable with 380 attached sensor housings; from Sergey and Iwan (30).

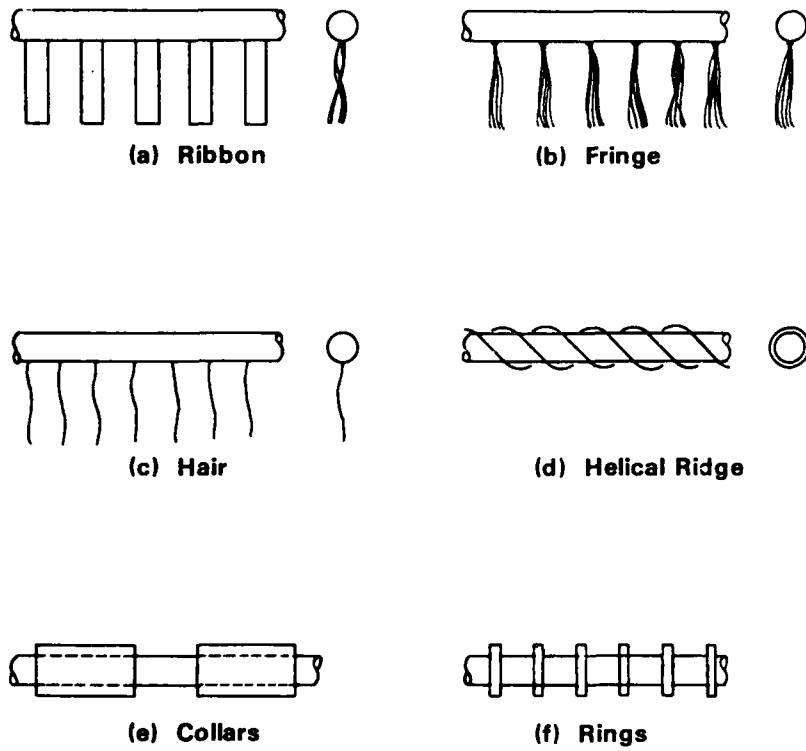


Fig. 12 — A line drawing of several common cable strumming suppression devices.
from Every, King and Weaver (31)

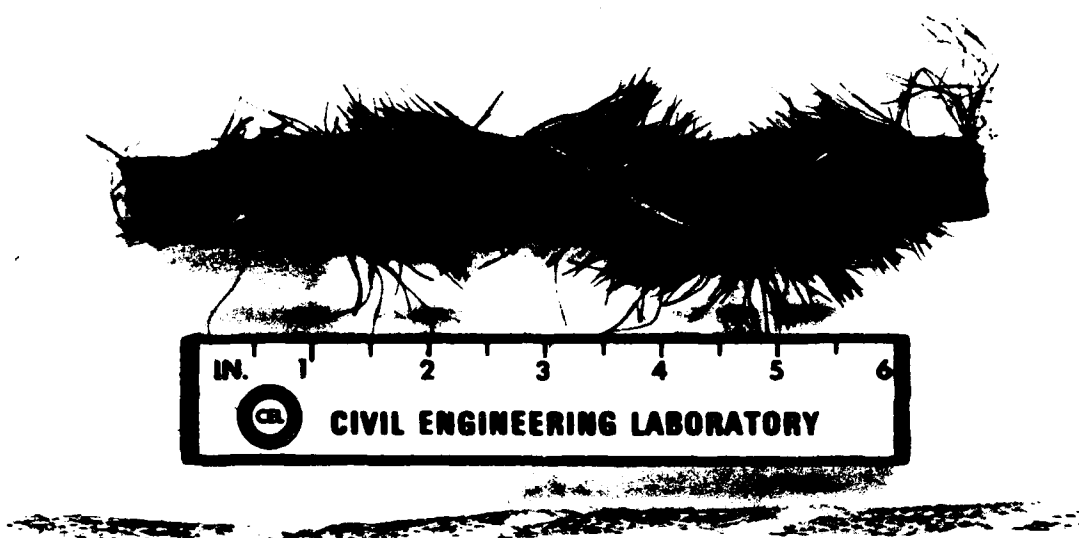


Fig. 13 — Examples of Philadelphia Resin Corporation haired fairings. Top: brush fairings applied helically on a 19.2 mm (0.75 in.) diameter cable. Bottom: cotton fuzz applied helically on a 6.4 mm (0.25 in.) diameter Kevlar cable. Photograph from Hafen and Meggitt (32).

MOORING DESIGN, DEPLOYMENT, AND OPERATION

W. O. Rainnie, Jr.
G. L. Timpe, LT USCG
R. L. Boy, LTJG USCG

NOAA Data Buoy Center
National Space Technology Laboratories
NSTL Station, Mississippi 39529

January 1983

INTRODUCTION

In January 1969, the National Data Buoy Development Project was established by the United States Coast Guard. The primary purpose of this organization was to verify and standardize the design and performance of environmental data buoys by establishing an extensive network of sophisticated buoys capable of delivering a wide variety of data, supplemented by smaller buoys of simpler design for special user needs. The project was transferred to the newly created National Oceanic and Atmospheric Administration (NOAA) in 1970. In 1972, user needs were re-evaluated and the program was redirected to be more responsive to these needs. Consequently, the goal of establishing a network of multipurpose buoys was discarded. In January 1973, the project was designated the NOAA Data Buoy Office (NDBO). Recently the name was again changed to NOAA Data Buoy Center (NDBC).

A major NDBC mission is to develop the technology required to gather and report environmental data from marine areas on an accurate, reliable, and synoptic basis. The provisioning of this data enables improved weather forecasting, including warnings of impending catastrophes. The essential ingredient in meeting the objective involves the deployment of a number of buoys moored in various gulfs and oceans. A supporting ingredient involves deployment of large numbers of small free-drifting buoys capable of measuring

meteorological parameters while simultaneously mapping ocean currents through Lagrangian tracking techniques. Finally, NDBC has deployed numerous custom-designed platforms designated to meet unique mission requirements and is also providing data systems for headland station and offshore platforms.

Since June 1972, NDBC has deployed environmental reporting data buoys in various gulf and ocean regions to provide synoptic data for weather reports and for scientific data archives. As of November 1982, 35 moored buoys have been reporting environmental data on a routine basis (see Figure 1). Accurate and reliable buoy sensors, electronics, and communications are required to support NDBC's mission of gathering and reporting environmental data from the marine areas of the world. The current complement of buoy electronics was determined by a series of hardware evolutions, which in turn were brought about by a continued quest for the most accurate and reliable equipment that technology could offer. The evolution of the data buoy hardware, together with the availability of microprocessor technology and suitable communication satellites, enables a fully automated, reliable approach for the acquisition of marine environmental data on a synoptic basis in severe weather conditions. These conditions include the underwater and surface open-ocean environment during all sea state conditions and, most importantly, during severe disturbances. In addition, the measurement and reporting of environmental data is accomplished on remote ocean platforms relatively inaccessible for maintenance.

NDBC's moored buoy system monitors surface meteorological parameters, one-dimensional wave spectra, and sea surface temperature, and provides this information to the National Weather Service and various other sponsoring government agencies. Buoys used in this system are designed for open ocean deployment and are of three basic configurations: the 12-m and 10-m discus, and the 6-m boat-shaped hull.

CURRENT BUOYS

Figure 2 shows the 12-m (40-ft) discus buoy displaces 95 ton and is presently the largest buoy in use by NDBC.¹ The steel hull uses all-welded construction and shipboard fittings. These buoys were originally equipped with twin diesel electric generators for power; however, they have all been modified to use a air-depolarized battery power source and the generators have been removed. Meteorological sensors are located at the 10-m level with oceanographic sensors installed in the hull. The 12-m discus buoys can be deployed at any depth in ice-free water. The mooring is typically single-point, semitaut or inverse catenary. Because of its size, the buoy must be towed to and from station. The towing speed is generally 8 kn in reasonable weather.

There are two classes of 10-m (33-ft) discus buoys in use. The first are equipped with a mast insulator, and originally had radial and cone wire antennas for high frequency (HF) date transmission. The second class is a value-engineered version of the hull, with no mast insulator. Both classes are steel, all-welded construction, and displace 57 tons. Like the 12-m hulls, the meteorological sensors are located at the 10-m level, and an air-depolarized battery power system is used. The 10-m buoys must be towed from site to site, at a maximum speed of 8 kn.

Both the 10-m and 12-m discus buoys are designed to remain on station for somewhat more than 2 years which is presently limited by battery life.

Figure 3 shows the 6-m (20-ft) boat-shaped hulls known (and have been for 30 years) as NOMAD (Navy Oceanographic Meteorological Automatic Device) buoys.² A NOMAD buoy is an all-aluminum hull that carries its meteorological sensors at the 5-m level. There are also two classes of this buoy. The first design was developed by the U.S. Navy as a floating weather station buoy in the late 1940's and early 1950's. The hull has eight compartments and four center-

line instrument wells. Currently in construction is a class of second generation NOMAD buoys, with lines identical to the original design but with a value-engineered hull structure. With a beam of 3 m (9'10") and a displacement of 10 tons, the NOMAD buoy is the easiest of the three types of buoys to handle and transport. It can be carried to station on the deck of a ship or can be towed. The option of transporting this buoy over land by rail or truck is also available. The NOMAD is powered by air-depolarized batteries, and can remain on station for up to about 2 years, depending on the mission. Newer electronics are expected to extend this to more than 3 years within the next year or so.

In addition, a new class of buoy is presently being developed for use in less-severe, near-shore environments. This class of buoy, known as the E-buoy, has a 3-m (10-ft) diameter aluminum discus hull with meteorological sensors located at the 3-m level, and displaces 2 tons. The E-buoy is powered by air-depolarized batteries and can remain on station for about 1 year. The prototype E-buoy hull is scheduled to be deployed for testing in late 1982, with the production series of the buoy scheduled for construction in early 1984.

NUMERICAL MODELS

The numerical model principally used in moored buoy system design is a frequency-domain model developed for NDBC by Oceanics, Inc., in 1972.³⁻⁶ It is used as a tool in buoy hull and mooring design to provide the following information:

- The station-keeping ability of a buoy system under a given set of environmental conditions
- The oscillatory motion (both angular and translational) of a buoy in various sea states

- The structural acceleration loadings on a buoy under a given loading condition
- The acceleration at stations along the mooring where instrument packages or floats are attached
- The tensions along the mooring line under a given set of environmental conditions.

The model was developed to predict the buoy and mooring's response as simply as possible without neglecting any significant factors. To cover the wide variety of hull and mooring types, the model was made as general as possible. In its simplest form, it consists of a surface float connected to the seafloor by some type of flexible cable. There are no limits on the water depth or on the mooring component size. To this simple model, a variety of possible buoy types, and use of cables that can vary in size, type, and elasticity along their lengths, was added. In addition, subsurface floats or instrument packages can be added at various locations along the cable. The type of mooring used can vary from slack to taut.

The model is a two-dimensional model, with buoy responses limited to the heave, pitch, and surge modes. Current, waves, and winds are all coplanar with the principal longitudinal axis of the buoy. The inputs to the model are the type of buoy, magnitude of wind, steady current profile, type of sea state, and mooring configuration. The possible buoy types are: spar, discus, boat-shaped, and catamaran hull. The wave system can be entered either as regular sinusoidal waves, or as a Neumann, Pierson-Moskowitz, or as a two-parameter wave spectra.

The numerical model arrives at two solutions. The first is a static solution (with no wave excitation), with the buoy and mooring in a steady-state equilibrium under the action of wind and current. Using the static solution as

a baseline, the dynamic effects of the waves are then added. These dynamic effects are linearized by assuming that they are small, sinusoidal perturbations about the static equilibrium condition. Both the static and dynamic system equations are two-point boundary-value problems. The static system is represented by a nonlinear, second-order equation, and the dynamic system represented by a linear, fourth-order equation.

For the static case, the cable is assumed to be flexible and elastic. It is acted on by steady hydrodynamic forces due to current flow, by the weight of the cable, by the forces on the cable due to the buoy, and by the forces induced by the attached floats or instrument packages. The buoy's response is dependent on its drag characteristics, its angular orientation to the waves, the degree of hull submergence, velocity of the current, and the force and moment of the wind acting on the exposed portion of the hull. Any aerodynamic lift on the buoy is ignored. All the forces and moments in the system: current, wind, weight, buoyancy, and cable forces must be in equilibrium. The static equation is solved by assuming a value of buoy submergence and then solving for buoy response. Then the buoy's response is used as an initial condition and the differential equations of the cable integrated. This routine is iterated until the point of zero cable slope coincides with the seafloor level.

For the dynamic case, it is assumed that all the buoy's added mass terms, and damping coefficients in motion that have a restoring action (heave, pitch, and roll), are constant and not frequency dependent. As a result, the general linear equations of motion represent a balance of inertial, damping, hydrostatic, mooring, and wave excitation forces.

$$\begin{aligned} a_{11}\ddot{x} + a_{12}\dot{x} + a_{13}x + a_{14}\ddot{z} + a_{15}\dot{z} + a_{16}z + a_{17}\ddot{\theta} + a_{18}\dot{\theta} + a_{19}\theta &= x_w \\ a_{21}\ddot{x} + a_{22}\dot{x} + a_{23}x + a_{24}\ddot{z} + a_{25}\dot{z} + a_{26}z + a_{27}\ddot{\theta} + a_{28}\dot{\theta} + a_{29}\theta &= z_w \end{aligned}$$

$$a_{31}\ddot{x} + a_{32}\dot{x} + a_{33}x + a_{34}\ddot{z} + a_{35}\dot{z} + a_{36}z + a_{37}\ddot{\theta} + a_{38}\dot{\theta} + a_{39}\theta = M_w$$

X_w , Z_w , and M_w are defined as the wave excitation forces, and moment respectively. From physical considerations, lack of coupling between the translatory motions of heave and surge, the lack of a surge restoring force, and the symmetry of the X_w excitation force with respect to θ , the equations of motion reduce to following:

$$a_{11}\ddot{x} + a_{12}\dot{x} + a_{17}\ddot{\theta} + a_{18}\dot{\theta} = X_w$$

$$a_{24}\ddot{z} + a_{25}\dot{z} + a_{26}z + a_{27}\ddot{\theta} + a_{28}\dot{\theta} + a_{29}\theta = Z_w$$

$$a_{31}\ddot{x} + a_{32}\dot{x} + a_{34}\ddot{z} + a_{35}\dot{z} + a_{36}z + a_{37}\ddot{\theta} + a_{38}\dot{\theta} + a_{39}\theta = M_w$$

These equations of motion are solved for each type of buoy using different methodologies. The forces on the buoy and resultant buoy motion for boat-shaped and catamaran hulls are solved using strip theory. The coefficients in the equation of motion for the discus hull are based on the results presented by Kim,⁷ while the coefficients for the spar buoy are based on the work by Newman.⁸

The dynamic problem for the cable then reduces to a two-point boundary-value problem, with one boundary condition at the anchor, and one at the buoy. This two-point boundary-value problem was then originally converted to an initial value problem using the Goodman-Lance method;⁹ however, this method allowed some instability in the solutions, especially in long cables at high frequencies. As a result, this portion of the model was subsequently modified to use the Godonov method¹⁰ of renormalization. After this renormalization, the cable's differential equations are integrated using the numerical method of Runge-Kutta-Gill, as modified by Thompson.¹¹

In conjunction with development of the numerical program, model tests were conducted to provide some verification of the program.^{5,12} The calculated

results corresponded closely with the experimental results from the model test; however, some type of full-scale verification was also desired. As a result, in 1976, NDBC, the Office of Naval Research (ONR), and Naval Civil Engineering Laboratory (NCEL) jointly funded an open-sea experiment to obtain engineering data on buoy and mooring dynamics for use in modeling verification.¹³ For the experiment, each of the involved organizations had tasks to perform. Woods Hole Oceanographic Institution (WHOI) under contract prepared the mooring hardware and was responsible for the data taking phase of the experiment. ONR provided contracting support. NDBC supplied a buoy hull and was responsible for archiving the data and issuing the results. Charles Draper Laboratories was responsible for the preparation and operation of the mooring line motion instruments and the temperature/pressure recorders.

In October 1976, the data taking phase of the experiment was conducted at the Pacific Missile Range Facility, Kauai, Hawaii. Five different moorings were tested, each constituting a separate experiment. These included:

- Discus buoy on a slack mooring
- Spar buoy with a spherical subsurface float
- Discus buoy on a taut mooring
- Spherical float on a high-performance mooring
- Spherical subsurface float.

All the experiments were conducted, but because of technical problems with the buoy motion package and uncertainties in the surface current measurements, the resultant experiment data were less than satisfactory.¹⁴ Afterwards, the experimental data were analyzed and compared with the computer-generated values. The results were far from conclusive, but in general at low frequencies both the experimental values of tension and transfer function were higher than calculated. At middle frequencies, comparison was good, and at high

frequencies, the calculated values of tension and transfer function were higher than the experimental values. However the results were not conclusive, so there is at present, no firm full-scale validation of NDBC's frequency domain model.

Another numerical model, used principally by NDBC in drifting buoy design, is a time domain program developed by Nath at Oregon State University.¹⁵ The model is used a tool to determine buoy motion, orientation, and tether and drogue stresses for a given set of environmental conditions.

It is a two-dimensional model in which wind, waves, current, gravity, and the resultant buoy motion all act in the same plane. Morrison's equation is used to compute the buoy's motions, and a lumped parameter technique is used to determine the motions of the tether and drogue.

Originally, the only types of buoy that could be analyzed were spar or NDBC-type drifting hulls. The program has been subsequently updated to include Coast Guard type Aids-to-Navigation (ATON) buoys, thick discus hulls, and ellipsoid-shaped buoys. Drifting buoys, with tethers and drogues, or buoys with single-point moorings can be analyzed. Environmental inputs to the model are a steady and uniform wind, a steady current profile, and waves that can be either regular linear or nonlinear finite amplitude waves. The model outputs the buoy's position, orientation, kinematics, and internal stresses in the line, all as a function of time.

PRESENT MOORING DESIGNS

The three primary generic types of moorings used by NDBC are slack, semi-taut, and inverse catenary. The specific type to use is highly dependent upon the depth of water. Other considerations include: the size of buoy, current, weather environment, mooring component cost and availability, watch

circle, the anchor/bottom interface, and the service vessels available to deploy and maintain them.

The slack moorings (Scope 3-5/1) are used in shallow water and are usually all-chain in construction (Figure 4). The ground chain and anchor see a lot of motion transferred down from the buoy. The chain must be of sufficient size to allow for accelerated wear in the chafe zone, yet be light enough to be supported by the buoy.

Semitaut (Scope 1.1/1) moorings are used in deeper water where a buoy cannot support a conventional all-chain mooring. High-strength, lightweight components are used in the upper portion of the moor to allow for greater depths with a given buoyancy. Synthetic rope has the characteristic of absorbing most of the buoy motion, thus the bottom chain will not wear as quickly as with an all-chain moor. Accurate depth measurement becomes important. A short mooring will result in heavy mooring loads on the buoy and a long mooring will expose the synthetic line to abrasion on the bottom.

Inverse catenary moorings (Scope: 1.25-1.4/1) are used in water deeper than about 600 feet (200 meters), or where very light mooring loads are desired (Figure 5). Subsurface floats on synthetic rope support the static weight of the lower mooring, thus lifting the synthetic line-chain connection, and allow for greatly reduced dynamic forces on the ground tackle. One of the other major advantages is that the inverse catenary allows for much less accurate depth measurements before deployment than the semitaut moorings. The catenary slack compensates for differences in actual depth. Two important factors to keep in mind with this type of mooring are 1) the added cost of the catenary slack, and 2) the increase in surface area exposed to high currents. These disadvantages are more than compensated for by the advantages previously mentioned, however.

As anyone in the buoy mooring field can attest, problems involving people and hardware do occur and must be taken into consideration when designing any mooring system. Those problems classified as human error are the most difficult to anticipate. They include assembly errors, deployment procedures, and inherent design errors. Hardware problems include quality control, corrosion and wear, and dissimilar metals in seawater. A third category to address is fishbite or "manbite." These problems range from bonafide fish attack to long-line and deep trawl abrasion to outright vandalism. Fishermen or seismic crews value their gear much more than buoy mooring line when the two become entangled.

The NOAA Data Buoy Center has taken the generic mooring types, enhanced them with the aid of computer modeling, and developed a series of standardized moorings. These are updated as specific mooring problems are addressed.

DEPLOYMENT AND OPERATIONS

The deployment procedures and operations of mooring systems are heavily dependent upon the servicing vessels available. NOAA has an Interagency Agreement with the U.S. Coast Guard (USCG). Therefore, NDBC uses Coast Guard facilities and vessels whenever practicable and has tailored the service operations to the specific cutters used.¹⁶ They range from 180-ft ocean going buoy tenders to small 44- to 55-ft service boats.

A typical discuss buoy deployment operation involves towing the buoy to location. On scene, the buoy is attached to the mooring which is then payed out, in the case of synthetic rope, down to end of the synthetic line. This is then connected to the lower chain portion of the moor on the ship. The anchor(s) is then released, dragging the bottom chain over the side mooring the buoy. This operation is known as the "anchor last" method of buoy deployment,

and is the one favored by NDBC and the USCG under all but the most unusual circumstances.

To recover or swapout the buoy, a tender will haul on the retrieval pennant to the main mooring holding the mooring in the chain stopper on deck. At this point, the existing buoy is disconnected and the new buoy is connected and will ride the existing mooring.

The only moorings which can be recovered at this time are the all-chain moorings. Attempts have been made to recover deep moorings that have exceeded their design life without success. The Coast Guard has had some success in recovering deep-water synthetic moorings using a modified traction winch. NDBC is looking into a similar device to be able to get data back on the condition of the lower moorings on the deep water semitaut and inverse catenary designs.

The design life of the synthetic moorings is 6 years. The all-chain moorings have versions allowing for a 2-year inspection cycle or a 6-year unattended design.

MOORING DEPLOYMENT AND FAILURE EXPERIENCE

Table I shows the summary of NDBC mooring experiences.

Table I

June 1972 - December 1982

Total Moorings Deployed	200
Total Number of Failures	63
Buoys Lost After Failure of Mooring	8*

*Three of these were small buoys in an early experimental stage, and three more were winter ice buoys for the Great Lakes

Table II shows the number of deployments and failures per year.

Table II

	1972 (6 mo)	1973	1974	1975	1976	1977	1978	1979	1980	1981	1982
Deployments	3	12	13	10	15	23	19	18	30	30	27
Failures	0	5	3	5	5	14	9	5	8	4	5*

* Two of these were winter ice buoys

Because of the abnormally high failures occurring in 1977, a mooring workshop was convened in May 1978.¹⁷

The major causes of failures as best determined from the evidence recovered or implied are shown in Table III. Although the category and cause assigned to a given event are somewhat arbitrary and not always the only one, this is the best information available to make a judgment.

Table III

Hardware/Design Error - 25

This includes improperly specified materials, corrosion, overstressed components, mechanical wear, etc., that have been or will be improved by design change or elimination

Operator/Assembly Error - 10

This includes assembly of material difference from that specified, improper assembly of the right materials, and seamanship errors. Most of these occur during operations

Vandalism/Collision - 5

Includes moorings cut by fishing gear, towed objects, theft, and collision with the mooring by ships or boats

Fishbite - 2

Unknown - 16

These were events where no evidence survived the failure, or subsequent events destroyed evidence of the initial failure

It should be noted from the above that in the experience of NDBC, fishbite has been confirmed only twice with one confirmed that did not result in failure and is not listed as a failure. For this reason, moorings are not presently designed to prevent failure from fishbite. A description of the problem is in the references.^{18,19}

SPECIAL MOORINGS

NDBC has long experimented with ways of reducing the relative motion, and thence damage of the electrical conductors, between the relatively inflexible conductors and synthetic line mooring materials. As a result of this experimentation, Kevlar as a composite integrated mooring material woven around the electrical conductors to protect them and be relatively strongly bonded to them, was designed and built by the Naval Ocean Research and Development Activity (NORDA) (Figure 6). The advantages of Kevlar for this application are high strength, low weight, and low stretch. Thus it was expected that the relative motion between mooring and conductors, housed in the same assembly, would be reduced and damage to conductors and sensors would be reduced, if not eliminated. During a test and evaluation (T&E) deployment lasting from September 1980 to May 1981 (see Figure 2 for the mooring design), the major objectives of minimizing sensor failure was achieved, but failures did occur. One that did not cause failure, but should have, was a documented case²⁰ of fishbite at the 280-m level.

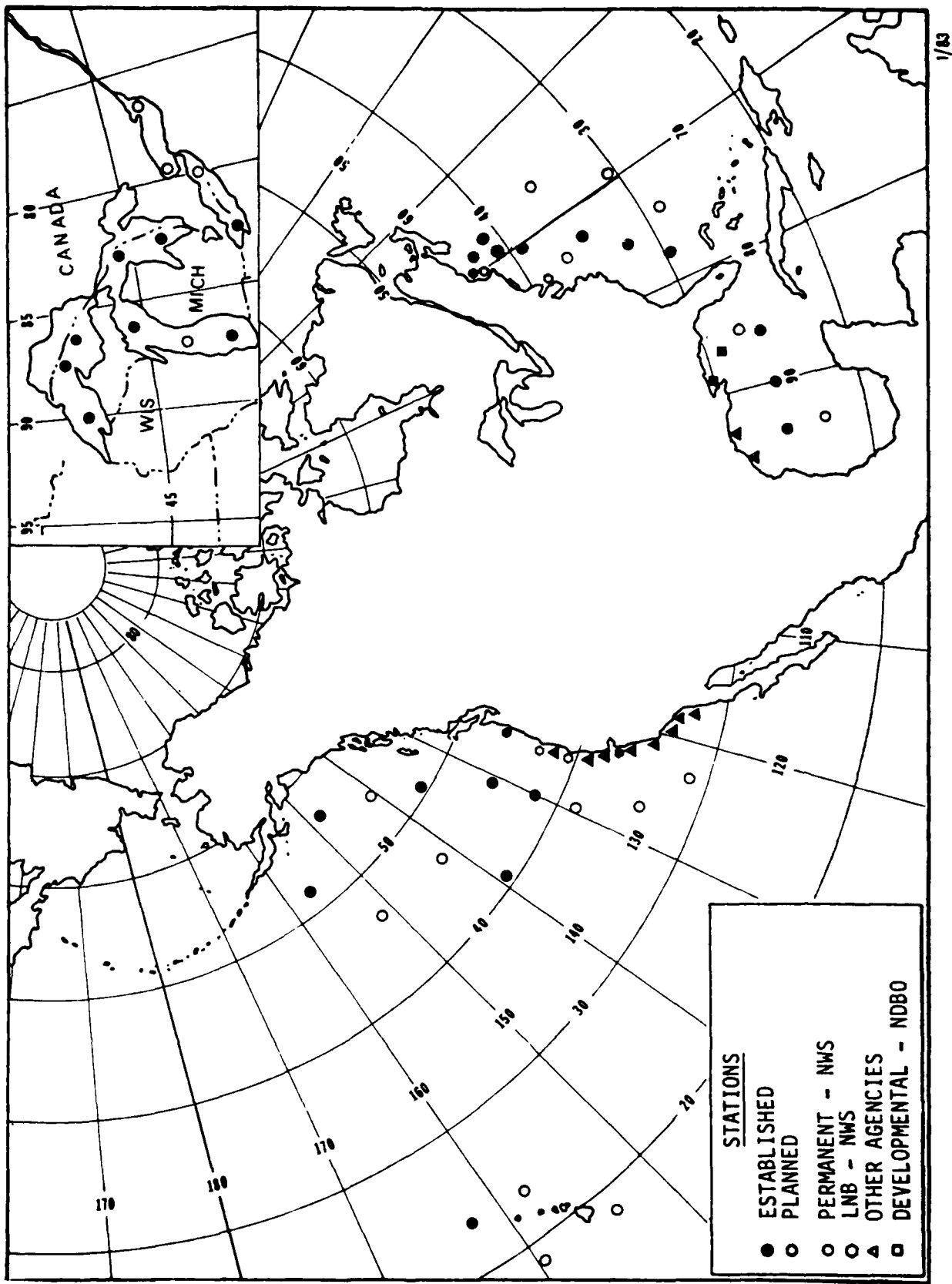
Kevlar lived up to its promise in this prototype. Two more full-scale prototype integrated thermistor-vs-depth mooring lines are being developed for further test and evaluation.

REFERENCES

1. Deverean, R. S. and Feenan D. Jennings, "The Monster Buoy," GeoMarine Technology, April 1966
2. Timpe, G. R., and W. O. Rainnie, Jr., "Development of a Value-Engineered NOMAD Buoy," MTS/IEEE OCEANS '82 Conference Record, pp. 605-609, September 20-22, 1982.
3. Goodman, T. R., P. Kaplan, T. P. Sargent, and J. Bentson, "Static and Dynamic Analysis of a Moored Buoy System," Oceanics, Inc., April 1972.
4. Sargent, T. P., A. Raff, and J. Bentson, "Computer Program Documentation Report, Buoy-Cable Dynamics Program," Oceanics, Inc., April 1972.
5. Kaplan, P., A. Raff, and T. P. Sargent, "Experimental and Analytical Studies of Buoy Hull Motions in Waves," Oceanics, Inc., April 1972.
6. "Modification of the NDBO Hull Mooring Simulation For Use In Shallow Water," Oceanics, Inc., June 1976.
7. Kim, W.D., "On the Forced Oscillations of Shallow-Draft Ships," Journal of Ship Research, Vol. 7, No. 2, October 1963.
8. Newman, J. N., "The Motions of a Spar Buoy in Regular Waves," DTMB Report 1499, May 1963.
9. Goodman, T. R., and Lance, G., "The Numerical Integration of Two-Point Boundary Value Problems," M.T.O.A.C., X, pp. 5482-86, 1956.
10. Godunov, S. K., "On the Numerical Solution of Boundary Problems for Systems of Linear Ordinary Differential Equations," Translated from Uspekhi Matematicheskikh Nauk. May-June, Vol. 16, No. 3 (89) pp. 171-174, 1961, Dept. of Commerce Report 63-10299, 1963.
11. Thompson, R. J., "Improving Round-Off In Runge-Kutta Computations with Gill's Method," Communications of the ACM 13, 12, pp. 739-740, December 1970.
12. Hoffman, Dan, E. S. Geller, and C. S. Niedermann, "Application of Mathematical Simulation and Model Tests to the Design of Data Buoys as Ocean Platform," SNAME Annual Meeting, 1973.
13. Walden, R. G., et al, "The Mooring Dynamics Experiment - A Major Study of the Dynamics of Buoys in the Deep Ocean," Offshore Technology Conference, 1977.
14. Shams, et al, "Evaluation of Programs NDBO and CABMOD Using Data From Experiments 1 and 3 of the Mooring Dynamics Experiment," Chi Associated, Inc., October 1981.

15. Nath, J. H., "Laboratory Validation of Numerical Model, Drifting Buoy-Tether-Drogue System," Developed for NDBO, 1977.
16. Anonymous, "NOAA Data Buoy Office Field Service Manual," NDBO F-444-1, Rev. A, June 1981.
17. Anonymous, "NDBO Buoy Mooring Workshop Report," NDBO F-320-2, September 1978.
18. Prindle, Bryce and Robert G. Walden, "Deep-Sea Lines Fishbit Manual," NOAA Data Buoy Office Report, 1976.
19. Prindle, Bryce, "Factors Correlated With Incidence of Fishbite on Deep-Sea Mooring Lines," WH01-81-57, June 1981.
20. Beacht, W. L., and B. F. Case, "Integrated Tz Line Test and Evaluation Final Report," NDBO Report No. F-342-1, April 30, 1982 (unpublished report).

NDBC BUOY LOCATIONS



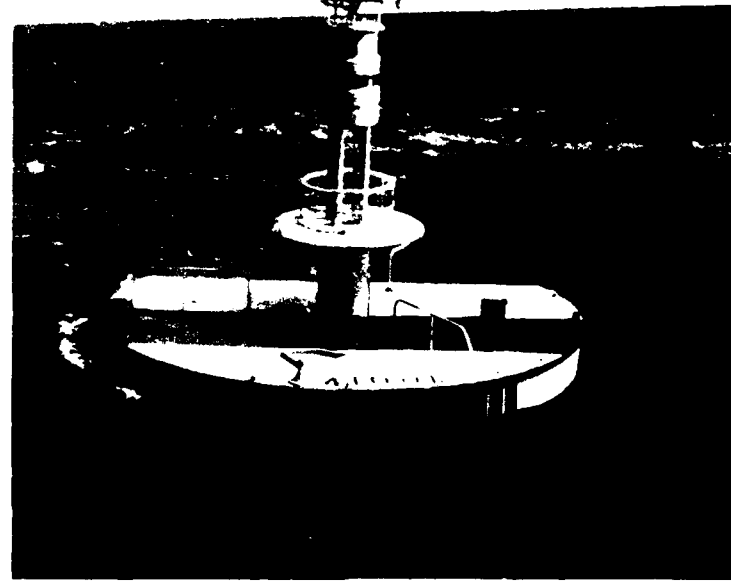


Figure 2. 100 ton discus buoy.

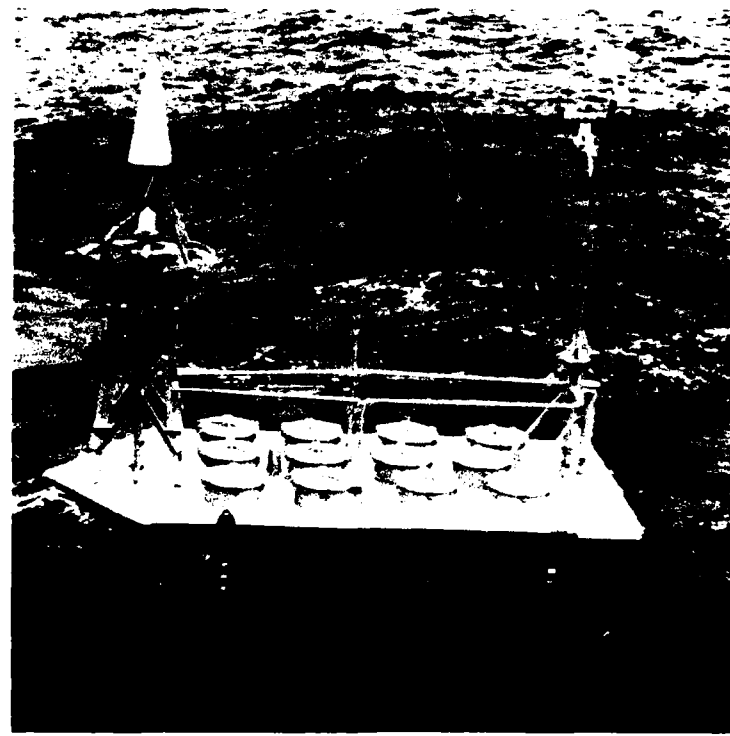
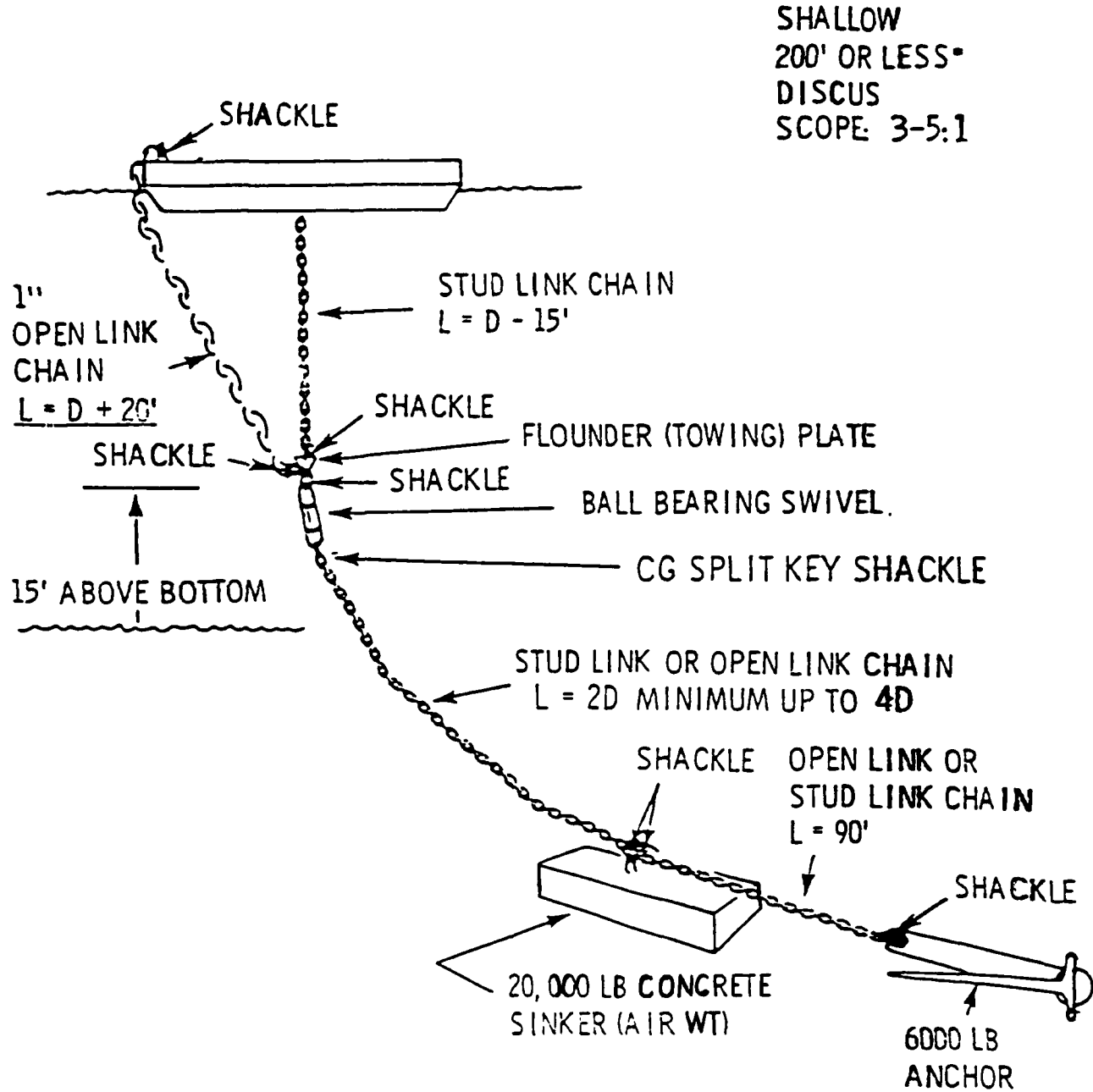


Figure 3. NOMAD data buoy configuration.

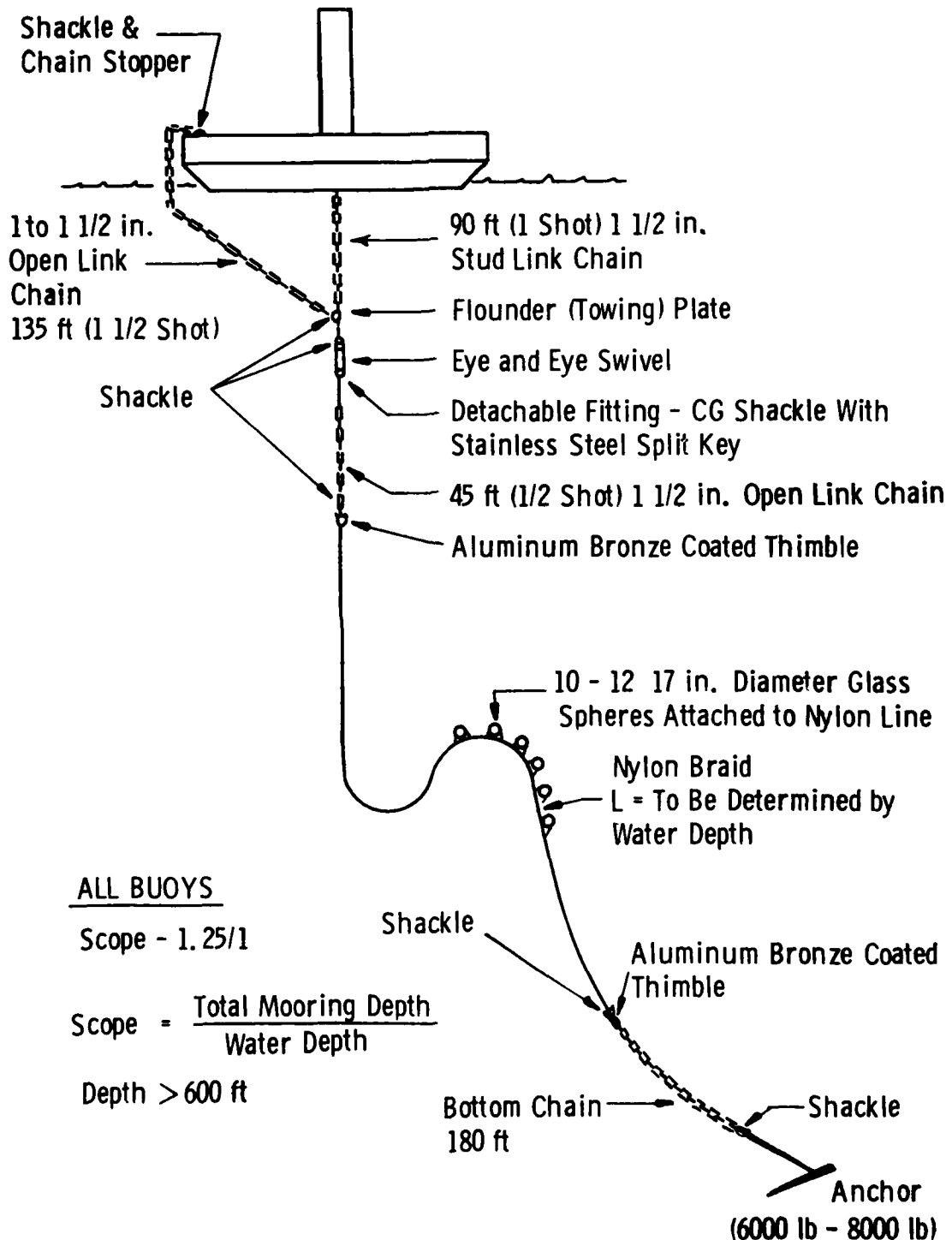
SHALLOW WATER MOORING FOR DISCUS BUOYS

NOMADS ARE SIMILAR

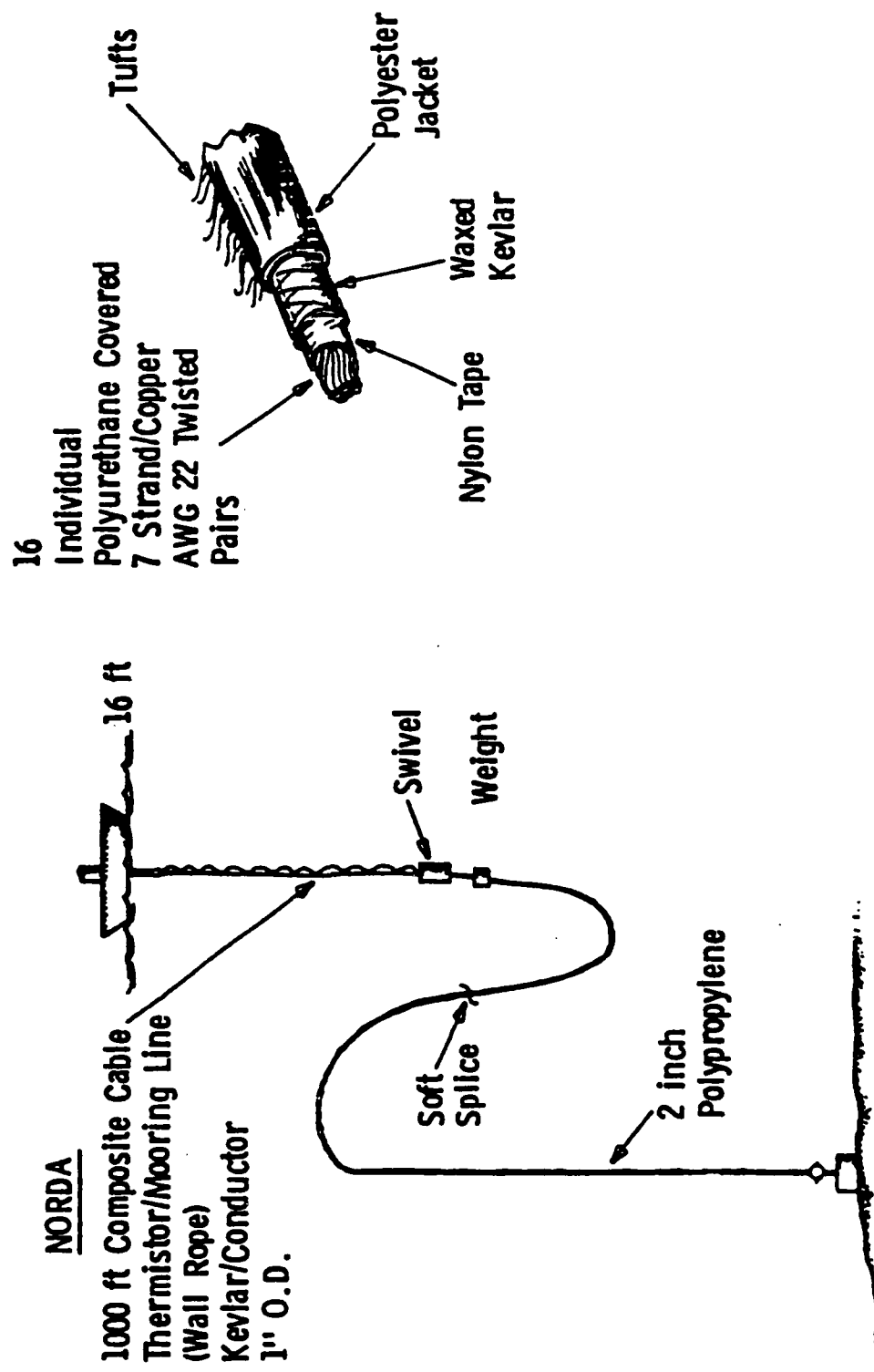


NOTE: FOR DEPTH BETWEEN 200 AND 600 FT, A SEGMENT OF NYLON WILL
USUALLY BE INCLUDED BELOW THE SWIVEL.

NDBC INVERSE CATENARY DEEP WATER MOORING FOR DISCUS AND NOMAD BUOYS



INTEGRATED MOORING LINE/THERMISTOR LINE TEST CONFIGURATION



FULL SCALE MEASUREMENTS, MODEL TESTS AND THE PREDICTION OF DYNAMIC RESPONSE

J. KIM VANDIVER
MASSACHUSETTS INSTITUTE OF TECHNOLOGY
JANUARY 10, 1983

INTRODUCTION

The ability to predict dynamic response is a key element in the design of fixed and floating offshore structures. The key components of most response prediction methods include:

1. A structural idealization utilizing analytic or numerical models.
2. A description of the expected environment.
3. Models of the excitation and the structure-environment interaction problems.

The role of scale model tests and full scale measurement programs can be viewed as the means by which the engineer can validate or improve his understanding of the three components given above. The discussion to follow uses these major elements of the response prediction problem as a framework on which to base a review of the state of the art of measurement and model testing. Response of large structures such as fixed platforms and TLP's is discussed as well as the response of long flexible cylinders to flow-induced vibration.

THE VERIFICATION OF STRUCTURAL IDEALIZATIONS USED IN DESIGN

Finite element models are frequently used. Except in special cases, such as in the post-elastic design of earthquake resistant structures most structural models are linear and well behaved. However, there are numerous sources of error in the models, with notable ones including the soil stiffness and joint flexibility. The accuracy of the dynamic properties of the models also depends on the accurate accounting of the structural mass. Non-loading bearing contributions to the total mass, such as equipment, marine growth, and expendable materials lead to frequent discrepancies between predicted and observed natural frequencies. Small errors in predicted natural frequencies can have rather severe consequences on expected fatigue life.

Measurements made on full scale structures are very useful in the validation of the structural model. The most commonly measured structural parameters on fixed offshore structures are the natural periods and damping ratios of the lowest bending modes. For structures deeper than 300 feet the natural periods commonly exceed two seconds and may be as high as five seconds

for structures in water 1000 feet deep. Such structures may have substantial dynamic response in commonly occurring low sea states, resulting in high cycle, low stress fatigue. The response at these long natural periods is also dependent on the modal damping ratio, which is very low for most structures. The accuracy of the prediction of fatigue life is for some structures dramatically dependent upon the accuracy of the prediction of the natural period and to a substantial, but lesser degree, on the estimated damping. Reference 1 shows that the rate of fatigue damage due to dynamic response at a structural natural period increases approximately as the estimated natural period raised to the 18th power, and varies inversely with the square of the damping ratio.

Lowest natural periods in bending for fixed jacket structures are commonly predicted to within 10% of the measured installed values. For structures whose fatigue is controlled by their resonant dynamic response, a 10% error in predicted natural period may result in a factor of six error in the estimated fatigue life.

Full scale measurement programs over the last eight years have led to a much improved understanding of the the dynamic properties of fixed jacket structures. References 2,3 and 4 were of particular value in addressing problems related to damping and natural frequency estimation. The natural periods and damping ratios for TLP'S and guyed towers are not so well understood, because data from full scale structures have as yet to be obtained. However accurate placement of several natural periods of both structural types is significant in their design. The TLP is intended to have natural periods in surge and sway on the order of one to two minutes and heave,pitch and roll periods in the range of two to four seconds. For these modes the natural periods are reasonably easy to predict. However, the damping ratios are not. Some insights may be gained from scale model tests and will be discussed later.

The guyed tower also has very long surge and sway periods, out of the range of linear wave excitation. However, such structures may have first bending modes of the frame which can be excited by waves. An oil production guyed tower for 1000 feet of water will have a first natural period in bending of approximately four to six seconds. With the natural period falling in the range of significant wave energy, the damping ratio of this mode must be accurately estimated. At this point in time damping ratios of such modes are not well understood. The damping will depend on current, sway motion and sea state. Due to lack of Reynold's scaling such damping can not be measured in small scale model tests. There is some recent evidence of fatigue failures due to bending of long articulated column loading facilities. First mode bending of such columns is very similar to that of guyed towers. To the author's knowledge no measurements of the damping ratios of such structures have been made, though to have them would be very helpful.

To this point no mention has been made of the accuracy of full scale measurements of natural periods and damping ratios. With modern spectral analysis techniques it is quite simple to obtain very accurate estimates of structural natural periods from time histories of deck acceleration. Unfortunately, this is not so true of damping estimates. Damping measurements are generally made in one of the following three ways: forced vibration tests, transient decay tests, and spectral analysis of ambient vibration response to environmental excitation. Each method has disadvantages. Some aspects of these are discussed in references 2,3, and 4. The damping on offshore structures is dependent both on response amplitude as well as seastate and current. Damping is amplitude dependent, primarily because of the non-linear behavior of the foundation. It is seastate and current dependent, because the viscous hydrodynamic sources of damping depend upon relative water particle velocity. Both forced vibration and snap back decay tests produce unrealistic response behavior and therefore result in damping estimates which are not necessarily characteristic of the structure. On the other hand, damping measurements made under ambient response equilibrium conditions are often frustrated by serious estimation errors in the spectral analysis.

Integrity Monitoring

Integrity monitoring has been an elusive goal of those in the full scale response measurement community. The goal is to detect damage on a structure by the measurement of changes in the dynamic properties of the structure, such as natural periods, damping ratios, or mode shapes. References 5,6,7 and 8 are typical of the literature in this area. The principal problem with most techniques is the lack of discrimination between failure and non-failure related sources of change in the vibration signature. For example, a change in the amount of fluid in a storage tank may have the same effect on the dynamic response parameter, being measured, as the failure of a member.

Several years ago the author made dynamic response measurements on the four Air Combat Maneuvering Range platforms located near Cape Hatteras (Figures 1 and 2). The measurements were made to confirm that the dynamic properties of the installed structures were acceptably close to the design goals. The measurements were also part of a research program then underway at MIT on the development of better spectral analysis tools for dynamic response analysis. Two sets of measurements were made. The first was in October of 1977, a few months after installation. The second was in August of 1980. Table 1 shows a comparison between the two measurements for the North, East, and West structures. The South structure was not measured in 1977. One remarkable change occurred. The fundamental or lowest natural frequencies in bending (those with the longest natural period) on the West platform in 81 feet of water (1977) changed

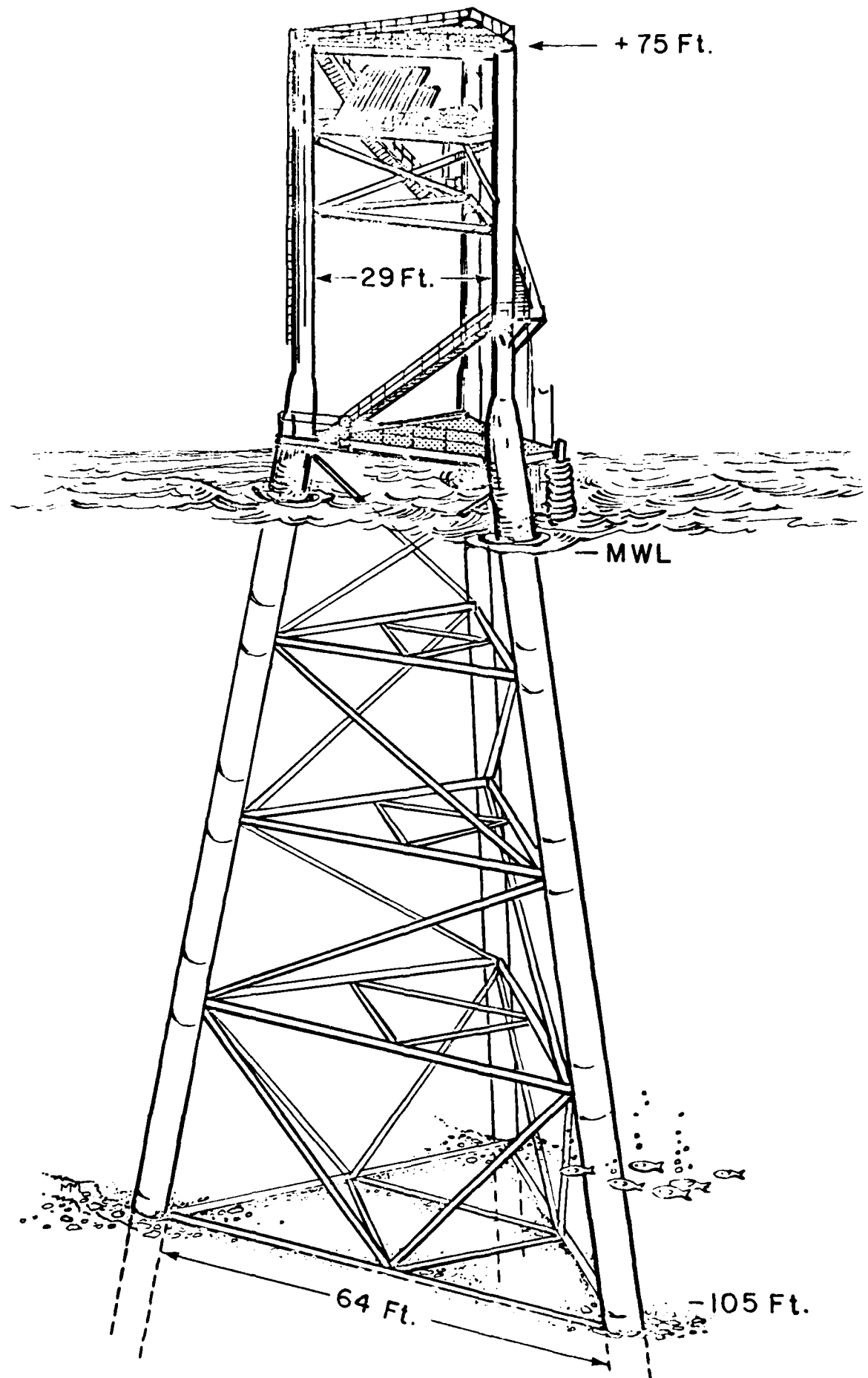


Figure 1. The ACMR East platform

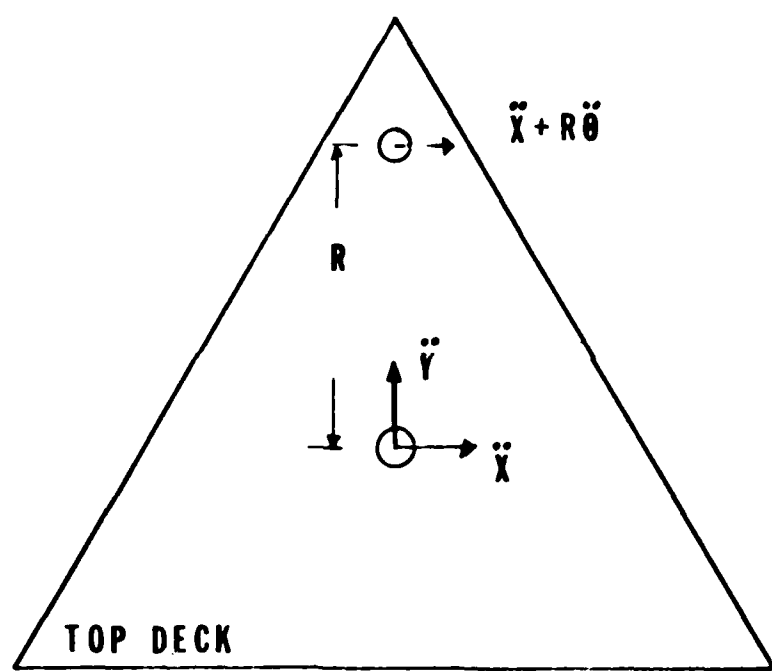


FIGURE 2. ACMR ACCELEROMETER PLACEMENT

dramatically in the three years between the measurements. A 10% reduction was measured. It is the author's opinion that the change is due to scouring of the foundation. The structure is located on a constantly shifting sandy bottom, which is occasionally exposed to the influence of the Gulf Stream. Note that the two lowest modes, representing vibration in orthogonal directions, are equally affected. This happens when the deck mass is known to have changed substantially, or when there is a change in the foundation conditions. In this case the deck mass was not changed. A similar shift in the lowest natural period was observed on the Union Oil Monopod structure in Cook Inlet, Alaska. That structure experienced a 15% reduction in the fundamental natural frequency of the structure. That too was attributed to a change in the foundation conditions, Reference 9. The second and third order modes on the ACMR platforms all show decreases in natural frequencies. This is probably due to marine growth and changes in foundations.

These experiences indicate that vibration measurements on full scale structures may be of use in assessing the condition of the foundations of structures such as TLP's, for which the condition of the foundation is critical to safety.

Recent progress has been made in the technology of integrity monitoring. Sheldon Rubin of Aerospace Corporation has proposed a new technique called 'flexibility monitoring'. The technique measures the flexibility of each vertical bay of a structure, relative to all of the other bays. Damage in one bay will reveal itself as a large change in flexibility of that bay, when compared to the undamaged baseline measurements. This technique requires accelerometers to be placed at the top and bottom of each bay while it is being tested. This may be accomplished by moveable accelerometers in chutes attached to the legs of the structure. This method will be presented in a paper at the 1983 Offshore Technology Conference, Reference 10.

ENVIRONMENTAL MEASUREMENTS

The second element required in the response prediction process is an adequate description of the expected environment. The desired data includes wind, current, and directional wave spectra. For the selection of worst case survival conditions to be met in the design, it is also necessary to know as much as possible about the extremal statistics for each of the environmental parameters of interest. To some degree it is possible to measure wind, waves and currents in most locations. Two measurements which will become increasingly important are current profiles in deep water and directional wave spectra. Current profiles will become increasingly important as longer tethers and mooring lines come into use and the prediction of drag forces becomes more critical. Near surface currents are especially difficult to measure in deep water, and yet they are very important in survival conditions and for structures expected to survive in high current conditions such as the Gulf Stream.

Table 1
Measured Natural Frequencies for the ACMR Platforms in Hz.

	f_{1x}	f_{1y}	$f_{1\theta}$	f_{2x}	f_{2y}	$f_{2\theta}$
West Platform (81 feet deep)						
1977 (Hz)	2.40	2.40	2.64	3.12	3.50	3.61
1980 (Hz)	2.17	2.19	2.26	3.37	3.22	3.23
$\Delta f (\%)$	-9.6	-8.8	-14.4	-6.9	-8.0	-10.5
North (93 feet deep)						
1977 (Hz)	2.39	2.43	2.69	3.54	3.57	3.59
1980 (Hz)	2.39	2.37	2.59	3.53	3.38	3.39
$\Delta f (\%)$	0	-2.1	-3.7	-1.7	-5.3	-5.6
East (105 feet deep)						
1977 (Hz)	2.19	2.28	2.48	3.48	3.44	5.39
1980 (Hz)	2.18	2.19	2.39	3.35	3.15	3.34
$\Delta f (\%)$	-.5	-3.9	-3.6	-3.7	-8.4	-1.5
South (105 feet deep)						
1977 (Hz)	Not tested due to weather					
1980 (Hz)	2.15	2.13		3.24	3.18	

Directional spectra measurements become increasingly important as fatigue problems become more severe. In the past large factors of safety were used to overcome ignorance of the environment. This was economically acceptable in shallow water. In deep water this practice must be replaced by a more and more refined understanding of the environment. Directional spreading must be taken into account to more realistically model the excitation processes. The use of unidirectional waves gives unrealistically high loads. The dynamic response of structures such as TLP'S is sensitive to directional spreading of the seas. Examples are presented in the next section.

MODELLING THE INTERACTION BETWEEN THE STRUCTURE AND THE ENVIRONMENT

The most difficult portion of the response prediction problem is the modelling of the interaction between the structure and the wind, waves, and current. Many features of the process are very complex, sometimes non-linear, and cannot yet be modelled reliably by numerical techniques. Scale model tests can resolve many problems, and sometimes reveal unexpected ones that would be disastrous to the full scale structure.

Full scale measurement programs are very important in the verification of the numerical calculations and the small scale model tests. In small scale model tests numerous assumptions have to be made, and the validity of these assumptions must be evaluated on the full scale structure. The remainder of this discussion focusses on a variety of topics which are relevant to predicting the performance of structures such as TLP's, guyed towers, and deepwater platforms. They include damping, wave spreading, and vortex shedding. Each of these present problems in response prediction and reflect many uncertainties in the present state of the art.

Wave Spreading

Dynamic response is known to be influenced by wave spreading. For structures excited by linear wave forces, such as a large TLP in low to moderate seas the influence of wave spreading on, for example, the pitch response of the structure can be expressed analytically. In Reference 10 the dynamic response energy of the pitch mode of a TLP is shown to be given by the following expression, which is equally applicable to other modes responding dynamically at structural natural frequencies.

$$E = C \frac{4 \rho g^3}{5 \omega_o^3} S_\eta(\omega_o) \frac{R_{RAD}(\omega_o)}{R_T(\omega_o)} \quad (1)$$

$R_{RAD}(\omega_o)$: wave radiation damping

$R_T(\omega_o)$: total damping

ρ : density of water

g : acceleration of gravity

ω_o : natural frequency

$S_\eta(\omega_o)$: wave amplitude spectrum

The factor C in the equation is dependent upon the wave amplitude to modal wave force or moment transfer function, of the structure and the directional spreading properties of the sea. In general such transfer functions are difficult to compute and require many approximations. However, it may be measured directly on a scale model held fixed in place by load cells. The results of such a model test are presented in Reference 11, and reviewed briefly here.

A 1 to 50 scale model, borrowed from Shell Oil Company, was attached to a rigid bridge spanning a towing tank, Figure 3. The attachment was via five load cells, three vertical and two horizontal. With these load cells the heave, pitch, roll, surge and sway rigid body forces and moments were measured. The heading of the model could be changed in 5 degree increments.

Measurements were made at headings from 0 to 45° and at seven wave periods corresponding to prototype wave periods of 4.7 to 14.1 seconds. Figure 4 is an example of the measured surge force and pitch moment transfer functions measured on the model for 10.5 second regular waves. The results as given are scaled up to prototype values. The dashed lines are numerical predictions made by a Shell Oil Company computer program.

These measured transfer functions may be used in either numerical or analytical computations of dynamic response. The factor C from equation 1 is shown to be given by

$$C = \frac{\frac{2\pi}{0} \int R^2(\theta) D(\theta) d\theta}{\frac{2\pi}{0} \int R^2(\theta) D\theta} \quad (2)$$

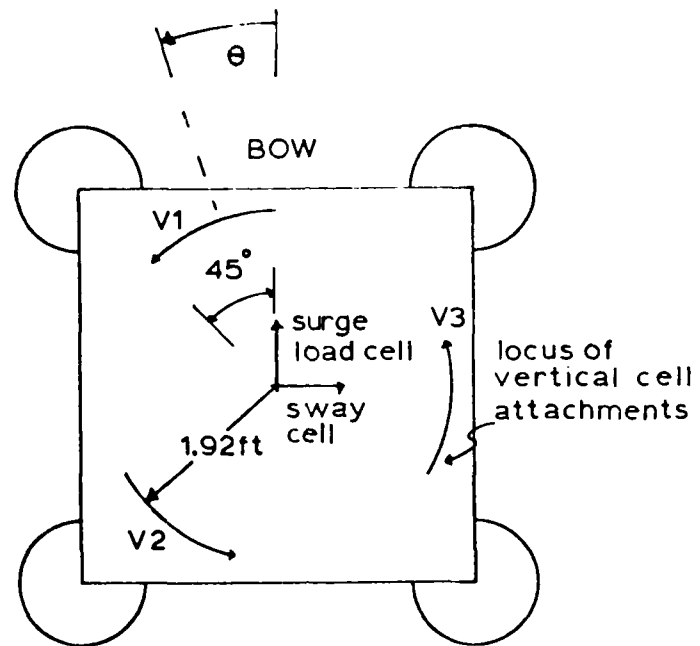


FIGURE 3. DECK ATTACHMENT POINTS FOR LOAD CELLS

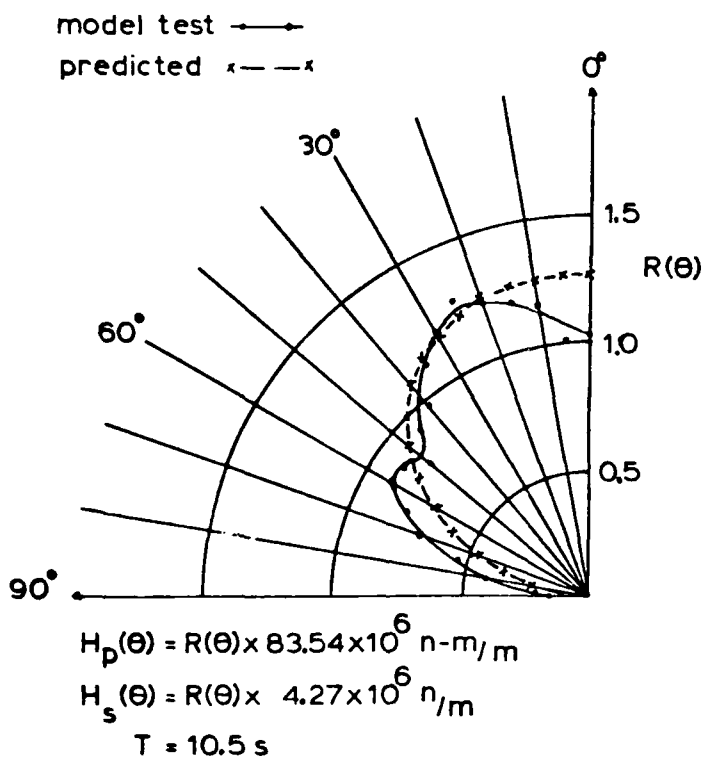


FIGURE 4. SURGE FORCE & PITCH MOMENT PER METER WAVE AMPLITUDE

where $D(\theta)$ is the spreading function of the directional wave spectrum and $R(\theta)$ is to within a scale factor the measured transfer function, such as is presented in Figure 4. It is shown in the paper (11) by way of an example that the energy of the pitch response of the TLP at a 6.25 second natural period is reduced by 39% in cosine squared directionally spread seas, compared to unidirectional head seas.

In addition to permitting a direct calculation of the effects of wave spreading on the dynamic response of a structural mode, such model test results in conjunction with Iaskind's relation can be used to calculate directly the radiation damping associated with a particular motion, such as pitch. An example computation is presented in Reference 11. The TLP has been used to demonstrate the usefulness of direct wave force measurements on models. The technique is applicable to a variety of structures. The theory behind the method is discussed in Reference 12.

The supporting theoretical work is restricted to linear wave forces. However, it is the author's opinion that the measurement of wave forces on a model held fixed in place may be equally useful for determining the variation of modal wave force with incidence angle even when non-linear wave force mechanisms are important. In particular, finite wave height affects and drag forces will be sensitive to incidence angle and can be measured directly. On any Froude scaled model, dynamic or fixed, Reynold's number discrepancies must be expected and accounted for.

The final aspect of wave spreading to be addressed here is on the mathematical formulations themselves. Several have been used in the past, including the cosine to $2n$ power model, and the circular normal. Recently a new model has been proposed which is a continuous function of a single spreading parameter, and automatically normalizes to 1.0 when integrated over all angles of incidence. Its versatility and simplicity make it very attractive.

The Elliptical Spreading Model

If at each frequency of interest a directionally spread sea is given as a product of a point wave spectrum and a spreading function, then

$$S_n(\omega, \theta) = S_n(\omega) D(\theta - \theta_o)$$

where $D(\theta - \theta_o)$ is a function which describes the directional distribution of the wave energy about some mean angle θ_o . The elliptical spreading model is given by

$$D(\theta - \theta_o) = \frac{\sqrt{1-e^2}}{2\pi(1-e \cos(\theta - \theta_o))} \quad (3)$$

In polar coordinates $D(\theta - \theta_0)$ describes a family of ellipses based on the eccentricity parameter e . One focus of the ellipse lies on the origin of the coordinate system and the other focus lies along the direction θ_0 . The eccentricity, e , can take on any value between zero and one. Zero corresponds to a completely diffuse sea with equal amplitudes of waves propagating in all directions. One corresponds to unidirectional seas from $\theta = \theta_0$.

Dynamic Scale Model Tests

Fixed model tests are valuable in determining the directional properties of the wave force transfer functions. However, dynamic models have a useful role as well, as demonstrated by model tests of the Hutton TLP, which is currently under construction. It underwent extensive model testing at NMI in the United Kingdom. These model tests were fully dynamic in that they modelled the natural resonances of the TLP in heave, pitch, roll, surge, sway, and yaw. In survival seas the model revealed one completely unanticipated form of response. The passage of large, very long period, head waves excited the pitch mode at its natural frequency, which in full scale is approximately two seconds. The problem was alleviated by rounding off the corners of the pontoons. A non-linear process which is not yet completely understood was responsible for this response. The early detection of this problem was a good example of the value of dynamic scale model testing.

A serious limitation of fully dynamic tests is that they often require that the water depth be modelled. This often results in unacceptably small models. When models are Froude scaled, the Reynolds number scaling problems result in unscalable viscous damping losses. If the dynamically amplified response at a natural period is important, then errors in damping may make it impossible to scale up the results.

Damping

Damping must be considered in the prediction of dynamic response of all deepwater designs. Response at natural frequencies is controlled by damping. Damping comes from many sources and each must be understood. Most sources are non-linear and many are not adequately modelled with scale models. One component which does scale and is basically linear in behavior is wave radiation damping. However, its role in the response prediction problem is frequently the least well understood.

The following discussion of damping will use the example of the dynamic response prediction of a simple vertical pile or caisson to illustrate the prediction problem.

Radiation Damping

The prediction of response at structural natural periods is especially difficult because it requires accurate wave force models, and accurate structural models, as well as precise estimates of damping. In finite element models, each of these issues is treated separately and direct relationships between, for example, exciting forces and damping mechanisms are frequently ignored. The most important of these relationships is between linear wave force mechanisms and wave radiation damping. By the use of Haskind's relation the modal wave force spectrum at the natural frequency of interest may be expressed in terms of the wave radiation damping coefficient of that mode.

This substitution leads to equation 1, presented in the section on wave spreading.

$$E = C \frac{4\pi\rho g^3}{5\omega_0^3} S_\eta(\omega_0) \frac{R_{RAD}(\omega_0)}{R_T(\omega_0)}$$

This is an expression for the energy of response of a resonant structural mode excited by linear wave forces, arising from a directionally spread random sea. This prediction accounts for the energy in the response spectrum, which is within the dynamically amplified peak centered on the natural frequency. This equation reveals the remarkable and frequently misunderstood role that radiation damping plays in determining response. The response energy is proportional to the ratio of the wave radiation damping to the total damping. It is generally and incorrectly assumed that any increase in damping will result in decreased response. In the case of radiation damping the reverse is true. A structural change which results in increased radiation damping also results in increased exciting forces, which result in increased dynamic response.

This equation accounts for linear wave exciting forces. In particular, drag exciting forces are not included. However all sources of damping are accounted for, including viscous hydrodynamic losses, by the use of a linear equivalent total modal damping (Reference 12).

A field experiment validating this response prediction technique was conducted in March of 1980 and presented at the 1982 Offshore Technology Conference (13). The structure was a free standing caisson, depicted in Figure 5. It stands in 90 feet of water at a site in the Gulf of Mexico. The structure is four feet in diameter in the wave zone and 7 feet at the base. It supports a single gas well. The helicopter deck is 76 feet above the water line. The dynamic response is dominated by resonant motion at a natural period in bending of 3.1 seconds.

The paper assesses the damping contributed by each of the following components: hydrodynamic viscous, wave radiation, soils, and structural hysteretic.

The total structural damping was estimated from field data by spectral techniques. The ratio of the analytically computed radiation damping to the measured total damping was used in a prediction of the mean square acceleration response of the structure in a directionally spread random sea. Table 2 presents a summary of the results. The 95% confidence bounds on the predicted response reflect the error introduced by the measurement of the total damping values. On the whole, the comparison between predicted and measured response are very good.

Table 2

Comparison of Predicted and Measured Helicopter Deck Acceleration Response

Date Recorded	3/25/80	3/28/80
Natural frequency f_o (Hz)	.323	.323
Measured Wave Spectrum at ₂ the Natural Frequency (ft ² /Hz)	1.2	0.7
$E_{RAD}(f_o)$ predicted (%)	.11	.11
$E_{TOTAL}(f_o)$ measured (%)	$1.0 \pm .4$	$.9 \pm .2$
E_{RAD}/E_T	.110	.122
σ^2 Predicted (ft ² /sec ⁴)	1.09	.71
(95% bounds on σ^2)	(.78-1.82)	(.58-.91)
σ^2 Measured (ft ² /sec ⁴)	.91	.72

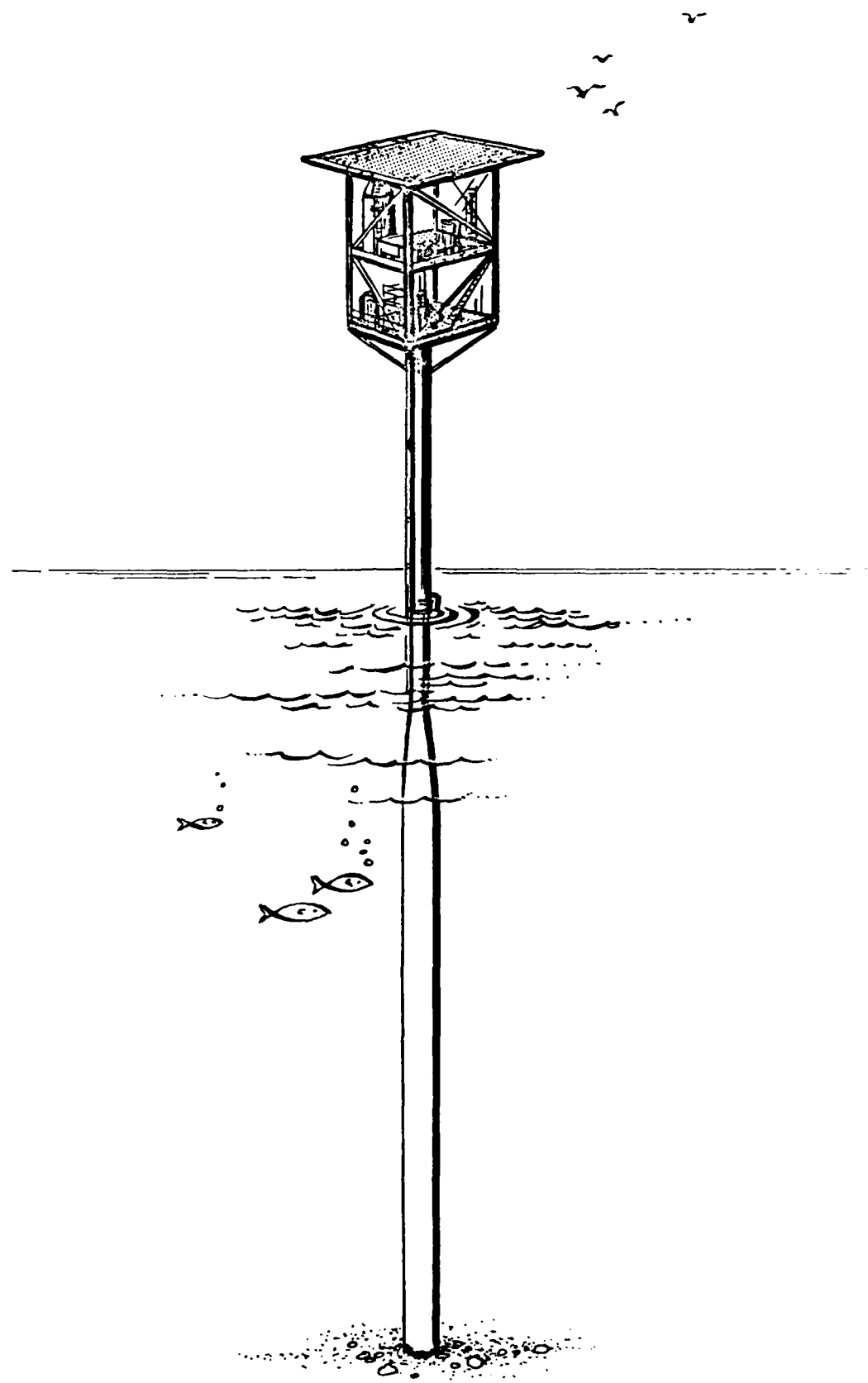


Figure 5. The Caisson Platform in 89 Feet of Water

The total damping for the response data shown in Table for 3/25/80 breaks down in the following way.

Wave Radiation	0.11%
Hydrodynamic Viscous	0.17%
Structural Hysteretic	0.24%
Soil Damping	<u>0.48%</u>
Total Modal Damping	1.0%

The wave radiation component was computed analytically. The steel hysteretic component was estimated from experience with steel structures in air.

The soils component accounts for one half the total damping. Present state of the art in soil dynamics makes it impossible to predict accurately. This value was arrived at by estimating the other components and subtracting them from the measured total damping. However, this value corresponds to a specific soil damping of 3%. A specific damping of .03 when multiplied by 4p is the fraction of soil strain energy lost per cycle. This value is consistent with current wisdom in soils engineering. Radiation damping in the soil for this structure was negligible.

The hydrodynamic viscous damping was predicted by a technique described by Dunwoody (Ref. 14). The method accounts for the relative motion between the structure and the fluid in random waves, but no current. The viscous losses are dependent on non-linear drag forces and therefore are sea state dependent. As the sea state increases so too does the damping. Dunwoody describes the results of an elegantly simple model test, which demonstrates the increase of damping with sea state. He also presents a non-linear stochastic, dynamic response prediction method for the case that drag exciting forces cannot be neglected. His approach is especially appropriate to dynamically amplified response at a natural frequency.

Sea state dependent damping has not been demonstrated on a full-scale structure. Hence the data is not yet available to compare to predictive models. A joint industry sponsored project is currently in progress.

A caisson in 175 feet of water has been instrumented with an automatic data telemetry system which transmits wind, wave, and acceleration data in all weather conditions. The measurement of damping as a function of sea state is one of the objectives of the experiment. The caisson is operated by MOBIL and the project is being conducted by the W.S. Atkins U.S. office in Houston.

The Dunwoody method for computing sea state dependent viscous damping cannot account for the presence of current. One technique which may be appropriate is stochastic linearization. This method has been described by Ghosh for calculating viscous hydrodynamic damping in the presence of a current and will be

used in comparisons with the W.S. Atkins caisson data (15).

THE FLOW INDUCED VIBRATION OF LONG FLEXIBLE CYLINDERS

There are numerous structures which involve the use of long flexible cylinders subject to flow induced vibration. Mooring lines, TLP tethers, and marine risers are examples. There are several documented examples where structural failure resulted from such vibration. A recent example is the loss of a 24 inch diameter casing during deployment in 1200 feet of water in a 3-knot surface current (16). There are several examples of problems with casing deployed from jack up rigs.

In some cases the vibration is directly responsible for failure. In other situations, the high drag that results from the vibration results in unacceptable performance.

Many scaling problems are encountered in laboratory attempts to model full scale systems. Full scale tests do not allow control of key experimental variables. Intermediate scale experiments in the ocean provide a useful stepping stone to understanding the full scale phenomena.

In the summer of 1981 a field experiment on the vortex excited vibration of long cylinders was conducted near Castine, Maine. The research was jointly sponsored by USGS, the Naval Civil Engineering Laboratory, and seven companies: The American Bureau of Shipping, Brown and Root, Chevron Oil Field Research, Conoco, Exxon Production Research, Shell Development Company, and Union Oil Company.

The test site was a sand bar which is exposed at low tide and covered by approximately ten feet of water at high tide. The test cylinders were 75 feet in length and were tensioned horizontally a few feet above the bar, between steel pilings. A schematic diagram of the test site is shown in Figure 6. Total drag force, tension, and current were recorded. The vibration response was monitored by seven biaxial pairs of accelerometers spaced throughout the test cable which was 1.25 inches in diameter. The vibration response of this cable to vortex shedding was measured in some tests, as was the vibration response of a steel pipe 1.625 inches in diameter with the cable fixed inside for others. An umbilical cable connected the site to the R/V Edgerton which was moored 100 yards away. Both digital and analog recording equipment were used.

The data was taken on the rising tide which exposed the test cylinder to currents up to 2.5 feet per second normal to the axis of the cylinder. The experiment lasted six weeks and a large variety of high quality data was obtained. A few sample results are presented here. A more extensive description of the experiment may be found in Reference 17 and more experimental data will be presented at the 1983 OTC (18).

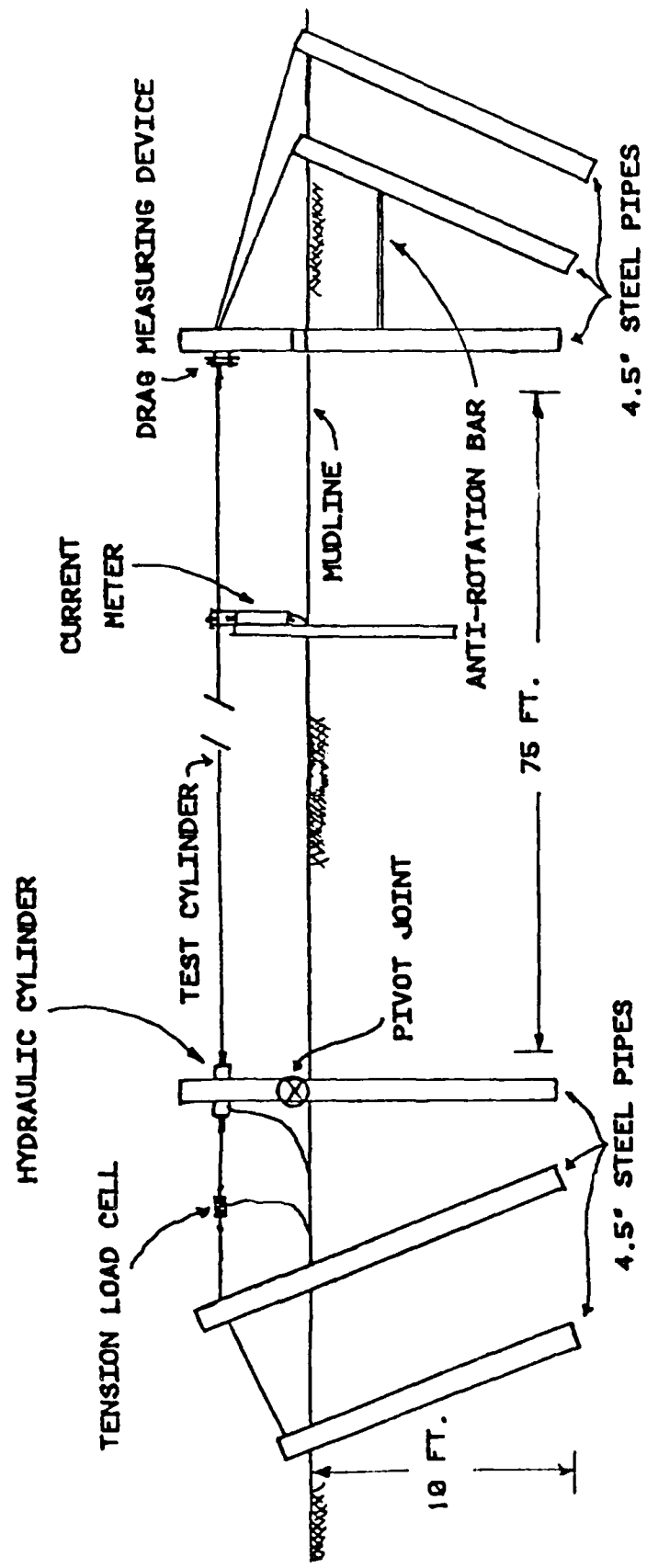


FIGURE 6 . SCHEMATIC DIAGRAM OF THE EXPERIMENT TEST SECTION

Figure 7 is a sample displacement time history observed at the midspan of the pipe. The flow velocity at the time was such that the natural frequency of the third mode in the cross flow direction coincided with the vortex shedding frequency, resulting in the synchronization of the vortices and the cross flow vibration in a phenomenon known as lockin. In this figure, the cross flow vibration is plotted vertically.

The inline, or horizontal, vibration was driven by fluctuating drag forces which occurred at twice the frequency of the lift forces. In this case, the natural frequency of the fifth mode of the pipe was resonant with the drag exciting forces. The resulting motion describes figure eights at the midspan of the cylinder, where both the third and fifth modes have points of maximum response.

Some of the most immediately useful results of the experiment were the measured drag coefficients for the cable and the pipe. Figure 8 summarizes the current, drag coefficient, and response data for a complete 2 1/2 hour data acquisition period for the pipe. In this figure are presented the current in feet per second, the cross flow (vertical) and in-line (horizontal) RMS response amplitudes in inches, and the mean drag coefficient. The RMS displacements are as measured at one location, 1/6 of the length from one of the ends. The drag coefficients are typically 2.5 to 3.0 and correlate very well to the cross flow vibration amplitudes. The rigid cylinder drag coefficient at the same Reynolds number would be approximately 1.2. Plateaus of high C_D are regions when cross flow lockin occurred. These values of C_D are substantially higher than generally used in present design practice.

The most pressing experimental problem is the accurate description and characterization of the vibration response of long flexible cylinders in a shear flow. It is not presently possible to predict the response spectrum of a cylinder in a shear, nor is it possible to predict the drag coefficient associated with the vibration. Experiments of this type are presently being discussed in many circles.

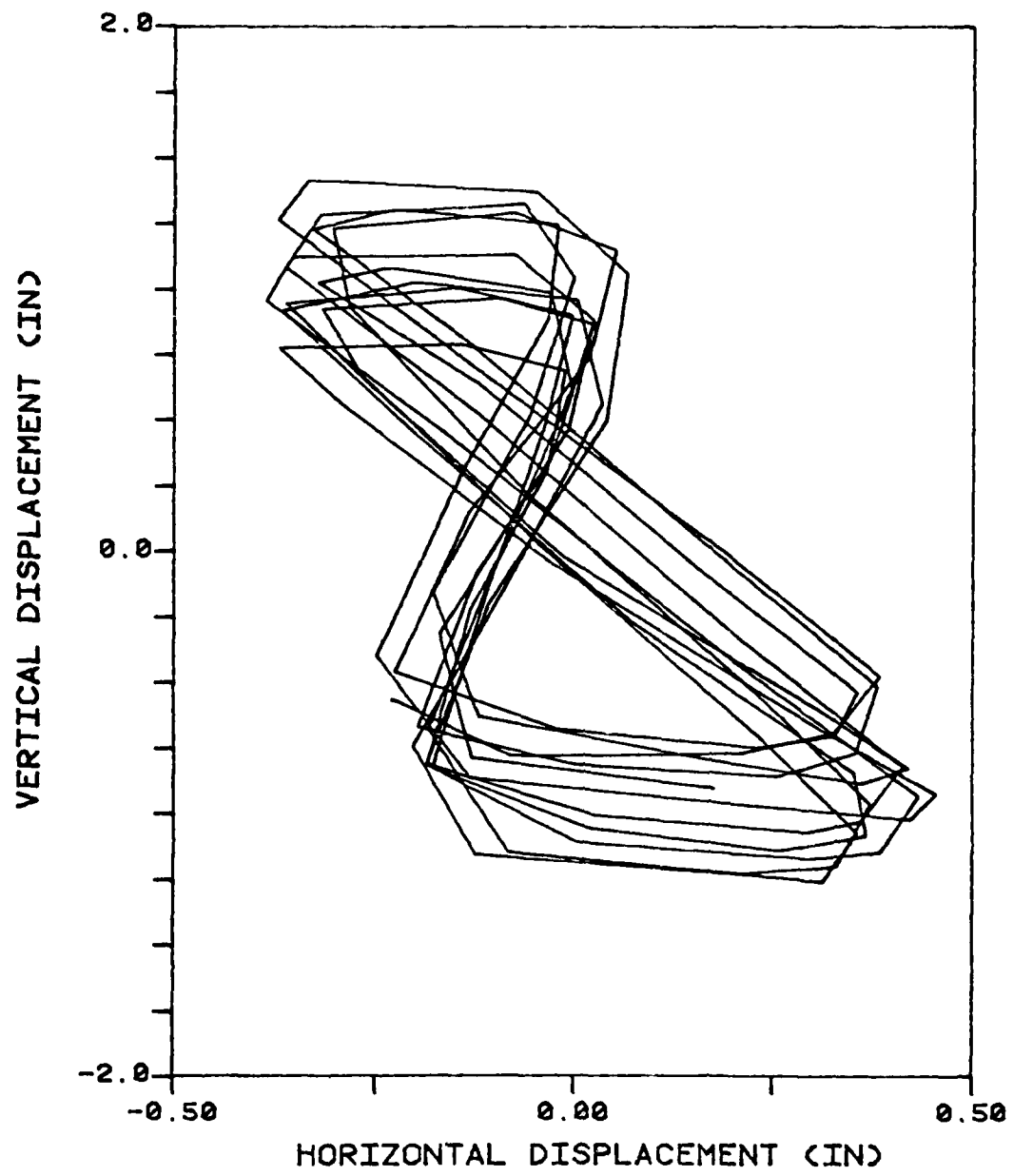


FIGURE 7. . LOCK-IN MOTION OF
THE STEEL TUBING AT POSITION L/6.

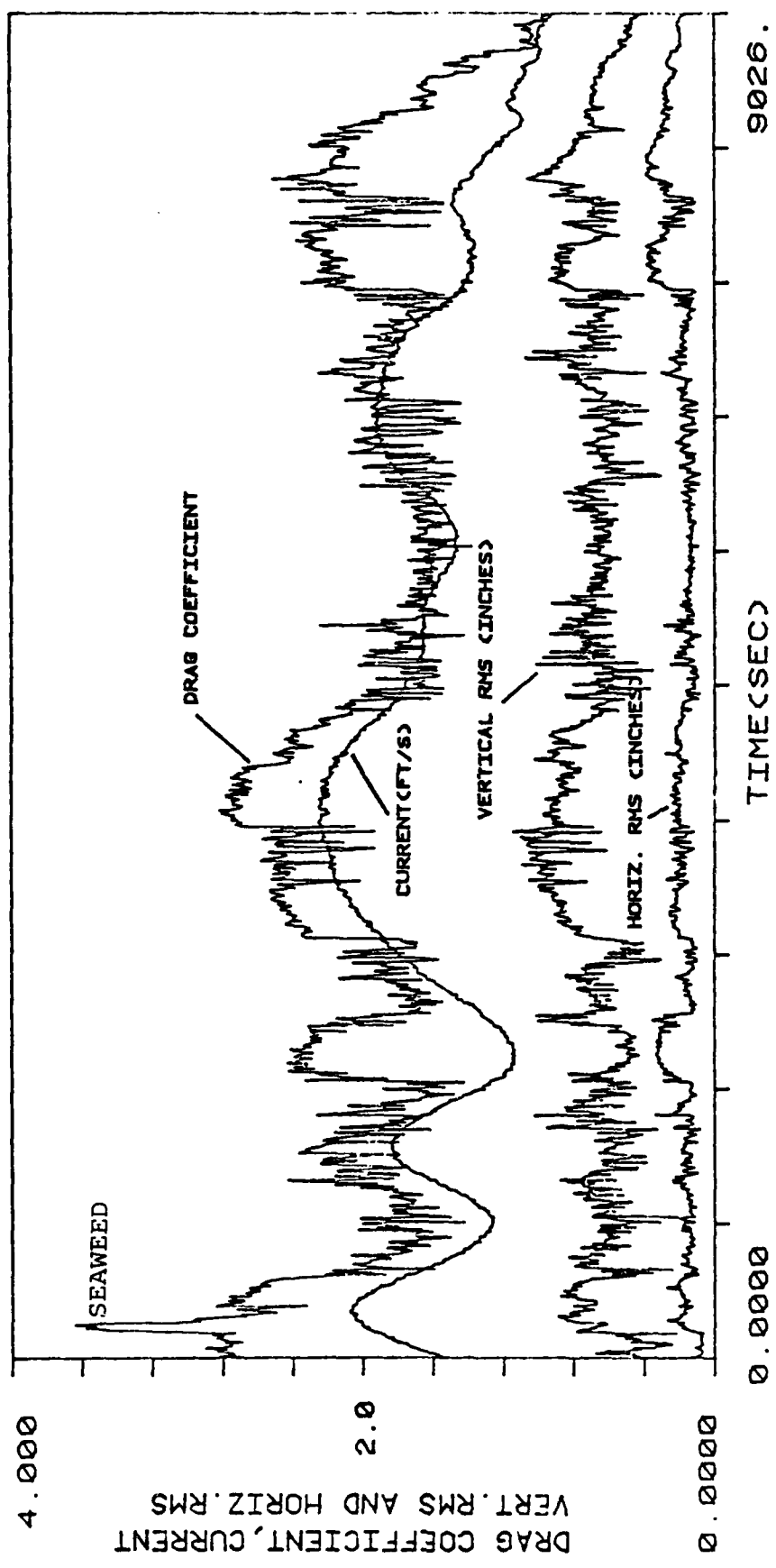


FIGURE 8 . 2 1/2 HOUR STEEL TUBING RECORD.
 VERTICAL AND HORIZONTAL RMS DISPLACEMENT FROM
 ACCELEROMETER PAIR LOCATED AT L/6.

CONCLUSIONS

Testing programs on models and full scale structures serve many purposes. A few of the most important have been emphasized here. The first one discussed was design verification. It is unwise to proceed with the development of analytical and numerical tools for the prediction of structural response to the ocean environment without constantly seeking verification of the predictions through measurement programs.

An area of active research in full scale response measurement is integrity monitoring. Techniques are being constantly improved for the purpose of examining the safety of structures through the evaluation of response records. One of the key requirements of most integrity monitoring techniques is that baseline signatures are needed for comparison to later tests. It is recommended that simple dynamic response measurements on new structures be made for archival purposes, anticipating the day that they may be useful in assessing damage.

Environmental measurements are also important. Now that both the oil industry and the U.S. Navy have interests in deploying structures in sites with deep water and current, better measurement techniques and enlarged data sets on sites such as in the Gulf Stream take on greater importance. Both current and directional wave spectra data are at present inadequate for many engineering design purposes.

The effect of wave spreading on dynamic response has been discussed, including a new model testing technique (the direct measurement of forces), and also including the introduction of the elliptical spreading function.

The accurate measurement of modal damping and the proper use of damping estimates in the prediction of response have been examined. In particular, wave radiation damping was shown to play a very unusual and significant role. Hydrodynamic viscous damping has an important dependence on sea state which is a topic of current research.

The final topic considered in this assessment of the state of the art in measurement and prediction of dynamic response was the flow induced vibration problem. The most pressing problem is the prediction of vibration response to spatially non-uniform flows. This is important because it impacts on the design of all long cylindrical members deployed in currents.

REFERENCES

1. Vandiver, J.K., "The Sensitivity of Fatigue Life Estimates to Variations in Structural Natural Periods, Modal Damping Ratios, and Directional Spreading of the Seas," Proceedings of the Third International Conference on the Behavior of Offshore Structures, MIT, 1982.
2. Ruhl, J.A., "Offshore Platforms: Observed Behavior and Comparisons With Theory," Proceedings of the 1976 Offshore Technology Conference, Paper No. 2553, Houston, Texas.
3. Ruhl, J.A., Berdahl, R., "Forced Vibration Test of a Deep Water Platform," Proceedings of the 1979 Offshore Technology Conference, Houston, Texas, May 1979.
4. Campbell, R.B., Vandiver, J.K., "The Determination of Modal Damping Ratios from Maximum Entropy Spectral Estimates," ASME Winter Annual Meeting, Paper No. 80-WA/DSC-29, Chicago, November 1980.
5. Vandiver, J.K., "Detection of Structural Failure on Fixed Platforms by Measurement of Dynamic Response," Journal of Petroleum Technology, Vol. XXIX, March 1977, OTC Paper No. 2267, 1975.
6. Begg, R.D. et al., "Structural Integrity Monitoring Using Digital Processing of Vibration Signals," Proceedings 1976 Offshore Technology Conference, Paper No. 2 ^, Houston, Texas.
7. Coppolino, R.N., Rubin S., "Detectability of Structural Failures in Offshore Platforms by Ambient Vibration Monitoring," Proceedings 1980 Offshore Technology Conference Paper No. 3865, Houston, Texas.
8. Duggan, D.M., et al., "Measured Vibrational Behavior of a Gulf of Mexico Platform," Proceedings 1981 Offshore Technology Conference, Paper No. 4137, Houston, Texas.
9. Utt, M.E., et al., "Estimation of the Foundation Condition of a Fixed Platform by Measurement of Dynamic Response," Proceedings 1976 Offshore Technology Conference, Paper No. 2625, Houston, Texas.
10. Rubin, S. and Coppolino, R.N., "Flexibility Monitoring of Offshore Jacket Platforms," Proceedings 1983 Offshore Technology Conference, Paper No. 4535, Houston, Texas.
11. Vandiver, J.K., "Direct Wave Force Measurements on a Model Tension Leg Platform," presented at the Ocean Structural Dynamics Symposium, Corvallis, Oregon, September 1982.

12. Vandiver, J.K., "Prediction of the Damping Controlled Response of Offshore Structures to Random Excitation," Society of Petroleum Engineers Journal, February 1980; also published in Proceedings: 1979 Offshore Technology Conference, Vol. II, Houston, Texas, May 1979.
13. Cook, M.F., Vandiver, J.K., "Measured and Predicted Dynamic Response of a Single Pile Platform to Random Wave Excitation," Proceedings of the 14th Annual Offshore Technology Conference, Paper No. 4285, Houston, Texas, May 1982.
14. Dunwoody, A.B., Vandiver, J.K., "The Influence of Separated Flow on the Dynamic Response of Offshore Structures to Random Waves," Proceedings of the Hydrodynamics in Ocean Engineering Conference, Trondheim, Norway, August 1981.
15. Ghosh, P., "The Prediction of Hydrodynamic Viscous Damping in Waves and Current by the Stochastic Linearization Method," SM Thesis, MIT, Department of Ocean Engineering, February 1973.
16. Gardner, T.N., "Deepwater Drilling in High Current Environments," Proceedings 1982 Offshore Technology Conference, Paper No. 4316, Houston, Texas.
17. Vandiver, J.K., Griffin, O.M., "Measurements of the Vortex Excited Strumming Vibrations of Marine Cables," presented at the Ocean Structural Dynamics Symposium, Corvallis, Oregon, September 1982.
18. Vandiver, J.K., "Drag Coefficients of Long Flexible Cylinders," Proceedings 1983 Offshore Technology Conference, Paper No. 4490, Houston, Texas.

EXTREME STATISTICS, RISK, AND RELIABILITY

by
Leon E. Borgman

Professor of Geology and Statistics
University of Wyoming
Laramie, Wyoming 82070

1. INTRODUCTION

Probabilistic design is widely applauded and usually ignored in engineering studies. By training and natural orientation, most engineers feel much more comfortable with deterministic design methods. However increasingly design situations arise whose correct treatment overwhelmingly requires elaborate probabilistic considerations, both in the selection of environmental forces and the structural response. This is particularly true in ocean engineering.

The following summary of basic probabilistic design methods is intended to provide an introduction to the young but vigorous field of reliability design, particularly as it relates to ocean engineering. The presentation will emphasize general, rather than specific techniques. Fixed-leg platforms, tension leg moored platforms, and self-positioning free-floating structures each have specific problems concerning reliability analysis of stress and motion response to environmental factors. Each could easily be the subject of a separate treatise. The presentation here, however, will emphasize common general aspects related to all of these.

A number of studies in reliability research have been concerned with the investigation of the function

$$Z = S - F \quad (1.1)$$

where S denotes the strength of a structure and F represents the force on the structure. Both S and F are considered to be probabilistic or random variables. The structure fails when $Z < 0$. The degree of safety is expressed by the average positive magnitude of Z . Since Z is random, the average magnitude of Z is given by the statistical expectation of Z , symbolized by

$$\mu_Z = E[Z] \quad (1.2)$$

It is convenient to scale the average magnitude of Z with the standard deviation of Z , denoted by σ_Z . Thus a reasonable measure of probabilistic safety is

$$\beta = \mu_Z / \sigma_Z \quad (1.3)$$

In words, β is the number of standard deviations by which the mean value of Z exceeds the failure boundary at $Z = 0$.

This simple, but typical, random failure function $Z = S - F$ is well treated in published literature and will not be explored further here. Rather, the analysis of more general analogous systems will be discussed and developed at various levels of design sophistication.

Any reliability analysis requires an often extensive study of the joint probability laws of characterizations of the environmental influences and of the structural properties. Typically, the analysis proceeds through (1) identification of potentially important variables (2) reduction to a minimal set of required variables (3) delineation of dependence and independence between variables, and (4) probability law development from historical data, coupled with physical analysis and engineering judgement.

This four step procedure requires a fairly thorough understanding of risk and the statistics of extremes, since often the reduction to a minimal set naturally introduces the near-extremes of the variables during the operational life of the structure. Such concepts as return period and non-encounter probability arise as appropriate parameters in the engineering analysis.

The investigation of failure modes for a modern offshore structure is a very complicated undertaking. Failures may be of many different types and have various levels of importance to the mission of the structure. One scheme which allows a realistic level of design complexity is based on the computer simulation of the design variables to produce a number of alternative "scenarios" of what might arise. For example, hydrodynamic flow properties at a number of loading points on a structure might be computer simulated for a given sea surface directional spectra in accordance with the random theory of ocean waves. Each of a number of such simulations might be combined with corresponding simulations of any randomness in the structural resistance behavior. An essentially deterministic analysis could be used for each scenario to determine some numerical measure of mission success. Since each alternative scenario is equally likely to arise, a frequency histogram of the numerical success measure directly gives an approximation to the probability law for a generalized Z function, and a safety measure $B = \mu_z/\sigma_z$.

The essential elements of reliability analysis will be presented in the three main topics: (1) Reliability Design, (2) Extremal Statistics at Risk, and (3) Computer Simulation Methods. Various subsidiary supporting topics will be introduced as needed.

2. STATISTICAL DEFINITIONS

Random variables will be denoted by capital letters. The corresponding sample or realization values for the random variable will be designated by lower case letters. Thus $X = x$ means that the random variable X takes on the sample value x . The distribution function for X is defined as

$$F_X(x) = P[X \leq x] \quad (2.1)$$

where $P[\cdot]$ represents the probability of the event within the bracket. The subscript on "F" designates which random variable is involved.

An underline will be used to designate vectors. For example \underline{X} is the random vector

$$\underline{x} = \begin{pmatrix} x_1 \\ x_2 \\ \vdots \\ x_n \end{pmatrix} \quad (2.2)$$

whose components are x_i . Vectors will always be considered to be column vectors. The transpose will be used to obtain a row vector if needed.

The distribution function of a random vector then may be written

$$F_{\underline{x}}(\underline{x}) = P[x_1 \leq x_1, x_2 \leq x_2, \dots, x_n \leq x_n] \quad (2.3)$$

The probability density of \underline{x} is given by

$$f_{\underline{x}}(\underline{x}) = \frac{\partial^n}{\partial x_1 \partial x_2 \dots \partial x_n} F_{\underline{x}}(\underline{x}) \quad (2.4)$$

Let $g(\underline{x})$ be a function of \underline{x} . The expected value of $g(\underline{x})$ is defined by

$$E[g(\underline{x})] = \int g(\underline{x}) dF_{\underline{x}}(\underline{x}) \quad (2.5)$$

where the integration is taken over the entire \underline{x} -space and the integral is interpreted as being of the Lebesgue-Stieltjes type.

The mean, variance, and correlation are defined in the usual ways as

$$\mu_{\underline{x}} = E[\underline{x}] \quad (2.6)$$

$$\sigma_{\underline{x}}^2 = E[(\underline{x} - \mu_{\underline{x}})^2] \quad (2.7)$$

$$\rho_{ij} = E[(x_i - \mu_i)(x_j - \mu_j)] / \sigma_i \sigma_j \quad (2.8)$$

where μ_i and σ_i have the obvious definitions as mean and standard deviation (square root of variance) for x_i .

3. RELIABILITY DESIGN

A structure may have a number of different modes of failure. The failure severity may range from an ultimate or catastrophic level down to consequences which interfere, at least temporarily, with the execution of the mission of the structure. Usually each failure mode is studied separately, and then an overall perspective is gained by examining the combined collection of separate mode studies.

3.1 A General Formulation: For a given mode of failure, let \underline{x} be the random vector of environmental and structural aspects relevant to the mode. Define the failure function $g(\underline{x})$ as some selected function such that

$$g(\underline{x}) \begin{cases} >0, & \text{if the structure does not fail when } \underline{X} = \underline{x} \\ <0, & \text{if the structure fails when } \underline{X} = \underline{x} \\ =0, & \text{on the boundary between failure and safety} \end{cases}$$

Let D be the failure domain in the \underline{x} -space. That is D is the set of values of \underline{x} such that $g(\underline{x}) \leq 0$. The probability of failure in the designated mode is given by

$$p_f = \int_D f_{\underline{X}}(\underline{x}) d\underline{x} = P[\underline{X} \in D] \quad (3.2)$$

where " \in " means "belongs to".

A very general decision structure may be developed by defining a utility function $V(\underline{x})$ which expresses degree of satisfaction (positive values) and dissatisfaction (negative values) with the magnitude of $g(\underline{x})$. Then the expected utility

$$E[V(\underline{X})] = \int V(\underline{x}) f_{\underline{X}}(\underline{x}) d\underline{x} \quad (3.3)$$

measures the adequacy of the design relative to that mode of failure, and provides a convenient value for comparing various designs. If

$$V(\underline{x}) = \begin{cases} 1.0, & \text{if } \underline{x} \in D \\ 0, & \text{otherwise} \end{cases} \quad (3.4)$$

then

$$E[V(\underline{X})] = p_f \quad (3.5)$$

However, it is usually desirable to use a more complicated utility function than this.

As an illustration of these concepts, consider a structure whose safety or failure is a function of the maximum wave height, H_m , during the operational life, and of the wave period, T_a , which is associated with the maximum wave when it happens. It will be presumed that the structure will fail for a region of values of H_m and T_a and not fail with various safety levels for other values of H_m and T_a . This general example is illustrated in Fig. 1. The intersection of the coordinate axes is not necessarily the origin of the coordinates. A utility matrix could be overlain on this figure as shown in Fig. 2. Then expected utility could be obtained by summing the products of the utility and the probability volume beneath the joint probability density within each rectangular cell of the grid.

In principle, the expected utility provides a fairly reasonable solution to probabilistic design. However in practice the dimensionality of \underline{X} is so large, the probability laws for \underline{X} are so difficult to determine, and the utility function is so subjective that simpler more direct methods are needed in most cases.

One approach was mentioned in the brief discussion of $Z = S - F$ earlier. This can be generalized as follows. Let

$$Z = g(\underline{x}) \quad (3.6)$$

$$\mu_z = E[Z] \quad (3.7)$$

$$\sigma_z = \sqrt{\text{Variance } Z} \quad (3.8)$$

Failure occurs when $Z \leq 0$. Hence the expected value of Z for the design, as scaled with the standard deviation of Z

$$\beta = \mu_z / \sigma_z \quad (3.9)$$

provides a measure of safety. Since the structure fails if $Z \leq 0$, the probability of failure is given by

$$\begin{aligned} p_f &= P[Z \leq 0] \\ &= P[(Z - \mu_z) / \sigma_z \leq -\mu_z / \sigma_z] \\ &= P[Z_N \leq -\beta] \end{aligned} \quad (3.10)$$

Let $F_{Z_N}(z)$ be the distribution function for Z_N . Then

$$p_f = F_{Z_N}(-\beta) \quad (3.11)$$

If $F_{Z_N}^{-1}(p)$ denotes the value of z such that

$$F_{Z_N}(z) = p \quad (3.12)$$

(i.e., the inverse function), it follows that

$$\beta = -F_{Z_N}^{-1}(p_f) \quad (3.13)$$

Consequently β and p_f are equivalent scales for risk or safety. The relation between β and p_f is illustrated in Fig. 3. A good discussion of these topics is given by Leporati (1979, pp. 1-30).

3.2 Linear, Second-Order Analysis

The above procedures are often called level 3 reliability analysis. They involve a rather complete formulation in terms of mathematical statistics. When various approximations are introduced in an attempt to simplify the techniques in terms of standard probability laws, the formulation is often referred to as level 2 analysis. Finally if the procedures are simplified to the point of allowing essentially deterministic design with percentiles of the various random variables concerned, the methods are often called level 1 analysis.

One of the common techniques in level 2 analysis is the linearization of $g(\underline{x})$ and use of second-order statistical moments, (Cornell, 1969; Hasofer and Lind, 1974). From a multivariate Taylor series expansion of $g(\underline{x})$ about $\underline{\mu}_x = E[\underline{x}]$, one obtains approximately

$$g(\underline{x}) \approx g(\underline{\mu}_x) + \sum_{i=1}^n a_i (x_i - \mu_i) \quad (3.14)$$

where

$$a_i = (\partial g / \partial x_i) \text{ at } \underline{x} = \underline{\mu}_x \quad (3.15)$$

To the same order of approximation, with $Z = g(\underline{x})$,

$$\underline{\mu}_z \approx g(\underline{\mu}_x) \quad (3.16)$$

$$\sigma_z^2 \approx \sum_{i=1}^n \sum_{j=1}^n a_i a_j \sigma_k \sigma_j \rho_{ij} \quad (3.17)$$

Then

$$\beta \approx g(\underline{\mu}_x) / \left(\sum_{i=1}^n \sum_{j=1}^n a_i a_j \sigma_k \sigma_j \rho_{kj} \right)^{1/2} \quad (3.18)$$

Within this framework, the failure function has value $g(\underline{\mu}_x)$ when $X_i = \mu_i$ and β measures the number of standard deviations this value is away from the failure region boundary where $g(\underline{x}) = 0$. The approximate failure boundary is given by

$$\beta \sigma_z + \sum_{i=1}^n a_i (x_i - \mu_i) = 0 \quad (3.19)$$

What is the distance between $\underline{x} = \underline{\mu}$ and the failure boundary plane, measured along the perpendicular? The perpendicular to the plane has direction cosines proportional to a_i . The equation of the line through $\underline{\mu}_x$ perpendicular to the plane, expressed in parametric form with parameter s is

$$x_i - \mu_i = a_i s \quad (3.20)$$

The point of intersection with the plane is obtained by substituting (3.20) into (3.19) and solving for s . Then (3.20) with this s value gives the coordinates of the intersection. Thus, s is the solution to

$$\beta \sigma_z + s \sum_{i=1}^n a_i^2 = 0 \quad (3.21)$$

or

$$s = -\beta \sigma_z / \sum_{i=1}^n a_i^2 \quad (3.22)$$

The intersection point is

$$x_i - \mu_i = -a_i \beta \sigma_z / \sum_{i=1}^n a_i^2 \quad (3.23)$$

and the length of the line from $\underline{\mu}_x$ to the boundary is

$$\text{length} = \left\{ \sum_{i=1}^n (x_i - \mu_i)^2 \right\}^{1/2} = \beta \sigma_z / \left\{ \sum_{i=1}^n a_i^2 \right\}^{1/2} \quad (3.24)$$

The length is proportional to β . If the X_i have $\mu_i=0$ and $\sigma_i=1.0$ and are independent, the length equals β . 7

The original x -space is not necessarily the best choice for reliability computations. It is often better to make a change of variables of the form

$$\underline{Y} = A(\underline{X} - \underline{\mu}_X) \quad (3.25)$$

where A is an appropriate non-singular matrix. A particularly good choice for A is related to the eigenvectors and eigenvalues for the covariance matrix of \underline{X} . Let C be the matrix whose (i,j) element is $\sigma_{ij}\sigma_{pj}$. The eigenvectors, \underline{v}_i , and eigenvalues, λ_i , of C are the n solutions to

$$C\underline{v}_i = \lambda_i \underline{v}_i \quad (3.26)$$

If V is the matrix whose i -th column is \underline{v}_i and L is a diagonal matrix (zeros for all off-diagonal elements) whose main diagonal is the eigenvalues, then (3.26) may be written

$$CV = VL \quad (3.27)$$

If A is defined as

$$A = L^{-\frac{1}{2}}V \quad (3.28)$$

where

$$V' = \text{matrix transpose of } V, \quad (3.29)$$

the transformation expressed by (3.25) has particularly desirable properties. The expectation of \underline{Y} is zero in all components and the covariance matrix for \underline{Y} is given by

$$\begin{aligned} \text{Cov } \underline{Y} &= E[\underline{Y}\underline{Y}'] = A E[(\underline{X} - \underline{\mu})(\underline{X} - \underline{\mu})'] A' \\ &= ACA' = L^{-\frac{1}{2}}V'CVL^{-\frac{1}{2}} \end{aligned} \quad (3.30)$$

It can be shown that V is an orthogonal matrix or may be made into one (generalized eigen vectors). With this property and (3.27), it follows from straightforward matrix operations on (3.30) that $\text{Cov } \underline{Y}$ becomes the identity matrix. Consequently, the components of \underline{Y} are uncorrelated with mean zero and unit variances. Even though the components of \underline{X} may have been interdependent, the transformation has produced a new uncorrelated set of variables. If $g(\underline{x}) = 0$ is transformed into $g^*(\underline{y}) = 0$, then the analysis can proceed in the y -space exactly as it did in the x -space. The function of $g^*(\underline{y})$ is expanded to second-order as before, the boundary plane is defined, and β is the distance from $\underline{\mu}_Y = 0$ to the plane. One property of orthogonal transformations is that they preserve distance. Thus, the β value is identical in the x -space and the y -space, except for scaling.

An illustration of the second-order analysis in x -space is given in Fig. 4. The linearization of $g(\underline{x}) = 0$ is shown as the dashed line. The distance from $\underline{\mu}_X$ to the plane, perpendicularly is $\beta\sigma_z / \sqrt{a_1^2 + a_2^2}$.

3.3 Partial Safety Factors and Level 1 Analysis: Suppose the vectors in \underline{x} can be subdivided into some terms related to structural strength and others related to environmental forces.

$$\underline{x} = \begin{bmatrix} S_1 \\ S_2 \\ \vdots \\ S_p \\ F_1 \\ F_2 \\ \vdots \\ F_q \end{bmatrix} \quad (3.31)$$

where S_i are the strength variables and F_j are the force variables. Let

$$S_i(.05) = \text{value of } s_i \text{ such that } F_{S_i}(s_i) = .05 \quad (3.32)$$

$$F_j(.95) = \text{value of } \phi \text{ such that } F_{F_j}(\phi) = .95 \quad (3.33)$$

That is $S_i(.05)$ is the 5-th percentile of S_i and $F_j(.95)$ is the 95-th percentile of F_j .

The quantities $S_i(.05)$ and $F_j(.95)$ are called the characteristic values for S_i and F_j . The use of .05 and .95 is completely arbitrary. Any convenient percentiles could have been selected.

One way to approximately take probabilities into account is to design deterministically with the characteristic values for the variables. A slight increase in generality is introduced by designing with

$$\begin{aligned} S_i &= S_i(.05)/\gamma_{S_i} \quad , \quad 1 \leq i \leq p \\ F_j &= F_j(.95)/\gamma_{F_j} \quad , \quad 1 \leq j \leq q \end{aligned} \quad (3.34)$$

The modifying factors, γ_{S_i} and γ_{F_j} , called partial safety factors, act in each case to move the design values in the direction of a more conservative design if the factors are greater than 1.0. If the partial safety factors equal 1.0, the design proceeds directly with the characteristic values.

It is convenient to introduce the coefficients of variation

$$c_{Si} = \sigma_{Si}/\mu_{Si} \quad (3.35)$$

$$c_{Fj} = \sigma_{Fj}/\mu_{Fj}$$

where μ_{Si} and μ_{Fj} are the means of S_i and F_j , respectively, and σ_{Si} and σ_{Fj} are the corresponding standard deviations. Let

$$k_{Si}(.05) = \{\mu_{Si} - S_i(.05)\}/\sigma_{Si} \quad (3.36)$$

$$k_{Fj}(.95) = \{F_j(.95) - \mu_{Fj}\}/\sigma_{Fj}$$

With these definitions, the design values in (3.34) become (Leporati, 1979, pp. 75-76)

$$S_i = \mu_{Si}\{1 - k_{Si}(.05) c_{Si}\}/\gamma_{Si} \quad (3.37)$$

$$F_j = \mu_{Fj}\{1 + k_{Fj}(.95) c_{Fj}\} \gamma_{Fj}$$

The failure function evaluated at these values

$$Z = g(S_1, S_2, \dots, S_p, F_1, F_2, \dots, F_q) \quad (3.38)$$

(where these capital letters specify numbers, not random variables) give a measure of risk.

3.4 General Comments: It appears that the complexity of most offshore structures will really require level 3, or possibly level 2 reliability analysis. Fortunately, the availability of modern computers overcomes many previous problems related to these more elaborate procedures.

4. EXTREMAL STATISTICS AND RISK

In many cases, the dimensionality of X may be quite large. For example, consider an offshore fixed-leg platform approximated with 40 loading points. The operational life of the platform will be taken as 50 years. Then, one excessively redundant choice for X would be all the time series for the velocities and acceleration at all loading points for the entire 50 years life. Considering three components for velocity and acceleration vectors and one second digitization of time series this would yield $6(40) 50(365) 24 (60)60 = 3.78(10)^{11}$ random variables. Clearly it is necessary to limit the analysis to extremal episodes during the 50 years, or further to work with the statistics of selected extremes. Thus, it is natural to introduce here a summary of extremal statistics and related parameters. A complete expository article on extremes is given by Borgman and Resio (1982a).

4.1 Basic Relations: Let X_1, X_2, \dots, X_N be N random variables. Define

$$X_{\max} = \max (X_1, X_2, \dots, X_N) \quad (4.1)$$

The probability law for X_{\max} is given by

$$\begin{aligned} F_{X_{\max}}(x) &= P[X_{\max} \leq x] \\ &= P[X_1 \leq x, X_2 \leq x, \dots, X_N \leq x] \end{aligned} \quad (4.2)$$

If the N random variables are independent, this becomes

$$F_{X_{\max}}(x) = \prod_{i=1}^N P[X_i \leq x_i] \quad (4.3)$$

where $\prod_{i=1}^N$ denotes the product of the terms for $1 \leq i \leq N$. Finally if the N random variables are identically distributed

$$F_{X_{\max}}(x) = F_X^N(x) \quad (4.4)$$

In many cases, the number of random variables, N , is also random. For example, if X_i is the maximum wave height in the i -th hurricane and N is the total number of hurricanes during the life of the structure, then the maximum wave height during the operational life will be the maximum of a random number of events.

Let

$$p_n = P[N = n], \quad n=0,1,2,3,\dots \quad (4.5)$$

be the probabilities that N events occur. The probability law for the maximum of N random variables is intimately related to the probability generating function

$$G_N(s) = \sum_{n=0}^{\infty} p_n s^n \quad (4.6)$$

For the case where X_1, X_2, \dots, X_N are independent and identically distributed

$$\begin{aligned} F_{X_{\max}}(x) &= \sum_{n=0}^{\infty} P[X_{\max} \leq x | n \text{ events}] P[n \text{ events}] \\ &= \sum_{n=0}^{\infty} p_n F_X^n(x) = G_N(F_X(x)) \end{aligned} \quad (4.7)$$

Here the convention is taken that

$$P[X_{\max} \leq x | 0 \text{ events}] = 1.0 \quad (4.8)$$

since, if no events happen, the value is less than or equal to any x .

4.2 Return Periods and Non-Encounter Probabilities: Let the non-encounter probability for an exceedance of x during the operational life of a structure be defined as

$$\begin{aligned} NE(x) &= P[\text{no exceedance of } x \text{ occurs during life } L] \\ &= P[X_{\max} \leq x] \end{aligned} \quad (4.9)$$

where X_{\max} is the maximum value during the life L . Thus

$$NE(x) = \begin{cases} \text{Case A} \\ F_X^L(x), \text{ if } L = \text{number of years and} \\ F_X(x) = \text{distribution function for annual maximum} \\ \text{Case B} \\ G(F_X(x)), \text{ if } G(s) = \text{probability generating function} \\ \text{for number of events during } L \text{ and } F_X(x) \text{ is} \\ \text{the distribution function for event maximums.} \end{cases} \quad (4.10)$$

The Poisson probability law is commonly used for p_n

$$p_n = e^{-\lambda t} (\lambda t)^n / n! , \quad 0 \leq n \quad (4.11)$$

This has the probability generating function

$$G_N(s) = \exp\{-\lambda t(1-s)\} \quad (4.12)$$

and gives a non-encounter probability of

$$NE(x) = \exp\{-\lambda L(1-F_X(x))\} \quad (4.13)$$

The return period, R , is the average length of time between exceedances of x . Usually x is referred to as the value of X with return period R . Thus, one may speak of the 100-year wave height or 50-year period wind velocity.

The waiting time in years for case A in (4.10) has probability law

$$P[W = w] = F_X^{w-1}(x)\{1-F_X(x)\} \quad (4.14)$$

and

$$E[W] = R = \{1-F_X(x)\}^{-1} \quad (4.15)$$

The waiting time for case B in (4.10) has probability law developed from

$$\begin{aligned} P[W > w] &= P[\text{no exceedances of } x \text{ in } (0, w)] = p_0 \\ &= \exp\{-\lambda\{1-F_X(x)\}w\} \end{aligned} \quad (4.16)$$

where the Poisson law has been used. It follows that

$$E[W] = R = [\lambda\{1-F_X(x)\}]^{-1} \quad (4.17)$$

The relation between $NE(x)$ and R may be developed by solving for $F_X(x)$ in (4.15) and (4.17) and substituting these into (4.10)

$$NE(x) = \begin{cases} (1-R^{-1})^L & , \text{ Case A} \\ \exp(-L/R) & , \text{ Case B} \end{cases} \quad (4.18)$$

It is interesting to note that if $R = L$, then $NE(x) = e^{-1}$ exactly for Case B and approximately for Case A. Consequently, there is a $1-e^{-1}=0.632$ chance of exceeding the event with return period L in L years. Obviously, one would not use an event with return period L for a structure with operational life L since there is almost a $2/3$ chance such an event will be experienced. What should one use? Leporati (1979, p.23) suggests $10 < R < 100$ years for failures which interrupt annual operations ($L \approx$ one year) and $1000 < R < 10,000,000$ for ultimate or catastrophic failures ($L \approx 100$ to 500 years). The hypothesized lives are not due to Leporati, but are suggested as reasonable operational lives corresponding to those return periods. It is interesting to examine the related non-encounter probabilities. These are shown in Tables I and II.

5. THE JOINT PROBABILITY METHOD

In data-rich investigations, it is often possible to develop the probabilities for extremes by direct extrapolation (See Borgman and Resio, 1982a, for a recent summary of these procedures and related problems). However most ocean engineering studies are data-sparse. It is usually necessary to use collateral meteorological information with physical models such as wave hind-casting to synthetically enlarge the data base.

5.1 The Basic Model: One physical-statistical model appropriate for developing extremal statistics from collateral information is the joint probability method. The basic formula underlying the joint probability method is

$$f_S(s) = \int f_{S|\underline{V}=\underline{v}}(s) f_{\underline{V}}(\underline{v}) d\underline{v} \quad (5.1)$$

Here $f_S(s)$ is the probability density for the basic random variable of interest, S . The function $f_{S|\underline{V}=\underline{v}}(s)$ is the conditional probability density for S , given that $\underline{V}=\underline{v}$ and $f_{\underline{V}}(\underline{v})$ is the joint probability density for \underline{V} . The vector \underline{V} is interpreted as a vector of random properties for the physical mechanism which produces the value of S . Thus, for hurricanes, the components of \underline{V} might be radius to maximum wind, central pressure, forward storm velocity, direction of travel, and distance from site to hurricane path. The random variable, S , might be interpreted as the maximum wave height at the site during the passage of the hurricane.

The function $f_{S|\underline{V}=\underline{v}}(s)$ is usually developed by methods somewhat as follows. A grid of values is laid over the portion of the \underline{v} -space, which has significant probabilities. Let the grid intersections be numbered arbitrarily with index j . That is \underline{v}_j is the value of \underline{v} at the j -th grid intersection. A physical model is used to predict $E[S] = \mu_S$ given $\underline{V}=\underline{v}_j$. Then either $f_{S|\underline{V}=\underline{v}_j}(s)$ is taken as normally distributed with a standard deviation related to the error of prediction for the physical model, or S , given $\underline{V}=\underline{v}_j$,

is taken as being deterministic or error-free. In the latter case, (5.1) reduces to the following procedure. (a) The value, S_j , is computed for each \underline{v}_j , $1 \leq j \leq J$. (b) Probabilities, p_j , are developed for the occurrence of \underline{v}_j

$$p_j = f_{\underline{v}}(\underline{v}) \Delta \underline{v} \quad (5.2)$$

where $\Delta \underline{v}$ is the grid cell volume. (c) The set of S_j for $1 \leq j \leq J$ are classified into a set of covering mutually exclusive and exhaustive cells, C_m , with midpoints s_m . Then (5.1) becomes

$$P[S = s_m] = \sum_{S_j \in C_m} p_j \quad (5.3)$$

In words, formula (5.3) is a sum of the probabilities for all grid points which lead to values of S in the vicinity of s_m .

5.2 A Generalized Model: Suppose that the extreme producing events can be classified into K meteorological types, each of which can be studied separately. For $1 \leq k \leq K$, let

$$F_{SRE \max, k}(s) = \int F_{S|\underline{v}_k=\underline{v}}(s) f_{\underline{v}_k}(\underline{v}) d\underline{v} \quad (5.4)$$

where \underline{v}_k is the random vector of properties characterizing the k -th type of extreme-producing event and $F_{SRE \max, k}(s)$ is the distribution function for $\max S$ in a single random event of type k . The formula in (5.1) has been re-expressed in terms of distribution functions, and $F_{S|\underline{v}_k=\underline{v}}(s)$ is the conditional distribution function for $\max S$ when $\underline{v}_k = \underline{v}$ an event of type k .

A single random event is taken as being of type k with probability p_k , for $1 \leq k \leq K$. Let $F_{SRE \max}(s)$ be the distribution function for S in a single random event drawn at random from the K possible types of events. Then

$$F_{SRE \max}(s) = \sum_{k=1}^K p_k F_{SRE \max, k}(s) \quad (5.5)$$

Finally if random events occur according to a Poisson probability law, the L -year $\max S$ value has distribution function

$$F_{L\text{-year max}}(s) = \exp[-\lambda L \{1 - F_{SRE \max}(s)\}] \quad (5.6)$$

Good characterizations of typical maximum S values are the median value of L -year $\max S$ and the value of S with a return period of R . The median value, s_m , is the solution to

$$F_{L\text{-year max}}(s_m) = 0.5 \quad (5.7)$$

The return period value, s_R , is, with good accuracy, given by the solution to

$$F_{R\text{-year max}}(s_R) = e^{-1} \quad (5.8)$$

The above model was used in a detailed study of maximum wave heights in the Gulf of Mexico (Ward, Borgman, and Cardone, 1979). A substantial study of procedures for the estimation of confidence intervals or reliability for the estimates s_m and s_R was made for the Waterways Experiment Station, U.S. Army Corps of Engineers, Vicksburg, Mississippi and is scheduled for eventual publication (Borgman, 1982c).

The problem with the reliability of the estimates in the joint probability method is that the errors depend on the accuracy of the physical prediction model, the skill of the meteorologist involved, the amount and reliability of the historical data, and other similar factors. These sources of error must be studied carefully before estimate reliability can be assessed. Unfortunately, the use of such estimates in subsequent reliability design requires such information. A great deal of further research is needed in this area of study.

6. COMPUTER SIMULATION OF EXTREMAL SCENARIOS

Extremal behavior of the structure may not be directly related to the largest wave height or any other single extreme value. Motion of a tension-leg platform may depend on wave grouping or second-order drift caused by the random wave field as a whole.

One way to study this type of problem is based on computer simulations of the hydrodynamic flow field in the more severe sea states likely to occur during the operational life of the structure. A number of independent simulations for the given extremal sea state may be used to provide equally-likely, alternative hydrodynamic flow fields which the structure must operate within. An analysis of the behavior of the structure for each simulation yields values for the extremes of the structure response. A frequency analysis of these values gives an approximation to the probability law for the extremal structural behavior.

6.1 Frequency Domain Simulations: Frequency domain simulations of wave properties are much faster than time domain simulations, in terms of computer time. Computer savings of 100 to 1 are common. The basic technique of frequency-domain simulation can be analyzed from formulas for the discrete Fourier transform. Let $n(t)$ be the water level elevation above mean water level at time t for some specified location. Define, for $0 \leq m \leq N$,

$$A_m = \Delta t \sum_{n=0}^{N-1} n(n\Delta t) e^{-i2\pi mn/N} \quad (6.1)$$

In general, A_m is complex valued and, if $n(t)$ is real valued,

$$A_{N-m} = \overline{A}_m \quad (6.2)$$

Here \bar{A}_m is the complex conjugate of A_m . The reverse transform is given by

$$n(n\Delta t) = \Delta f \sum_{m=0}^{N-1} A_m e^{+i2\pi mn/N} \quad (6.3)$$

where $\Delta f = (N\Delta t)^{-1}$ and $i = \sqrt{-1}$. For $0 < m < N/2$ (Borgman, 1976), if $n(t)$ is a real-valued, mean zero, stationary Gaussian stochastic process and $A_m = U_m - iV_m$, it follows that U_m and V_m are normally distributed with mean zero and variance $N\Delta t S(m\Delta f)/2$. Here $S(f)$ denotes the spectral density of $n(t)$. Also (U_m, V_m) are independent of $(U_{m'}, V_{m'})$ for $m \neq m'$, $0 < m < N/2$ and $0 < m' < N/2$. Finally U_m and V_m are independent of each other. In essence, the correlated, constant variance sequence $n(n\Delta t)$ is replaced with an uncorrelated, changing-variance sequence (U_m, V_m) for $0 < m < N/2$.

Computer simulations can proceed as follows: (a) Generate independent normal variables, U_m and V_m , with mean zero, and variance $N\Delta t S(m\Delta f)/2$ for $0 < m < N/2$. (b) Set $U_0 = V_0 = U_{N/2} = V_{N/2} = 0$ (c) Define $A_{N-m} = \bar{A}_m$. (d) Then inverse transform the complex sequence $\{A_m, 0 < m < N\}$ by (6.3) to obtain $\{n(n\Delta t), 0 < n < N\}$. The computer speed of the procedure follows from the great efficiency of the so-called fast Fourier transform algorithm, and the independence of the A_m in frequency domain.

A detailed discussion of computer simulation techniques for ocean waves, both in time and in frequency domains, is given by Borgman (1982b). Procedures for simulating multiple wave properties are also developed. In particular, the Fourier coefficients, A_m , for each wave property are independent for each m value within the interval $0 < m < N/2$, but are correlated between wave properties at the given m .

The best procedure for developing the intercorrelated, normal Fourier coefficients at a given m is by a procedure based on eigenvectors (Borgman, 1982b, p.392). The basic definitions for eigenvectors were developed earlier in (3.26) - (3.30). Let C be the covariance matrix for the combined set of U_m and V_m values for all the wave properties at a fixed m . If V is the eigenvector matrix for C and L is the diagonal matrix of eigenvalues, as defined previously then

$$\underline{X} = VL^{\frac{1}{2}}\underline{Z} \quad (6.4)$$

is a vector with covariance matrix C and mean zero. Here \underline{Z} is taken as a vector of independent, standard normal random variables (mean zero, variance one). The vector \underline{X} provides the simulated U_m and V_m values for each wave property. When all Fourier coefficients with significant wave energy have been developed this way, each wave property is reverted from the frequency to the time domain by the inverse fast Fourier transform.

6.2 Conditional Simulations: The above procedure is quite satisfactory for structural response behavior which depends on the average behavior of the extreme sea state. However, if one wants a group of successive very large waves, a quite long computer simulation may be required to obtain a small time piece with the desired behavior. Conditional simulations may be made which

force large wave groups to the present. The technique for achieving this is outlined by Borgman (1982b, pp. 406-407). Conditional simulation procedures are quite new within ocean engineering but show great promise for future applications.

7. RECOMMENDATIONS FOR FURTHER RESEARCH

The present paper has emphasized broad general principles applicable to a diversity of offshore structures. When these principles are applied to a specific structure, particularly with level 3 or level 2 reliability analysis, all of the mathematical problems of identification, reduction, delineation of dependence, and probability law development must be resolved for that structure. In addition, there are the questions of possible use of computer simulations, and of confidence interval determination for the reliability estimates. Almost every structure of any magnitude and complexity unavoidably requires statistical research to guide the choices in the reliability analysis. Reliability investigations are most emphatically not of a "cook book" nature. They demand a substantial level of mathematical and statistical sophistication.

In addition to research on the specific methods most appropriate for a given structure, research is needed on a number of theoretical aspects of the field. If one is going to advocate reliability design then, in all honesty, it is logically necessary to examine the reliability of the reliability design estimates. But the whole area of confidence intervals for reliability estimates is relatively undeveloped and is loaded with research questions. For example, what types of procedures should be introduced to evaluate the meteorologist procedures and skill in the joint probability method and to infer the related enlargement of the confidence intervals on the final return period variables? This and many similar questions through reliability analysis are largely unexplored.

The continuing increase in capacity of large main frame computers makes reliability analysis by computer simulation more and more appealing. However, even with the present substantial capacity, large problems require finesse if they are to be done with dispatch and not exceed available memory. In particular, the method of conditional simulation offers great promise as a technique to alleviate a reasonable number of computer time and memory difficulties. The method of conditional simulation was developed in mining geostatistics and is relatively new in ocean engineering. Even in mining geostatistics, there are still questions demanding research. This is doubly so, when the technique is transferred over to the new field of application in ocean engineering.

In summary then, the primary research topics which appear important in ocean engineering reliability analysis are (1) development of methods for specific types of structures, (2) study of reliability of reliability estimates, and (3) continuing extension of more efficient procedures for computer simulation of sea states, particularly the method of conditional simulations.

8. REFERENCES

Borgman, L.E. (1976), "Statistical Properties of Fast Fourier Transform Coefficients", Tech. Paper 76-9, U.S. Army Corps Engineers, Fort Belvoir, VA.

Borgman, L.E. and Resio, D.T. (1982a), "Extremal Statistics in Wave Climatology", Topics in Ocean Physics, pp. 439-471, Italian Physical Society, Bologna, Italy.

Borgman, L.E. (1982b), "Techniques for Computer Simulation of Ocean Waves", Topics in Ocean Physics, pp. 387-417, Italian Physical Society, Bologna, Italy.

Borgman, L.E. (1982c), "Final Report on Feasibility for Quantitative Assessment of Available Margins Inherent in Flood Protection of Nuclear Plants", A report to the Wave Dynamics Division, U.S. Army Waterways Exp. Station., Vicksburg, Mississippi.

Cornell, C.A. (1969), "Structural Safety Specification based on Second-Moment Reliability Analysis", Proc. IABSE Symposium, London.

Hasofer, A.M. and Lind, N.C. (1974), "Exact and Invariant Second-Moment Code Formal", Jour. Eng. Mech. Div., American Society of Civil Engineers.

Leporati, Ezio (1979), The Assessment of Structural Safety, Research Studies Press, P.O. Box 92, Forest Grove, Oregon, 97116, 133 pp.

Ward, E.G.; Borgman, L.E.; and Cardone, V.J. (1979), "Statistics of Hurricane Waves in the Gulf of Mexico", Jour. Petr. Tech., vol. 632.

Table 1. Service life non-encounter probabilities

R	L	Years	
		1	2
10		.905	.819
20		.951	.905
30		.967	.936
40		.975	.951
50		.980	.961
60		.983	.967
70		.986	.972
80		.988	.975
90		.989	.978
100		.990	.980

Table II. Ultimate life non-encounter probabilities

R	L	Years				
		100	200	300	400	500
1,000		.905	.819	.741	.670	.607
10,000		.990	.980	.970	.961	.951
100,000		.999	.998	.997	.996	.995
1,000,000		.9999	.9998	.9997	.9996	.9995
10,000,000		.99999	.99998	.99997	.99996	.99995

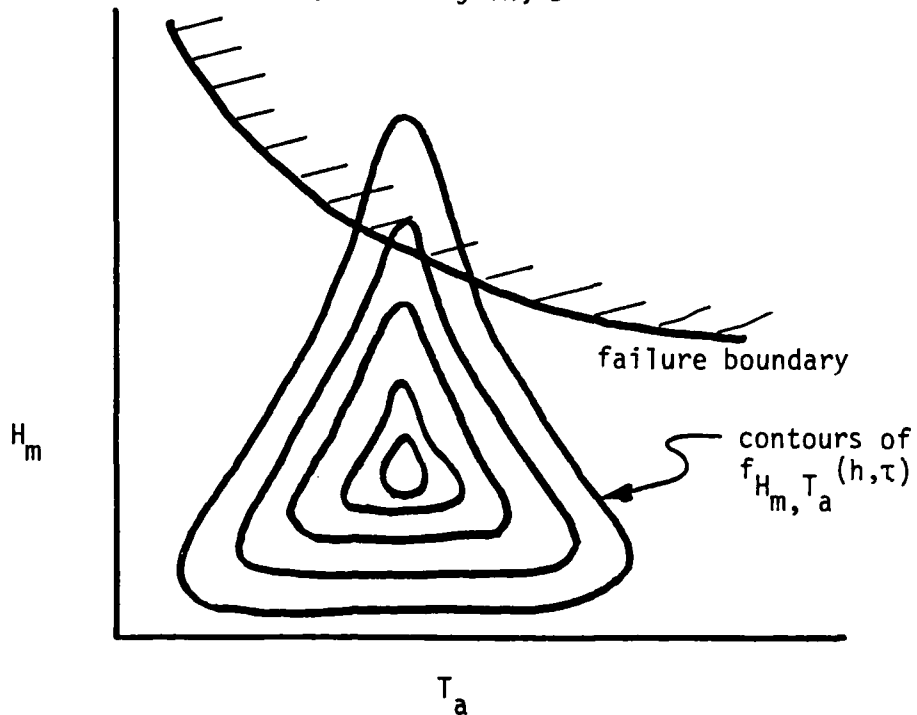


Fig. 1. A simple example. (H_m = max. wave height, T_a = associated wave period.

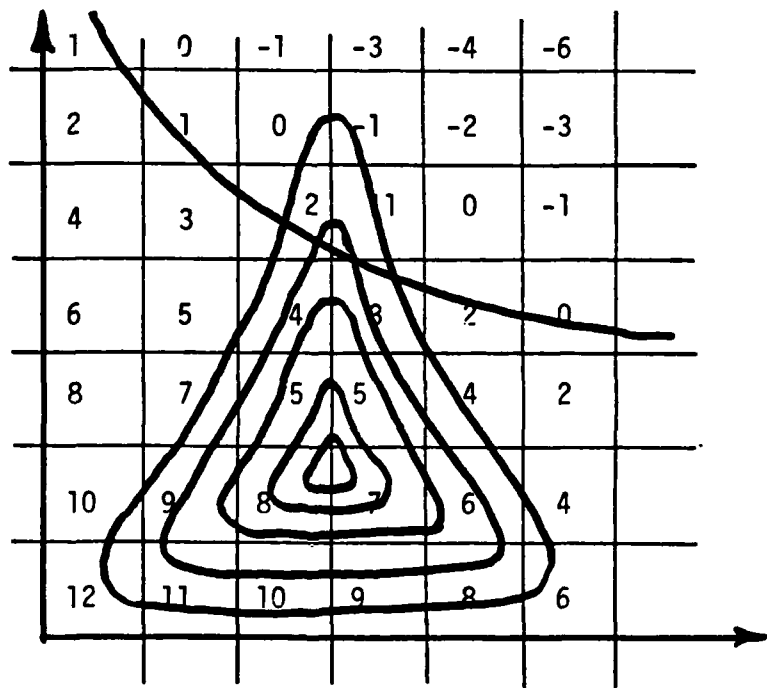


Fig. 2. Overlay of a utility field on the space x.

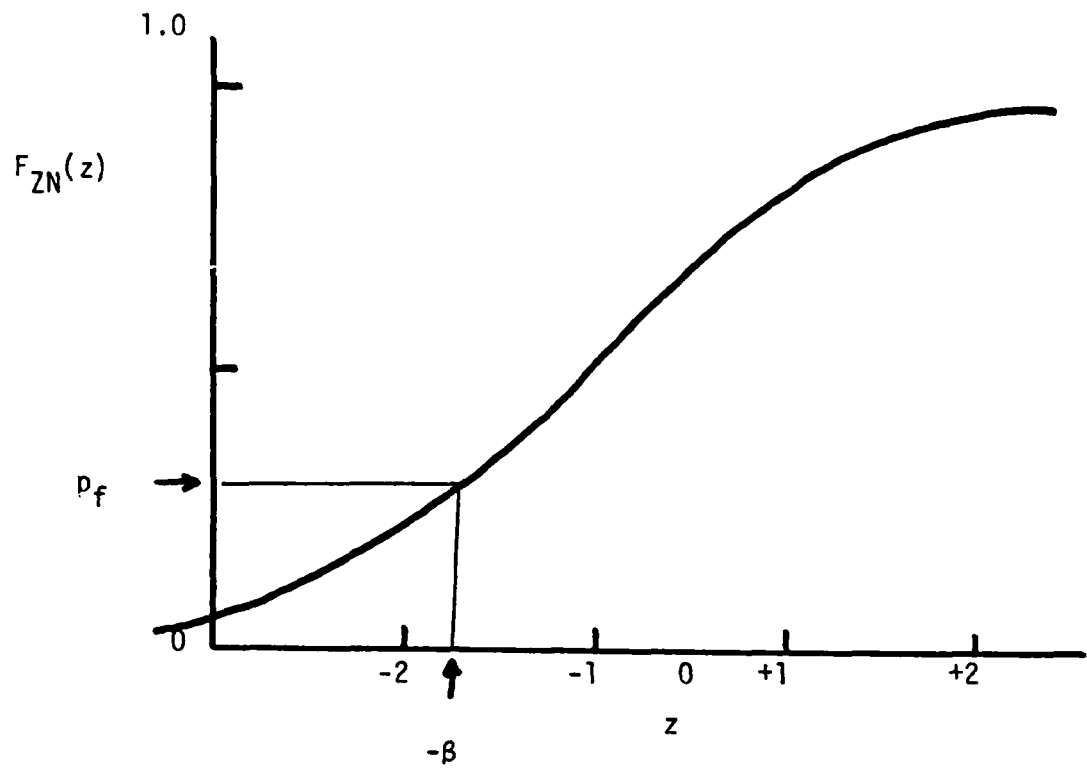


Fig. 3. Relation between failure probability and β .

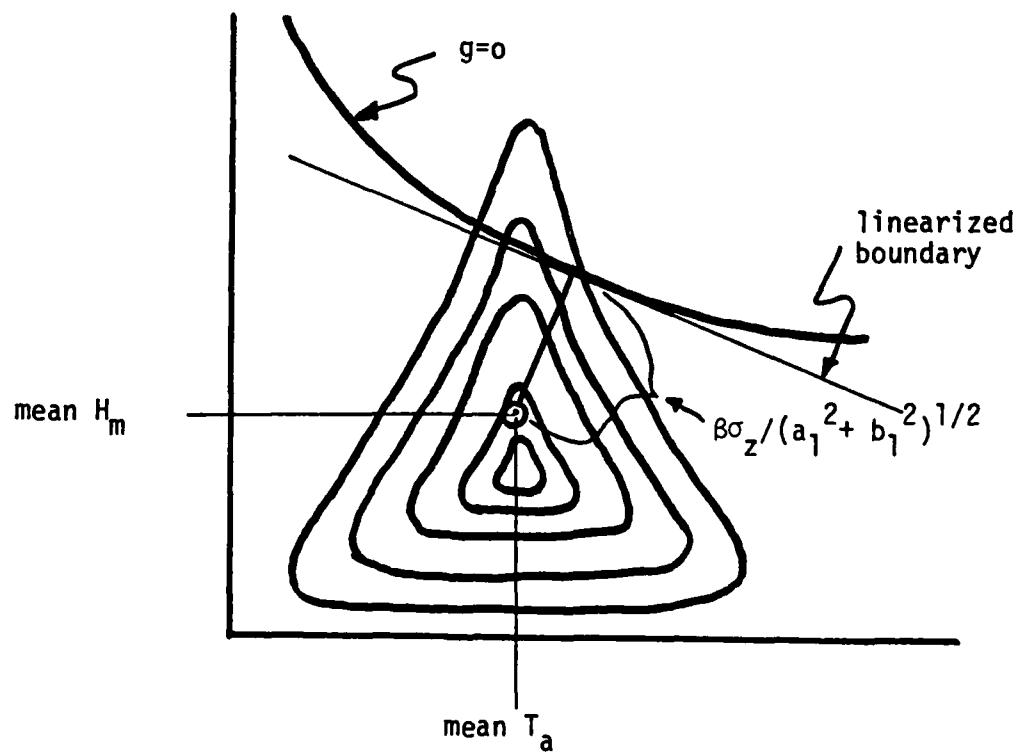


Fig. 4. Second-order analysis.

SEMINAR SUMMARIES

NCEL OCEAN PLATFORMS SEMINAR

Recommendations
by C. L. Vincent

1. The seminar at NCEL indicated that the Navy had extensive needs for the accurate specification of environmental design parameters for a variety of engineering problems. It was also apparent that there was no consistent or set methodology for obtaining these information which are critical to safe and economic design. For many of the applications discussed there are very few places where adequate environmental information is available (where adequacy is determined by having appropriate probability distributions with estimated error statistics). In most cases the information available is of unknown quality and may often be from multiple sources of unknown quality that present inconsistent values for parameters.
2. Therefore, I recommend that NCEL proceed to develop (or have developed for them):
 - a. Consistent, state of the art methodology for the specification of the environmental parameters needed for the design problems that the Navy is likely to face. The methodology should specify how events are to be specified on a probabilistic or joint probabilistic basis, which probabilities are appropriate for which design and how the expected errors are to be specified so that risk calculations can be made where needed. Documentation standards should be set so that, for major design problems, the procedures used to arrive at critical parameter values can be clearly stated.
 - b. The Navy should work toward development of a data base containing the environmental data they need for design that would be available by computer. Such a data base should include data of known or specified quality. The Navy may find it desirable to work with other agencies developing similar systems in order to decrease the cost. Over a period of years the systematic establishment of such information is less costly than developing the information (from "scratch") each time a project needs it. Further, the information insures high quality design information for both large and small projects. Since the Navy would be aware of how the information was generated in the data base, the Navy would be better aware of how reliable the information should be.
 - c. Based on a and b above, the Navy could present some often used design data in atlas form for easy access.
2. Many of the structures discussed in the seminar seem particularly sensitive to short period (less than 5 second) waves especially in terms of structure life. Most of this information is obtained from theoretical information about the shape of the wind wave spectrum in the saturation range. Recent research indicates that in shallow water this part of the wind wave spectrum can deviate substantially from the deep water case. Further, there is a theoretical basis suggesting that the spectral shape in the presence of a current (whether in deep or shallow water) will be altered from the deep water case. If the Navy is likely to pursue this type of structure, then an investigation of the effects of currents on this portion of the wind wave spectrum should be conducted to determine how to obtain realistic estimates for energy in these frequency components for arbitrary locations where the engineers may require it.

NCEL OCEAN PLATFORMS SEMINAR
SUMMARY OF RESEARCH OBJECTIVES
by
DR. ROBERT T. HUDSPETH

During the two-day seminar conducted by NCEL on 11 and 12 January 1983, the following research objectives were identified:

1. Selection of force coefficients for and identification of regions of validity for the **relative motion** generalization of the Morison equation.
2. Application of the **relative-motion** Morison equation to wave-current dynamic loadings.
3. Effects of member shielding on platform dynamics.
4. Interaction and shielding between Morison (slender body) members and diffraction members on complex platforms.
5. Dynamic interaction between hydrodynamically loaded tethers and platform motions.

RELATIVE MOTION MORISON EQUATION

The numerical comparisons by Garrison (1982) and by Paulling (1981) raise some fundamental concerns regarding the generalization of the Morison equation to relative-motion platform dynamics which merit further research and experimental verification. These concerns are most easily demonstrated by the comparison between the relative-motion generalization of the Morison equation with the extended form of the MacCamy-Fuchs theory for a vertical circular pile (Garrison, 1982).

In diffraction theory for large members, the generalized hydrodynamic pressure from loadings are linearly decomposed into two separate boundary value problems: viz. 1) the **exciting** force on a **fixed body** (the diffraction problem) and 2) the **restoring** force on a body **oscillating** in otherwise still water (the wavemaker problem). The **exciting** force is given by

$$F_e = \frac{2\gamma}{kb} \frac{Hb}{kh} \frac{[\sinh kh - \sinh k(h-D)]}{\sqrt{A(kb)}} \cos(\omega t - \delta) \quad (1a)$$

and the restoring force by

$$F_r = -\rho b^3 (C_m \ddot{x} + C_D \dot{x}) \quad (1b)$$

in which the added-mass coefficient, C_m , is

$$C_m = \frac{4\pi}{(kb)^2} \frac{W(kb)[\sinh kh - \sinh k(h-D)]}{A(kb)[2kh + \sinh 2kh]} + \quad (2a)$$

$$+ 4\pi \sum_{m=1} \frac{K_1(k_m b)}{(k_m b)^2} \frac{[\sin k_m h - \sin k_m (h-D)]}{K_1(k_m b)[2k_m h + \sinh 2k_m h]}$$

and the hydrodynamic radiation damping coefficient, C_D , is

$$C_D = \frac{8[\sinh kh - \sinh k(h-D)]}{(kb)^3 A(kb)[2kh + \sinh 2kh]} \quad (2b)$$

$$\text{and } A(kb) = \dot{J}_1^2(kb) + \dot{Y}_1^2(kb) \text{ and } W(kb) = Y_1(kb)\dot{Y}_1(kb) + J_1(kb)\dot{J}_1(kb).$$

(Garrison, 1982). It is obvious by comparing Eqs.(1) with Eqs.(2) that the hydrodynamic coefficients for the exciting force are distinct from the force coefficients for the restoring force.

In contrast, the generalized relative-motion Morison equation is given by

$$F = (1+C_m) \frac{\rho\pi b^2}{4} \frac{du}{dt} - C_m \frac{\rho\pi b^2}{4} \ddot{x} + 1/2 C_D b(u\dot{x}) |u\dot{x}| \quad (3)$$

In this case, the restoring force coefficients are directly related to the exciting force coefficients. These force coefficients are not obtained separately as in the case of large bodies by computing the exciting forces on a fixed body and by computing the viscous damping of an oscillating body in otherwise still fluid.

A research objective needs to be initiated both to verify the application of a generalized Morison equation to relative-motion platform dynamics and to obtain the appropriate force coefficients for these applications. Experimental verification of Eq. (3) is lacking as well as the parametric dependency of the coefficients.

WAVE-CURRENT GENERALIZATION OF THE MORISON EQUATION

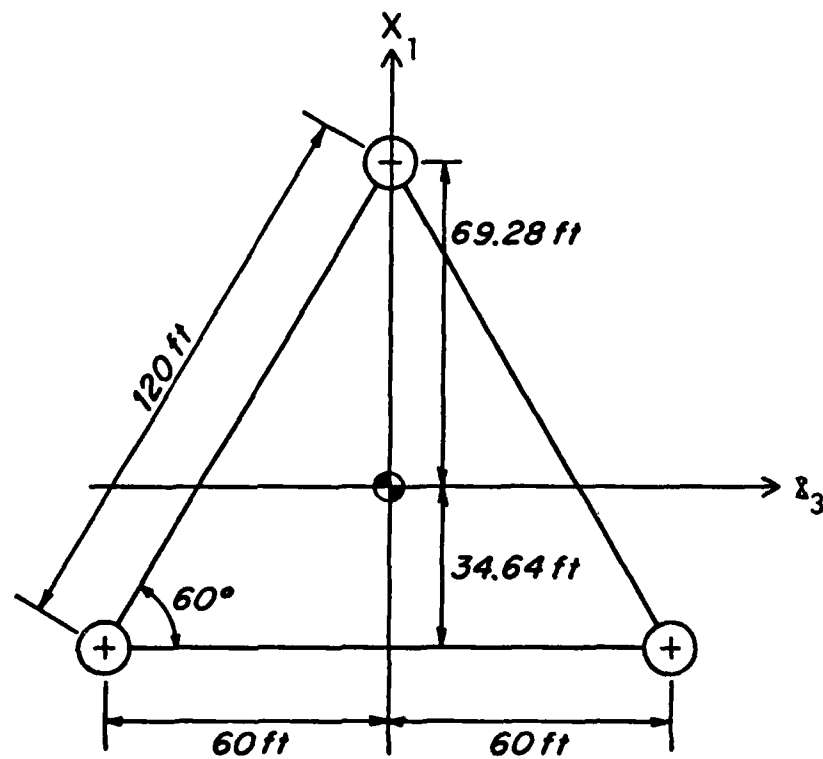
Potential design sites discussed during the seminar were located in regions of potentially high ocean currents. Force loadings on slender members at these sites will be computed by a generalization of the Morison equation to include wave-current interactions. Reliable force coefficients for ocean applications are not presently available. Limited experiments in U-tubes have indicated that the Morison equation force coefficients computed from harmonic flows with a steady motion are significantly different from those computed without the steady motion. While application of these U-tube observations to ocean wave-current forces is not entirely clear, it is clear that a research objective is required to define these coefficients for the NCEL platform program. Wave-current force coefficients are not presently available for design applications.

SHIELDING EFFECTS ON PLATFORM DYNAMICS

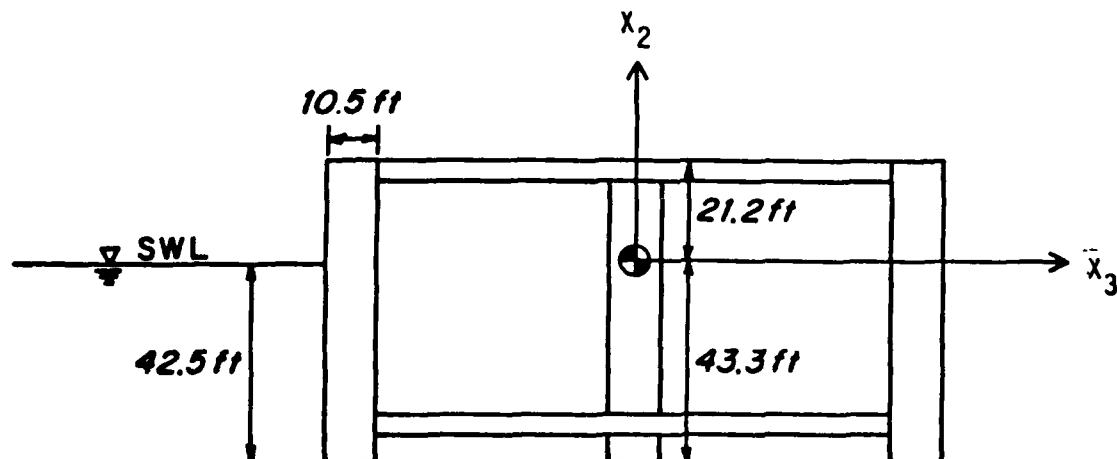
Significant dynamic effects have been demonstrated numerically (Garrison, 1982, and Huang et al., 1983) for both Morison equation forces (slender members) and diffraction forces (large members). Experimental verification is almost entirely lacking for the design concepts identified for potential applications by NCEL. A thorough parametric study needs to be initiated for determining the sensitivity of platform dynamics to member shielding for both large and small members. The DOT-TLP data appear to be representative of the type of TLP platform applicable to the NCEL design payloads. Analyses of these or other similar data should be incorporated into the NCEL Research objectives.

INTERACTION AND SHIELDING FOR COMBINATION MEMBERS

Some of the potential platform concepts reviewed by NCEL during the seminar include both large and small members. An example of the importance of including both of these force loadings has been demonstrated by Garrison (1982) and by Hudspeth and Leonard (1982). The analysis by Hudspeth and Leonard (1982) is of interest here since it represents a structure of the size and type that would have potential application in the NCEL platform program; viz., the DOT-TLP.



DECK PLAN VIEW



ELEVATION

FIG. 1 DEFINITION SKETCH OF DOT TLP

The generalized dynamic equations of motion for the DOT-TLP shown in Fig. 1 are given by

$$\sum_{n=1}^N \{ \vec{F}_n^I + \vec{F}_n^D + \vec{F}_n^H + \vec{F}_n^M \} + \sum_{n=1}^{N'} \{ \vec{F}_n^I + \vec{F}_n^V \} + \vec{F}_G = \sum_{n=1}^N \vec{F}_n^e + \sum_{n=1}^{N'} \vec{F}_n^e \quad (4a)$$

$$\sum_{n=1}^N \{ \vec{M}_n^I + \vec{M}_n^D + \vec{M}_n^H + \vec{M}_n^M \} + \vec{M}_G + \sum_{n=1}^N \vec{R}_n \times \{ \vec{F}_n^I + \vec{F}_n^D + \vec{F}_n^H + \vec{F}_n^M \}$$

$$+ \sum_{n=1}^{N'} \vec{R}_n \times \{ \vec{F}_n^I + \vec{F}_n^V \} = \sum_{n=1}^N \vec{M}_n^e + \sum_{n=1}^N \vec{R}_n \times \vec{F}_n^e + \sum_{n=1}^{N'} \vec{R}_n \times \vec{F}_n^e \quad (4b)$$

in which N = total number of large vertically axisymmetric buoyant members; N' = total number of small member elements; and n = mode of response.

Experimental response data recorded for the DOT-TLP were compared with numerical results obtained from an algorithm which included diffraction forces and moments computed for the three corner legs by an axisymmetric Green's function and for the slender member cross bracing by the Morison equation. No interactions between the diffracted wave field and the slender members were included in the Morison equation wave kinematics. Linear wave theory was applied for wave force computations on both large and small members.

The moments of inertia for each local member were computed and compared with the DOT values. The local members analyzed are identified on the DOT-TLP shown in Fig. 2. The 1:3 scale model DOT-TLP shown in Fig. 1 consists of 3 vertically axisymmetric buoyant caissons located at each apex of the triangular shaped dock structure (denoted as #1a, b, and c in Fig. 2); 3 each exterior and interior horizontal cross bracing members (#2 and 7 in Fig. 2); 3 vertical small member columns (#4 in Fig. 2); 6 diagonal interior struts (#5 in Fig. 2); and 3 main deck cross braces (#6 in Fig. 2).

The discretization scheme used to compute the forces/moment on the DOT-TLP is shown in Fig. 3. Each vertically axisymmetric buoyant pontoon was discretized into 8 nodal points beginning at the submerged centerline of the vertically axisymmetric member (0, - 42.6) and ending at the stillwater level (5.25,0). Each of the 3 horizontal exterior cross bracing members were discretized into 10 equal segments for analysis by the linearized relative-motion Morison equation (vide Fig. 3). Each of the 3 vertical small member columns

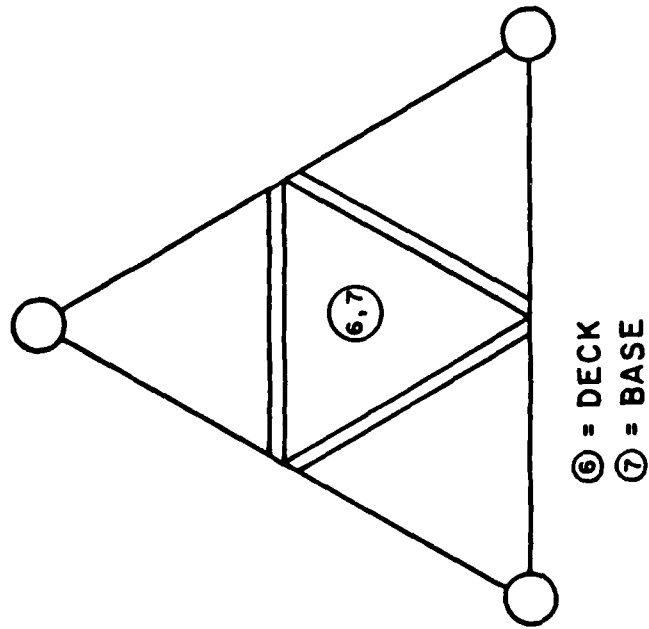
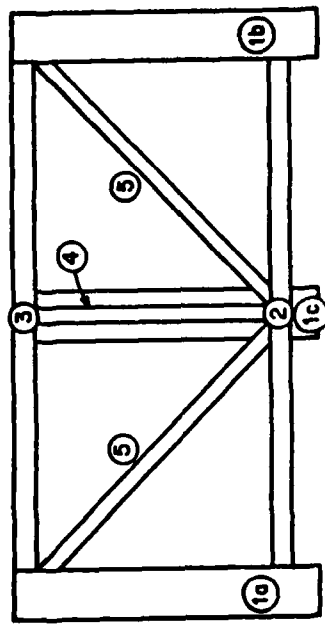


FIG. 2 SUMMARY OF DOT TLP INERTIA CALCULATIONS

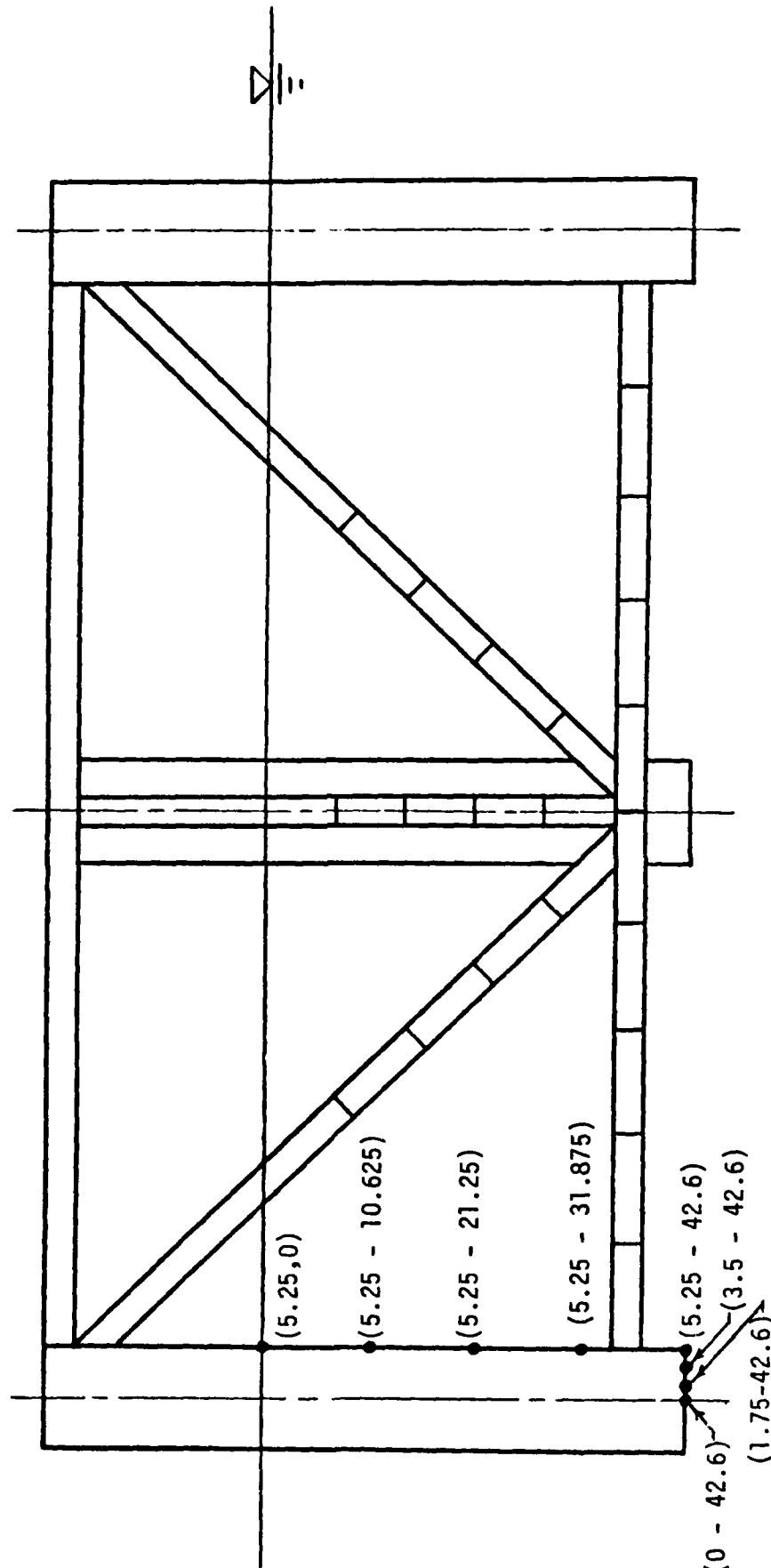


FIG. 3 DISCRETIZATION OF DOT TIP

and each of the 6 diagonal small member interior struts were discretized into 5 equal segments for analysis by the linearized hydroelastic Morison equation (vide Fig. 3).

The measured dynamic response of the DOT-TLP in the surge mode is compared in Fig. 4 with the numerical results of the TLP algorithm for various combinations of diffraction and Morison forces and moments. It can be seen that as more slender members are included in the model the surge results converge to the measured data for both the accelerometer and microwave measurements. The results which include the Morison equation are better than the results for diffraction only. This is because the vertically axisymmetric buoyant members are only marginally large enough to consider diffraction effects. The prototype TLP results are expected to be more inertially dominated. The 5 frequencies used to compute the surge mode RAO in Fig. 4 were taken from the DOT WAVE-2 spectrum for 0° angle of attack in the global coordinate axis.

This example (which neglected the shielding and interaction between the diffracted wave and Morison equation wave kinematics) clearly demonstrates the importance of including both diffraction and Morison equation effects. NCEL should initiate a research objective to develop a parametric study of the importance of interaction and shielding in structures with both large and slender members such as the DOT-TLP. The DOT-TLP data are available and their analyses should be considered in the NCEL Research Objectives.

DYNAMIC INTERACTION WITH HYDRODYNAMIC TETHERS

Dr. R. A. Skop demonstrated during the seminar the differences in the dynamic response of a body having a constant tether stiffness compared to a time-varying tether stiffness. Dr. J. R. Paulling also demonstrated this effect with his analysis of the Mathieu instability in the dynamic response of a TLP.

Since some of the potential platforms to be considered by NCEL will experience dynamic tether interactions, a research objective on this topic should also be initiated.

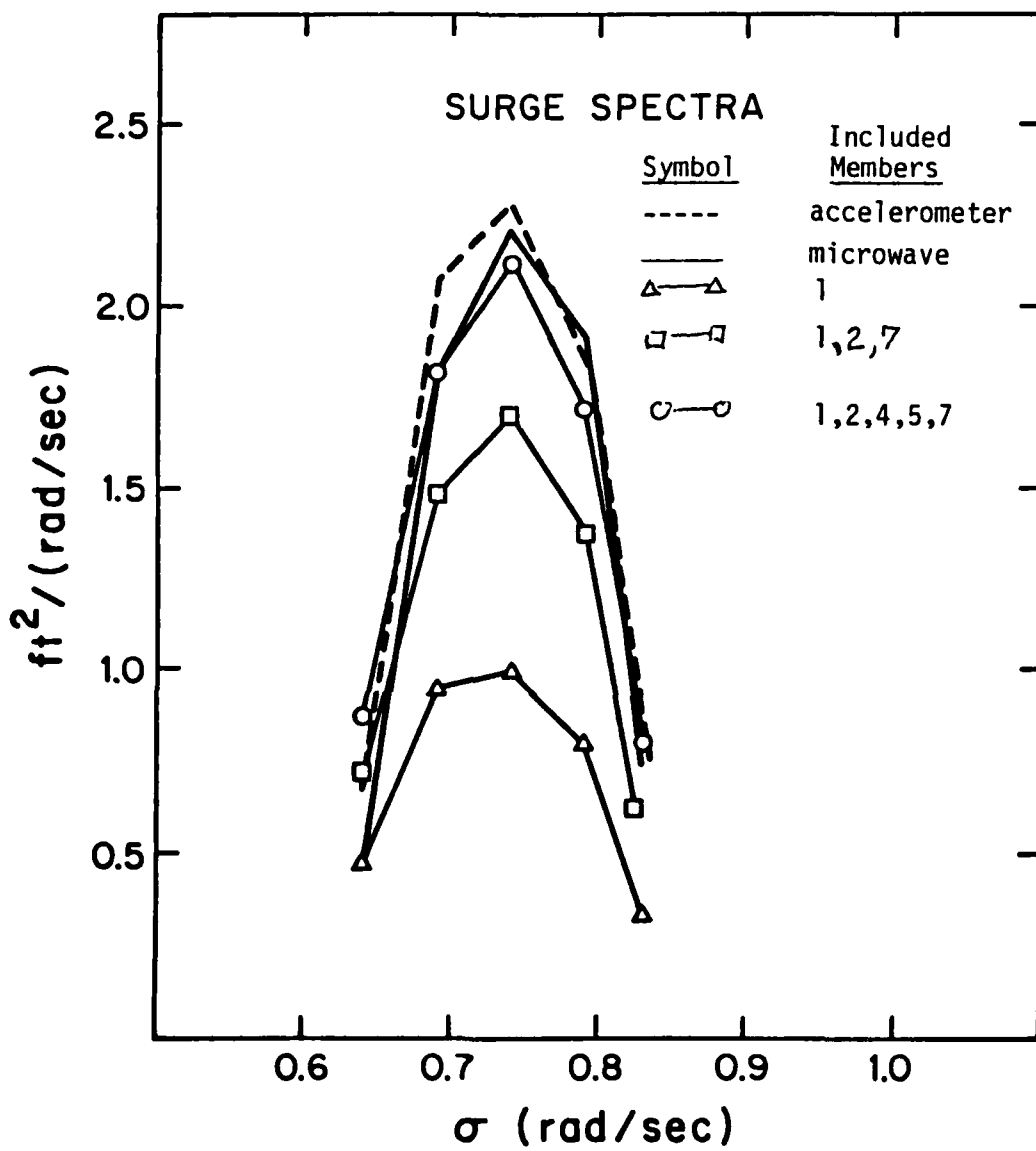


FIG. 4 SURGE SPECTRA FOR DOT TLP

Naval Civil Engineering Laboratory
Ocean Platform Seminar

Closing discussion by J. R. Paulling

GENERAL COMMENTARY. Both the semisubmersible and the tension leg platform may be considered as attractive candidates for certain of the navy's deep water sensor platform applications. The motion characteristics of each type must, however, be kept in mind when formulating operational specifications. In some cases, it may not be possible to achieve the navy's target motion specifications with a platform of reasonable size or cost. For both TLPs and semis, the horizontal motions of surge and sway, and for the semi, the heave as well, will be in the range of one-fourth to one-half the wave amplitude. This will be less for a large platform and greater for a small one and cannot be improved significantly through geometric changes alone. Angular motions will be similar to the wave slope in the medium to long period waves. In such cases, consideration should be given to the possibility of downgrading the motion requirements of the platform, and to incorporate suitable motion compensation characteristics and capabilities into the electronics or software used for signal processing.

The TLP does not, at present, appear to be the cure-all for extremely deep water applications which it once was expected to be, but will probably be most successful in a range of depth between 1000 and 5000 feet. This comes about because of the great weight sensitivity of the concept coupled with a rapid increase of the weight of mooring members with increased water depth. It is a principal design requirement for the TLP that the mooring members remain taut at all times in order to avoid large impulsive loads which would follow a

momentary slackening of a member in heavy wave conditions. This requirement, coupled with the desire to keep the mean tensions as low as possible, results in a need for very close control of variable weights.

This weight sensitivity may not pose as severe a problem for a navy sensor platform as it does for a large oil drilling/production platform since the former may well operate with a nearly constant payload. The limitation imposed by mooring member weight may sometimes be alleviated in the smaller navy sensor platform through the use of synthetic material or mooring members having distributed buoyancy.

In designing for an operating life measured in several tens of years, consideration must be given the inspection, maintenance and repair of mooring members. Moored oil drilling vessels rarely remain on station for periods exceeding six months, although there is one catenary moored semisubmersible platform which has now been in service for between five and ten years. A production TLP would have an expected life of twenty to thirty years on one location. No large TLP has yet entered service but retrieval, inspection and replacement of mooring members has formed an important design consideration for the Conoco Hutton TLP presently under construction.

The mooring installation may be simplified somewhat for a small platform if gravity anchors can be utilized in place of the drilled and grouted tension piles envisioned for most large oil field TLPs.

It is expected that a small navy sensor platform will experience relatively more severe wave conditions than a drilling platform solely because of its size. Since much of

the design analysis currently in use is based upon linearized techniques or has been developed through a process of extrapolation of past experience, there exists a need for the development of more fundamentally sound design procedures for navy sensor platforms. Aside from a fundamental desire to carry out the design in a more thorough and exact manner, this need exists in order to avoid the possibility of overlooking some effects which may be unimportant in large platforms solely because of scale, but which are important in the smaller absolute size range. Differences between navy and oil industry maintenance and construction practices should also be considered when selecting appropriate design procedures and standards.

Design codes or rules have been developed for semis and are under development for TLPs by the American Bureau of Shipping, API, Lloyds, DNV and other agencies. The existing rules are somewhat loose and are based largely upon experience. The ABS is currently developing a reliability-based TLP code utilizing the best available rational analysis procedures, and this work is expected to be completed during the present year. Related work being sponsored by ABS involves the development of a comprehensive hydrodynamic loads, structural analysis and long term fatigue computer software package for TLPs and semisubmersible platforms.

RESEARCH AND DEVELOPMENT NEEDS. The following list is repetitive to some extend of the list included in the original notes for the seminar. The order of the items is not intended to indicate priority.

- (1) Improved basis for the computation of hydrodynamic loads and motions for large, closely-spaced members in extreme wave environments.

- (2) Improved methods for the prediction of the low frequency and drift forces caused by wave reflection and wave-current acting simultaneously.
- (3) Improved methods of predicting wind effects, especially the unsteady wind over high waves.
- (4) Improved knowledge of the dynamics of the mooring lines and the interactions with platform motions. NCEL SEADYNE has the capability for providing this information for a semisubmersible. There may be other effects present in the TLP mooring such as vortex-generated strumming and Mathieu instability which require additional attention.
- (5) Structural design optimization in a fatigue environment. The reason for this is the weight sensitivity of the TLP. The ABS code development may produce some useful output and it would appear desirable for the navy to keep informed of these developments.

OCEAN PLATFORM SEMINAR
NCEL, Port Hueneme, CA

January 11 and 12, 1983

SUMMARY AND AREAS OF FURTHER RESEARCH

by

H.O. Berteaux

SUMMARY. The Seminar was well planned, well organized and well conducted. The formal presentations were of the highest quality.

The environment factors were well reviewed with perhaps too much emphasis on waves and not enough on currents. The lecture on extreme statistics was most enlightening. How to apply these advanced mathematical concepts to moored structures deployed in the ocean will require further work.

Modern techniques to predict the response of large platforms to ocean waves were reviewed in detail by several participants, with some overlap. Differences in definition of drag types and drag coefficients and in proposed linearization techniques are worth noting and exploring. Also noteworthy is the increased complexity of the models as platform dimensions grow in comparison to wave length and amplitude.

The "users" point of view, presented by FINN, RAINNIE and BERTEAUX gave a realistic touch to the meeting.

At this time, and as presented, the Navy needs appear somewhat undefined. Among unresolved uncertainties:

- ° Payload weight and location on platform.
- ° Allowable displacement (of Antenna I presume). There a distinction should be made between horizontal displacement of the platform with respect to known coordinates, and horizontal, vertical, and angular displacements of the antenna with respect to the platform c.g. The first is current induced, the second is wind and wave induced. The first could be specified in terms of absolute maxima. The second should be specified in terms of

statistical averages (RMS, significant etc.). Types of antenna displacement should also be listed in order of tolerance.

For example, vertical displacement could be a lesser problem than horizontal or angular displacements.

- ° Perhaps equally relevant would be a definition of the allowable rates of displacements.
- ° Operational limits due to bad weather. (Wind force and sea state beyond which the platform can have motions larger than those prescribed.)

Platform service life expectancy (20 years) may be achieved in shallow waters. It is doubtful that it can be achieved for deep sea moored platforms without some form of mooring line inspection and replacement.

An attempt was made at associating plausible types of platform (jacket, semisubmersible, spar buoys etc...) with various water depths. The audience response, including the vigorous statements of Dr. Shun Ling was a good index of the great interest that all participants share in the project.

FURTHER RESEARCH. It appears that implanting stable platforms in "shallow" water is well within the state-of-the-art. On the other hand, implanting a "stable" surface piercing platform in deep waters will require an extensive study, particularly if severe currents prevail at the projected deployment sites. Research areas relevant to such endeavor could include:

- ° Environment. Current measurements should be available or made at locations transecting the area of projected deployment. Ideally these measurements should be continuous and extending over a period

long enough - at least a year - to assess the presence and the magnitude of large perturbations (eddies). These measurements should extend from the surface to the seafloor.

A knowledge of the general current regime prevailing in the area would permit to:

1. Provide additional rationale for final selection of implantation sites.
2. Provide invaluable input data for the analysis and the design of mooring dominated platform systems.
- Mathematical modeling of wave induced platform response. In my opinion, statistical expectations of means and maxima of moored platform response to random waves would be more representative and informative than solutions obtained for regular waves of discrete periods and amplitudes. Linearization techniques (Taylor expansion, least square fit, energy equivalence etc...) which permit these expectations to be calculated should be compared as to ease of manipulation and coherence of results. Published values of drag and inertia coefficients should be used to establish error bounds on calculated platform response. Coefficients leading to large discrepancies may need to be evaluated further by experimentation.
- Sensitivity study of current induced mooring response. A sensitivity study of different mooring/platform configurations should be conducted to assess platform response against prescribed requirements.

This study should investigate:

1. Types of platform which will provide required surface expression within motion tolerances.

2. Types of moorings to maintain platform on station (single moor, multileg moor, auxiliary buoys, etc...).
3. Types of mooring materials (steel, Kevlar, nylon) which will provide best service life for investment.

° Drag Research. In mooring dominated systems, mooring drag could be singled out as the parameter having most bearing on mooring performance. As pointed out by VANDIVER, a better understanding of drag increase due to strumming is certainly timely and relevant. Equally important, in my opinion, would be a parallel effort at devising ways of decreasing mooring line drag. For example, if moorings could be equipped with neutrally buoyant, rigid, strut-shaped fairings of the type sold by FATHOM OCEANOLOGY, LTD. (Canada), then possibly:

1. Strumming would be reduced, or suppressed.
2. The drag of a nonstrumming rope would be greatly reduced. (Cut in half or better.)

How these well advertised fairings actually work when deployed in long lengths (thousands of meters) in currents which change direction with depth and time has never been measured. How would they work on a mooring line at 45 degrees or so from the vertical as the case would be in a trimoor? What other solutions could be devised to reduce drag?

POST SEMINAR SUMMARY

by J. Kim Vandiver

Deepwater Structures

The participants in the seminar reviewed the essential topics relevant to the design and placement of structures in water depths of up to 6000 feet of water. In very deep water no existing structural design concept can meet the desired restrictions on vessel horizontal excursion and pitch, roll, and yaw angles. It is not likely that major breakthroughs will occur, leading to substantial reductions in motion or cost. There are some topics for which research and development would lead to refinements in present understanding and predictive capability, allowing for more optimal design of structures.

This seminar was convened to review the state of the art in the ocean engineering of deepwater systems, rather than a review of the overall project. However, it became evident in the discussions of the second day that the system designers of the range had set very high standards for the performance and availability of the support structures making up the range. Of course a precedent had been set by the outstanding performance of the ACMR platforms near Cape Hatteras. They were, however, in very shallow water and that design concept is not acceptable in deep water. The present requirements of low cost and high performance at very deep water sites is unrealistic.

Success will require a compromise between a number of competing factors. One tradeoff is in the cost of improving the performance of the support structures versus the cost of making the electronics capable of tolerating greater structural motion. The second tradeoff is in the availability of the range as a function of weather conditions versus the motion restrictions placed on the structure.

It was apparent in the discussions that the system designers had hopes of adapting the electronics technology, presently used on the nearshore fixed structures, to the deepwater sites. A number of alternative suggestions came up in the discussion. For example, a conventional moored buoy in 6000 feet of water will have a enormous watch circle. However, the rate of change of position is very slow. In the time frame of an aerial engagement of 10 to 20 minutes, the moorings will move very little horizontally. If a method is developed to track the buoys over long periods of time, then it may be possible to use conventional buoy technology at relatively low cost. The suggestion was made to make use of the rapid advances in satellite global positioning systems or very accurate Loran-C.

The desired limitations placed on pitch, roll, and yaw are not realistic for low cost systems in deep water. Might it be less costly to use more powerful transmitters and wide beam antennas?

Availability is the other area in which a less costly structure may be achieved. If for a substantial fraction of the time in poor weather conditions, the structure did not have to stay within the motion restrictions required for good radio transmission, then a much simpler structure would result.

In my own area of expertise one particular topic for useful R and D work comes to mind. Deepwater structures of all types being considered here, including TLP's, semi-submersibles, buoys, and guyed towers, require mooring elements. At the present time it is not possible to accurately predict the drag coefficient on these elements. The reason is that it is not currently possible to predict the vortex induced vibration level on the mooring elements in current environments which vary greatly with depth as they do in and near the Gulf Stream. The state of the art is limited to the prediction of response levels and drag coefficients for cylinders in uniform flows. Anecdotal evidence on oceanographic moorings indicates that the drag coefficients do not often exceed 1.4 to 1.8. However, uniform flow experiments have revealed drag coefficients in excess of 3.0. The non-uniform flow result will fall somewhere between these two extremes, depending on conditions. The present understanding is very limited, and some field experimental work would benefit many deepwater projects.

Shallow Water Structures

Numerous types of structures will work in shallow water depths and meet the stringent performance requirements presently in use. The ACM structures are excellent examples of shallow water technology which is perfectly applicable to the task. However, in the hopes of decreasing costs even further, the most promising structure discussed at the seminar is the free standing caisson. In somewhat deeper water the articulated column may be an alternative as may be the guyed caisson.

SUMMARY REVIEW:
NCEL OCEAN PLATFORM SEMINAR,
11-12 JANUARY 1983

By: Leon E. Borgman
Re: Extreme Statistics, Risk and Reliability

1. SUGGESTED TOPICS FOR FURTHER RESEARCH

The paper which was presented emphasized broad general principles applicable to a diversity of offshore structures. When these principles are applied to a specific structure, particularly with level 3 or level 2 reliability analysis, all of the mathematical problems of identification, reduction, delineation of dependence, and probability law development must be resolved for that structure. In addition, there are the questions of possible use of computer simulations, and of confidence interval determination for the reliability estimates. Almost every structure of any magnitude and complexity unavoidably requires statistical research to guide the choices in the reliability analysis. Reliability investigations are most emphatically not of a "cook book" nature. They demand a substantial level of mathematical and statistical sophistication.

In addition to research on the specific methods most appropriate for a given structure, research is needed on a number of theoretical aspects of the field. If one is going to advocate reliability design then, in all honesty, it is logically necessary to examine the reliability of the reliability design estimates. But the whole area of confidence intervals for reliability estimates is relatively undeveloped and is loaded with research questions. For example, what types of procedures should be introduced to evaluate the meteorologist procedures and skill in the joint probability method and to infer the related enlargement of the confidence intervals on the final return period variables? This and many similar questions throughout reliability analysis are largely unexplored.

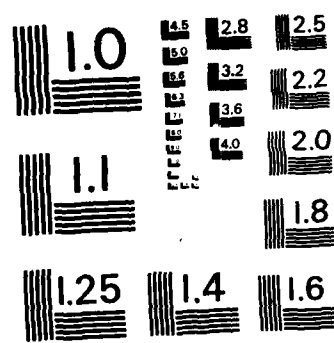
The continuing increase in capacity of large main frame computers makes reliability analysis by computer simulation more and more appealing. However, even with the present substantial capacity, large problems require finesse if they are to be done with dispatch and not exceed available memory. In particular, the method of conditional simulation offers great promise as a technique to alleviate a reasonable number of computer time and

AD-A139 419 NCEL (NAVAL CIVIL ENGINEERING LAB) OCEAN PLATFORMS
SEMINAR(U) NAVAL CIVIL ENGINEERING LAB PORT HUENEME CA
D R SHIELDS NOV 83 NCEL-TN-1681 4/4

UNCLASSIFIED

F/G 13/13 NL





MICROCOPY RESOLUTION TEST CHART
NATIONAL BUREAU OF STANDARDS - 1963 - A

memory difficulties. The method of conditional simulation was developed in mining geostatistics and is relatively new in ocean engineering. Even in mining geostatistics, there are still questions demanding research. This is doubly so when the technique is transferred over to the new field of application in ocean engineering.

All of the reliability procedures require a careful development of probabilities related to the hydrometeorological design variables and to the structural response and strength variables. The development of these probabilities from data is a nontrivial research task which is fundamental to the subsequent computations.

2. IMPLEMENTATION DETAILS FOR THE SUGGESTED RESEARCH

The suggested research is concerned with (a) development of hydrometeorological and structural input, (b) specification of response for each combination of input variables for the particular structure being studied, (c) description of failure modes and associated failure domains together with the related reliability analysis, and (d) confidence interval development for the reliability estimates. Each of these will be discussed briefly.

2.1. Hydrometeorological and Structural Input: The hydrometeorology is generally independent of the structure and forms a necessary prerequisite for any design procedure. The Wave Dynamics Group at the Waterways Experiment Station (U.S. Army Corps of Engineers, Vicksburg, Mississippi) have developed a substantial database of wave hindcasts for a network of locations along the Atlantic Coast during a twenty-year time interval. These hindcasts could be processed to give probability tabulations such as the joint distribution of maximum wave height and associated wave period and travel direction. The current software in the retrieval system at the Waterways Experiment Station will provide the joint distribution of maximum wave height and associated wave period. The mathematics for including associated direction has been developed in a recent Ph.D. thesis at the University of Wyoming (Ogbi, 1983). Other statistics related to various aspects of structural response can also be computed from the W.E.S. database. Statistics on winds and currents would need to be developed also.

The collection and compilation of the hydrometeorological input is a research project in its own right. It should involve cooperative efforts among individuals possessing statistical, meteorological, and engineering expertise and should be carefully coordinated with the Civil Engineering Laboratory relative to the overall requirements of the planned subsequent engineering analysis.

2.2. Response Specification: Some aspects of the structural

response for a given set of hydrometeorological variables may be predicted from standard deterministic structural design procedures. However others, particularly the dynamic response, involve nonlinear aspects and may require research. For example, mooring restraints and the current-wave environmental forces introduce nonlinearities. Both the tension-leg and moored structures experience a second-order drift or displacement under wave attack which requires some type of nonlinear treatment. Two design tools which aid in the attack on response specification are ocean wave simulation techniques (Borgman, 1982a) and the use of Volterra integrals (Borgman, 1982b). Both of these tools would need some mathematical development and the preparation of computer software to facilitate their use in the CEL design study. A computer package for simulation of ocean wave hydrodynamics would appear to be very useful in many aspects of the overall study.

2.3. Reliability Design for Each Structure: Although there would be certain computer software items that might be best prepared by outside contractors, it appears desirable for the majority of the actual reliability design to be carried out cooperatively between personnel at the Civil Engineering Laboratory and one or more outside consultants. This procedure would guarantee that whatever was developed would be applicable within the framework of the Laboratory design process, and that the resulting capabilities and experience in reliability design would be available within the Laboratory staff for future problems.

2.4. Confidence Interval Computations: This particular topic is a very valid subject for ongoing theoretical research. Confidence intervals for reliability estimates are particularly hard to define because they involve the meteorological uncertainties of the environmental input, as well as many other uncertainties in the reliability design process. Nevertheless, some guidance can be taken from recent studies (Borgman, 1983 and others). It would be useful in the proposed CEL study to include a survey and summarization of published techniques which might help in approximating the confidence intervals for the results of the reliability design.

3. RESEARCH PRIORITIES

Within the topics suggested here, the following ranked list appears to represent the importance of the proposed research topics to the CEL study.

1. Development of hydrometeorological input statistics.
2. Design of ocean wave simulation computer software.
3. Cooperative reliability design effort between CEL staff and selected consultants.

4. Derivation of Volterra integral or other nonlinear methods for treating structural response.
5. Review and summarization of techniques to approximate confidence intervals for estimates developed by reliability analysis.

REFERENCES

Borgman, L. E. (1982a), "Techniques for Computer Simulation of Ocean Waves", Topics in Ocean Physics, pp. 387-417, Italian Physical Society, Bologna, Italy.

Borgman, L. E. (1982b), "Specification of the Wave Environment", Proceedings of a Conference on Dynamics of Structures in the Ocean, Oregon State University, Corvallis, Oregon.

Borgman, L. E. (1983), "Final Report on Feasibility for Quantitative Assessment of Available Margins Inherent in Flood Protection of Nuclear Plants", Nuclear Regulatory Agency, Washington, D.C.

Ogbi, M. (1983), The Study of the Joint Probability Densities for Ocean Waves, Ph.D. Thesis, Statistics Dept., University of Wyoming, Laramie, Wyoming.

DISTRIBUTION LIST

AF HA Armament Div - YHI (R. Ballard); HQ Armament Div - YI (R. Warren)
AFB AF Tech Office (Mgt & Ops), Tyndall, FL; AFESC/TST, Tyndall FL; CESCH, Wright-Patterson
NATL ACADEMY OF ENG. Alexandria, VA
ARMY - CERL Library, Champaign IL
ARMY COE Philadelphia Dist. (LIBRARY) Philadelphia, PA
ARMY CORPS OF ENGINEERS Seattle Dist. Library, Seattle WA
ARMY CRREL Library, Hanover NH
ARMY ENG WATERWAYS EXP STA Library, Vicksburg MS; Coastal Eng Rsrch Cntr, Vicksburg, MS
ARMY ENGR DIST. Library, Portland OR
CNO Code OP 987 Washington DC
COMFLEACT, OKINAWA PWD - Engr Div, Sasebo, Japan
COMOCEANSYSLANT PW-FAC MGMNT Off Norfolk, VA
COMOCEANSYSPAC SCE, Pearl Harbor HI
DEFFUELSSUPPCEN DFSC-OWE, Alexandria VA
DOD Explosives Safety Board (Library), Washington DC
DOE Div Ocean Energy Sys Cons/Solar Energy Wash DC
DTIC Defense Technical Info Ctr/Alexandria, VA
DTNSRDC Code 522 (Library), Annapolis MD
LIBRARY OF CONGRESS Washington, DC (Sciences & Tech Div)
MARITIME ADMIN (E. Uttridge), Washington, DC
NAS PWO Belle Chasse, LA; PWO Key West FL
NATL BUREAU OF STANDARDS E. Simiu, Washington, DC
NATL RESEARCH COUNCIL Naval Studies Bd, Washington, DC; Naval Studies Board, Washington DC
NAVAIRDEVcen Code 813, Warminster PA; PWD, Engr Div Mgr, Warminster, PA
NAVAIRSYSCOM Range Instrumentation Div (R. Day) Washington DC
NAVCOASTSYSCEN CO, Panama City FL; Code 715 (J Quirk) Panama City, FL; Code 715 (J. Mittleman)
Panama City, FL; Code 719, Panama City, FL; Library Panama City, FL; PWO Panama City, FL
NAVELEXSYSCOM Code PME 124-61, Washington, DC; Commander, Washington, DC
NAVFACENGCOM Alexandria, VA; Code 03 Alexandria, VA; Code 03T (Essoglou) Alexandria, VA; Code
0451 (P W Brewer) Alexandria, Va; Code 0451, Alexandria, VA; Code 0453 (D. Potter) Alexandria, VA;
Code 0454B Alexandria, Va; Code 04A1 Alexandria, VA; Code 04B (M. Yachnis) Alexandria, VA; Code
PC2 (H Herrmann) Alexandria, VA
NAVFACENGCOM - CHES DIV. Code 101 Wash, DC; Code 407 (D Scheesele) Washington, DC; Code
FPO-1C Washington DC; FPO-1 (E. Spencer) Washington, DC; FPO-1 (S. Ling) Washington, DC; FPO-1
(T.J. O'Boyle) Washington, DC; FPO-1 Washington, DC; FPO-1EA5 Washington DC; FPO-1P/1P3
Washington, DC; Library, Washington, D.C.
NAVFACENGCOM - LANT DIV. Library, Norfolk, VA; RDT&ELO 102A, Norfolk, VA
NAVFACENGCOM - NORTH DIV. CO; Code 04AL, Philadelphia PA
NAVFACENGCOM - PAC DIV. Code 402, RDT&E, Pearl Harbor HI; Library, Pearl Harbor, HI
NAVFACENGCOM - SOUTH DIV. Library, Charleston, SC
NAVFACENGCOM - WEST DIV. Library, San Bruno, CA
NAVMAG SCE, Subic Bay, R.P.
NAVOCEANO Code 3432 (J. DePalma), Bay St. Louis MS; Library Bay St. Louis, MS
NAVOCEANSYSCEN Code 09 (Talkington), San Diego, CA; Code 4473 Bayside Library, San Diego, CA;
Code 4473B (Tech Lib) San Diego, CA; Code 5204 (J. Stachiw), San Diego, CA; Code 5214 (H. Wheeler),
San Diego CA; Code 5221 (R.Jones) San Diego Ca; Code 5322 (Bachman) San Diego, CA; Hawaii Lab (R
Yumori) Kailua, HI; Hi Lab Tech Lib Kailua HI
NAVPGSCOL C. Morers Monterey CA; E. Thornton, Monterey CA
NAVSCOLCECOFF C35 Port Hueneme, CA
NAVSEASYSCOM Code PMS 395 A 3, Washington, DC; Code SEA OOC Washington, DC; SEA 04E (L Kess)
Washington, DC; SEA-99611, Washington, DC
NAVSHIPYD Code 202.4, Long Beach CA; Code 280, Mare Is., Vallejo, CA; Library, Portsmouth NH; Tech
Library, Vallejo, CA
NAVSTA Dir Engr Div, PWD, Mayport FL; PWD - Engr Dept, Adak, AK; PWO, Mayport FL; SCE, San
Diego CA
NAVTECHTRACEN SCE, Pensacola FL
NAVWPNSTA PWO, Seal Beach CA
NCBC Library, Davisville, RI; PWO, Gulfport, MS; Technical Library, Gulfport, MS
NOAA (Mr. Joseph Vadus) Rockville, MD; (M. Ringenbach), Rockville, MD; (Mr. Joseph Vadus) Rockville,
MD; Library Rockville, MD
NOAA DATA BUOY OFFICE Engrng Div (Riannie) Bay St. Louis, MS
NORDA CO, Bay St. Louis, MS; Code 350 (Swenson) Bay St. Louis, MS; Code 410 Bay St. Louis, MS; Code
500, (Ocean Prog Off-Ferer) Bay St. Louis, MS

NRL Griffith, Wash., DC
NUSC DET Code 131 New London, CT; Code 332, B-80 (J. Wilcox) New London, CT; Code EA123 (R.S. Munn), New London CT; Code SB 331 (Brown), Newport RI
ONR Cagle, Pasadena, CA; Central Regional Office, Boston, MA; Code 481, Bay St. Louis, MS; Code 485 (Silva) Arlington, VA; Code 700F Arlington VA
PERRY OCEAN ENG R. Pellen, Riviera Beach, FL
PHIBCB 1 P&E, San Diego, CA
PMTC Code 4253-3, Point Mugu, CA
PWC Code 120, Oakland CA; Code 154 (Library), Great Lakes, IL; Library, Guam; Library, Norfolk, VA; Library, Pearl Harbor, HI; Library, Pensacola, FL; Library, Yokosuka JA
UCT ONE OIC, Norfolk, VA
UCT TWO OIC, Port Hueneme CA
U.S. MERCHANT MARINE ACADEMY Kings Point, NY (Reprint Custodian)
US DEPT OF INTERIOR Bur of Land Mgmt Code 583, Washington DC
US GEOLOGICAL SURVEY (Chas E. Smith) Minerals Mgmt Serv, Reston, VA (F Dyrkopp) Metairie, LA; (R Krahl) Marine Oil & Gas Ops, Reston, VA; Off. Marine Geology, Pitmekei, Reston VA
USCG (G-MP-3/USP/82) Washington DC
US GEOLOGICAL SURVEY (Chas E. Smith) Minerals Mgmt Serv, Reston, VA
USCG G-EOE-4 (T Dowd), Washington, DC; Library Hqs Washington, DC
USCG R&D CENTER CO Groton, CT; D. Motherway, Groton CT; D. Paskausky, Groton, CT; Library New London, CT
USGS Gregory, Reston, VA
USNA Ch. Mech. Engr. Dept Annapolis MD; USNA/SYS ENG DEPT ANNAPOLIS MD; USNA/SYS Eng. Dept (T. Dawson), Annapolis, MD
AMERICAN CONCRETE INSTITUTE Detroit MI (Library)
CALIF. DEPT OF NAVIGATION & OCEAN DEV. Sacramento, CA (G. Armstrong)
CALIF. MARITIME ACADEMY Vallejo, CA (Library)
CALIFORNIA INSTITUTE OF TECHNOLOGY Pasadena CA (Keck Ref. Rm)
CALIFORNIA STATE UNIVERSITY LONG BEACH, CA (CHELAPATI); LOS ANGELES, CA (KIM)
DAMES & MOORE LIBRARY LOS ANGELES, CA
DUKE UNIV MEDICAL CENTER B. Muga, Durham NC
UNIVERSITY OF DELAWARE (Dr. S. Dexter) Lewes, DE
FLORIDA ATLANTIC UNIVERSITY Boca Raton FL (W. Hartt); Boca Raton, FL (McAllister)
FLORIDA INSTITUTE OF TECHNOLOGY (J Schwalbe) Melbourne, FL
INSTITUTE OF MARINE SCIENCES Dir, Port Aransas TX
WOODS HOLE OCEANOGRAPHIC INST. Woods Hole MA (Berteaux)
JOHNS HOPKINS UNIV Ches Bay Rsch Inst Rsch Library Shady Side MD
LEHIGH UNIVERSITY BETHLEHEM, PA (MARINE GEOTECHNICAL LAB., RICHARDS); Bethlehem PA (Linderman Lib. No.30, Flecksteiner)
MAINE MARITIME ACADEMY CASTINE, ME (LIBRARY)
MIT Cambridge MA; Cambridge MA (Rm 10-500, Tech. Reports, Engr. Lib.); Vandiver, Cambridge, MA
OREGON STATE UNIVERSITY (CE Dept Grace) Corvallis, OR; (CE Dept, R. Hudspeth) Corvallis, OR; Corvallis OR (School of Oceanography); Corvallis, OR (Ocean Engr Prgm-J. Nath)
PENNSYLVANIA STATE UNIVERSITY State College PA (Applied Rsch Lab)
PORTLAND STATE UNIVERSITY H. Migliore Portland, OR
SEATTLE U Prof Schaebler Seattle WA
STATE UNIV. OF NEW YORK Fort Schuyler, NY (Longobardi)
TEXAS A&M UNIVERSITY College Station TX (CE Dept. Herbich); Galveston, TX (Marine Engr-H. Alexander); Hyd Rsch Lab College Station, TX; J.M. Niedzwecki, College Station, TX; J.R. Morgan, College Station, TX
UNIVERSITY OF ALASKA Doc Collections Fairbanks, AK; Marine Science Inst. College, AK
UNIVERSITY OF CALIFORNIA BERKELEY, CA (CE DEPT, GERWICK); Berkeley CA (Dept of Naval Arch.); Berkeley, CA (Dept of Naval Arch, Paulling); Engr Lib., Berkeley CA; La Jolla CA (Acq. Dept, Lib. C-075A)
UNIVERSITY OF CONNECTICUT Groton CT (Inst. Marine Sci, Library)
UNIVERSITY OF HAWAII HONOLULU, HI (SCIENCE AND TECH. DIV.); Ocean Engng Dept
UNIVERSITY OF ILLINOIS Metz Ref Rm, Urbana IL; URBANA, IL (LIBRARY)
UNIVERSITY OF NEW HAMPSHIRE (Corell) Durham, NH
UNIVERSITY OF RHODE ISLAND Narragansett, RI (Pell Marine Sci. Lib.)
UNIVERSITY OF SO. CALIFORNIA Univ So. Calif
UNIVERSITY OF TEXAS Inst. Marine Sci (Library), Port Arkansas TX
UNIVERSITY OF TEXAS AT AUSTIN AUSTIN, TX (THOMPSON)
UNIVERSITY OF WASHINGTON SEATTLE, WA (OCEAN ENG RSCH LAB, GRAY); SEATTLE, WA (PACIFIC MARINE ENVIRON. LAB., HALPERN)
UNIVERSITY OF WISCONSIN Milwaukee WI (Ctr of Great Lakes Studies)
VIRGINIA INST. OF MARINE SCI. Gloucester Point VA (Library)

WOODS HOLE OCEANOGRAPHIC INST. Doc Lib LO-206, Woods Hole MA
AMETEK Offshore Res. & Engr Div
ATLANTIC RICHFIELD CO. DALLAS, TX (SMITH)
BELL TELEPHONE LABS Sashoty, Whippany, NJ
BRITISH EMBASSY M A Wilkins (Sci & Tech Dept) Washington, DC
CHEVRON OIL FIELD RESEARCH CO. LA HABRA, CA (BROOKS)
COLUMBIA GULF TRANSMISSION CO. HOUSTON, TX (ENG. LIB.)
CONTINENTAL OIL CO O. Maxson, Ponca City, OK
CUBIS DEFENSE SYSTEMS C. Whitney, San Diego, CA
EXXON PRODUCTION RESEARCH CO Houston, TX (L.D. Finn)
FURGO INC. Library, Houston, TX
GIANNOTTI ASSOC A.T. Morris, Berkeley, CA; Annapolis, MD
HUGHES AIRCRAFT Culver City CA (Tech. Doc. Ctr)
NUSC DET Library, Newport, RI
LIN OFFSHORE ENGRG P. Chow, San Francisco CA
LOCKHEED MISSILES & SPACE CO. INC. Dept 57-22 (Rynewicz) Sunnyvale, CA
MARATHON OIL CO Houston TX
MARINE CONCRETE STRUCTURES INC. MEFARIE, LA (INGRAHAM)
MC CLELLAND ENGINEERS INC Corp Library Houston, TX
MOBIL R & D CORP Manager, Offshore Engineering, Dallas, TX; Manager, Offshore Engineering, Dallas, TX
MOFFATT & NICHOL ENGINEERS (R. Palmer) Long Beach, CA
NEWPORT NEWS SHIPBLDG & DRYDOCK CO. Newport News VA (Tech. Lib.)
NOBLE, DENTON & ASSOC., INC. (Dr. M Sharples) Houston, TX
OFFSHORE & COASTAL TECHNOLOGY C.L. Vincent, Woodbridge, VA
PORTLAND CEMENT ASSOC. Skokie IL (Rsch & Dev Lab, Lib.)
R J BROWN ASSOC (McKeehan), Houston, TX
SANDIA LABORATORIES Seabed Progress Div 4536 (D. Talbert) Albuquerque NM
SEA DATA CORP (M. Lanza) Newton, MA
SHELL DEVELOPMENT CO. Houston TX (E. Doyle)
SHELL OIL CO. HOUSTON, TX (MARSHALL); Houston TX (R. de Castongrene); I. Boaz, Houston TX
UNIVERSITY OF CALIFORNIA Santa Barbara (Dept of Mech Engr-Anmanel)
UNIVERSITY OF WYOMING (Statistics Dept. - L.E. Borgman) Laramie, WY
WESTINGHOUSE ELECTRIC CORP. Annapolis MD (Oceanic Div Lib, Bryan); Library, Pittsburgh PA
WESTINSTRUCORP Egerton, Ventura, CA
WOODWARD-CLYDE CONSULTANTS (Dr. R. Dominguez), Houston, TX; Library, West. Reg., Walnut Creek, CA; PLYMOUTH MEETING PA (CROSS, III)
BRAHTZ La Jolla, CA
GERWICK, BEN C. JR San Francisco, CA
WM TALBOT Orange CA

INSTRUCTIONS

The Naval Civil Engineering Laboratory has revised its primary distribution lists. The bottom of the label on the reverse side has several numbers listed. These numbers correspond to numbers assigned to the list of Subject Categories. Numbers on the label corresponding to those on the list indicate the subject category and type of documents you are presently receiving. If you are satisfied, throw this card away (or file it for later reference).

If you want to change what you are presently receiving:

- Delete - mark off number on bottom of label.
- Add - circle number on list.
- Remove my name from all your lists - check box on list.
- Change my address - line out incorrect line and write in correction (DO NOT REMOVE LABEL).
- Number of copies should be entered after the title of the subject categories you select.

Fold on line below and drop in the mail.

Note: Numbers on label but not listed on questionnaire are for NCEL use only, please ignore them.

Fold on line and staple.

DEPARTMENT OF THE NAVY

NAVAL CIVIL ENGINEERING LABORATORY
PORT HUENEME, CALIFORNIA 93043

OFFICIAL BUSINESS
PENALTY FOR PRIVATE USE, \$300
1 IND-NCEL-2700/4 (REV. 12-73)
0630-LL-L70-0044

POSTAGE AND FEES PAID
DEPARTMENT OF THE NAVY
DOD-316



Commanding Officer
Code L14
Naval Civil Engineering Laboratory
Port Hueneme, California 93043

DISTRIBUTION QUESTIONNAIRE

The Naval Civil Engineering Laboratory is revising its primary distribution lists.

SUBJECT CATEGORIES

- 1 SHORE FACILITIES**
- 2 Construction methods and materials (including corrosion control, coatings)
- 3 Waterfront structures (maintenance/deterioration control)
- 4 Utilities (including power conditioning)
- 5 Explosives safety
- 6 Construction equipment and machinery
- 7 Fire prevention and control
- 8 Antenna technology
- 9 Structural analysis and design (including numerical and computer techniques)
- 10 Protective construction (including hardened shelters, shock and vibration studies)
- 11 Soil/rock mechanics
- 12 BEO
- 13 Airfields and pavements
- 15 ADVANCED BASE AND AMPHIBIOUS FACILITIES**
- 16 Base facilities (including shelters, power generation, water supplies)
- 17 Expedient roads/airfields/bridges
- 18 Amphibious operations (including breakwaters, wave forces)
- 19 Over-the-Beach operations (including containerization, materiel transfer, lighterage and cranes)
- 20 POL storage, transfer and distribution
- 24 POLAR ENGINEERING**
- 24 Same as Advanced Base and Amphibious Facilities, except limited to cold-region environments

TYPES OF DOCUMENTS

- 85 Techdata Sheets
- 86 Technical Reports and Technical Notes
- 83 Table of Contents & Index to TDS

28 ENERGY/POWER GENERATION

- 29 Thermal conservation (thermal engineering of buildings, HVAC systems, energy loss measurement, power generation)
- 30 Controls and electrical conservation (electrical systems, energy monitoring and control systems)
- 31 Fuel flexibility (liquid fuels, coal utilization, energy from solid waste)
- 32 Alternate energy source (geothermal power, photovoltaic power systems, solar systems, wind systems, energy storage systems)
- 33 Site data and systems integration (energy resource data, energy consumption data, integrating energy systems)

34 ENVIRONMENTAL PROTECTION

- 35 Solid waste management
- 36 Hazardous/toxic materials management
- 37 Wastewater management and sanitary engineering
- 38 Oil pollution removal and recovery
- 39 Air pollution
- 40 Noise abatement
- 44 OCEAN ENGINEERING**
- 45 Seafloor soils and foundations
- 46 Seafloor construction systems and operations (including diver and manipulator tools)
- 47 Undersea structures and materials
- 48 Anchors and moorings
- 49 Undersea power systems, electromechanical cables, and connectors
- 50 Pressure vessel facilities
- 51 Physical environment (including site surveying)
- 52 Ocean-based concrete structures
- 53 Hyperbaric chambers
- 54 Undersea cable dynamics

82 NCEL Guide & Updates

- 91 Physical Security

None -

remove my name

END

FILMED

4-84

DTIC